

June 2020

Development of Water Coning Control Design Metrics in Naturally Fractured Reservoirs

Samir Prasun

Louisiana State University and Agricultural and Mechanical College

Follow this and additional works at: https://repository.lsu.edu/gradschool_dissertations



Part of the [Energy Systems Commons](#), [Geological Engineering Commons](#), [Operational Research Commons](#), and the [Other Engineering Commons](#)

Recommended Citation

Prasun, Samir, "Development of Water Coning Control Design Metrics in Naturally Fractured Reservoirs" (2020). *LSU Doctoral Dissertations*. 5283.

https://repository.lsu.edu/gradschool_dissertations/5283

This Dissertation is brought to you for free and open access by the Graduate School at LSU Scholarly Repository. It has been accepted for inclusion in LSU Doctoral Dissertations by an authorized graduate school editor of LSU Scholarly Repository. For more information, please contact gradetd@lsu.edu.

DEVELOPMENT OF WATER CONING CONTROL DESIGN METRICS IN NATURALLY FRACTURED RESERVOIRS

A Dissertation

Submitted to the Graduate Faculty of the
Louisiana State University and
Agricultural and Mechanical College
in partial fulfillment of the
requirements for the degree of
Doctor of Philosophy

in

Craft & Hawkins Department of Petroleum Engineering

by

Samir Prasun

B.S., Indian Institute of Technology (ISM), 2009

M.S., University of Oklahoma, 2013

August 2020

To my Parents, *Raghubar Narain Barnwal* and *Chanda Barnwal*
Who always stood there for me during the hard times,
Who always cared and prayed for me,
I want to tell you I love you

To my wife, *Nisha Kumari* and my baby, *Kiaan Prasun*
Whom I love more than myself,
Whom I want to give a comforting/healthy life in the future
Thanks for your moral support and patience

Acknowledgements

I would like to express my special thanks of gratitude to my advisor, Dr. Andrew K. Wojtanowicz, for his guidance, supervision, and support during the five-year long PhD study. At the beginning, it was quite difficult for me to pace with the quality of his research and level of perfection. I had hard time with the continuing need for improving quality of my work that seemed to be still insufficient, but I kept up with the demand by working harder. In this long journey, there were periods of failure and confusion and moments of adjoining success and rejoice. Towards the end, however, my PhD study turned out to provide me with a meaningful accumulation of knowledge and skills, and also to result in the improved communication and understanding between two of us.

I would also like to thank Dr. Mayank Tyagi, Dr. Mehdi Zeidouni, and Dr. Edward Laws for being on my examining committee panel and providing me the help and technical support whenever needed.

I wish to express my gratitude to the LSU Downhole Water Sink Technology Initiative (DWSTI) and Petroleum Engineering Department for supporting this research.

Table of Contents

Acknowledgements	iii
Nomenclature	vi
Abstract	xiii
Chapter 1. Introduction	1
1.1. Water Coning/Channeling in NFR.....	1
1.2. Water Coning Control Design Metrics	3
1.3. Objectives	8
1.4. Methodology And Limitations	9
1.5. Dissertation Outline and Logic	12
Chapter 2. Water Coning Control Metrics	14
2.1. Critical Oil Rate – Coning Severity	14
2.2. Well Placement	23
2.3. Water-Cut Pattern.....	26
2.4. Well Spacing	30
2.5. Well Completion Design	33
Chapter 3. Critical Oil Rate in NFR	35
3.1 Apparent Critical Rate in DPDP Model of NFR	36
3.2 Limitations of Apparent Critical Rate Model	39
3.3 Grey-Box Model of Critical Rate in NFR	42
Chapter 4. Well Placement and Significance	46
4.1 Qualification of Single And Dual-Completed Well Placement in NFR	46
4.2 Well Completion Placement Simulation Model	47
4.3 Well Placement Significance in Planar Network NFR.....	56
4.4 Effect of Well Placement on Critical Rate	72
Chapter 5. Water-Cut Pattern and Well-Spacing	81
5.1 Water-Cut vs. Well Spacing in SPR	81
5.2 Water-Cut Stabilization Effect on Well’s Recovery in SPR	92
5.3 Water-Cut Pattern in NFR	96
5.4 Analytical Model of Stable Water-Cut in NFR	104
5.5 Effect of Well Spacing and Production Rate on Stabilized Water-Cut	107
5.6 Well Spacing Optimization.....	110
Chapter 6. Oil Recovery Prediction in NFR with Fracture Corridors	119
6.1 Well’s Recovery vs Completion Placement	120
6.2 Probabilistic Prediction of Reservoir Recovery.....	124
Chapter 7. Feasibility of Downhole Water Loop (DWL) Wells in NFRs.....	139

7.1 DWL Well Concept and Applications	139
7.2 DWL Well in NFRs with Fracture Corridors	140
7.3 DWL Well in NFRs with Planar Fracture Network	148
7.4 DWL Feasibility Model	158
Chapter 8. Conclusions	165
Appendix A: Experimental Data on Critical Rate	172
Appendix B: Properties of Single and Dual Completed Wells in NFR.....	176
Appendix C: Derivation of Pseudo WCULT Formula	179
Appendix D: Effect of Production Rate on Minimum Well Spacing.....	182
Appendix E: Verification of Stabilized Water-Cut Formula.....	184
Appendix F: Previous Publication Agreements	186
References	189
Vita.....	201

Nomenclature

α = angle of relative inclination between well (vertical or subvertical) and fracture or dip angle of fracture

β = regression coefficient

β_a = azimuth of parallel fractures

ρ_o = oil density

Φ_m = matrix porosity, fraction

φ_f = fracture porosity, fraction

μ_o = viscosity of oil, cp

μ_w = viscosity of water, cp

$\Delta\rho$ = difference in density between water and oil, lb/ft³

Δt = small time increment, days

Δh_o = decrease in oil-column thickness due to water advancement towards oil-pay, ft

Δh_w = increase in aquifer thickness due to water advancement towards oil-pay, ft

Δt_p = duration of project, days

$\frac{\Delta h}{\Delta t}$ = upward velocity of water invasion in matrix, ft/sec

$\frac{\Delta(WC)}{\Delta t}$ = rate of water-cut increase

ΔP = pressure drawdown, psi

ΔP_{fr} = pressure drawdown in fracture-well, psi

A = laminar flow coefficient

A_c = cross-sectional area of the reservoir, sq.ft

B = turbulence coefficient derived from well testing

BOR = balanced-oil-rate

B_o = formation oil volume factor, rb/stb

B_w = formation water volume factor, rb/stb

C1 = event associated with the well intersecting fracture corridors

C2 = event associated with the well intersecting matrix-block

CSI = coning severity index

D = Radial size of matrix-zone/exclusion-zone, ft

d_w = well diameter, ft

dz = differential element in direction from top to bottom of oil-zone column, ft

DPDP = dual porosity dual permeability

$E(F_w)$ = expected fracture corridor width, m

$E(S_p)$ = expected fracture spacing, m

$E(k_f)$ = expected value of effective fracture permeability, md

F_A = equivalent fracture width for a system of fractures

F_{bc} = dimensionless factor for poor cementation

F = spatial distribution density, fracture/m

F_w = fracture corridor width, m

g = acceleration due to gravity, 32.174ft/sec²

h_o = oil-zone thickness, ft

h_{op} = perforated length, ft

$\frac{h_{op}}{h_o}$ = penetration ratio

h_t = total reservoir thickness (including water-zone), ft

h_w = aquifer thickness, ft

k_f = average permeability of fracture network, md
 k_{fh} = effective mean horizontal permeability of the fracture network, md
 k_{fv} = effective vertical fracture permeability, md
 K_e = anisotropic permeability in principle directions
 k_{fx} = effective permeability of fracture network in X-direction, md
 k_{fy} = effective permeability of fracture network in Y-direction, md
 k_{fz} = effective permeability of fracture network in Z-direction, md
 k_h = horizontal permeability in single porosity reservoir, md
 k_m = average matrix permeability, md
 k_{mh} = horizontal permeability of the matrix blocks, md
 k_{mv} = vertical matrix permeability, md
 k_o = effective horizontal permeability of oil, md
 k_{ro} = relative permeability of oil
 k_{roe} = end point oil relative permeability of matrix at connate water saturation, fraction
 k_{rw} = relative permeability of water
 k_{sp} = spherical rock permeability, md
 k_{spw} = effective spherical permeability of water, md
 k_v = vertical permeability in single porosity reservoir, md
 k = reservoir permeability, md
 k_{ff} = Intrinsic permeability of fracture/fracture corridor, md
 k_f = effective permeability of fracture in any direction, md
 $k_{f,m}$ = overall permeability of NFR, md
 k_v/k_h = anisotropy ratio of matrix blocks, fraction

k_w = effective horizontal permeability of water, md

M = mobility ratio between water and oil, fraction

NFB = no-flow boundary

OWC = oil-water contact

pseudoWCult = pseudo-ultimate water cut, fraction

P_2 = reservoir pressure at R_2

P_c = reservoir pressure at R_c

P_i = initial reservoir pressure, psi

P_b = bubble point pressure, psi

P_c = capillary pressure, psi

P_F = probability of well intersection within orthogonal vertical fracture network

P(C1) = probability that the well intersects the fracture-corridors

P(C2) = probability that the well intersects the exclusion (matrix) block

$p(F_w)$ = probability density function of fracture corridor width

$P(F_w)$ = Cumulative probability function

q_c^* = dimensionless critical oil rate defined by Chaperon (1986)

q_{CD} = dimensionless critical oil rate by Papatzacos

$q_{c,max}^*$ = maximum dimensionless stable critical oil rate

$q_{cr,fr}$ = critical-rate for a fracture-well in NFR, bopd

$q_{cr,matrix-zone}$ = critical-rate for coning in an exclusion-zone, when well is completed in matrix blocks of NFR, bopd

$q_{cr,fractured-zone}$ = critical-rate for coning in a fractured-zone, when well is completed in matrix blocks of NFR, bopd

$Q_{capillary}$ = hypothetical matrix oil replacement rate due to negative capillary pressure, bbl/day

Q_m = liquid production through matrix-well, bbl/day

Q_{opt} = optimum total production rate in NFR, bbl/day

$Q_{m,o}$ = oil flow-rate through matrix, bopd

Q_{max} = maximum liquid production rate at bottom-hole pressure equal to bubble-point pressure, bpd

$Q_{m,gravity}$ = oil displacement rate due to gravity force, bpd

$Q_{m,viscous}$ = oil displacement rate due to viscous force, bpd

q_{cr} = critical oil rate, bbl/day

q_o = oil production rate, bbl/day

q_w = water flow rate, bbl/day

Q = total production rate, bbl/day

Q_{fmax} = maximum liquid production rate of fracture well, bbl/day

Q_o = cumulative oil, bbl

R_1 = turbulence radius

R_2 = drainage radius

R_c = critical radius at which stable water cone forms

r_D = dimensionless radius

r_w = wellbore radius, ft

r_e = reservoir radius, ft

r_{eTh} = threshold drainage radius, ft

r_s = semi-spherical flow radius, ft

r_{ms} = matrix-zone radius, ft

$(r_{ms})_{cr}$ = critical matrix-zone radius, ft

r_{Ds} = dimensionless semi-spherical water inflow radius

r_{ws} = spherical water sink radius, ft

RF = recovery factor, fraction

$r_{e,eq}$ = Equivalent drainage size of matrix-zone after replacing the fractured-zone with an equivalent matrix-zone, ft

S_p = fracture spacing

S = partial penetration skin

S_m = skin factor due to well-inflow in matrix block

S_f = skin factor due to well-inflow in fractured zone

$S_{oi}(z)$ = initial oil-saturation as a function of depth, fraction

S_{or} = irreducible oil saturation, fraction

S_w = water-saturation, fraction

S_{wc} = connate water saturation

$S_{w,stab}$ = average water saturation at the end of stabilized water-cut stage

S_y = fracture spacing in Y-direction

S_x = fracture spacing in X-direction

S_{pmean} = mean fracture spacing, ft

T_{stab} = duration of stabilized water-cut stage, years

t = actual time elapsed after the start of production, days

t_{BT} = breakthrough time, days

t_D = dimensionless time

WC = water-cut, fraction

WC_{ec} = economic limit of water-cut, fraction

WC_{stab} = stabilized water-cut, fraction

W_s = well spacing, ft

$W_{s,opt}$ = optimum well spacing, ft

w_x = fracture aperture in X-direction

w_y = fracture aperture in Y-direction

w = fracture aperture

WC_D = dimensionless water-cut

WC_{ult} = ultimate water cut, fraction

x = independent variable

y = objective function

Z_s = Distance of the apex of stable cone from the point source-well, ft

Abstract

Naturally fractured reservoirs (NFRs) with bottom-water are known for their instant water breakthrough and severe water coning that reduces oil recovery. This is because water channels through the highly permeable fractures easily connecting the well to the aquifer bypassing the oil contained in the matrix. Remedial techniques such as producing below critical-oil rate, optimizing the well spacing and installing the downhole water sink (DWS)/ downhole water loop (DWL) technology, have already been successfully tested in single-porosity reservoirs (SPR). However, applicability of these techniques in NFRs are unknown since only a few studies have been performed on their feasibility in NFRs, to date. Moreover, metrics used for assessing severity of coning and performance of remedial techniques in single porosity reservoirs are insufficient or irrelevant for NFRs.

Two objectives of the study are: 1) to develop the water coning control design metrics specific for NFRs; and, 2) to optimize these metrics for oil recovery improvement in NFRs.

Critical oil rate is an important metric for coning severity. Consequently, the study develops a new semi-analytical “grey-box” model of critical oil rate for NFRs using the mechanistic model of single porosity reservoir and statistically calibrating it with the results from simulated experiments covering wide ranges of NFR. The study also relates critical rate to the placement of well’s completion in fracture network – in fractures or in rock matrix.

Based on the literature, natural fracture systems are classified as planar and channel (fracture corridor-type) fracture networks. A dual porosity/dual-permeability (DPDP) two-dimensional radial-cylindrical model is used for simulating planar networks and a 3-D Cartesian model - for simulating fracture corridor-type network. The study classifies the planar fractures as

densely or sparsely distributed networks based on the minimum fracture spacing - critical fracture spacing – when the well’s placement (on or off fractures) has significant effect on the recovery.

The analysis of water-cut patterns in NFR identifies a stabilization stage that is a characteristic metric of the water coning process and can be controlled by well spacing design. The study correlates the duration of the stabilized WC stage with production rate and well-spacing, thereby providing a basis for optimizing NFR oil recovery.

Another metric – uniquely specific for NFRs – is the location placement of well’s completion within fracture network which controls the pattern and severity of water coning. The study compares recovery performance of well placement on/off-fractures for single and dual-completed wells. Due to uncertainty of well completion’s location with respect to the distributed fracture network, a field case of NFR is studied to make probabilistic prediction of well’s oil recovery.

Well completion design – is an operational metric of water coning control. The study addresses the DWL well’s feasibility for on/off fracture well placement in NFRs.

Chapter 1. Introduction

Excessive water production has always been a concern for operators all round the world. Produced water is the largest waste stream from oil and gas fields. The large volume (15 to 20 billion barrels) of water generated annually along with its high salinity (5000 to 270,000 mg/L TDS) may pose a severe threat to environment under inadequate disposal. There may be either lack of sufficient infrastructure near fields to process the produced water before discharge or high treatment cost of water may render the oil production unviable. Naturally fractured reservoirs (NFRs) are the heterogeneous reservoirs where highly permeable fractures intercepting the matrix block typically improves the conductivity of the formation. The large contrast in the properties including permeability, porosity and capillary pressure between the fracture and matrix in NFR causes the recovery mechanism in the bottom-water NFRs different from that of conventional reservoirs with bottom-water. Severe water coning/channeling in NFRs poses a severe threat to the recovery of these reservoirs.

1.1 Water Coning/Channeling in NFR

Though water coning has been categorized as the most difficult water production problems in conventional reservoirs, it is even more severe in NFRs (Alblooshi and Wojtanowicz 2018). Often the wells pass through multiple conductive fractures, faults and high permeable streaks connecting the wellbore to the underlying aquifer and the mobility advantage results in rapid water channeling through the fractures, thereby causing large amount of bypassed oil (Haugen 2010). Water coning occurs when the oil-water contact surface under the well forms a cone-shaped profile due to well's pressure drawdown in the vicinity of the wellbore. Higher mobility of water as compared to oil favors the water coning whereas the gravity difference between water and oil opposes it. Coning occurs because of the dynamic viscous force in the vertical direction exceeding

the static gravity forces. Both water coning/channeling causes production of large amount of water that results in (a) the need for more complex water–oil separation (b) rapid corrosion of well equipment (c) rapid decline in hydrocarbon recovery and (d) ultimately, premature abandonment of the well. In naturally fractured reservoirs (NFRs), with vertical fractures, severe coning is observed as vertical conductive fractures accelerate the bottom-water migration to the well. In contrast to conventional (single permeability) reservoirs, there are two concurrent conduits for fluid flow in NFRs- fractures and matrix in dual-permeability NFRs. It has been reported from the water coning studies in NFR that the invading bottom water builds two cones- one in the fractures and other in matrix (Namani et al. 2007; Al-Afaleg and Ershaghi 1993). Depending on the rate and reservoir properties, it may be a fast-moving cone in fractures and slower one in matrix. The lag time between the two cones are influenced by fracture storativity, transmissivity and matrix-fracture interporosity effects (Al-Afaleg and Ershaghi 1993). The extent of the cone growth and advancement would depend on different factors such as fracture and matrix permeability, fracture storativity, mobility ratio, oil-pay thickness and production rate (Namani et al. 2007). Shadizadeh and Ghorbani (2001) further, confirmed that in NFR, the fractures cone development would follow the path of least resistance. The ratio of K_v/K_h is very high in fractures in NFR and is a key parameter in deciding the water coning tendency.

Reiss (1980) showed that, though in water-wet NFR, capillary imbibition reinforces the gravity effects; in oil-wet rock, capillary forces oppose the penetration of water in matrix and displacement of oil from matrix is possible only if gravity forces overcome the capillary displacement pressure. Hamon (1988) also reported limited oil recovery by water-oil gravity segregation that could be obtained for oil-wet NFRs at high matrix permeability and large block height with vertical capillary continuity of matrix blocks (Pratap et al. 1997). In contrast, for water-

wet NFRs, capillary imbibition controls the significant oil recovery and the effect of gravity drainage due to capillary continuity is not significant (Pratap et al. 1997).

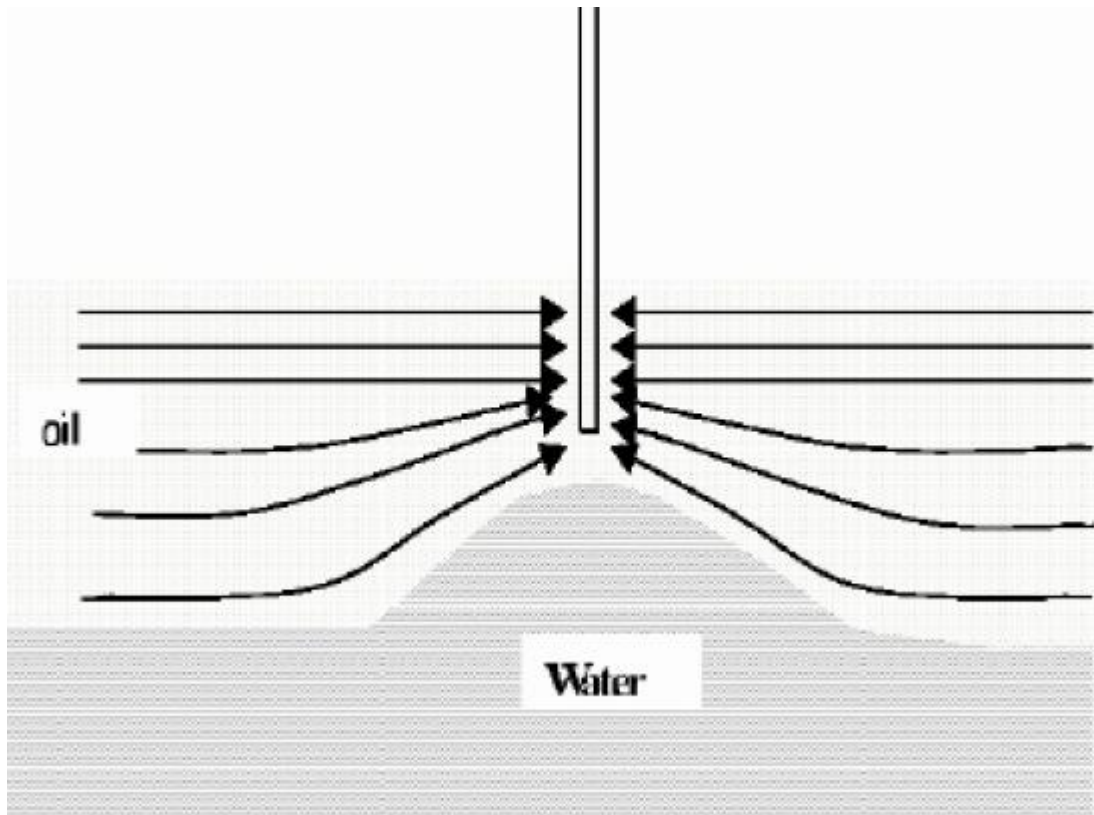


Fig. 1.1. Water coning and production below critical-rate (Namani 2007)

The design of the water coning control methods can be analyzed using certain metrics which can help assess and improve the water coning performance. There is a need to identify these metrics, optimize them and derive their functional relationship for controlling water coning in NFRs.

1.2 Water Coning Control Design Metrics

Metrics are parameters or measures of quantitative assessment used for measurement, comparison, or to track performance of a process. In this study, the process is the oil production with controlled water coning. The process performance is determined by the final recovery. The process alternatives are the conventional/ downhole water sink/downhole water loop wells in

NFRs. The process design metrics are the parameters/variables of the process which may be either known or uncertain. There are different water coning control design metrics that can help assess and design the strategies, which include;

Critical oil rate: The critical oil rate is the maximum oil production rate without water breakthrough, which is a typical characteristic of the reservoir with bottom water coning. The critical oil rate is a metric of coning severity. It can also be used to assess the efficiency of a coning control technique. The basic presumption is that if we produce at a low rate, local pressure drawdown will be minimized which will not allow the coning to occur and only oil is produced. The upward force due to drawdown results in upward movement of water till the point at which the dynamic force is balanced by the height of water beneath that point. The locus of balance point is the oil-water cone-shaped interface which is shown in Fig. (1.1). Above the interface, lies the moving oil while below the interface is the stable water. However, when coning is severe, producing below the critical-rate may pose a practical difficulty and economic unfeasibility if the rate becomes too low. Previous models of critical production rate both in single-porosity reservoirs (SPR) and NFRs are discussed in Chapter 2. Though the models are up-to-date for SPR, they fail to account for all properties of NFRs, which is addressed in Chapters 2 and 3.

Well-placement: Well completion placement in SPR is an operational metric that help assess the design of water coning control. It influences the pattern and severity of water coning. Completion is preferably placed at the top of oil-zone to mitigate the severity of coning. Because of the heterogeneity introduced in dual-porosity reservoirs due to the presence of highly permeable and slightly porous fractures, water coning is greatly affected by the placement of well completion within the fracture network. Thus, spatial well placement on/off fractures become an important water coning metric specific for NFRs addressed in Chapters 2 and 4. Further, because of the

uncertainty of well placement with respect to location of fracture network, recovery estimation becomes probabilistic problem, which is addressed in Chapter 6.

Water-cut pattern: Water-cut pattern is a metric for identifying different water problems. Different water problems display different diagnostic log-log plot of WOR vs. time patterns. For example, a) water channeling through faults and fractures or channeling from behind the casing – shows a very rapid increase of the curve; b) edge-water flow or moving oil-water contact – shows a rapid increase after breakthrough followed by a straight line curve; and c) water coning – shows a gradual buildup of WOR – (Bailey et al. 2000) as shown in Fig. 1.2.

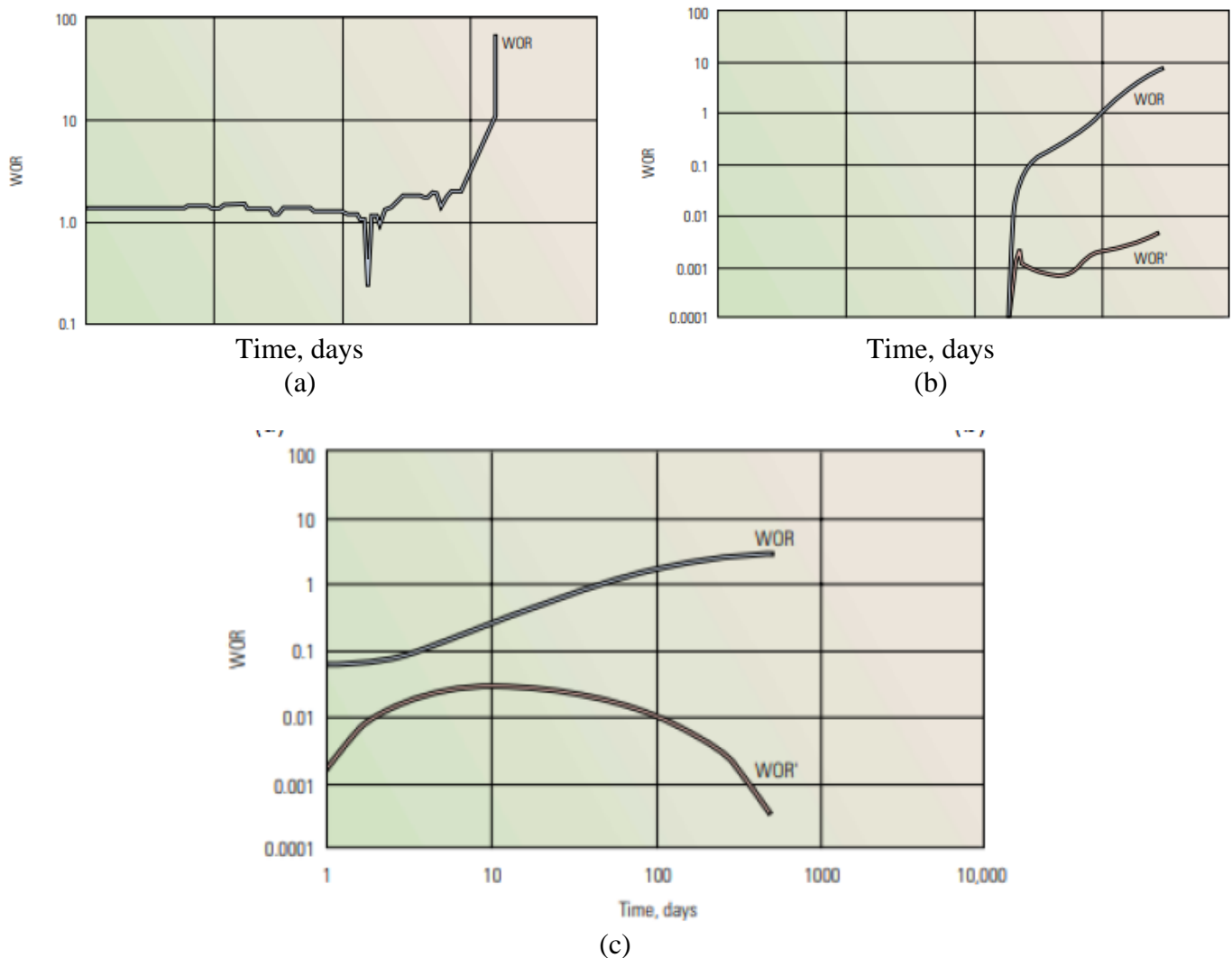


Fig. 1.2. Water-oil ratio (WOR) diagnostic plots for different water problems characterizing different breakthrough mechanisms (Bailey et al. 2000)

Water-cut pattern in SPR would depend on the size of drainage area affecting oil depletion rate, which is addressed in chapters 2 and 5. In NFRs, water-cut pattern would be a function of well completion location within the heterogeneous fracture network, which is addressed in chapters 2 and 5.

Recovery: Recovery is a metric of process performance. Well's productive life is defined by the economic limit of water-cut representing the break-even cost (zero-profit) of daily production. At economic limit of water-cut (say 97%), revenue due to oil production becomes equal to the oil producing cost and water processing-disposal cost. Ultimate recovery is determined at economic limit of water-cut or 20 years duration of project, which ever reaches first. Higher ultimate recovery is the metric for improved water coning control design. Both deterministic and probabilistic recovery computation in NFRs is addressed in Chapter 6.

Well Spacing: Well spacing is an important water coning metric in single-porosity reservoirs (SPR), as it controls the performance of water coning. Higher well spacing or drainage area in bottom-water SPR would be detrimental to oil recovery, because of the locality of water coning sweepage resulting in vast amount of by-passed oil regions. In this way, well spacing controls the recovery performance. Well spacing estimation becomes a challenge for NFRs because of the simultaneous water channeling issue along with water coning in a heterogeneous fracture network, which is addressed in Chapters 2 and 5.

Well Completion Design: Well completion design is another operational metric that controls the severity and performance of water coning. Length of vertical completion placed at the top of oil-zone determines the inflow performance of oil and water. Horizontal wells where water cresting is a common phenomenon would considerably reduce the water-cut severity due to its low-pressure drawdown requirements. Since pressure gradient is the highest at heel of the well, first water

breakthrough happens at the heel of the well. Perforation design where more holes are perforated towards the end of a horizontal well would prevent the immediate water breakthrough at the heel end of the well. There are other designs being considered in SPR to control the water coning, which include Downhole water Sink (DWS) and Downhole water loop (DWL) completions. DWS is a completion technique that involves installing an additional completion in the aquifer beneath the oil-water contact (Fig. 1.3). This additional completion drains the water which creates the pressure sink at the oil water contact suppressing the water cone progression around the wellbores, thereby reducing or completely eliminating the water-cut from the top completion. This helps in maximizing the recovery of reservoir. However, a large amount of water is drained from the bottom completion, which may create the environmental problem on the surface. Further, removal of water from aquifer would deplete it and lower the strength of aquifer.

In downhole water loop (DWL) technology, we install a third completion deep down the wellbore as shown in Fig. 1.3. The third completion injects the water drained from the completion just beneath the oil-water contact. The injection of water back into the aquifer helps maintain reservoir pressure and eliminate any environmental concern of water disposal. This allows to keep the advantage of DWS technology, while minimizing its drawback. Though feasibility of DWL wells is already proved for SPR (chapter 2), it needs to be addressed for NFRs (chapter 7 – future work).

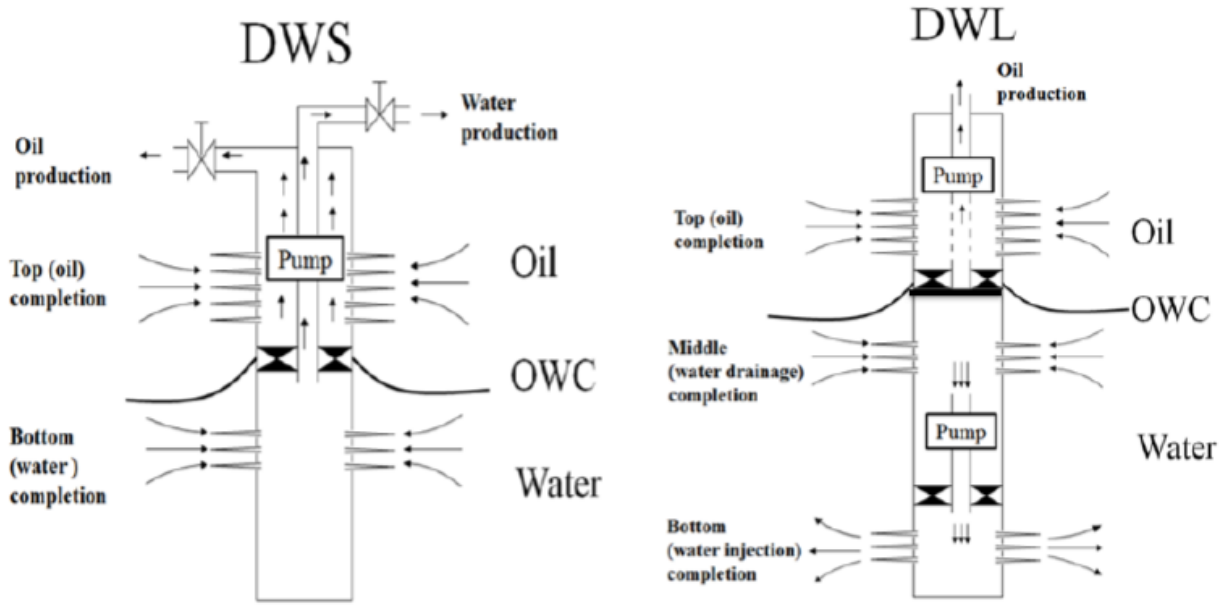


Fig. 1.3. Schematic of DWS and DWL well completions (Jin 2013)

1.3 Objectives

The main objectives of this study are to evaluate the water coning control metrics and determine a functional relationship between them:

1. Study well placement modeling and significance in NFRs.
2. Develop an improved model of critical oil rate in NFR as a function of well placement in fracture-network.
3. Investigate the water-cut pattern in a single porosity reservoirs (SPR) developed using a multi-well project, and relate it with the well-spacing design for maximum recovery.
4. Study the water-cut pattern in NFR and develop an analytical model of stabilized water-cut in NFR which has implications on well-spacing design for maximum recovery.
5. Investigate the well placement uncertainty in fracture networks and its recovery implications.
6. Assess the feasibility of downhole water loop technology in NFRs

1.4 Methodology and Limitations

Following methods are used to achieve the objectives:

Grey-box Modelling: Many theoretical models are derived from simplified assumptions and hence are unable to closely match experimental results that invariably include additional physics ignored in the models. Purely theoretical models are also called *white-box* models. As the name suggests, the parameters of the model are generally known or quantifiable using law of physics. Alternatively, there are purely empirical or *black-box* models comprising correlations developed statistically using experimental data. Therefore, the models cannot capture the physical mechanisms of the process. There are also grey-box models that represent a combination of analytical and empirical modeling (Amisigo 2006; Clarkson and Qanbari 2015). Such models, underline methodology used in this study. The grey-box modelling approach comprises three steps:

Step a) Simplified Analytical Modeling: Any physical process can be represented by mechanistic/physical forces that govern their mechanism, which can be used to model the process. However, these models can be more computationally demanding and may not be precise under extreme conditions, so may not represent entire dataset. In that case, we may look for assembling data-driven modelling into analytical modelling approach using virtual experiments.

Step b) Experiments (Virtual): Simulation experiment involves running the black oil reservoir simulator IMEX (using Computer Modelling Group (CMG)) on dual porosity/dual permeability (DPDP) NFR models. However, it is necessary to evaluate the performance of simulation tool against the actual processes occurring in sub-surface reservoirs. Following are the advantages/disadvantages of DPDP model that needs to be acknowledged considering the other physical models:

- a) DPDP models allows highly adjustable matrix/fracture transfer physics, which are important for NFR with water-drive/water flooding conditions to account for the transfer of fluids determined by capillary imbibition and gravity drainage. Discrete fracture network (DFN) model do not allow adjustable modelling of matrix/fracture fluid transfer, so their applicability for full-field simulation is limited (Narr et al. 2006).
- b) These models require twice the data used for single-porosity simulation which are not known most of the time. This may result in erroneous complex model. Also, computation run time may be 5 times longer than single-porosity models (Narr et al. 2006).
- c) Fractures as geological discontinuities introduce a high level of complexity into the entire reservoir modeling workflow. In current practice, the geological modeling of fractures and the current flow simulation are considerably disconnected, simply because current commercial simulators cannot handle the complexity of current fracture models. To enable a manageable computation, these NFR simulator (DPDP) must work on a coarser grid, hence, the only way is to upscale a fine scale fracture description to a continuum flow simulation model. This is possible by computing effective permeabilities for fractured system. This averaging can lead to severe errors as it ignores much of the geological information leading to less predictive power (Karimi-Fard et al. 2006).
- d) In contrast to the DFN models, DPDP models fails to consider the geometry, orientation, and connectivity of the fracture networks.
- e) DPDP Model fracture spacing may not be equal to the true geological average fracture spacing, which can be highly variable and non-orthogonal/conjugate. However, the value of fracture spacing for DPDP model in any direction is computed based on the orthogonality of fracture network (Narr et al. 2006).

Number of experiments may increase exponentially with the increase in the number of factors, so that the entire effect of each input variable is captured. The experimental saving thus becomes more important which is possible by performing design of experiment (DOE). Following are the experimental design methods used in my research study:

Taguchi Design: It is a 2-level experimental design. This method utilizes two, three and mixed-level fractional factorial design, which favors large screening designs and makes the process more robust.

Fractional Factorial Design: This design considers the main effects and few of the two/three-factor interactions of input variables. By considering, only a fraction of the factorial design, fractional factorial designs drastically reduces the number of simulations required to uniquely estimate the significance all the input variables on the responses (Polidasu et al. 2016). The disadvantage of the fractional factorial design is that it assumes linearity between the input and response variables, and hence, it cannot be used to formulate the proxy model.

Box-Behnken Design: The full three-level factorial design requires 3^k experiments where k is the number of factors. To minimize the number of runs while at the same time capturing the entire effect of each input variable and the interactions of these input variables, we use the Box and Behnken method for three-level design to fit the second order responses. Compared to full three-level factorial design, Box and Behnken design (BBD) significantly reduces the number of experiments. For five factors, BBD manages to reduce the number of experiments to 46 as compared to full three-level factorial designs which requires 243 number of experiments. BBD requires three levels: minimum, center and maximum which are coded as -1, 0 and +1.

Step c) Model modification to match experiments: The physics-based model can be fit to the virtual experimental results using two different techniques 1) complementary modeling

where discrepancy or error between the predicted values (from analytical model) and measured values (from experiments) is modelled separately by a complementary model (Jemberie 2004). 2) model calibration, where the theoretical model may be calibrated to include the effect of parameters not defined in the physical model or difficult to quantify analytically. Specifically, as we do not have or cannot estimate the values of the mechanistic model's parameters, we estimate these parameters from experimental data using the correlation-regression approach. The second order (quadratic) models which can be used to fit the discrepancy or the additional physics-based parameter in the modified model, is given by (Myers and Montgomery 1995, Jin 2013),

$$y = \beta_0 + \sum_{j=1}^k \beta_j x_j + \sum_{j=1}^k \beta_{jj} x_j^2 + \sum_{i=1}^{k-1} \sum_{j>1}^k \beta_{ij} x_i x_j \quad (1.1)$$

Where, y is the objective function; x is the independent variable; β is the regression coefficient; j and i are the variable index; k is the total number of independent variables. $\sum_{j=1}^k \beta_j x_j$ and $\sum_{j=1}^k \beta_{jj} x_j^2$ represent the linear and quadratic effects of the variables, respectively, while the interaction effects between variables are expressed by $\sum_{i=1}^{k-1} \sum_{j>1}^k \beta_{ij} x_i x_j$. The final grey-box model would be computationally less demanding and would represent wide variations in the data.

1.5 Dissertation Outline and Logic

Based on the objectives of research, the dissertation will be organized in the following chapters:

Chapter 1 focuses on the mechanism of oil recovery in bottom-water NFR, problems of water coning/channeling in NFR, and water coning/channeling control design metrics in NFR. The first chapter gives a brief explanation of reasons undertaken to the study, the objectives of the study, the methods used in the research and the limitation of the methodology.

Chapter 2 presents the literature review on water coning control design metrics both in non-fractured and fractured reservoir, which include critical oil rate in single porosity reservoirs (SPR) and NFRs, well placement modeling, water-cut pattern in SPR and NFRs, well spacing and water

coning completion design. Subsequent chapters address the metrics separately by deriving the analytical expression of the relationships between the design metrics and their compound effect on the process performance.

Chapter 3 proposes a new semi-analytical model of critical rate for NFRs which uses the mechanistic approach of Chaperon (1986) and then statistically modifies it.

Chapter 4 summarizes with well placement modeling and qualification of NFRs and its effect on critical oil rate in NFRs

Chapter 5 investigates on the water-cut pattern in single porosity reservoir and NFRs and proposes the way to optimize the well spacing in these reservoirs based on their water-cut characteristics.

Chapter 6 evaluates the deterministic and probabilistic well's oil recovery considering uncertain well placement in NFR with distributed fracture network.

Chapter 7 investigates the feasibility of dual completed wells with downhole water loop in NFRs.

Chapter 2. Water Coning Control Metrics

This chapter reports the literature review on coning control design metrics which include critical oil rate, well-placement, water-cut, well spacing, and well completion design alternatives. Most of the research work, to date, has been done for single porosity reservoirs (SPR) with some studies for NFRs.

2.1 Critical Oil Rate – Coning Severity

2.1.1 Critical Oil Rate in SPR

Dupuit (1863) was the first one to consider inverse coning of air into aquifer. He developed a steady state relationship between the water production rate and water table elevation in the vicinity of single wellbore, assuming segregated flow and vertical equilibrium (VE). Meyer and Gardner (1954) followed by Pirson (1977) extended the Dupuit approach to single phase flow of oil in a gas/oil/water reservoir. To address the segregated flow in their derivation of the analytical model, Johns et al. (2005) developed a new analytical solution of “Dupuit form” that include the effects of capillary pressure and relative permeability on fluid interfaces. The major limitation of their work is the assumption of VE which implies maximum crossflow of fluids in the vertical direction. This may cause their solutions to overestimate the coning effect.

The first work in analyzing water coning in oil production reservoirs theoretically was carried out by Muskat and Wyckoff (1935). They suggested that water coning is induced by pressure differential existing between the well and the reservoir, and the advancement rate of oil-water contact (OWC) is directly proportional to this pressure differential.

Though the earlier works were focused on the experimental and simulation study of isotropic conventional reservoirs; correlations were later developed for anisotropic homogenous formation.

Bournazel and Jeanson (1971) also developed the correlation to compute the critical oil rate for anisotropic reservoir:

$$q_{cr} = 5.14 \times 10^{-5} \frac{k_o^2 h_o^2 \Delta \rho g \left(1 - \frac{h_{op}}{h_o}\right)}{\mu_o k_v B_o} \quad (2.1)$$

Where, all the parameters are in field units. Where, $\Delta \rho$ is the density difference between water and oil, lb/ft³; k_o is the effective permeability of the oil-zone; h_o is the oil-zone thickness, ft; h_{op} is the perforated interval, ft; μ_o is the oil viscosity, cp; r_e is the drainage radius of the reservoir, ft; r_w is the well radius, ft; B_o is the oil formation volume factor.

Schols (1972) developed an empirical correlation of water coning based on results of experimental study on Hele Shaw model and numerical simulation as:

$$q_{cr} = 0.0783 \times 10^{-4} \left[\frac{\Delta \rho k_o (h_o^2 - h_{op}^2)}{\mu_o B_o} \right] \left[0.432 + \frac{\pi}{\ln \frac{r_e}{r_w}} \right] \left(\frac{h_o}{r_e} \right)^{0.14} \quad (2.2)$$

Where, all the parameters are in field units.

Chaperon (1986) developed the first semi-analytical model to estimate the critical rate for very short perforations in vertical well in an anisotropic reservoir, as,

$$q_{cr} = 0.0783 \times 10^{-4} \left[\frac{\Delta \rho k_o (h_o^2)}{\mu_o B_o} \right] \left[0.7311 + \frac{1.943}{\frac{r_e}{h_o} \sqrt{\frac{k_v}{k_h}}} \right] \quad (2.3)$$

Where, k_h is the horizontal permeability and k_v is the vertical permeability of the reservoir. In her development of semi-analytical model, she first introduced the mechanistic model of critical-rate for point source well at the top of oil-zone and later, modified it statistically to simplify it as shown in Eq. (2.3).

Another analytical solution, based on single phase, compressible fluid and infinitely conductive wellbore was presented by Hoyland et al. (1989) to predict critical oil rate for partially penetrated well in an anisotropic formation:

$$q_{cr} = 0.246 \times 10^{-4} \left[\frac{\Delta \rho k_o h_o^2}{\mu_o B_o} \right] q_{CD} \quad (2.4)$$

They used the methodology of Papatzacos (1986), where method of images and superposition is used to address boundary conditions. After running large number of simulations using a reservoir simulator, they plotted dimensionless critical rate, q_{CD} vs. dimensionless radius,

r_D ($r_D = \frac{r_e}{h_o} \sqrt{\frac{k_v}{k_h}}$) for a different penetration ratio. Hoyland et al. (1989) also proposed an empirical

correlation for isotropic reservoir, given by:

$$q_{cr} = \frac{\Delta \rho k_o \left[1 - \left(\frac{h_{op}}{h_o} \right)^2 \right]^{1.325} h_o^{2.238} [\ln(r_e)]^{-1.99}}{10822 \mu_o B_o} \quad (2.5)$$

A new analytical solution, based on single phase, compressible fluid and infinitely conductive wellbore was presented by Hoyland et al. (1989) to predict critical oil rate for partially penetrated well in an anisotropic formation. They used the methodology of Papatzacos (1986), i.e. the method of images and superposition to address boundary conditions. Using analytical solution, they plotted dimensionless critical rate vs. dimensionless radius for different penetration ratio. Then, following correlation can be used to estimate critical rate from the dimensionless critical rate (q_{CD}) value obtained from graph:

$$q_{cr} = 0.246 \times 10^{-4} \left[\frac{\Delta \rho k_h h_o^2}{\mu_o B_o} \right] q_{CD} \quad (2.6)$$

Hoyland et al. (1989) also proposed a general correlation to predict the critical rate for water coning in anisotropic reservoirs. The correlation is based on a large number of simulation runs with a numerical model and is presented in a single graph, with dimensionless critical rate as a function of dimensionless radius between 0.5 and 50, at five different well penetrations. For isotropic reservoirs, the correlation is given by:

$$q_{cr} = 9.23 \times 10^{-5} \frac{k_o \Delta \rho}{B_o \mu_o} \left[1 - \left(\frac{h_{op}}{h_o} \right)^2 \right]^{1.325} [\ln(r_e)]^{-1.990} h_o^{2.238} \quad (2.7)$$

Where, all parameters are in field units.

Guo and Lee (1993) presented an analytical model to predict the critical rate, where the flow in the water coning system is approximated by the radial/spherical/combined (RSC) field model. The RSC 3D flow field is a combination of uniform line-sink radial flow field at the upper part and a point-sink semi-spherical flow field at the lower part as shown in Fig. 2.1. The analytical solution demonstrated that the optimum wellbore penetration into an oil zone is less than one-third of the total pay zone thickness. Their correlation is given by:

$$q_{cr} = 0.0783 \times 10^{-4} \frac{\Delta\rho k_v}{\mu_o} \left[r_e - \sqrt{r_e^2 - r_e(h_o - h_{op})} \right]^2 \left[\frac{k_v}{\sqrt{k_h^2 + k_v^2}} + \frac{h_{op} \left[\frac{1}{r_w} - \frac{1}{r_e} \right]}{\ln \frac{r_e}{r_w}} \right] \quad (2.8)$$

Where, all the parameters are in field units.

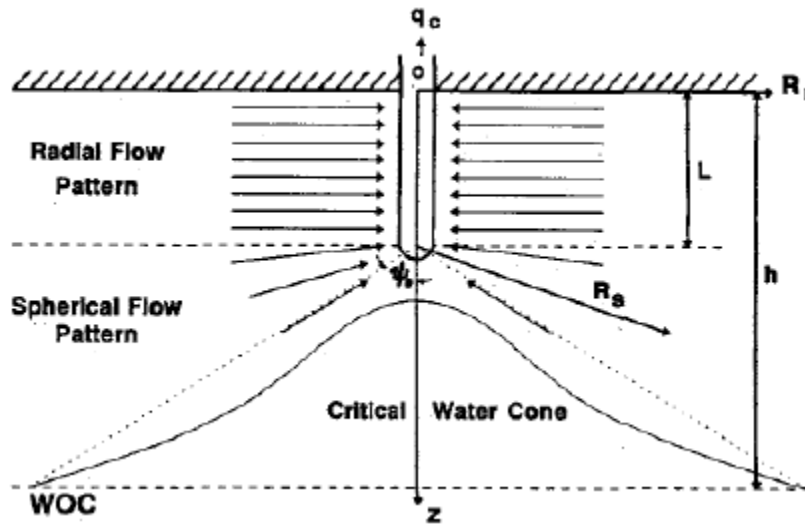


Fig. 2.1. An Radial/Spherical/Combined Flow Field (Guo and Lee 1993)

Tabatabaei et al. (2012) also presented an analytical model of critical rate assuming the same RSC 3D flow field similar to the model of Guo and Lee (1993). Their developed model is given by,

$$q_{cr} = \frac{1.13 \times 10^{-4} k_o \Delta \rho (h_o - h_{op} - r_w)}{\mu \left(\frac{1}{r_w} - \frac{1}{r_e} \right)} \times \left[\frac{1}{\sqrt{\left(\frac{k_h}{k_v} \right)^2 + 1}} + \frac{h_{op} \left(\frac{1}{r_w} - \frac{1}{r_e} \right)}{\ln \frac{r_e}{r_w}} \right] \quad (2.9)$$

Where, all the parameters are in field units.

The Tabatabaei et al. model is applicable only to low pressure gradient or high conductivity reservoirs, whereas the Guo and Lee (1993) model predicts critical rate for both high pressure gradient and low-pressure gradient reservoirs. Though both the models consider the effect of limited wellbore penetration on oil's productivity, they oversimplify the combined existence of the radial and hemispherical flow field, which may overestimate the critical oil rate.

Evidently, critical oil rate model development in matrix-only reservoir is already concluded, and there is no need of any new model.

2.1.2 Critical-Oil Rate in NFRs

Theory used for single-porosity reservoir (SPR) can also be applied to NFR using the concept of equivalent permeability of fractured-media (instead of permeability of matrix). The concept assumes the fracture-network as an equivalent continuous porous medium. The concept was used in the Perez-Martinez (2012) model of critical oil rate in NFR.

The challenge of the equivalent continuous medium approach is to estimate the equivalent permeability of fractured-media which would accurately represent the equivalent fracture network. Previous attempts have been made to estimate the effective permeability of the fracture-network using the tensor approach (Snow 1969; Oda 1985; Long et al. 1985; Durlofsky 1991). Dershowitz et al. 2000 recommended the use of discrete fracture network (DFN) simulations to compute the equivalent permeability tensors which can address the issue of connectivity. They also showed how to find the optimal grid cell size which can reproduce the actual connectivity of DFN. Further,

they demonstrated the way to calculate the equivalent fracture spacing and hence the shape factor for an equivalent orthogonal fracture system.

There are also correlations of critical-rate developed specifically for NFRs either assuming fracture network as a single fracture or continuous porous media. Using the well testing derived parameters (laminar flow coefficient, A), Birk (1963) represented the system of fractures as a single fracture characterized by equivalent fracture width, F_A , as,

$$F_A = 0.19 \left[\frac{\mu_o B_o}{A} \log_{10} \frac{R_2}{R_1} \right]^{1/3} \quad (2.10)$$

Where, laminar flow coefficient, A is obtained from the quadratic flow equation: $\Delta p = A \cdot q_o + B \cdot q_o^2$, which considers turbulence around the wellbore. 'B' is the turbulence coefficient derived from well testing. The values of turbulence radius, R_1 and drainage radius, R_2 are calculated from Eqs. (2.11) and (2.12):

$$R_1 = 0.045 \cdot \frac{\rho_o \cdot q_o \cdot B_o}{\mu_o} \quad (2.11)$$

$$R = 0.00715 \frac{\mu_o q_o \cdot B_o}{\frac{\partial P}{\partial R} \cdot F_A \cdot \ln(10)} \quad (2.12)$$

Where, $\frac{\partial P}{\partial R}$ reaches a defined minimum value at $R = R_2$ close to zero, as the pressure at drainage boundary is assumed constant. In his derivation, Birk supposedly assumed the flow regime changes from laminar to turbulent as the flow approaches close to the wellbore defined by turbulence radius, R_1 .

As shown in Fig. 2.2, R_c is the critical radius at which flowing pressure gradient in the oil-zone becomes equal to the difference in the gradient of water and oil in the direction of flow. The critical radius, R_c , which defines the radius at which stable water cone forms, is given by,

$$R_c \cos \phi = h_{rc} = \frac{0.98 \mu_o B_o q_o}{F_A^3 \Delta \rho \cdot \ln(10)} \quad (2.13)$$

During stable water cone formation at the critical rate condition, gravitational head of water is given by,

$$h_{cw} = \frac{140(P_2 - P_c)}{\Delta\rho} \quad (2.14)$$

Where; P_2 is reservoir pressure at R_2 ; P_c is the reservoir pressure at R_c ; q_o is the oil production-rate.

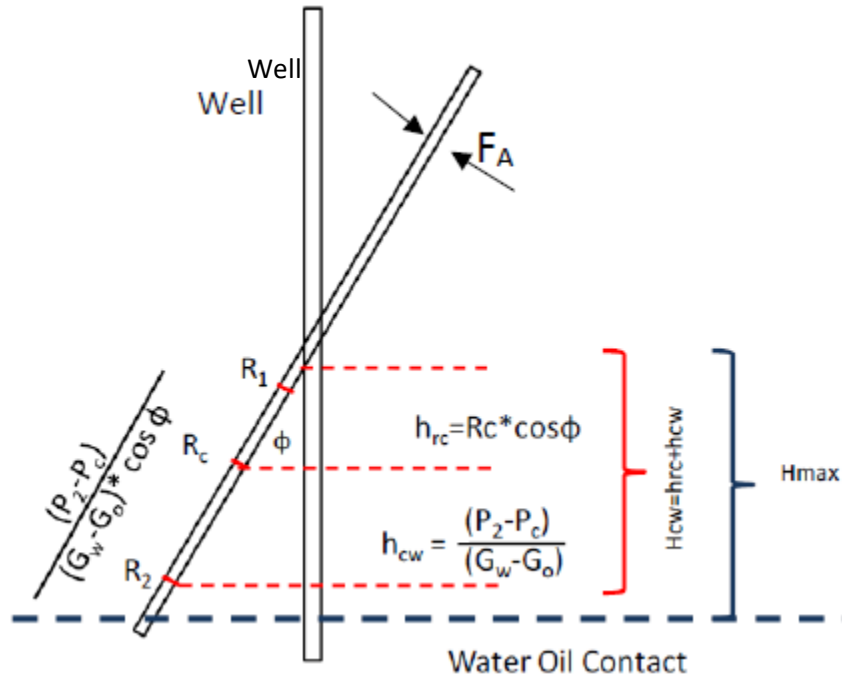


Fig. 2.2. Schematic of unique equivalent fracture, active radii and cone heights (Hidalgo 2009)

At critical rate condition, we also know that,

$$H_{cw} = h_o - h_{op} = h_{rc} + h_{cw} \quad (2.15)$$

Where, h_{op} is the perforated length, ft, and h_o is the oil-pay thickness.

Substituting Eqs. (2.13) and (2.14) in Eq. (2.15), we can write the critical rate formula as,

$$q_{cr} = \frac{[\Delta\rho(h_o - h_{op}) - (P_2 - P_c)]F_A^3 \cdot \ln(10)}{0.98\mu_o B_o} \quad (2.16)$$

The pressure difference ($P_2 - P_c$) is the viscous pressure drop, given by,

$$P_2 - P_c = \frac{0.007\mu_o B_o q_o}{F_A^3} \cdot \log_{10} \frac{R_2}{R_c} \quad (2.17)$$

Saad et al. (1995) presented a theoretical relationship between critical radius and production rate in fractured basement reservoir. They came out with the same critical rate equation based on Birk's (1963) methodology; however, their approach is different. Considering a fracture of width 'W' having a large lateral extent making an angle α with vertical and intersected by well, the critical rate can be represented by:

$$q_{cr} = \frac{100F_A^3 \Delta\rho R_c \cos\alpha}{\mu_o B_o} \quad (2.18)$$

Hidalgo et al. (2009) also reviewed the Birks (1963) method for calculation of critical rate in naturally fractured reservoir. They also followed the same methodology as Birks (1963), however, they didn't consider the fixed drainage radius, $R_2 = 1000ft$, as assumed by Birks to calculate equivalent fracture width, F_A . They proposed the explicit use of minimum radial pressure gradient ($\frac{\partial P}{\partial R} = 0.001psi/ft$) to compute variable drainage radius, R_2 using Eq. 2.12.

The major limitation of Hidalgo's and Birks (1963) model is the uncertainty in defining minimum value of $\frac{\partial P}{\partial R}$, which can incorrectly predict the critical rate for NFRs. Above methods by Birk's (1963), Saad et al.'s (1995) and Hidalgo et al. 2009 require expensive well testing operation in order to evaluate the laminar flow coefficient, A and hence the critical rate for the given NFR. Moreover, equivalent fracture width concept would be valid when well intersects the fractures, which may not be applicable in all NFR cases.

In 2012, Perez-Martinez presented an empirical correlation for maximum height of water cone in NFR for a given production rate, assuming fracture network as a continuous porous media. He showed that for a closed boundary reservoir, cone will reach the critical height when the radial growth of the cone reaches the well's drainage boundary, so the further production would cause

the water breakthrough not by coning itself, but due to the advancement of OWC. He empirically correlated the critical cone height, as

$$h_{wc} = (9.721 + F_{bc}) \left[\frac{q_o B_o \mu_o \ln \left(\frac{r_e}{r_w} \right)}{k_{fh} \Delta \rho} \right]^{0.5} \quad (2.19)$$

Where, F_{bc} is 0.712 for poor cement in the annular space, and F_{bc} is 0 for a good cemented well. The major limitation of this correlation is that they did not consider the effect of anisotropy ratio.

All the parameters are in field units. $\Delta \gamma_{wo}$ is in gm/cm³.

Perez-Martinez also formulated the equation for time of formation of the cone when the base of cone reaches the drainage radius, given by:

$$t_{wc} = 182.9 \left(\frac{k_{fh}}{\mu_o} \right)^{-0.26} (q_o B_o)^{-0.72} \quad (2.20)$$

Where, k_{fh} is the fracture permeability in Darcy.

t_{wc} is the time of formation of the water cone, in days.

Most of the above correlations (Muskat and Wyckoff, 1935; Schols, 1972; Hoyland et al. 1989, Perez-Martinez, 2012), do not take into account the anisotropy ratio in matrix or fracture, which may significantly affect the flow of oil and water, and hence the critical-rate value. Further, the above correlations except the Chaperon's (1986) model neglect the water cone instability issue in a high-pressure gradient reservoir or low conductivity reservoir (Tabatabaei et al. 2012). Low permeability or high-pressure gradient reservoirs would result in the water cone instability near the bottom of perforation when the flowing pressure gradient of oil becomes greater than the gravitational pressure gradient of water in oil-zone. This implies that the actual critical rate may be smaller than the theoretical critical rate at which water cone is allowed to reach the bottom of perforation, where the positive net pressure gradient may cause the water cone to lose its stability

and may result in eventual water breakthrough. Obviously, neglecting this issue would overpredict the critical rate. The above reasons qualify the need to improve the critical rate formula for the NFRs in the fracture-well (on-fracture completion) (Chapter 3). Further, because of the possible well placement in the matrix blocks of NFR, critical-rate needs to be investigated for the matrix-wells as a function of well's distance to the nearest fractures (Chapter 4).

2.2 Well Placement

2.2.1 Well Placement in SPR

Often well patterns are deployed based on uniform permeability models; however, we cannot ignore the role of heterogeneity and anisotropy in such reservoirs. We also cannot ignore the presence of water drive support in SPR. Due to the small area drained by local water coning, well placement depends on the lateral extent of water cones, which is further dependent on the properties of reservoir. In addition, one of the strategies to delay the water breakthrough in a bottom-water drive or edge-water drive reservoir is to place the well completions high in the oil-zone (Joshi 1991, Perez-Martinez et al. 2012). Since, in our study, we assume the homogeneous matrix, we won't consider well placement as a concern in SPR as long as it is placed high in the oil-zone.

2.2.2 Well placement in NFR

Well completions in NFRs may or may not intersect fractures depending on the completion placement in the fracture-network which is difficult to determine. This is because of the complexity of fracture network geometry within the rock matrix.

Based on the network connectivity, fracture network can be classified as planar fracture network (Fig. 2.3) and channel fracture (fracture corridor) network (Fig. 2.4) (Van Siclen 2002; Elmouttie et al. 2015; Figueiredo et al. 2016). Planar fracture network system may result from

folding due to external tectonic forces or from internal forces like high pore pressure and temperature-inducing-thermal stresses. These fracture-networks are well connected and regular in distribution (Fig. 2.3). Their fracture spacing either follows a normal, or log-normal or power-law distributions (Hooker et al. 2014). Moreover, the strata bound fractures which terminate at the bedding exhibit a regular spacing proportional to the height of layer thickness (Guerriero et al. 2011).

However, many natural fractures are not regularly spaced but are systematically clustered - Fracture corridors (Ozkaya 2010; Ozkaya and Richard 2006; Hooker et al. 2014) - categorized as channel fracture network. These clustered fracture corridors have widely spaced matrix blocks defined by exclusion-zones. The corridors are generally oriented in one direction (Fig. 2.4), however, they can also cross-cut each other. These fracture corridors are associated with faults and resemble fault damage zones (Ozkaya and Minton 2005; Ozkaya and Minton 2007). They are described as subvertical cluster of fractures that transverses the entire reservoirs and extend for several tens to hundreds of meters laterally. Their widths may vary from 1-10 m (Questiaux et al. 2010). Ozkaya and Minton (2005) reported spacing ranges from 33ft (10m) to 1300ft (393m).

Wells in fracture corridors act as a high permeable pathway for water channeling in bottom-water NFRs. Large spacing of fracture corridors provides high probability of the off-fracture well completions in the exclusion-zones. The exclusion zones may contain diffuse fractures (Bockell-Rebelle et al. 2004) and their properties are usually controlled by matrix properties (Ray et al. 2012). Diffuse fractures or layer-bound fractures are tensile fractures and hence their density and height are controlled by mechanical layer thickness and lithology (Ozkaya 2010). Permeability of connected diffuse fractures system is few tens of mD, and can be as large as 10 times that of the rock matrix permeability (Gouth et al. 2006).

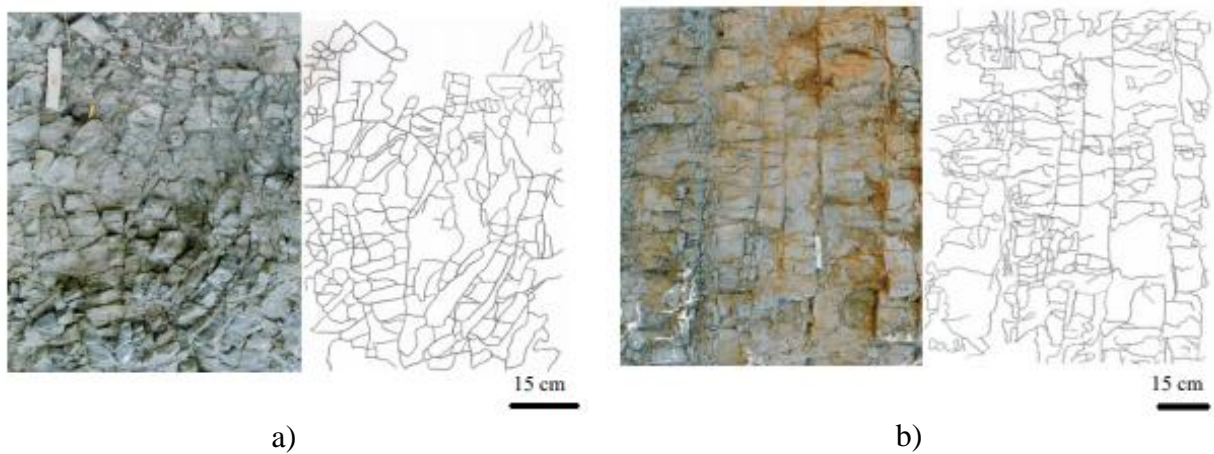


Fig. 2.3. Outcrop of fractured formation with fracture trace map (Jafari and Babadagli 2010) – Outcrop of a producing formation in the a) Germeneik field, and b) Kizildere field

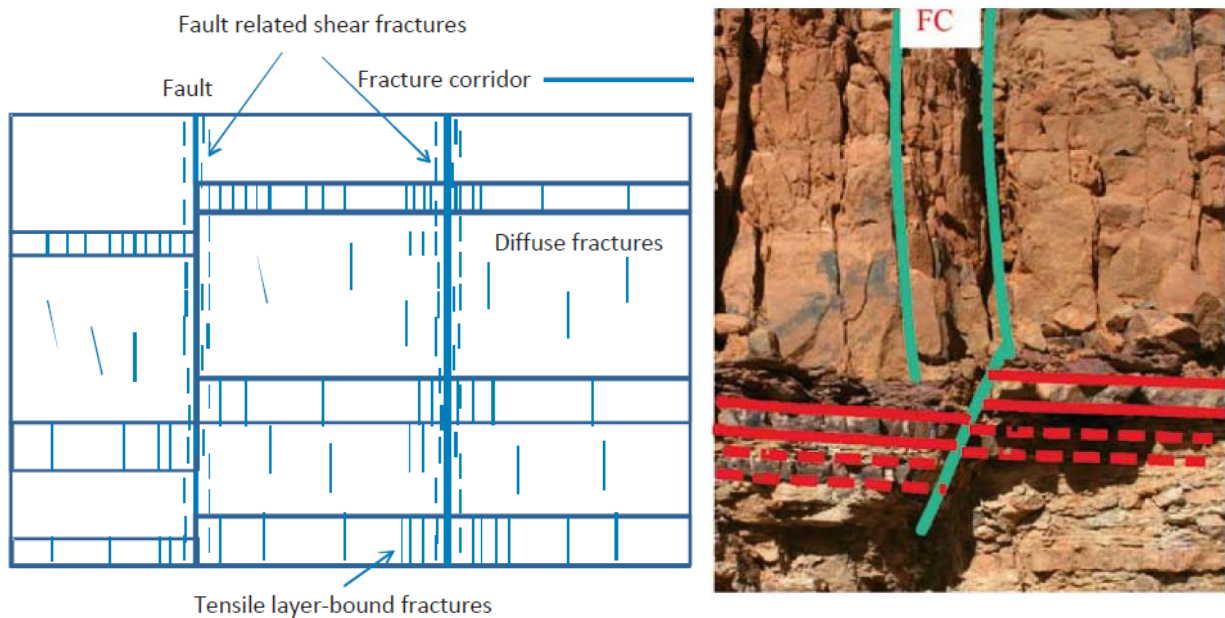


Fig. 2.4. Cross-sectional view of fracture corridors (FC) and diffuse fractures (Ozkaya 2013; Singh 2008)

The abundance of fractures and their size distribution can be determined using seismic data, coring, and image logs (Hooker et al. 2014). Due to the uneven distribution of fracture-network coupled with uncertain location of a well in the network, the well's performance would be stochastic in nature. It depends upon probable well location in the fracture network. Probability

of well's intersection with fracture studied by researchers before (Martel 1999; Carlson 2003) considered constant “mean” values of the network properties with no consideration given to the distribution of fracture-attributes. They simply assumed an idealized fracture-network. Carlson computed probability of well intersection within orthogonal vertical fracture network, P_F , as,

$$P_F = \frac{4 \times (S_{pmean} - d_w) \times d_w}{S_{pmean}^2} \quad (2.21)$$

Where, S_{pmean} is the mean fracture spacing and d_w is the well diameter. Further, Martel 1999 estimated the probability of encountering a set of natural fracture having particular orientation with wellbore which depends on fracture spacing (S_{pmean}), orientation of the fractures with respect to wellbore (α), and well completion length (h_{op}) assuming that $h_{op} < S_{pmean}/\sin\alpha$,

$$P_F = \frac{h_{op}}{S_{pmean}/\sin\alpha} \quad (2.22)$$

To date, no studies addressed the probability of well's location in the fracture network based on the distribution of fracture network in a given NFR. Moreover, no studies compared the oil recovery with the fracture and matrix-wells for the same NFR developed using single-completed or dual-completed wells (dealt in chapters 4 and 6). There is also a need to develop a method for probabilistic estimate of total recovery from a fully-developed NFR (Chapter 6).

2.3 Water-Cut Pattern

2.3.1 Water-Cut in SPR

A simple analytical model for water-cut prediction in bottom water drive single-porosity reservoirs was developed by Kuo and Desbrisay (1983). They performed the number of simulation experiments shown in the semi-log plots in Fig. 2.5. They simulated a well producing at constant rate from an uncontained oil pay-zone with constant pressure boundary. They varied the parameters such as anisotropy ratio (0.01 to 1.0), the completion penetration (from 20 % to 80%

of oil column), constant production rate (from 500 to 2000 rb/day), and the oil/water mobility ratio (from 1.0 to 10). Based on the results, they developed a mathematical relationship of dimensionless water cut, (WC_D), versus dimensionless time, t_D , as,

$$WC_D = 0 \quad \text{for } t_D < 0.5 \quad (2.23a)$$

$$WC_D = 0.94 \log t_D + 0.29 \quad \text{for } 0.5 < t_D < 5.7 \quad (2.23b)$$

$$WC_D = 1 \quad \text{for } t_D > 5.7 \quad (2.23c)$$

Where,

$$t_D = \frac{t}{t_{BT}} \quad (2.24)$$

$$WC_D = \frac{WC}{WCult} \quad (2.25)$$

$$WCult = \frac{Mh_w}{Mh_w + h_o} \quad (2.26)$$

Where M is the mobility ratio of water and oil,

h_w is the thickness of aquifer, ft

h_o is the thickness of oil-pay, ft

t = time (in days)

WC = Water cut (fraction)

For the breakthrough time, t_{BT} , value, Kuo and Debrisay (1983) suggested the use of Bounazel and Jeanson's (1971) correlation of breakthrough time. They also observed constant value of ultimate water-cut (WCult) (Eq. 2.26), but refrained from addressing the late water-cut pattern in developed multi-well reservoir where drainage area becomes affected by no-flow boundary.

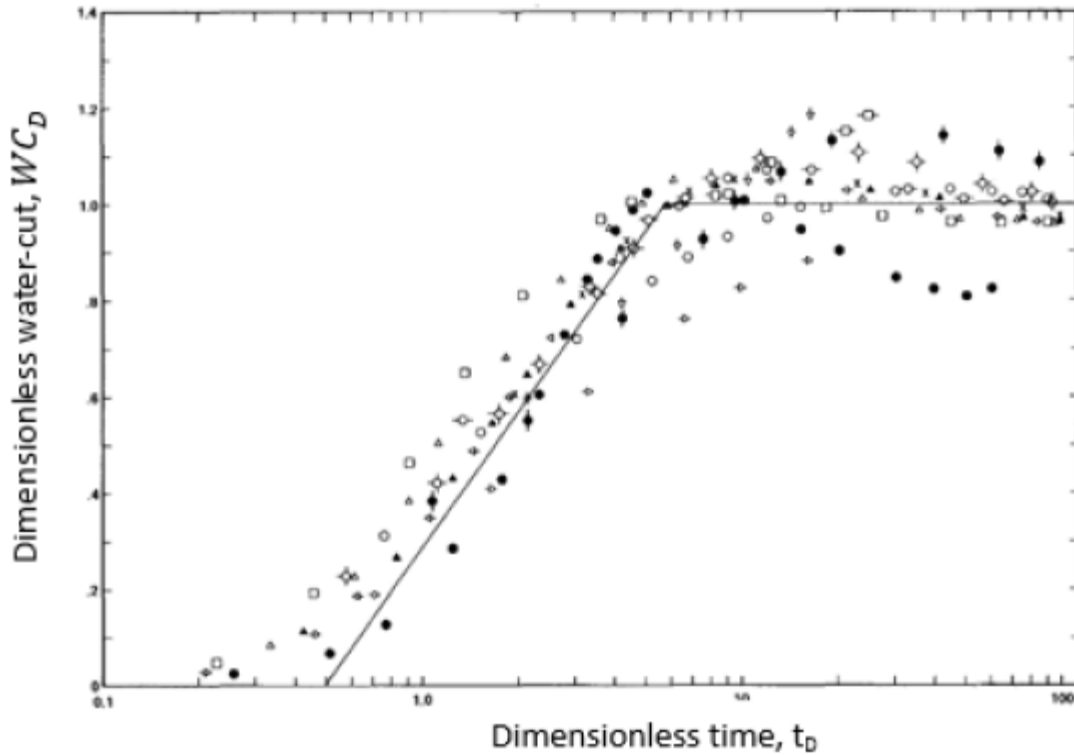


Fig. 2.5. Plot of dimensionless water-cut and dimensionless time (Kuo and Debrisay 1983)

While Kuo and Desbrisay (1983) assumed no dependence of production rate on ultimate water-cut; other authors (Meyer and Searcy 1956, Shirman and Wojtanowicz 2000, Van Golf-Racht and Sonier 1994, Shirman and Wojtanowicz 1997) showed that stabilized water-cut for a balanced-oil rate boundary is dependent on production rate. According to them, for production rates slightly higher than critical rates, water-cut would stabilize at value lower than ultimate water-cut.

Shirman and Wojtanowicz (2000) analyzed data from their laboratory experiments and found out that the water-cut stabilization value predicts the Kuo and Desbrisay (1983) model only for high production rate. They modified Eq. (2.26) by adding the production-rate effect as,

$$WC_{ult} = \left(1 - \frac{q_{cr}}{Q}\right) \frac{Mh_w}{Mh_w + h_o} \quad (2.27)$$

The rise of water-cut before final stabilization is due to the rising water-cone development which covers larger area of oil completion. Eventually, the ratio of well completion producing oil and water becomes equal to the ratio of oil and water zone thickness, when ultimate water-cut is reached. The above model draws implicitly from assumptions including 1) Flow distortion in oil-zone and aquifer due to partially penetrating well is ignored; 2) Steady state flow and equal pressure drop in both oil-zone and water-zone; and 3) Permeability anisotropy is ignored, which needs to be addressed (Chapter 5).

2.3.2 Water-Cut in NFR

In NFRs, water-cut pattern is investigated both qualitatively and quantitatively. Ozkaya and Minton 2007 observed that instant water breakthrough and steplike water-cut rise are indicative of fractured-reservoirs. However, post-breakthrough analysis of water-cut pattern in NFRs have never been performed in detail. For example, Joshi in 1991 showed different water-cut patterns in the SPR and NFR, by comparing plots of water-cut vs. recovery factor for the two systems. Though the plots could be helpful in identifying NFRs, there was no attempt to analyze the late water-cut development further. Van Golf-Racht and Sonier in 1994 analyzed the reservoir simulation results of bottom-water fractured reservoir at the end of 100 days and indicated a parabolic relationship between coning water-cut and total production-rate. However, they refrained from showing the mechanism or pattern of water cone growth in NFR and did not provide an analytical tool to predict water-cut. Analytical treatment was attempted by Bahrami et al. (2004) who developed a correlation of water-cut versus time using multi-variable regression, after running series of simulations with sensitivity analysis, as shown below,

$$t_{BT} = 0.001054(\phi_m + 0.091)^{1.954}(1 + 87.06\phi_f)^{0.989} 0.9591(K_{mh}^{0.0118}(5.9654 - \exp(-10.213K_{mv}))K_{fh}^{0.3955}K_{fv}^{-0.0476})^{2.6655} \left(1.3875 \left(\frac{(h_o^2 - h_{op}^2)\Delta\rho}{Q_o\mu_o B_o}\right)^{0.68} (1 + M)^{0.64}\right)^{1.6647}$$

(2.28)

$$WC = m(t - t_{BT}) \quad (2.29)$$

Where,

$$m = 0.0196(\phi_m^{-0.63514}(1 - 20.714\phi_f))^{0.96582}(K_{mh}^{-0.05479}K_{fh}^{0.16523})^{0.98495}\left(1.3875\left(\frac{(h_o^2 - h_{op}^2)\Delta\rho}{Q_o\mu_oB_o}\right)^{0.68}(1 + M)^{0.64}\right)^{-1.3854}$$

However, the main shortcoming of their correlation is the assumption of constant slope of water-cut versus time at all time. Moreover, since their correlation is purely empirical it does not asymptotically come to a limit of water-cut. There is a characteristic pattern of water-cut for different well location within the fracture-network NFR. Studies (Ozkaya 2010, Ozkaya and Minton 2007) have shown that there is a rapid water increase after instantaneous breakthrough in a fracture well (well intercepting fractures), however, a more gradual water-cut rise in matrix-well (well in exclusion-zone) (Fig. 2.6). BSW (basic sediments and water), as shown in Fig. 2.6, defines the impurities contained in the crude oil in the form of suspended solids and water; whereas the gross-rate is the total production rate including oil and water. Bustos et al. 2010 reported that the rate of water-cut rise is indicative of the nearby fracture corridors or faults. They reported that the constant water-cut trend at later times, is typical of well located near the fracture corridors. However, the observation was only qualitative and not supported by physical explanations and quantitative models.

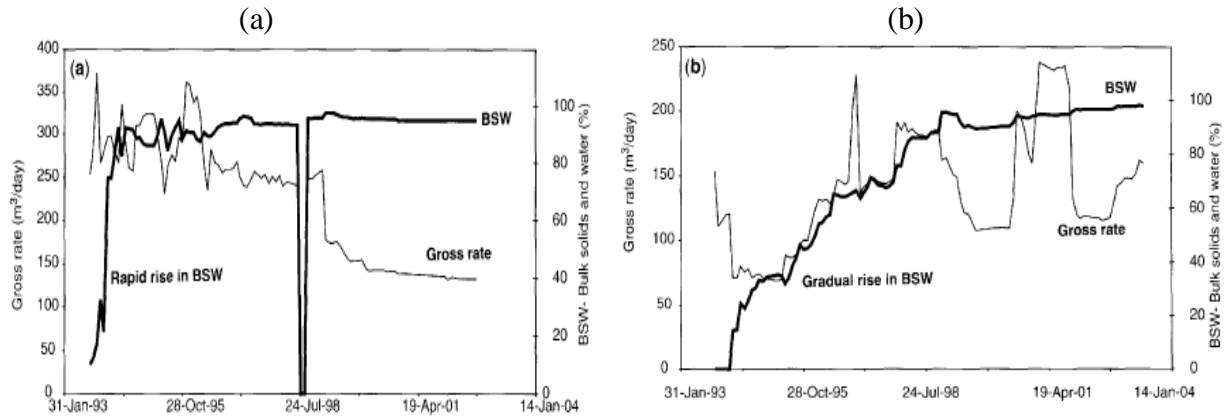


Fig. 2.6. a) WC in Fracture- well (Ozkaya and Minton 2007); b) WC in matrix well (Ozkaya and Minton 2007)

The above discussions show incomplete knowledge of water-cut behavior in NFR to date, but it shows two characteristics: 1) rapid stepwise WC increase; and 2) stabilization. Thus, there is a need to perform both qualitative and quantitative analysis of post-breakthrough water-cut development and its pattern with emphasis given to WC stabilization stage. Similar to single-porosity reservoirs (Kuo and Desbrisay 1983; Shirman and Wojtnaowicz 2000; Prasun and Wojtanowicz 2016; Prasun and Wojtanowicz 2018), there is a need to develop a mathematical model of the stabilized WC stage and relate the pattern to well spacing and recovery performance of wells in NFR (Chapter 5).

2.4 Well Spacing

2.4.1 Well Spacing in SPR

Several studies (Matthews et al. 1992; Longxin et al. 2015; Qin et al. 2016) have shown that *well-spacing* has considerable effect on oil recovery in matrix-only SPR with bottom-water. Matthews et al. 1992 developed an analytical model to optimize the well spacing and showed that smaller spacing (20-40 acres) compared with traditionally employed in the North Sea could improve the economic recovery. This is because water coning is a local phenomenon, and so only

small area of reservoir close to well is displaced by water during water coning, making the recovery inversely proportional to the drainage area or well spacing.

Qin et al. 2016 studied heavy oil recovery underlain with bottom-water and found that low ultimate oil-recovery is caused by the combination of small drainage area and water bypassing oil after breakthrough. They stated that the oil recovery could be improved only if mobilized oil zone can be enlarged which is possible by reducing the well-spacing/drainage area. They derived an analytical model to determine the actual drainage distance mathematically. Above studies assume ultimate water-cut (when the cone growth is full and complete) is equal to or greater than the economic limit of water-cut, so the recovery is only from the water cone drainage area. Consequently, the well spacing must be reduced to recover more oil. However, when the ultimate water-cut is smaller than the economic limit of water-cut, additional oil can be recovered from the process of oil-water contact advancement occurring after the cone growth is complete, which needs to be addressed (Chapter 5).

2.4.2 Well Spacing in NFR

In NFRs, well spacing effect on recovery may not be a function of the local nature of water coning. Studies have shown that in NFRs, there are two water cones – one in the fractures and other in the matrix. Water cone in the fractures is relatively abrupt followed by water invasion from the other connected fractures in the drainage space while the water coning in matrix is still developing. Therefore, depending on the extent of connected fractures in the reservoir, water invasion may no longer restrict to the near wellbore phenomenon.

To date, no studies have been reported into the effect of well spacing in NFR beyond the knowledge pertaining to SPRs, discussed above. It could be hypothesized, however, that in the distributed network of fractures and random placement of well completion, regular spacing of the

wells in NFR may not be more important than in SPR. Particularly, relationship of well spacing and fracture spacing and the ultimate water-cut value may define additional oil recovered when the water cone become stable, which needs to be addressed (Chapter 5).

2.5 Well Completion Design -Downhole-Water Sink/Downhole-Water Loop

Dual completion design including down-hole water sink (DWS) and down-hole water loop (DWL) have proven to be effective in controlling water coning, thereby improving the recovery (Shirman and Wojtanowicz 2000; Jin 2013). In dual-completed DWS well, bottom completion is installed below the oil-water contact, which drains the water from aquifer, and the top completion above the oil-water contact, which is designated for oil production. The rate of water drainage is adjusted according to the production rate, so that water-cut is greatly minimized. Previous studies while comparing DWS with single-well completions for water coning control (Shirman and Wojtanowicz 1997b, 1998), showed better performance of DWS in single porosity reservoirs.

Operational and design principles of DWS wells have been studied theoretically and experimentally since 1991 (Wojtanowicz et al. 1991; Wojtanowicz and Xu 1992; Wojtanowicz and Shirman 1996; Shirman 1996; Shirman and Wojtanowicz 1997a). Recently, Shirman et al. (2014) demonstrated the effect of drainage to production rate ratio on the recovery advantage in DWS. They showed that for a drainage rate 5-fold greater than the production rate, recovery can be improved by 1.65 fold. These authors focused on qualitative design of operational parameters for water coning control performance without considering the well productivity or oil recovery as a design parameter. Arslan 2005 developed an empirical model of improved productivity ratio for DWS well, as a function of reservoir properties and operational parameters. He found that oil productivity index is most sensitive to mobility ratio and operating pressure drawdown, and least sensitive to the drainage radius. This was the first study to screen candidate reservoir for DWS

technology. Later, Jin (2013) developed a proxy model of oil recovery to help assess the feasibility of downhole water loop (DWL) well for single porosity reservoirs. In a triple-completed DWL well, there is an additional third completion installed further deep in the aquifer, which loops the water drawn from the water drainage completions back to the aquifer. The proxy model which considered scaling groups developed for DWL-SPR system based on dimensional analysis, considerably reduced the dependence of recovery on (20+) dimensional physical properties. Although above studies provided a feasibility study of DWS or DWL in single porosity reservoirs, no studies have been performed until date testing this technology in NFRs.

Chapter 3. Critical Oil Rate in NFR

Critical oil rate is a metric for coning severity, which can be defined quantitatively using coning severity index (CSI) as,

$$CSI = \frac{Q_{max} - q_{cr}}{Q_{max}}$$

Where, q_{cr} is the critical oil rate for a given reservoir, and Q_{max} is the maximum liquid production rate at bottom-hole pressure equal to bubble-point pressure. So, when critical oil rate is theoretically equal to zero, or, $CSI = 1$, it implies coning severity is maximum, and when critical rate is theoretically equal to q_{max} , or $CSI = 0$, it implies coning severity is minimum. However, in order to evaluate the coning severity index for NFRs, we need to model critical oil rate addressed in this chapter.

The chapter develops a semi-analytical formula of critical-oil rate in NFRs (planar fracture network) considering the well completion placement either in fractures (fracture-well) or in matrix blocks (matrix-well) of NFR. The development derives from mechanistic principles employed by Chaperon (1986). Since the mechanistic model is only valid for point-source completion, the modeling requires statistical calibration to include the effect of long penetration, resulting in a semi-analytical or grey-box model.

The following steps are carried out in the development of grey-box model of critical-rate:

- 1) Simplifying the planar fracture network using continuum-based approach where discrete fracture networks are upscaled to continuum porous media.
- 2) Adopting critical rate model in SPR (Chaperon 1986) to develop apparent critical rate model for NFR with statistical correction of the model's limitation.

All sections of this chapter previously appeared as Journal paper 2019 on “Semi-Analytical Prediction of Critical Oil Rate in Naturally Fractured Reservoirs with Water Coning” published in Journal of Petroleum Science and Engineering, 180 (2019): 779-792. Reproduced with permission of Journal of Petroleum Science and Engineering. See Appendix F for more details.

- 3) Calibrating the apparent critical rate model with designed series of simulated experiments to develop a grey-box model.

3.1 Apparent Critical Rate in DPDP Model of NFR

The following assumptions are considered for applying present critical rate formula to NFR:

- 1) The oil reservoir is naturally-fractured having mixed-wettability.
- 2) Fracture system is modeled using a 2D radial-cylindrical DPDP model.
- 3) Assuming DPDP continuous porous media in a steady state flow can be represented by a single media (single porosity reservoir) having a combined effective permeability of fractures and matrix, we can write the effective permeability of the matrix-fracture system, $k_{f,m}$ (following Parsons' (1966) work), as,

$$k_{f,m} = k_{fh} + k_{mh} \quad (3.1)$$

Where, k_{fh} is the Darcy flow effective-horizontal permeability of the fracture network (Parsons 1966; Aguilera 1998). Rock matrix permeability can be determined from cores. Average permeability, $k_{f,m}$ for a radial system can be determined from the production data (Song et al. 2019) as,

$$k_{f,m} = \frac{141.2Q\mu B_o \left(\ln \frac{r_e}{r_w} + S \right)}{2\pi\Delta P} \quad (3.2)$$

- 4) Steady-state flow is maintained by replacing the produced oil at the reservoir boundary, so below the critical rate, water breakthrough would never happen. However, in a real multi-well reservoir represented by closed drainage areas, water-breakthrough would always happen as the oil-water contact never stops advancing upwards even for production rate below critical-rate.

Chaperon (1986) idealized a short well completion by placing a point source oil sink (O) at the top of oil-zone, inducing a semi-spherical inflow in the oil-zone as shown in Fig. 3.1, and derived critical oil-rate analytically, as,

$$q_{cr} = 0.0783 \times 10^{-4} \frac{k_{ro} k h_o}{B_o \mu_o} (\Delta \rho h_o) q_{c,max}^* \left(\frac{r_e}{h_o} \sqrt{\frac{k_v}{k_h}}, \frac{Z_s}{h_o} \right) \quad (3.3)$$

$$\text{Where, } q_c^* = 2\pi \left(1 - \frac{Z_s}{h_o} \right) / \sum_{n=-\infty}^{+\infty} \left[\frac{1}{\left| \frac{Z_s}{h_o} + 2n \right|} - \frac{1}{\left(\left(\frac{r_e}{h_o} \sqrt{\frac{k_v}{k_h}} \right)^2 + (2n+1)^2 \right)^{1/2}} \right] \quad (3.4)$$

Where, $\frac{Z_s}{h_o}$ is a critical cone dimensionless height; q_c^* is the critical dimensionless oil rate.

$q_{c,max}^*$ can be obtained graphically by finding the maxima of the plot $q_c^* \text{ vs. } \frac{Z_s}{h_o}$ for a given value of

$\frac{r_e}{h_o} \sqrt{\frac{k_v}{k_h}}$. The maximum value of q_c^* (or $q_{c,max}^*$) would help determine the maximum stable critical-

rate for a point-source well at the top of oil-zone.

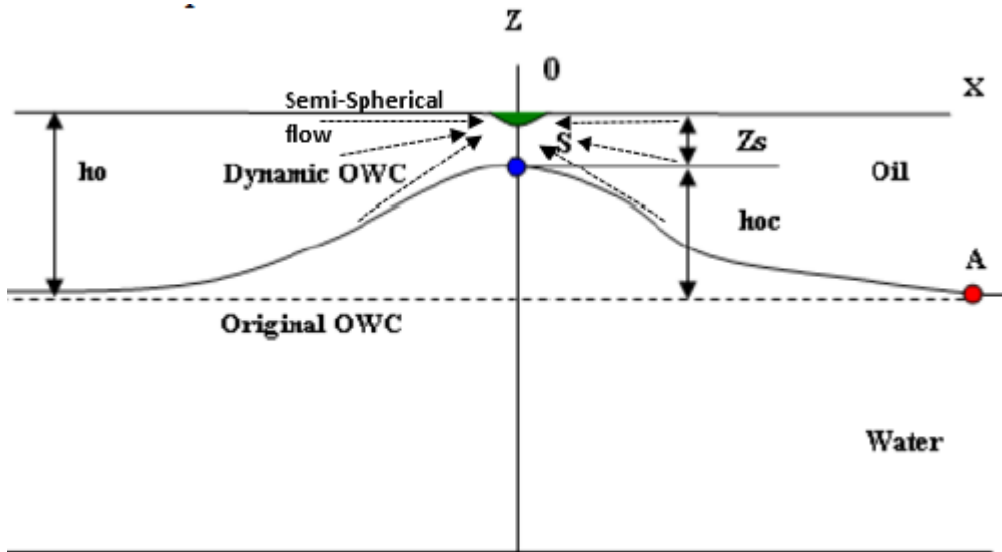


Fig. 3.1. Water coning in a partially penetrating well

After plotting q_c^* vs. $\frac{z_s}{h_o}$ for various value of $\frac{r_e}{h_o} \sqrt{\frac{k_v}{k_h}}$, Chaperon (1986) reported nearly constant critical cone dimensionless height, $\frac{z_s}{h_o}$ (ranging between 0.34-0.43 for values of $(\frac{r_e}{h_o} \sqrt{\frac{k_v}{k_h}})$ ranging from 4 to 13). Assuming $\frac{z_s}{h_o} \cong \text{constant}$, Chaperon further correlated q_c^* as a function of $\frac{r_e}{h_o} \sqrt{\frac{k_v}{k_h}}$ empirically to obtain a semi-analytical model of critical oil rate as,

$$q_{cr} = 0.0783 \times 10^{-4} \left[\frac{\Delta \rho k_o (h_o^2)}{\mu_o B_o} \right] \left[0.7311 + \frac{1.943}{\frac{r_e}{h_o} \sqrt{\frac{k_v}{k_h}}} \right] \quad (3.5)$$

Based on assumption 3, formula Eq. (3.3) can be applied to fracture-well in NFR after replacing conventional horizontal permeability (k_h) by an effective homogenized horizontal permeability of NFR ($k_{f,m}$). The resulting apparent critical rate formula is,

$$q_{cr,fr} = 0.0783 \times 10^{-4} \frac{k_{f,m} h_o^2}{B_o \mu_o} (\Delta \rho) q_{c,max}^* \left(\frac{r_e}{h_o} \sqrt{\frac{k_{fv}}{k_{fh}}}, \frac{z_s}{h_o} \right) \quad (3.6)$$

Where, q_c^* is given by Eq. 3.4.

In NFR, invading bottom-water builds two cones -- one in fractures and other in matrix (Namani et al. 2007; Al-Afaleg and Ershaghi 1993). Since the cone moves faster in fractures (being highly conductive) than in matrix, critical-rate should be governed by fracture properties. This implies that while modeling critical-rate in NFR, a) we can ignore the effect of capillary pressure (since fractures have large apertures and do not demonstrate preferential wettability to any fluids), and b) we need to use the anisotropy ratio of fractures, $\frac{k_{fv}}{k_{fh}}$ in Eq. 3.6. Irrelevance of the effects of capillary pressure on critical oil-rate is further demonstrated by running the simulations for the base case NFR properties (Appendix A-Tables A1 and A2) as shown in Fig. 3.2. Also, formula Eq. 3.6 implies that critical rate of fracture-well is independent from either fracture spacing or

fracture density at a given equivalent permeability of NFR, except for the fact that the effective permeability of the fractures (k_{fn}) is itself a function of spacing (Reiss 1980).

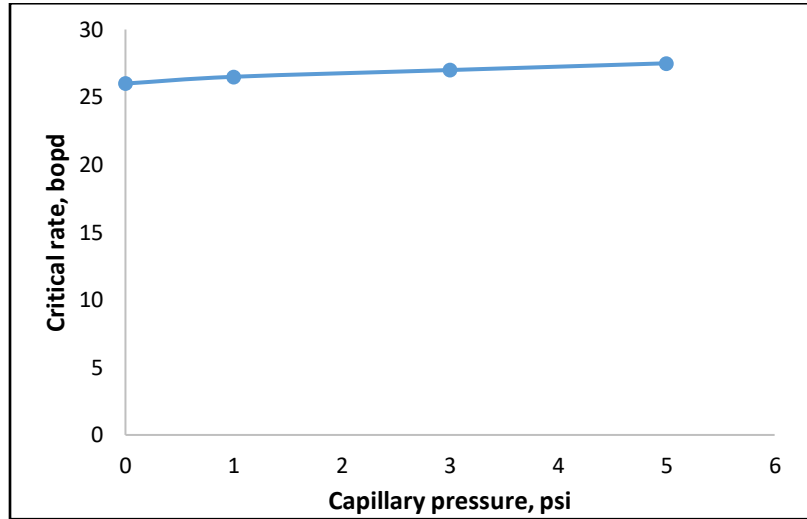


Fig. 3.2. Critical oil rate vs. capillary pressure (base case NFR)

3.2 Limitations of Apparent Critical Rate Model

For verifying and validating apparent model of critical rate in NFR, we design matrix of simulated experiments. We employed 3-level Box-Behnkein design approach to create 63 simulated matrix of experiments as shown in Table A4 (Appendix A). The 3-level design addresses any non-linearity in the factors affecting critical rate. The designed matrix of simulated experiments represent wide varieties of NFRs (including the most common type II and type III NFRs) (Gallagher et al. 1993; Hassall et al. 2004; Gouth et al. 2006; Shibasaki et al. 2006; Meehan 2011; Williams et al. 2011) which considers reservoir properties including matrix permeability, fracture permeability, mobility ratio, penetration ratio, drainage radius and anisotropy ratio. Anisotropy ratio of natural fractures is considered to be always higher than 1 (Zhang and Koutsabeloulis 2010). From core measurements, Lorenz and Hill (1991, 1994) found individual fracture spacing ranging from 0.1 to 18 ft (Gomez et al. 2003) for a given NFR. Assuming the

infinite length of fracture, intrinsic permeability of the fracture, k_{ff} , can be determined using the cubic law (Lamb 1945; Witherspoon et al. 1980), in which fracture is modeled as two parallel plates with planar, uniform aperture. The formula is given as,

$$k_{ff} = \frac{w^2}{12} \quad (3.7)$$

Where, ‘w’ is the width of fracture aperture. From the Darcy law definition, effective permeability of fracture can be written as,

$$k_f = \frac{w^3}{12S_p} \quad (3.8)$$

Using the eqs. (3.7) and (3.8), two unknowns ‘w’ and ‘ k_{ff} ’ can be determined. For this designed matrix of experiments study shown in Table A4, ‘w’ is back calculated and is found to vary from 0.03 to 0.5 mm (shown in Table A4), which is within the typical range between 0.02 and 2mm in a highly fractured rock (Bear 2013; Zhang and Koutsabeloulis 2010). Similarly, fracture field intrinsic permeability ‘ k_{ff} ’ is found to vary from $10^{-10}m^2$ to $2 \times 10^{-8}m^2$ (shown in Table A4), which is within the typical field range between $2 \times 10^{-12}m^2$ and $2 \times 10^{-7}m^2$ (Zhang and Koutsabeloulis 2010). This justifies the considered range values of fracture properties for this study.

Simulated Critical-rate is determined by using the trial and error approach in which the first initial guess of critical rate for the given simulated case is estimated from the Chaperon’s model of NFR for short penetration ratio. Then, we reduce the rate by a step change of 0.1 bbl/day till we observe no water breakthrough, considering the maximum duration of typical field life for each simulation run to be approximately 40 years.

Subsequently, we test the apparent critical rate model for NFR given by Eq. 3.6 using designed series of the matrix of experiments as shown in Table A3 representing wide variety of

NFRs. The properties are considered based on the included parameters in Eq. 3.6 assuming other parameters do not play significant role in critical rate determination. We run the simulation for these series of experiments for each penetration ratio beginning from 0.1 to 0.6, and compare them with the apparent critical rate model (from Eq. 3.6) as shown in Fig. 3.3a. The deviation of the slope of the line from 1 provide an estimate of the average discrepancy of the critical rate at short penetration ratio. From fig. 3.3a and fig. 3.3b, we can infer that the discrepancy is minimal (less than 5%) when critical rate is below penetration ratio of 0.35. This implies that Chaperon’s model for NFR is good for NFRs as long as the penetration ratio is below 0.35. However, discrepancy increases significantly (>5%) beyond 0.35, rendering the model unfit for longer penetration ratio in NFRs. So, there is a need to statistically calibrate the model (grey-box model) to include the effect of penetration ratio.

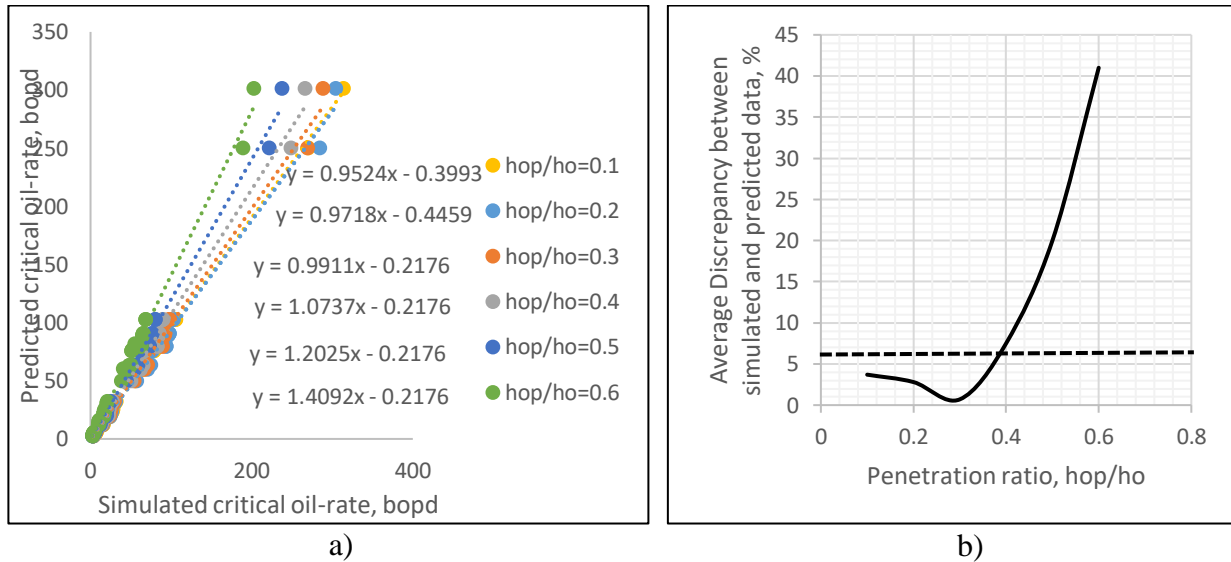


Fig. 3.3. a) Predicted vs. Simulated critical rate for matrix of experiments of NFRs (Table D1) (for $0.1 \leq \frac{h_{op}}{h_o} \leq 0.6$); b) Average discrepancy between simulated and predicted critical rate, (in %), determined from the % deviation of slope from value of 1

3.3 Grey-Box Model of Critical Rate in NFR

In the derivation of grey-box model, we revisited the apparent critical rate model (Eq. 3.6) to redefine the dimensionless critical oil rate, $q_c^* \left(\frac{r_e}{h_o} \sqrt{\frac{k_{fv}}{k_{fh}}}, \frac{Z_S}{h_o} \right)$ concept that originally represents semi-spherical flow regime occurring towards the oil-sink placed at the top of oil-zone. However, for a longer penetration ratio greater than 0.35, the flow regime would change from semi-spherical to distorted non-radial flow, whose effects needs to be subsequently adjusted in the model. This can be done by empirically calibrating q_c^* to include the effects of longer penetration ratio and aspect ratio $\left(\frac{r_e}{h_o} \sqrt{\frac{k_{fv}}{k_{fh}}} \right)$, since they mainly control the flow regime (Moncada et al. 2005; Chaperon 1986). After making the above adjustments, a new semi-analytical model can be written from Eq. 3.6, as,

$$q_{cr,fr} = 0.0783 \times 10^{-4} \frac{k_{f,m} h_o^2}{B_o \mu_o} (\Delta\rho) q_c^* \quad (3.9)$$

$$\text{Where, } q_c^* = f\left(\frac{h_{op}}{h_o}\right) f\left(\frac{r_e}{h_o} \sqrt{\frac{k_{fv}}{k_{fh}}}\right) \quad (3.10)$$

Based on the analytical works of Dupuit (1863), Meyer and Gardner (1954), Pirson (1977) and Johns et al. (2005); and the empirical works of Schols (1972) and Hoyland et al. (1989), we observe the following relationship between critical rate and penetration ratio, $\frac{h_{op}}{h_o}$, as,

$$q_{cr,fr} \propto 1 - \left(\frac{h_{op}}{h_o}\right)^2 \quad (3.11)$$

In order to verify this relationship for NFRs, we plot the simulated critical rate values for different values of $1 - \frac{h_{op}}{h_o}$ greater than 0.35, for the base case, and the cases 1, 2 and 3 from Table A4 (Appendix A), as a function of $1 - \left(\frac{h_{op}}{h_o}\right)^2$ (shown in Fig. 3.4).

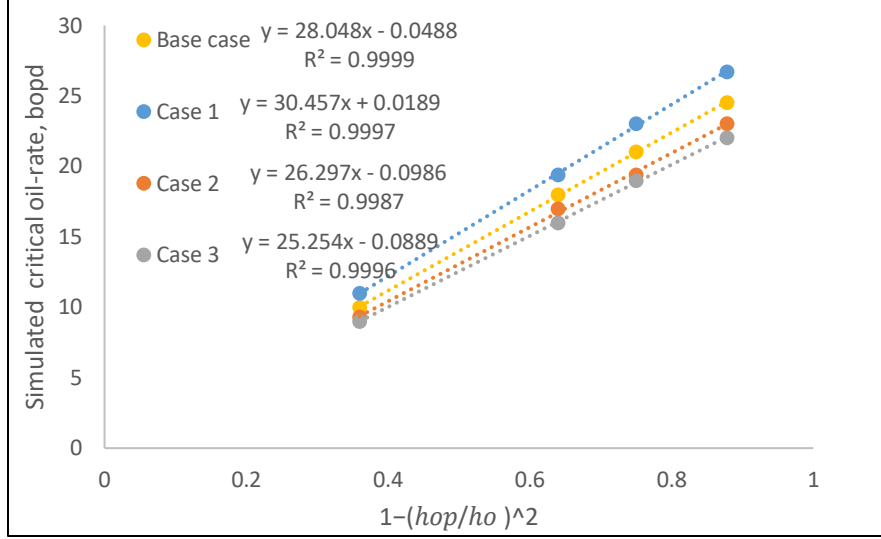


Fig. 3.4. Simulated Critical rate vs. $1-(h_{op}/h_o)^2$ for the base case-NFR and cases 1, 2 and 3 from Table A4

The plot shows that there is a straight-line relationship between critical rate and $1 - \left(\frac{h_{op}}{h_o}\right)^2$ having intercept that can be neglected. This implies,

$$f\left(\frac{h_{op}}{h_o}\right) = 1 - \left(\frac{h_{op}}{h_o}\right)^2 \quad (3.12)$$

Substituting $f\left(\frac{h_{op}}{h_o}\right) = 1 - \left(\frac{h_{op}}{h_o}\right)^2$ in Eq. (3.9), we obtain,

$$q_{cr,fr} = 0.0783 \times 10^{-4} \frac{k_{f,m} h_o^2}{B_o \mu_o} (\Delta\rho) \left(1 - \left(\frac{h_{op}}{h_o}\right)^2\right) f\left(\frac{r_e}{h_o} \sqrt{\frac{k_{fv}}{k_{fh}}}\right) \quad (3.13)$$

For determining the empirical component of the model, $f\left(\frac{r_e}{h_o} \sqrt{\frac{k_{fv}}{k_{fh}}}\right)$, we designed series of simulated matrix of experiments for penetration ratio > 0.35 , as shown in Table A4. Evidently, as $\frac{r_e}{h_o} \sqrt{\frac{k_{fv}}{k_{fh}}}$ decreases, critical rate would increase suggesting an inverse relationship between them.

Hence, the function, $f\left(\frac{r_e}{h_o} \sqrt{\frac{k_{fv}}{k_{fh}}}\right)$ is correlated with the inverse of $\frac{r_e}{h_o} \sqrt{\frac{k_{fv}}{k_{fh}}}$ using a linear regression (shown in Table 3.1) after matching semi-analytical formula (Eq. 3.13) with the simulated data from 62 experimental runs.

Table 3.1. Regression model of empirical parameter, $f \left(\frac{r_e}{h_o} \sqrt{\frac{k_{fv}}{k_{fh}}} \right)$

Variable	Coefficients	t Value	p-value
Intercept	0.735	193	0
$\frac{1}{\frac{r_e}{h_o} \sqrt{\frac{k_{fv}}{k_{fh}}}}$	1.86	15.3	0

The regression model shows the good fit with experimental data at R-Squared value of 0.8. The final equation of the critical rate for the fracture-well in NFR for longer penetration ratio greater than 0.35, can be written as,

$$q_{cr,fr} = 0.0783 \times 10^{-4} \frac{k_{fm} h_o^2}{B_o \mu_o} (\Delta\rho) \left(1 - \left(\frac{h_{op}}{h_o} \right)^2 \right) \left(0.735 + 1.86 \frac{1}{\frac{r_e}{h_o} \sqrt{\frac{k_{fv}}{k_{fh}}}} \right) \quad (3.14)$$

Formula Eq. 3.14 is only as good as the estimated value of effective permeability of fractured media for accurately predicting the critical-oil rate for a real NFR. In other words, the new model ignores any deviation of actual NFR properties due to the idealization of discrete fractures as equivalent continuous porous media in NFR. Moreover, any possible discrepancy due to the semi-spherical flow pattern in discrete fracture network as compared to that of equivalent porous media, is also ignored. Further improvements in the model can be made by calibrating the analytical model with the experiments performed on the discrete fracture network model.

Summary

Inference of the above study on semi-analytical modeling of critical-rate in NFRs with bottom-water can be summarized as:

1) Simulations performed on the designed matrix of experiments (representing wide varieties of NFRs) reveal that critical production rate in NFRs (with bottom-water) can exceed 200bopd, which

is viable enough to be investigated. High critical rate suggests that some NFRs can be produced at those rates for longer time avoiding water breakthrough. This led us to develop a critical oil rate formula for fracture-well in NFR for known effective flow properties of the planar network.

2) The critical oil rate model considers mechanistic principle assuming vertical equilibrium of viscous and gravity forces for a hemispherical flow in any reservoir using Chaperon's (1986) approach. For NFRs with bottom-water, the permeability in the model is replaced by the equivalent permeability of a dual-porosity/dual-permeability (DPDP) NFR, and anisotropy ratio is replaced by that of fractures.

3) The analytical model of NFR considers water cone instability and anisotropy ratio for a point source oil sink at the top of oil-pay. As a result, while testing the model with the designed experiments representing wide variety of NFRs, it is found that the model is only good for NFRs having well's penetration ratio smaller than 0.35.

4) The model's limitation prompted us to derive a new model for NFRs for longer well's penetration ratio. This is performed by statistically calibrating Chaperon's apparent model for NFR (valid for short penetration) for longer penetration ratio, using designed matrix of simulated experiments covering wide ranges of NFR properties. The calibration approach redefined the flow regime from semi-spherical to non-radial distorted flow due to longer completion.

Chapter 4. Well Placement Model and Significance

The chapter brings forth the reservoir modeling techniques of different well placement settings in dual-porosity/dual permeability (DPDP) NFR, and shows how single and dual well placement can have significant impact on recovery. The study also reveals that the effect of well placement on recovery is a function of the type of NFR, thereby, proposing the criteria of classifying NFRs based on its well placement significance. Further, the chapter investigates the effect of well placements on critical rate.

4.1 Qualification of Single and Dual-completed Well Placement in NFR

Single well completions in NFRs may or may not intersect the fractures depending on the completion placement in the fracture-network which depends upon the network structure and complexity of fracture network geometry. Similarly, dual completed or DWS well which can serve as the technology to mitigate water coning (Wojtanowicz et al. 1991; Shirman 1996; Shirman and Wojtanowicz 1997a; Shirman et al. 2014), may also have top and bottom completions placement either in fractures or in matrix, resulting in different recovery performances (discussed later in the chapter). Based on the pattern of fracture network, NFRs are classified as planar and channel fracture network (fracture corridor network) as discussed in chapter 2. Because of the relatively dense network, we assume the planar fracture networks are well connected. In the study, we consider the connected planar fracture network based on the distributed fracture spacing size as, a) densely distributed planar fracture network and b) sparsely distributed planar fracture network.

Section 4.3.1 and 4.3.2 of this chapter previously appeared as OMAE paper (OMAE2019-96836) on “Probabilistic Estimation of Recovery From Naturally Fractured Bottom-Water Reservoir With Uncertain Well Placement in Fracture Network” in ASME 2019 38th International Conference on Ocean, Offshore and Arctic Engineering. Reproduced with permission of ASME. See Appendix F for more details.

Section 4.4 of this chapter previously appeared as Journal paper 2019 on “Semi-Analytical Prediction of critical Oil Rate in Naturally Fractured Reservoirs with Water Coning” published in Journal of Petroleum Science and Engineering, 180 (2019): 779-792. Reproduced with permission of Journal of Petroleum Science and Engineering. See Appendix F for more details.

This is done in order to qualify the NFR based on its well placement performance in the two planar network.

4.2 Well Completion Placement Simulation Model

In the simulation study, we simplify the fracture network using DPDP model. This is assuming capillary continuity exists in the fractured reservoir (Thomas et al. 1987, Gilman and Kazemi 1988, Labastie 1990, Horle et al. 1990, Thomas et al. 1991, Boerrigter et al. 1993, Tabola and Baldwin 1995). DPDP model is preferred as it considers matrix-matrix flow and matrix/fracture transfer. However, since DPDP is based on simplified continuum approach, well placement modeling can be a challenge. In the study, we attempt to address well placement modeling in DPDP NFR with 1) connected planar fracture network and 2) fracture corridor (channel) network.

4.2.1 Well Placement Simulation in Connected Planar Fracture Network

A 2-D radial cylindrical dual porosity/dual permeability (DPDP) model built with IMEX software is used to simulate planar fracture network (Gilman 1986; Gilman and Kazemi 1988; Gilman 2003; Tan et al. 2018). For a DPDP NFR model, average fracture permeability, k_f for a radial system can be obtained by subtracting the core rock matrix permeability, k_m from the average permeability (Eq. 3.2) obtained from production data (Song et al. 2019),

$$k_f = k_{f,m} - k_m k_{ro} = \frac{141.2Q\mu B_o \left(\ln \frac{r_e}{r_w} + S \right)}{2\pi\Delta P} - k_m k_{ro} \quad (4.1)$$

Where, Q is the oil production rate, μ is the oil viscosity, r_e is the reservoir drainage radius, and ΔP is the pressure drawdown.

Since matrix permeability is usually very small compared to fracture effective permeability, we can write Eq. (4.1) as,

$$k_f = \frac{141.2Q\mu B_o \left(\ln \frac{r_e}{r_w} + S \right)}{2\pi\Delta P} \quad (4.2)$$

However, NFRs are highly anisotropic and heterogeneous which brings a problem of modeling them. Such reservoirs containing fractures which fails to be defined by a single Darcy permeability, are defined by full permeability tensor. Song et al. 2019 demonstrated the work to integrate the full permeability tensor of fractures to a single Darcy permeability, which can be used for reservoir simulation purpose. The fracture logs would give the complete permeability tensor of fractures. For an arbitrary set of parallel fractures having azimuth β_a , dip angle α , and average permeability, k_f , complete permeability tensor is given by,

$$\overline{K_e} = k_f \begin{bmatrix} \cos^2\alpha \cdot \cos^2\beta_a + \sin^2\beta_a & \sin^2\alpha \cdot \cos\beta_a \cdot \sin\beta_a & \cos\alpha \cdot \sin\alpha \cdot \cos\beta_a \\ \sin^2\alpha \cdot \cos\beta_a \cdot \sin\beta_a & \cos^2\alpha \cdot \sin^2\beta_a + \cos^2\beta_a & -\cos\alpha \cdot \sin\alpha \cdot \sin\beta_a \\ \cos\alpha \cdot \sin\alpha \cdot \cos\beta_a & -\cos\alpha \cdot \sin\alpha \cdot \sin\beta_a & \sin^2\alpha \end{bmatrix} \quad (4.3)$$

The next approach is to compute the anisotropic permeability parameters, which are the principal directions and principal values of permeability for fractured media. For the principal direction, it can be determined by the fracture orientation data from logging. Based on the identified principal directions, the axis direction of the global coordinate is set to be aligned with the principal direction. In this case, off-diagonal terms of the permeability tensor can be eliminated. So, the anisotropic permeability in principle directions (X, Y and Z) is given by,

$$\overline{K_e} = k_f \begin{bmatrix} \cos^2\alpha \cdot \cos^2\beta_a + \sin^2\beta_a & 0 & 0 \\ 0 & \cos^2\alpha \cdot \sin^2\beta_a + \cos^2\beta_a & 0 \\ 0 & 0 & \sin^2\alpha \end{bmatrix} = \begin{bmatrix} k_{fx} & 0 & 0 \\ 0 & k_{fy} & 0 \\ 0 & 0 & k_{fz} \end{bmatrix} \quad (4.4)$$

The average permeability, k_f can be derived and related to the three anisotropic permeability (Muskat 1937) as;

$$k_f = (k_{fx}k_{fy}k_{fz})^{1/3} \quad (4.5)$$

For an infinite length of orthogonal fractures, effective permeability is determined by considering laminar flow in a slot with planar, uniform fracture (Lamb 1945; Witherspoon et al. 1980), so,

$$k_{fx} = \frac{w_y^3}{12S_y}; k_{fy} = \frac{w_x^3}{12S_x} \quad (4.6)$$

Other types of complex fracture network can be integrated with DPDP model (Fig. 4.1) using method shown by Dershowitz et al. 2000. Dershowitz introduced a method for converting non-orthogonal fracture network to an equivalent continuous porous medium by representing the fracture network as an equivalent orthogonal network system (Dershowitz et al., 2000). This approach couples the advantage of high accuracy using discrete fracture network and increased computational speed using DPDP model. Use of DPDP further solves the problem of multiphase flow in NFR.

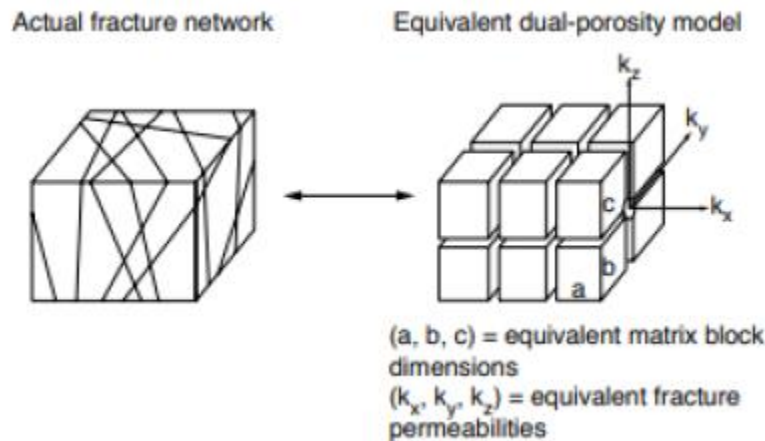


Fig. 4.1. Conventional dual-porosity representation of actual fracture network (BourBiaux et al. 1988)

As the DPDP IMEX software considers only wells intercepting fractures it implicitly models fracture-well placement shown in Fig. 4.2. In order to model well placed in rock matrix, we assume a well completed at the center of cubical/cylindrical matrix-block surrounded by orthogonal fractures as shown in Fig. 4.3. Matrix-wells are modeled by assigning zero fracture

porosity to the matrix block around the well. In the cylindrical model, radius of the well-containing matrix block is determined by the distance to the nearest fracture, $0.5S_p$.

The modeling relevance can be verified for the matrix well by comparing the results of model's simulation with the analytical model of high permeability single porosity reservoir having a low permeability damage skin near the wellbore. This is done considering the fractured-zone as the single porosity high permeability zone, whose average permeability can be derived from Eq. (4.1). For an example demonstration, we compare the simulated oil production rate of fully-penetrating matrix-well in an oil NFR with the Darcy's law derived production rate using the properties of two NFRs listed in Table 4.1. The analytical Darcy's law derived production rate is given by,

$$Q = \frac{k_{f,m}h_o\Delta P}{141.2\mu_o(\ln(\frac{r_e}{r_w})+Skin)} = \frac{(k_{fh}+k_{mh}k_{ro})h_o\Delta P}{141.2\mu_o(\ln(\frac{r_e}{r_w})+Skin)} \quad (4.7)$$

Where, low permeability damage skin, $Skin = \left(\frac{k_{f,m}}{k_{mh}} - 1\right) \ln\left(\frac{r_{ms}}{r_w}\right)$

Table 4.1. Reservoir properties of two NFRs -1 and 2

Reservoir properties	Value (NFR-1)	Value (NFR-2)
Fracture effective permeability, k_{fh}	600md	400md
Matrix permeability, k_{mh}	20md	40md
Oil relative permeability at connate water saturation, k_{ro}	1	1
Thickness of oil-zone, h_o	40ft	60ft
Oil viscosity, μ_o	2 cp	5 cp
Pressure drawdown, ΔP	1000 psi	2000 psi
Reservoir radius, r_e	1000ft	500ft
Well-bore radius, r_w	0.25ft	0.25ft
Matrix-zone radius, r_{ms}	3ft	10ft

Table 4.2. Oil production rate comparison of simulation and analytical model for two NFRs -1 and 2

Simulation NFR-1	Analytical – NFR-1	Simulation – NFR-2	Analytical – NFR-2
1070bbl/day	1094bbl/day	1750bbl/day	1833bbl/day

Clearly, Table 4.2 shows the oil production rate obtained from model simulation matches well with the analytical model results, which clearly validates the use of simulation model for matrix-well simulations’ studies carried later in the dissertation.

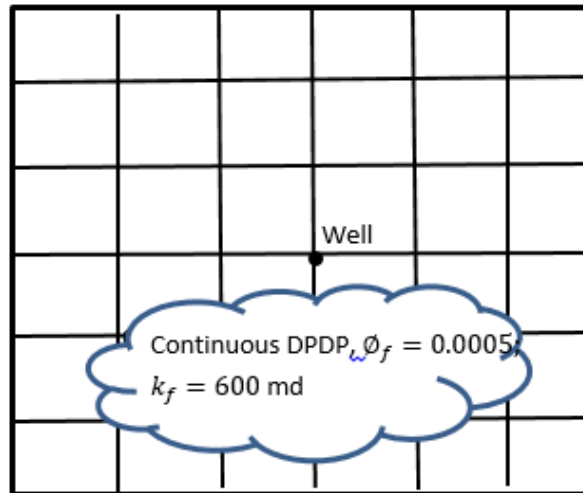


Fig. 4.2. Simulation DPDP model of fracture-well in planar fracture network

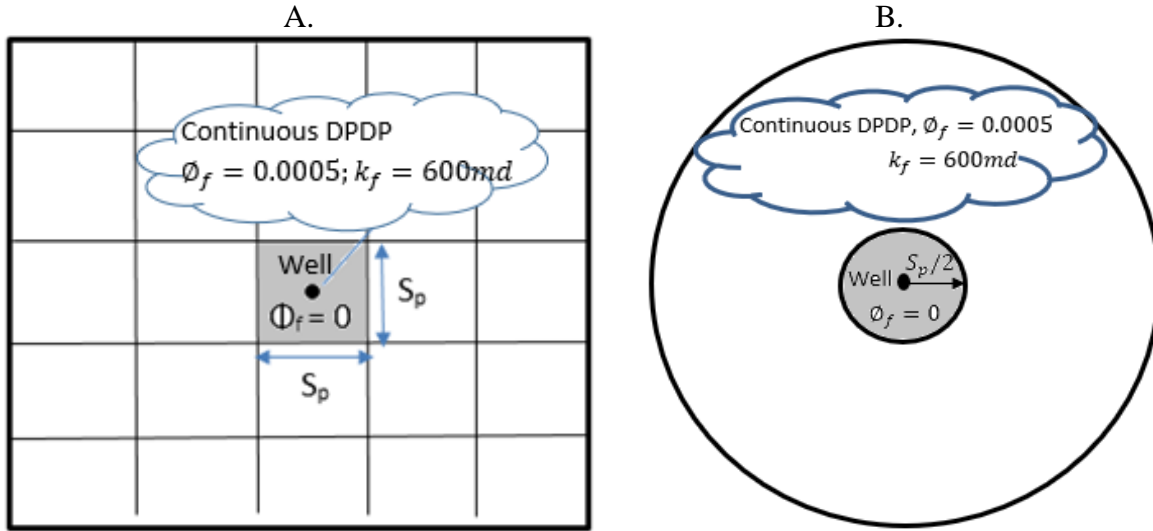


Fig. 4.3. A) Simulation model of matrix-well in DPDP cartesian model; (B) Simulation model of radial cylindrical model representing planar fracture network

4.2.2 Well Completion Placement Simulation in Channel (Fracture Corridor) Network

In contrast to connected planar networks, modeling of wells in corridor NFR might require different approach as the continuous DPDP model may not represent properly water coning around wells. Water coning occurs locally around wells so large corridor spacing and their non-orthogonal alignment may disqualify the orthogonal DPDP approach and necessitate a discrete model of fracture network.

The regular corridor alignment shown in Fig. 4.4a, implies that fracture corridor distribution could be idealized as a sheet-like network shown in Fig. 4.4b that would require a discrete rather than continuous model to accurately simulate the locality of water coning.

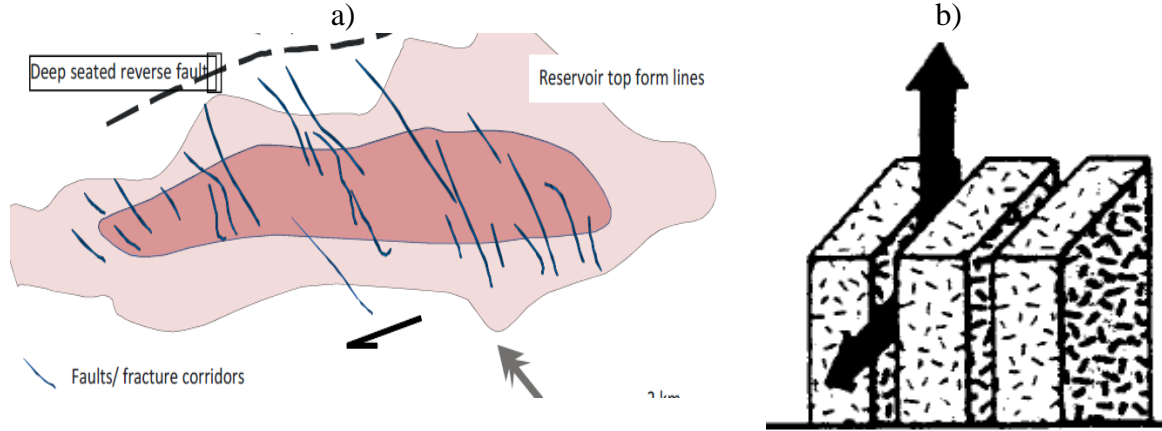


Fig. 4.4. a) Parallel fracture corridors network (Ozkaya 2013); b) Idealized sheet like network representing fracture corridors (Reiss 1980)

A partially discrete DPDP model is built by assigning zero fracture porosity in the exclusion-zone containing the well as shown in Fig. 4.7 and to the exclusion-zone next to the corridor intercepted by the well – Fig. 4.6. Outside the exclusion-zone, the fracture corridor network is homogenized using continuous DPDP model. Effective permeability of the homogenized part of NFR – in the discrete DPDP model, and the entire NFR for the continuous DPDP model is computed from the corridor size, F_W , permeability, k_{ff} , and spacing, S_p , as,

$$k_f = \frac{k_{ff} \times F_W}{S_p} \quad (4.8)$$

The partially discrete DPDP model's accuracy is verified by comparing its simulation recovery performance with that of a complete discrete model, considered to be more physically representative, where all the corridors specific grids having fracture porosity of 0.0005, and the exclusion-zone specific grids are assigned zero fracture porosity. Table 4.3 refers to the two extreme corridor type NFR cases 1 and 2 considered for the comparison. Figs. 4.5 shows that similar recovery performances between partially and complete discrete DPDP model for two NFR cases – 1 and 2. This implies that the partially discrete DPDP model can be used in place of complete discretized (corridor) model which consumes more simulation time and energy.

Moreover, as shown in Fig. 4.5b, the partially discrete DPDP model result is also compared with the complete homogenized DPDP model to justify the use of partially discrete DPDP model. Predictably, the homogenous DPDP model would fail to completely replicate the more simulation results of more physically representative model of corridor-type NFRs, and so is not used in the study.

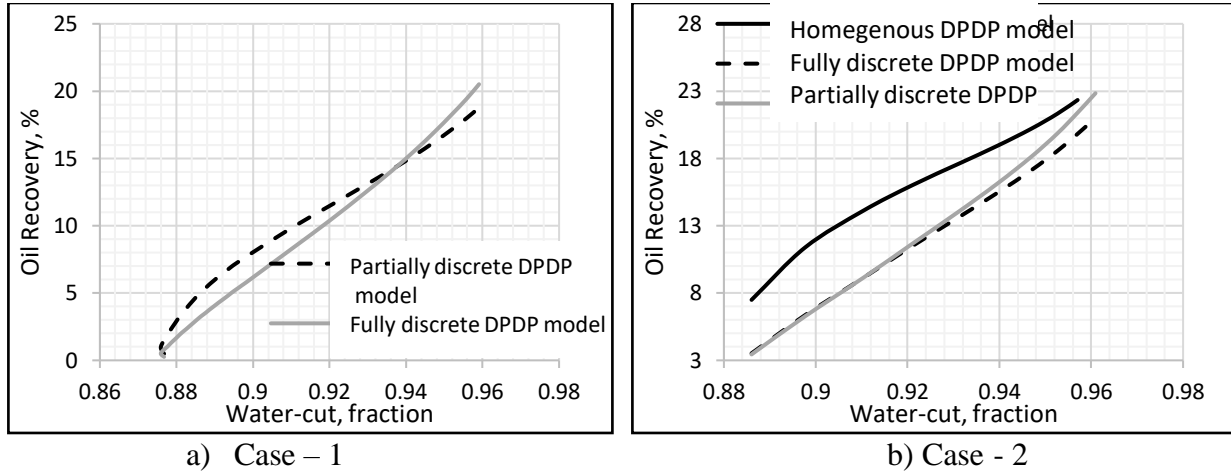


Fig. 4.5. Comparison of different DPDP models (Discrete DPDP, complete discrete corridor, and homogenized DPDP) for two different NFRs – a) Case - 1; and b) Case-2

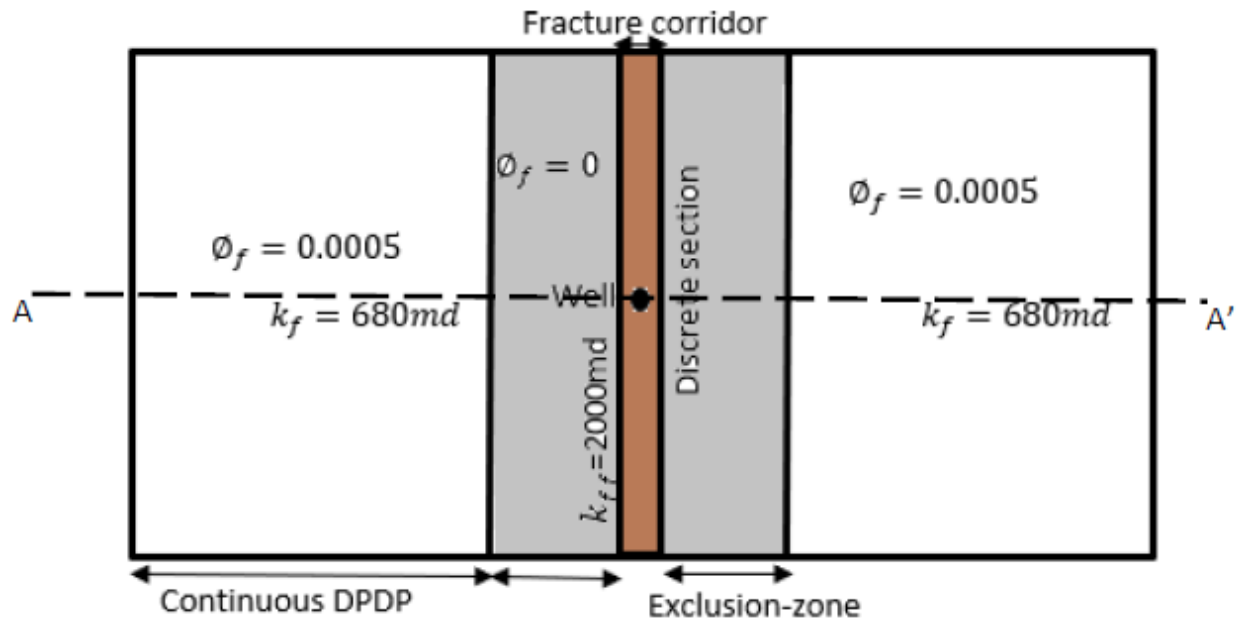


Fig. 4.6. Top view of partially discrete DPDP model of well placed in fracture corridor (Case 1)

Table 4.3. Input data for Discrete DPDP model of sparsely distributed fracture corridor

NFR Properties	Discrete DPDP model	
	Case 1	Case 2
Fracture corridor horizontal permeability	2000md	2000md
Fracture corridor vertical permeability	10000md	10000md
Matrix permeability	30md	30md
Corridor width (size)	20ft	10ft
Corridor spacing	200ft	50ft
Oil-water contact from top of reservoir	40ft	40ft
Reservoir size	1320ft×1320ft×80ft	350ft×350ft×80ft
Oil viscosity	1cp	1cp
Water viscosity	0.8cp	0.8cp
Reservoir pressure	3000psi	3000psi
Fracture porosity	0.0005	0.0005
Matrix porosity	0.3	0.2
Liquid Production rate	2000 bbl/day	2000 bbl/day

In the model, matrix-well is placed at the center of the zero-fracture-porosity exclusion-zone equal to the size of corridor spacing (Fig. 4.7).

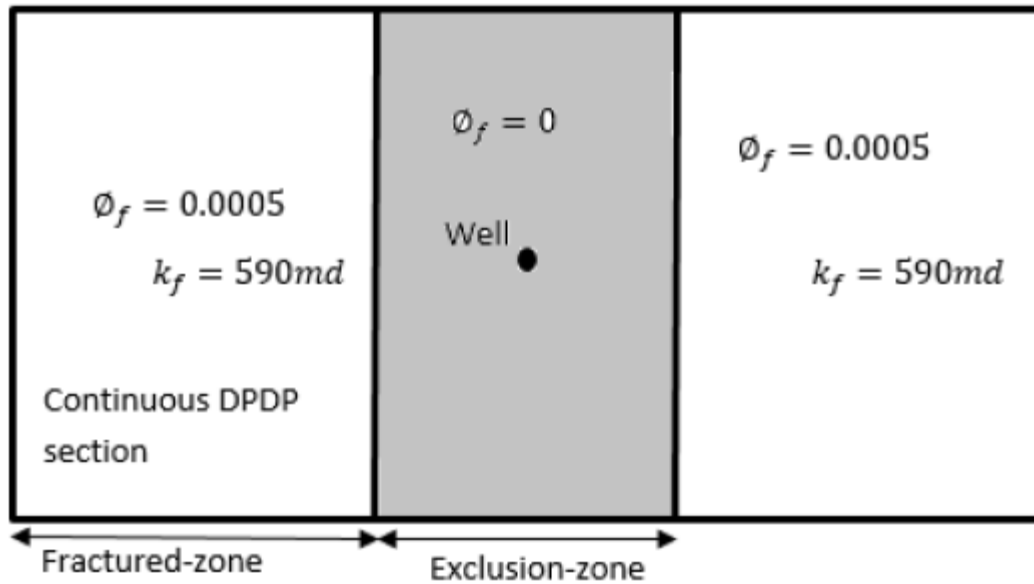


Fig. 4.7. Simulation model of matrix-well in fracture corridor network (Exclusion-zone shown by shaded region)

4.3 Well Placement Significance in Planar Network NFR

Placement of well completion in NFR may only be important if it would affect the well's recovery performance. Physically, the well placement effect shall be significant in the fracture-corridor NFR with large spacing of fracture corridors. However, in case of the planar fracture network NFR recovery from wells placed in fractures may or may not be different to that from wells completed in the rock matrix.

Objective of this study, is, firstly, to compare recovery performance of single-completed and dual-completed (DWS) wells placed in the fracture or the rock matrix of NFR with planar network having different network density – densely-distributed and sparsely distributed network. In this study, an oil recovery factor (RF) over 20 years production period or until the water-cut value comes to 97% is used as a metric of well performance. The second objective is to develop analytical criterion for assessing significance of well placement in such NFRs.

4.3.1 Single-Completed Well in Densely Distributed Fracture Network

For studying densely-distributed fracture networks, we choose two different classes of NFRs - Type II and type III (with different wetting properties) shown in Tables B1 and B2. Type II NFR is mixed-wet and type III NFR is water-wet. In type III NFR, fracture provides “permeability assistance” to the matrix permeability; whereas in type II NFR, fracture provides essential permeability (Nelson 2001).

In a densely distributed fracture network of type II NFR, water breakthrough to matrix-well is controlled by the water invasion to fractures. As water invasion to fractures results from the fractured zone pressure drawdown, *a relevant comparison of fracture-well and matrix-well* requires using the *same value of fractured zone pressure drawdown*. We can do so, by setting the same production rate and ignoring very small pressure drop (in the matrix well) across the matrix separating the well from adjacent fracture.

Figure 4.8 compares the water-cut patterns (vs. cumulative oil) of the matrix-well and fracture-well completed in type II and type III NFRs having properties shown in Tables B1 and B2. Using cumulative oil instead of time in the plots (Chan 1995) removes the scatter caused by the variation of liquid production rate and provides the direct measure of invasion of water per incremental oil – water-cut severity per barrel of oil recovered. Such plots have been already used to demonstrate different pattern of water coning in single-porosity reservoirs and NFRs (Joshi 1991).

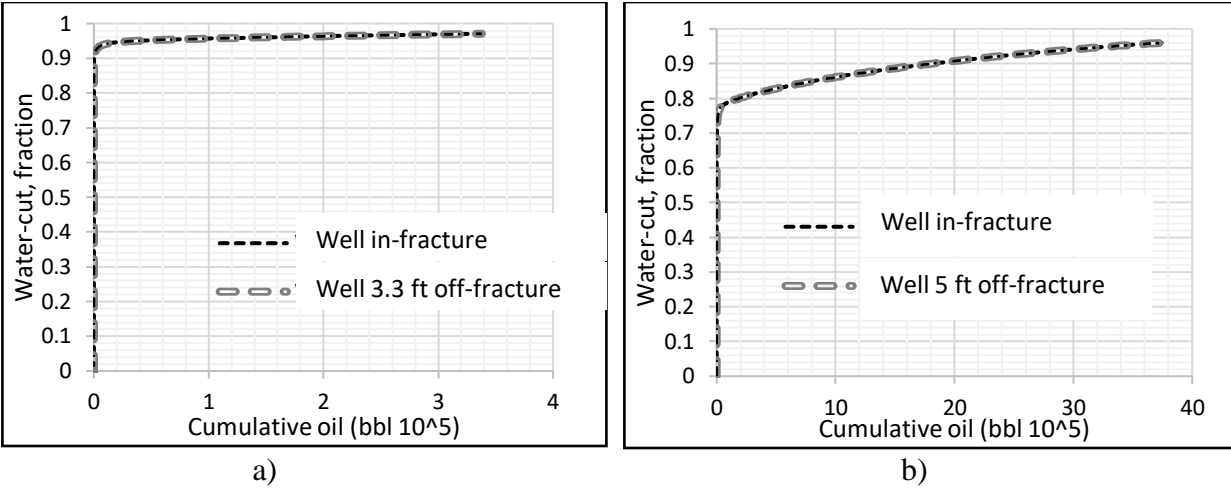


Fig. 4.8. Water-cut vs. cumulative oil for matrix-well and fracture-well in a) type II NFR (liquid production rate =2400bbl/day); and b) type III NFR liquid production-rate=2000bbl/day)

The plots clearly show that both wells (matrix and fracture-well) display the same water-cut-cumulative oil pattern for both types of NFR (type II and type III), and hence exhibit the same performance in densely distributed NFRs. This implies that uncertainty of the well completion placement in densely-distributed fracture network NFRs is not a problem of concern.

4.3.2 Dual-completed (DWS) Well in Densely Distributed Fracture Network

DWS wells discussed in Section 4.1, are dual completed wells with an additional bottom completion below oil-water contact, which serve to minimize water coning in the oil-zone, thereby, improve oil recovery. There are four possible cases of DWS completions location in the fracture network shown in Fig. 4.9:

- a) Both the top and bottom well completions intersect the fracture-network. This is possible for deviated well and inclined fractures, as shown in Fig.4.8, and for vertical wells and fractures.
- b) There is a misalignment between the well and fracture so that the top well completion intersects a fracture while the bottom completion is in the rock matrix;

- c) Similar to (b), the top completion is in rock matrix and the bottom completion intersects the fractures;
- d) The two well completions are placed in rock matrix.

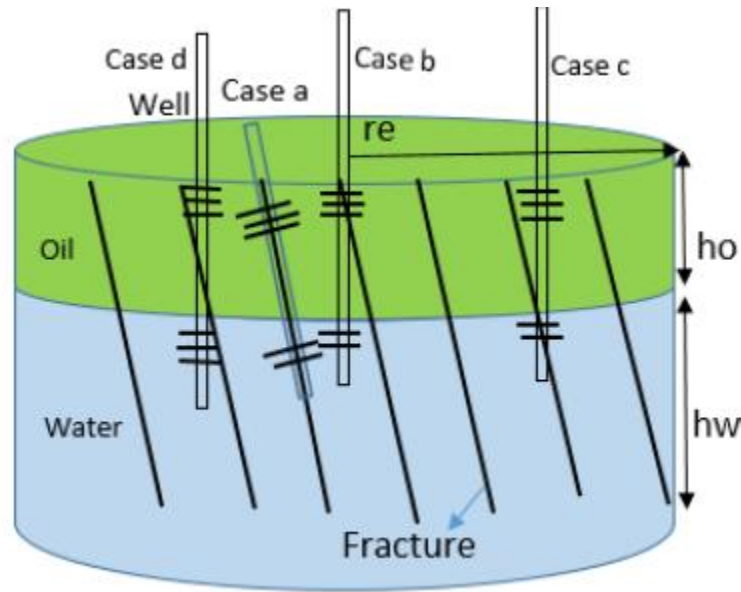
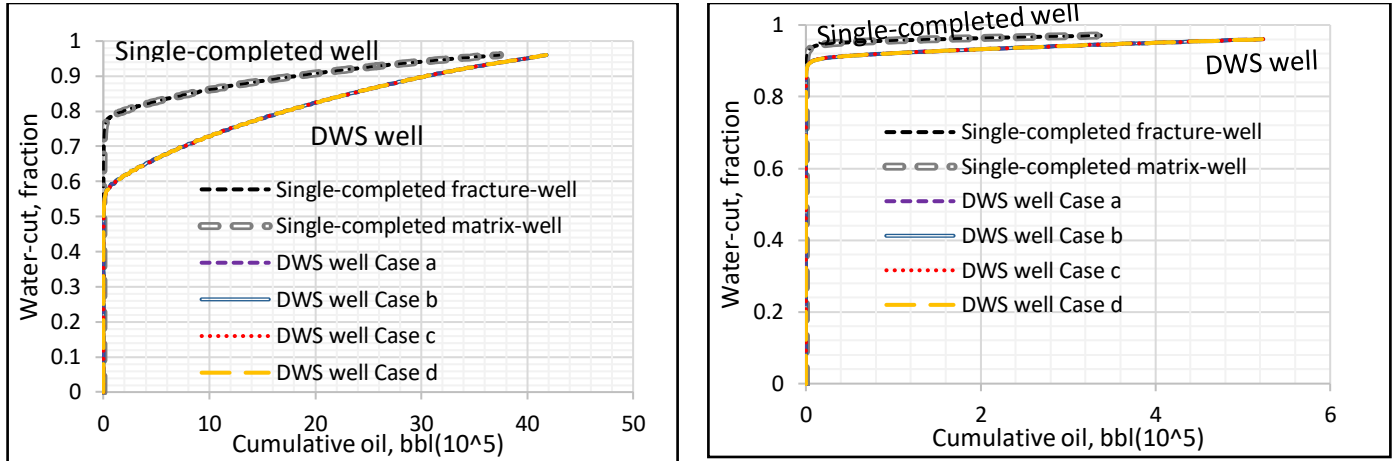


Fig. 4.9. DWS well completions placement variants in NFR with densely-distributed fracture network

Similar to the single-completed well study, above, for DWS well in the densely-distributed fracture network we assume the same production rates at the oil (top) and water sink (bottom) completions for all four variants of completions' placement. This approach represents the scenario of designing DWS well operation for maximum pressure drawdown in the top matrix completion such that the bottom-hole pressure is above the bubble point pressure, and b) there is no inverse coning of oil to the bottom completion.

We conduct the DWS well simulations using properties of type II and type III NFRs shown in Tables B1 and B3. The results show a considerable improvement in recovery comparing to single-completed wells for all four cases (Fig. 4.10 and Table 4.4). DWS wells increase recovery from 20% to 25% in type III NFR, and from 15% to 18% in type II NFR. The results also show

the same DWS recovery, 18% and 25% in Type II and Type III NFR, respectively, for four placements of DWS well completions, a, b, c, and d. It is then concluded that in densely-distributed type II and type III NFRs, DWS completion placement in fracture network has no effect on recovery performance. Thus, the problem of DWS completion placement uncertainty is irrelevant in densely-distributed fracture network NFRs.



a) Single-completed well ($Q=2000$ bfpd) vs. DWS well ($Q_{top} = Q_{bot} = 2000$ bfpd) in type III NFR b) Single-completed well ($Q=2400$ bfpd) vs. DWS well ($Q_{top} = Q_{bot} = 2400$ bfpd) in type II NFR

Fig. 4.10. Water Cut pattern (top completion) with on/off fracture completion placement variants for DWS and single-completed wells in NFRs with densely-distributed fracture network

Table 4.4. Well recovery in densely-distributed fracture network (Type III and Type II NFRs)

Well type	Completions		Average RF, %		Production rate, bfpd	
	Upper	Lower	Type III NFR	Type II NFR	Type III NFR	Type II NFR
Single-completed	Fracture	-	20.2%	15%	2000/0	2400/0
	Matrix	-	19.9%	15.2%	2000/0	2400/0
Dual-completed	Fracture (a)	Fracture (a)	25.4%	18.3%	2000/2000	2400/2400
	Fracture (b)	Matrix (b)	25.2%	18.2%	2000/2000	2400/2400
	Matrix (c)	Fracture (c)	24.9%	17.9%	2000/2000	2400/2400
	Matrix (d)	Matrix (d)	24.7%	17.6%	2000/2000	2400/2400

Predictably, qualification of densely-distributed (when the well placement does not affect recovery), and sparsely-distributed fracture network (when the recovery depends on on/off fracture well placement) would be dependent on the NFR properties. The proposed work is to analytically derive the threshold fracture spacing as a function of NFR properties which would qualify the well placement significance in planar fracture network.

4.3.3 Single-Completed Well in Sparsely Distributed Planar Fracture Network – Critical Fracture Spacing

We continue here on the study in Section 4.3.1 to assess significance if fracture spacing effect in planar network NFR. Our hypothesis is that increased spacing would significantly change well's recovery and the difference can be associated with a critical (minimum) value of fracture spacing. Consequently, the critical fracture spacing becomes a design metric for preferable location of well completion in NFR with the planar fracture network – in the fracture (fracture well) or in the matrix (matrix well). Thus, we define critical fracture spacing as the minimum distance between fractures that results in significant difference in recovery performance of fracture well vs. matrix well.

Our study, above in Section 4.3.1, shows that when fractures are densely distributed performance of the two wells is almost the same if the wells are produced at the same rate. The bottomhole flowing pressures in such case are not much different due to proximity of the matrix well to the nearest fracture. However, for larger spacing pressure drawdown in the two wells becomes different and the matrix well rate becomes limited by the minimum value of bottom flowing pressure so the two wells should not perform the same. Thus, there is a minimum value of fracture spacing – critical fracture spacing, that delineates sparsely - distributed fracture network from densely - distributed fracture system. In this study, we analytically determine a correlation for finding critical fracture spacing

The concept is demonstrated in Figs. 4.11 and 4.12 showing comparison of recovery performance of the fracture and matrix wells vs. fracture spacing for NFR with properties listed in Table 4.5. The recovery is computed when water-cut reaches 97%. Clearly, for small fracture spacing (up to 4ft (Fig. 4.11)) the two wells' recovery is the same. For larger spacing, however, the matrix well production rate drastically reduces with increased spacing as its maximum rate of production (maximum pressure drawdown) becomes constrained by the bubble - point pressure. Nevertheless, matrix well's recovery would increase from 47% to 52% (Fig. 4.11) when the well's life - is limited by 97% water-cut. This occurs due extended production time with water cut below 97%. However, as shown in Fig. 4.12, if the well's life (duration of project) is limited to 20 years, matrix well recovery becomes strongly dependent on fracture spacing and significantly smaller than that for the fracture well, which is not affected by fracture spacing. As demonstrated in Figure 4.13a, even though the fracture well produces with very high water cut it still recovers more oil due to its high production rate – unlike the matrix well at large fracture spacing =20ft. However, Fig. 4.13b, shows that for both matrix and fracture well producing at same rate (low fracture spacing =3ft), would result in almost similar water-cut and oil production rate for these wells. Also, as shown in Fig 4.11, the matrix well performance rapidly reduces with small increase of fracture spacing if the spacing is smaller than 20 ft in this example case. We also conclude that NFR fracture spacing appears to be the main property that controls well performance. Since there is no control of well placement (in a fracture or matrix), well performance variation depends on the reservoir property – fracture spacing, with the disparity being greater for larger spacing. Moreover, for NFRs with small fracture spacing the disparity is negligibly small and can be ignored. The concept gives rise to quantify definition of two categories of NFR – with closely and sparsely – distributed natural fractures.

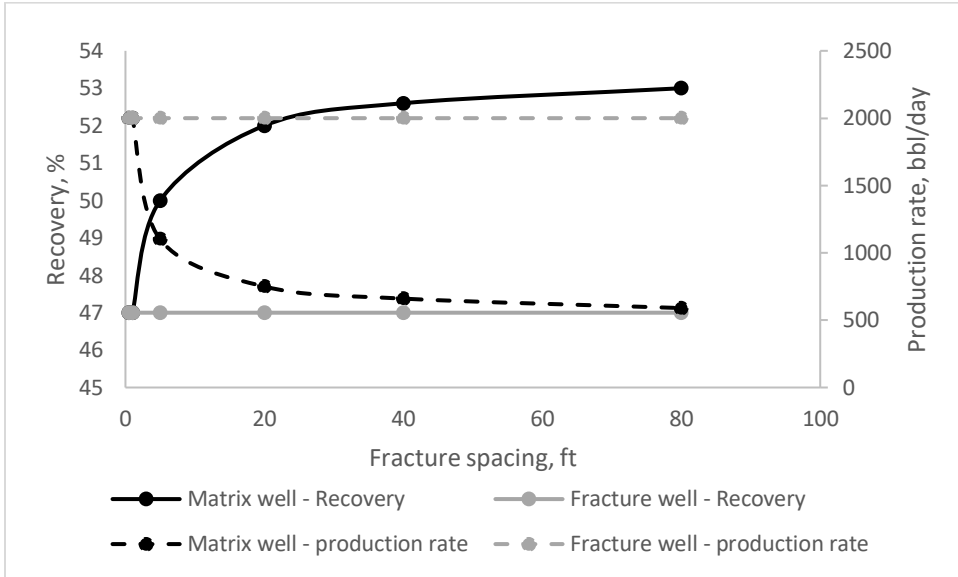


Fig. 4.11. Recovery comparison of fracture and matrix well vs. fracture spacing in same NFR (Table 4.5). Critical spacing \approx 4 ft. (Based on 97% water-cut project life)

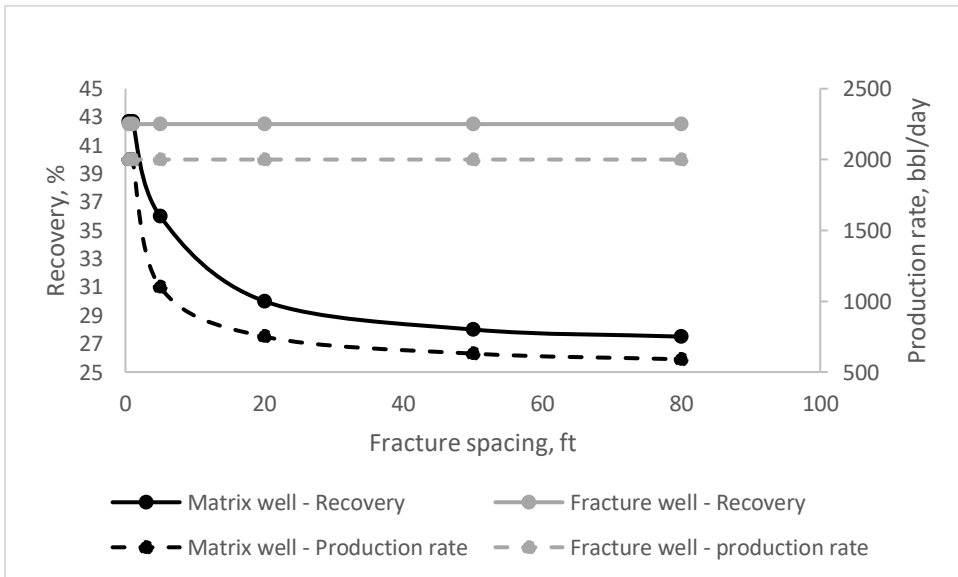
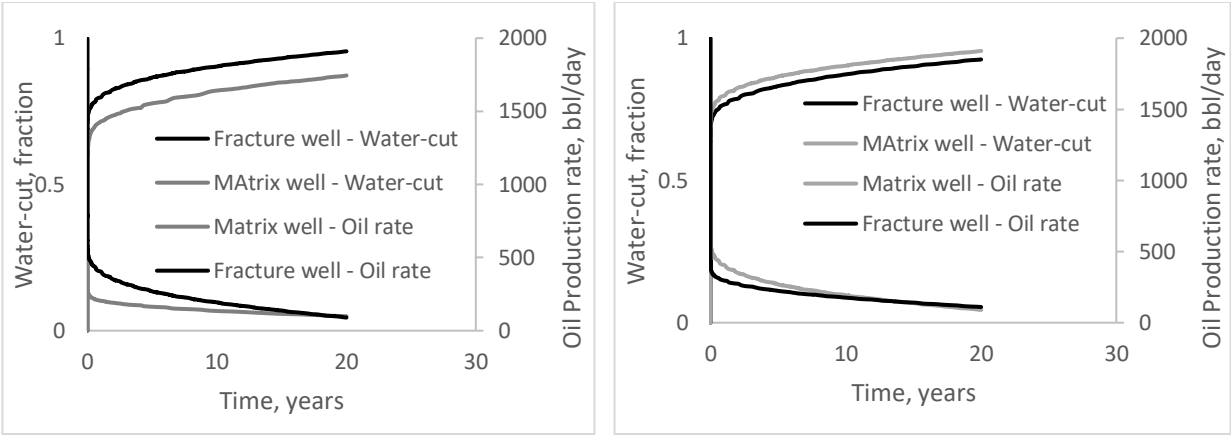


Fig. 4.12. Recovery comparison of fracture and matrix well vs. fracture spacing in same NFR (Table 4.5). Critical spacing \approx 4 ft. (Based on 20 years duration of project life)



(a) Fracture spacing = 20ft

(b) Fracture spacing = 3ft

Fig. 4.13. Water-cut and oil production rate comparison for matrix and fracture-well until 20 years project life for a) fracture spacing = 20ft, and b) fracture spacing = 3ft

Table 4.5. Reservoir and Operational Input Parameters

Reservoir and Operational parameters	Value
Fracture effective horizontal permeability	500md
Matrix permeability	50md
Fracture effective vertical permeability	5000md
Fracture porosity	0.0005
Matrix porosity	0.2
Oil-zone thickness	40ft
Aquifer thickness	50ft
Oil viscosity	1cp
Water viscosity	0.8cp
Maximum production rate	2000 bpd
Reservoir radius	1000ft
Reservoir pressure	3000psi
Bubble point pressure	500psi
Perforated length	20ft

Following on the above concept, we presume that for any given maximum production rate of the fracture-well (yielding maximum recovery) there is a minimum (critical) fracture spacing above which production rate of matrix well must be reduced below that of the fracture well, to satisfy the constraint of bottomhole pressure not exceeding bubble point pressure. Consequently, fracture spacing greater than the critical spacing is the reason for significant recovery difference between the two options for well placement. Since rates comparison predominantly controls the pattern of recovery comparison (shown in Fig. 4.11), we can use rates for modeling critical fracture spacing. So, in the result, critical fracture spacing is defined not only by NFR properties but also by the value of maximum well production rate. Thus, the study objective is to develop a formula for critical spacing above which matrix well cannot be produced at the same rate as the fracture well. Mathematically, this condition is to determine the maximum value of fracture spacing that matrix well rate is equal to the fracture well's rate, or

$$(Sp)_{cr} = \max (Sp), \text{ for } Q_m = Q_{fmax} \quad (4.9)$$

Where, Q_{fmax} is the maximum liquid production rate of fracture well (constrained by maximum well performance and surface installation) and Q_m is the liquid production rate of the matrix well at its maximum pressure drawdown (constrained by bubble point pressure, for example). The forthcoming analytical model of critical fracture spacing considers the same value of maximum production rate for comparing the fracture and matrix wells: $Q_{fmax} = Q_{mmax}$, where Q_{mmax} is the maximum rate of matrix well with bottomhole pressure equal to bubble-point pressure.

4.3.3.1 Analytical Formulation of Critical Fracture Spacing

Considering the simplified model of matrix well inflow in Fig. 4.3, used for the simulation, maximum pressure drawdown of the matrix-well, ΔP_{max} , is the sum of the pressure drawdown of two zones – fractured zone and matrix-zone, constrained by bubble point pressure, given by,

$$\Delta P_{max} = P_i - P_b \quad (4.10)$$

P_i is the reservoir pressure and P_b is the bubble-point pressure.

For modelling inflow to the fracture well (at the end of project life) we use the effective permeability (Kdpdp) concept so production rate of fracture well operating at the given pressure drawdown, ΔP_{fr} , is given by,

$$Q_{fmax} = \frac{k_{f,m} h_t \Delta P_{fr}}{\mu B (\ln(\frac{r_e}{r_w}) + S_f)} = \frac{(k_{fh} + k_{mh} k_{rwa}) h_t \Delta P_{fr}}{\mu B (\ln(\frac{r_e}{r_w}) + S_f)} \quad (4.11)$$

Where, $k_{f,m}$ is the overall permeability of the system, given by (Eq. 4.1)

$$k_{f,m} = k_{fh} + k_{mh} k_{rwa} \quad (4.12)$$

Where, μ can be approximated by water viscosity since water-cut reaches 97% at the end of project life. In order to estimate the average water relative permeability of the matrix-zone, k_{rwa} at the end of project life, we compute the fractional flow of water, f_w as shown in Table 4.6, which can be approximated by,

$$f_w = \frac{1}{1 + \frac{\mu_w k_{ro}}{\mu_o k_{rw}}} \quad (4.12)$$

Where, μ_o is the oil viscosity, μ_w is the water viscosity, k_{ro} is the oil relative permeability and k_{rw} is the water relative permeability of the matrix-zone. We choose the average water relative permeability, k_{rwa} corresponding to the fractional flow of water at economic limit of water-cut \approx 97%.

For the given relative permeability table as shown in Table 4.6, fractional water flow \approx 0.97 (or water-cut = 97%) occurs when relative permeability of matrix block with respect to water, $k_{rwa} = 0.3$.

Table 4.6. Matrix Relative permeability and fractional water flow

Sw	Krw	Kro	fw
0.15	0	1	0.00
0.2	0	0.8	0.00
0.3	0.013	0.6	0.03
0.4	0.05	0.37	0.14
0.5	0.1	0.18	0.41
0.6	0.2	0.08	0.76
0.7	$k_{rwa} = 0.3$	0.015	0.96
0.8	0.4	0	1.00

S_f is the partial penetration skin in NFR would be given by (Papatzacos 1987):

$$S_f = \left(\frac{1}{h_{pD}} - 1 \right) \ln \frac{\pi}{2r_D} + \frac{1}{h_{pD}} \ln \left[\frac{h_{pD}}{2+h_{pD}} \left(\frac{A-1}{B-1} \right)^{1/2} \right] \quad (4.14)$$

where, $r_D = (r_w/h_t) \left(k_{fv}/k_{fh} \right)^{1/2}$, $h_{pD} = h_{op}/h_t$, $A = 4/h_{pD}$, $B = 4/3h_{pD}$

Where, k_{fv} is the vertical effective permeability of the fracture-network and k_{fh} is the horizontal effective permeability of the fracture network.

For modeling inflow to the matrix well, we use the concept of the average permeability of the fractured zone and matrix block in series depicted in Fig. 4.3B, so the average permeability, $k_{av,m}$, can be given by,

$$k_{av,m} = \frac{\ln \left(\frac{r_e}{r_w} \right)}{\ln \left(\frac{r_e}{r_{ms}} \right) / k_{f,m} + \ln \left(\frac{r_{ms}}{r_w} \right) / k_{mh} k_{rwa}} \quad (4.15)$$

Therefore, production rate of the matrix-well is,

$$Q_m = \frac{k_{av,m} h_t \Delta P_{max}}{\mu B (\ln(\frac{r_e}{r_w}) + S_m)} \quad (4.16)$$

Where, r_{ms} is the radius of matrix-zone (or half the radius of fracture spacing (Fig. 4.3B)), S_m is the partial penetration skin due to the matrix-zone (inflow to the matrix-well Fig. 4.3B), which can be obtained from Eq. (4.13) after the following modifications:

$$S_m = \left(\frac{1}{h_{pD}} - 1 \right) \ln \frac{\pi}{2r_D} + \frac{1}{h_{pD}} \ln \left[\frac{h_{pD}}{2+h_{pD}} \left(\frac{A-1}{B-1} \right)^{1/2} \right] \quad (4.17)$$

$$r_D = (r_w/h_o) \left(k_{mv}/k_{mh} \right)^{1/2}, \quad h_{pD} = h_{op}/h_t$$

Where, k_{mv} is the matrix-zone vertical permeability, k_{mh} is the matrix-zone horizontal permeability, and h_t is the total reservoir thickness (sum of oil-pay and aquifer thickness).

$$\text{At critical fracture spacing, } Q_{fmax} = Q_m \quad @ \quad r_{ms} = (r_{ms})_{cr} = 0.5(Sp)cr \quad (4.18)$$

Or, from Eqs. 4.11, 4.16, and 4.18, we can write,

$$\frac{(k_{fh} + k_{mh} k_{rwa}) h_t \Delta P_{fr}}{\mu B (\ln(\frac{r_e}{r_w}) + S_f)} = \frac{k_{av,m} h_t \Delta P_{max}}{\mu B (\ln(\frac{r_e}{r_w}) + S_m)} \quad (4.19)$$

Or Substituting Eq. (4.15), we get,

$$\frac{\frac{\ln(\frac{r_e}{r_w})}{\ln(\frac{r_e}{r_{ms}}) / k_{f,m} + \frac{\ln(\frac{r_{ms}}{r_w})}{k_{mh} k_{rwa}}} - h_t \Delta P_{max}}{\mu B (\ln(\frac{r_e}{r_w}) + S_m)} = \frac{(k_{fh} + k_{mh} k_{rwa}) h_t \Delta P_{fr}}{\mu B (\ln(\frac{r_e}{r_w}) + S_f)}$$

Solving above Eq. for critical radius, $(r_{ms})_{cr}$, we get.

$$(r_{ms})_{cr} = \left[\frac{r_w \left(\frac{1}{k_{mh} k_{rwa}} \right)}{r_e \left(\frac{1}{k_{f,m}} \right)} \exp \left(\frac{\left(\ln \left(\frac{r_e}{r_w} \right) + S_f \right)}{\left(\ln \left(\frac{r_e}{r_w} \right) + S_m \right) \left(\frac{P_i - P_b}{\Delta P_{fr}} \right) \times \ln \left(\frac{r_e}{r_w} \right)} \right) \right] \left[\frac{1}{k_{mh} k_{rwa}} - \frac{1}{k_{f,m}} \right] \quad (4.20)$$

Where, ΔP_{fr} is the maximum pressure drawdown in the fracture-well corresponding to its maximum production rate, given by Eq. 4.11, S_f is given by Eq. 4.14, S_m by Eq. 4.17, and $k_{f,m}$ by Eq. 4.12.

Above Eq. (4.20) qualifies one of the metric to delineate the sparsely distributed from densely distributed fracture system in a dynamic flow model. The maximum fracture spacing is not only a function of static NFR properties, but also dynamic well-design and operational condition as demonstrated from Eq. (4.20). This implies that the critical fracture spacing which would demarcate the densely and sparsely distributed NFR may be different for the same NFR depending on the maximum operating constraints.

4.3.3.2 Validation

We use the fractional factorial design for 4 factors to create 8 testing sample of experiments shown in Table 4.7. The two-level design considers the factors including fracture to matrix permeability ratio, anisotropy ratio of fractures, drainage radius, and penetration ratio. In the validation study using DPDP reservoir simulator CMG (IMEX), we assume $Q_{fmax} = 2000\text{bbl/day}$ as the maximum well's production rate allowed due to surface constraint and bottom-hole pressure exceeding bubble point pressure (500psi). Simulated recovery vs. fracture spacing is shown in Figs. 4.14. The plots show critical values of fracture spacing where recovery (at 97% economic limit of water-cut) of matrix-well starts diverting upwards (increases), resulting from the longer duration of the project life of matrix-well as compared to the fracture-well.

The simulated critical fracture spacing is compared with analytical model (Eq. 4.20) results as shown in Table 4.7, which shows they are in close agreement to each other. Values of critical fracture spacing obtained for different NFRs (Table 4.7), reveals that such characteristic spacings are mostly on the lower range of typical planar fracture network spacing (0.2-20ft), which implies

that only few planar network NFRs can be classified as densely distributed. Moreover, for few NFRs shown in Table 4.7, simulated critical fracture spacing (for values < 2ft) is too small to be identified using reservoir simulation.

Table 4.7. Comparison of simulated vs calculated critical fracture spacing for testing sample of experiments (Bubble point pressure, $P_b=500$ psi; $k_{rwa} = 0.3$)

Case	Fracture-to-matrix perm ratio, k_{fh}/k_{mh}	Anisotropy ratio, k_{fv}/k_{ft}	Drainage radius, r_e	Penetration ratio, h_p/h_o	Fracture effective permeability, k_{fh}	Maximum production rate, Q_{fmax}	pressure drawdown, ΔP_{max}	Calculated critical spacing, (Sp)cr	Simulated critical spacing, (Sp)cr
1	10	2	400	0.2	500	2000	193	3	3
2	25	2	400	0.5	500	2000	102	2.5	2
3	10	10	400	0.5	500	2000	87	26	25
4	25	10	400	0.2	500	2000	155	1.0	NA
5	10	2	1000	0.5	500	2000	106	38	35
6	25	2	1000	0.2	500	2000	200	1.0	NA
7	10	10	1000	0.2	500	2000	158	3.6	3
8	25	10	1000	0.5	500	2000	93	3	3

Using the simulated data obtained from Table 4.7 and Figs.4.14, we can plot the maximum possible ultimate recovery difference between matrix and fracture well (at an arbitrary large fracture spacing equal to 80 ft fracture spacing) vs. critical fracture spacing for a given NFR as shown in Fig. 4.15. The reason to randomly choose 80ft fracture spacing, is to consider extremely sparse distributed planar network NFR for which well placement effects are identified. The plot Fig. 4.15 reveals the inverse relationship between recovery difference (at large fracture spacing) and critical fracture spacing where power-law curve showed better match with the data points at R-squared value of 0.87. This implies that lower the critical fracture spacing, higher would be the contrast in matrix and fracture well recovery for sparsely distributed planar network NFR, which makes well placement on/off fracture an important decision for operator. Since Fig. 4.15 reveals that most of the critical fracture spacing data points are below 5ft, for such low range values of critical spacing implies that most of the planar network NFRs would be sparsely distributed.

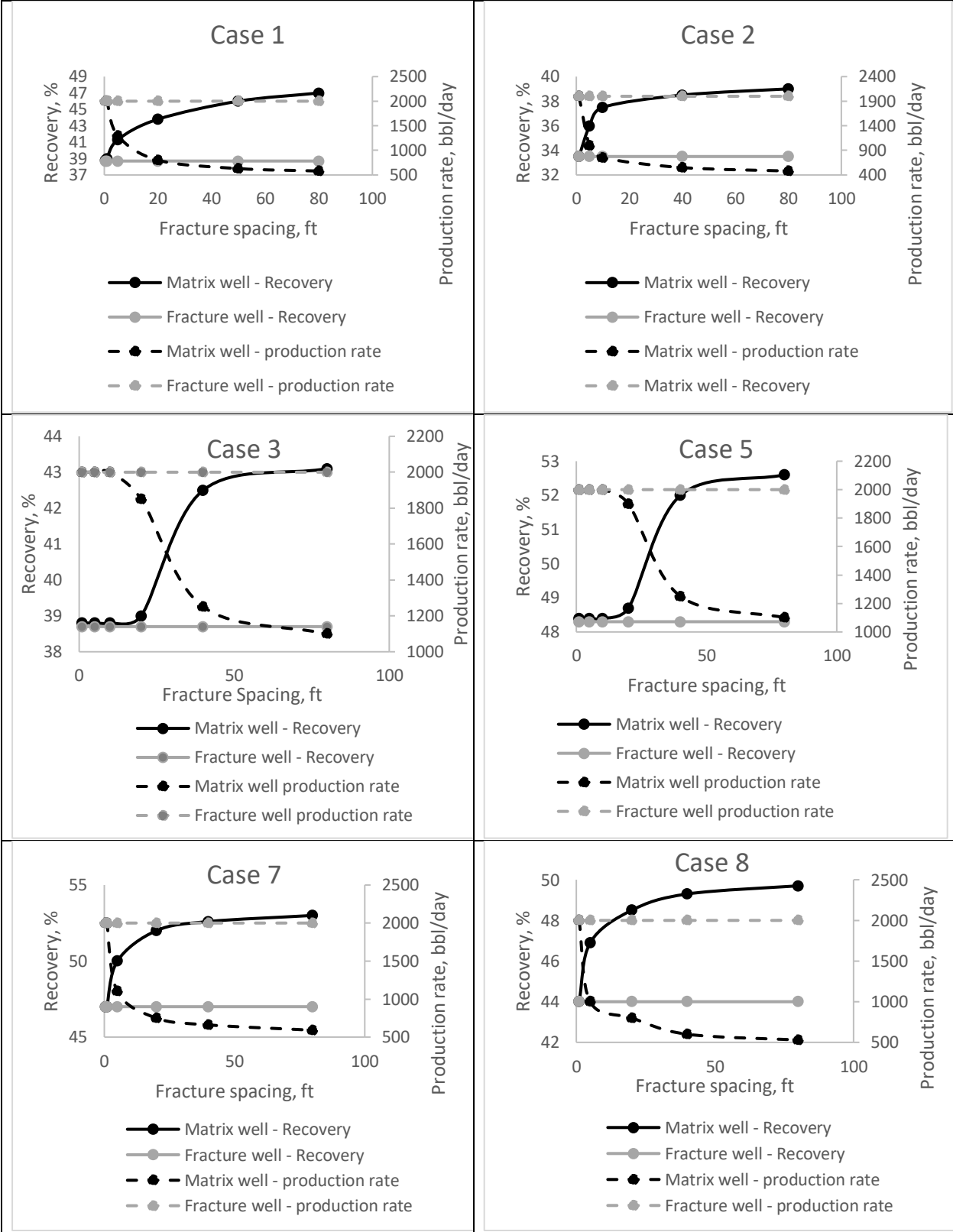


Fig. 4.14. Simulated recovery and production rate as a function of fracture spacing for matrix and fracture well for case 1, 2, 3, 5, 7 and 8 shown in Table 4.7

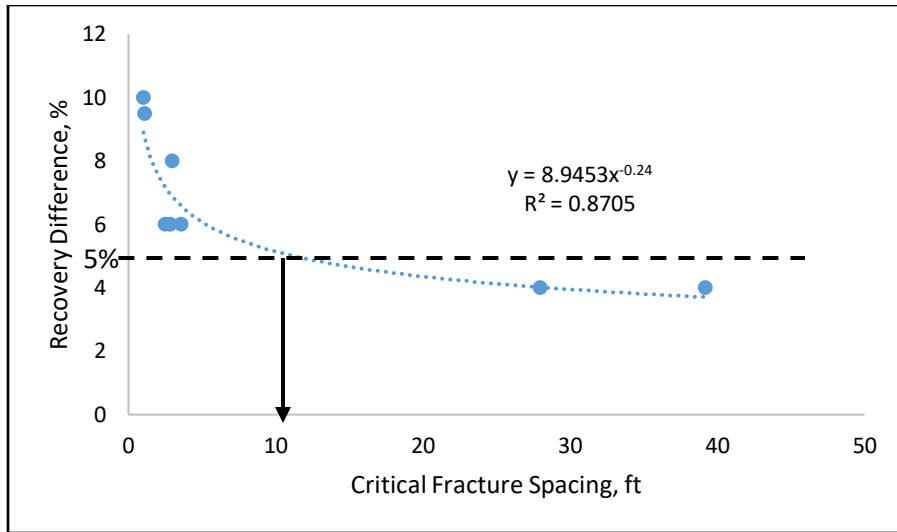


Fig. 4.15. Ultimate recovery difference between matrix and fracture well (for fracture spacing=80ft) as a function of critical fracture spacing revealing an inverse relationship

Placement of well completion in NFRs with planar fracture network would also have an impact on critical oil rate, which needs to be addressed.

4.4 Effect of Well Placement on Critical Rate

In previous chapter, we derived the critical oil rate model for on-fracture completions (Eq. 3.14). However, the critical rate value may significantly vary for matrix-wells with increased fracture spacing as compared to the on-fracture completion in same NFR. Thus, there is a need to study the effect of well-placement on critical-rate values for sparse planar fracture network.

After running simulation for the base-case NFR (Appendix A- Tables A1 and A2) matrix-well (as shown by saturation maps in Fig. 4.16), we observed two coning phenomena occurring at the same time - one in matrix-zone (exclusion-zone), and another in fractured-network zone, that causes the typical cone profile as shown in Figs. 4.16 and 4.17a. From Fig. 4.17a, it can be inferred that the cone in matrix-zone would breakthrough from underneath the wellbore, while cone in fractured-zone (being far from the well) would breakthrough after reaching the level until the bottom of perforation, and then flowing horizontally across the matrix-zone. Critical-rate of such matrix-well would depend on whichever cone reaches well first.

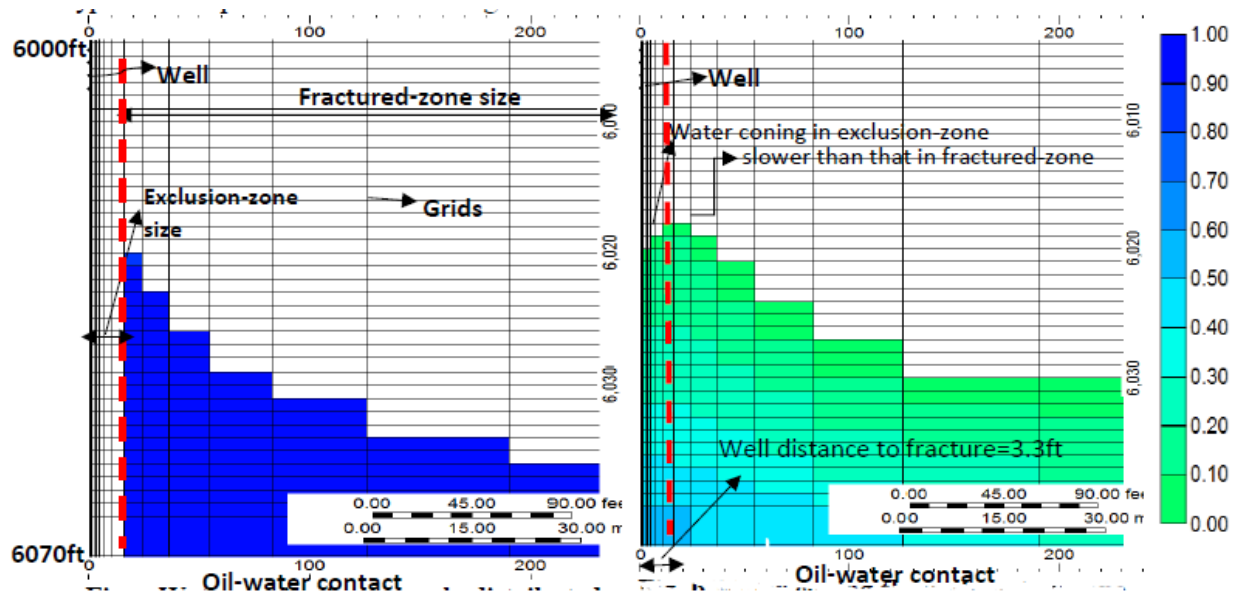


Fig. 4.16. Dual water coning in a matrix-well (NFR-base case)-base case properties Tables A1 and A2

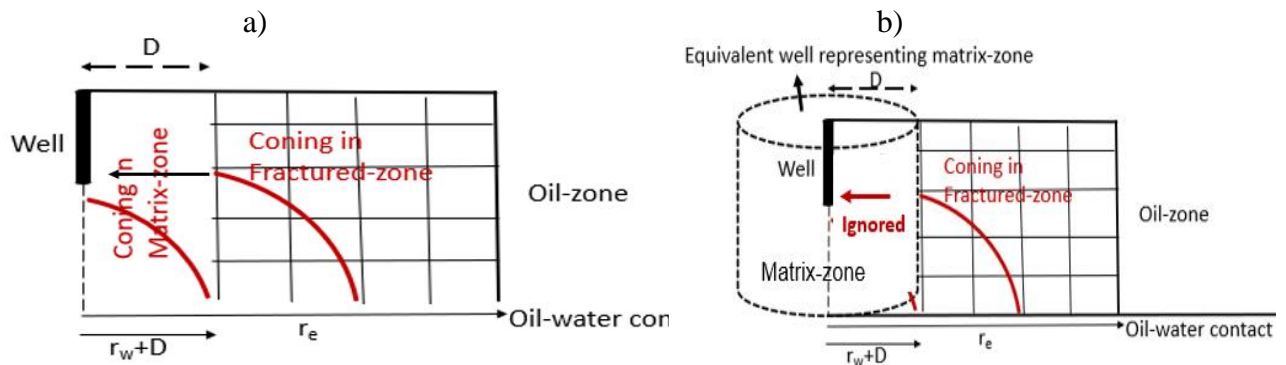


Fig. 4.17. a) Dual water coning profile in matrix-well; b) Equivalent well representing matrix-zone for modeling the critical-oil rate of a cone in fractured-zone

Critical-rate for coning in the fractured-zone (of a matrix-well) can be obtained from an already developed formula for fully fractured-zone i.e. Eq. 3.14 by considering a radial matrix-zone with an equivalent well, so that the new replaced system can be assumed to have an equivalent well intersecting the fractured-zone as shown in Fig. 4.17b. The main assumption is that flow across the matrix-zone is ignored (Fig. 4.17b). Since the well's critical pressure drop (without water breakthrough) derives from near wellbore phenomena, it would be independent of NFR

lateral (drainage) size for fracture-well. This implies that critical pressure drawdown would be the same for two different reservoir sizes. Or,

$\Delta P_{critical}$ for an equivalent fracture-well = $\Delta P_{critical}$ for a fracture-well from same NFR

Or,

$$q_{cr, equivalent\ fracture-well} \times \left(\ln \left(\frac{r_e}{r_w + D} \right) + S \right) = q_{cr, fr} \times \left(\ln \left(\frac{r_e}{r_w} \right) + S \right) \quad (4.21)$$

Since, critical rate for an equivalent fracture-well replacing the matrix-zone is same as the critical rate for a fractured-zone, above formula Eq. 4.21 can be written as,

$$q_{cr, fractured-zone} = q_{cr, fr} \times \frac{\left(\ln \left(\frac{r_e}{r_w} \right) + S \right)}{\left(\ln \left(\frac{r_e}{r_w + D} \right) + S \right)} \quad (4.22)$$

Substituting Eq. (3.14) as a formula for $q_{cr, fr}$ in Eq. (4.22), we get,

$$q_{cr, fractured-zone} = 0.0783 \times 10^{-4} \frac{k_{fm} h_o^2}{B_o \mu_o} (\Delta \rho) \left(1 - \left(\frac{h_{op}}{h_o} \right)^2 \right) \left(0.735 + 1.86 \frac{r_e}{h_o \sqrt{\frac{k_{fv}}{k_{fh}}}} \right) \times \frac{\left(\ln \left(\frac{r_e}{r_w} \right) + S \right)}{\left(\ln \left(\frac{r_e}{r_w + D} \right) + S \right)} \quad (4.22a)$$

where, D is the radial size of matrix-zone in a matrix-well and S is the partial-penetrating skin factor (Papatzacos 1986), given by,

$$S = \left(\frac{1}{h_{pD}} - 1 \right) \ln \frac{\pi}{2r_D} + \frac{1}{h_{pD}} \ln \left[\frac{h_{pD}}{2+h_{pD}} \left(\frac{A-1}{B-1} \right)^{1/2} \right] \quad (4.23)$$

$$r_D = (r_w/h_o) \left(\frac{k_{fv}}{k_{fh}} \right)^{1/2} ; \quad h_{pD} = h_{op}/h_o ; \quad A = 4/h_{pD} ; \quad B = 4/3h_{pD}$$

The critical-rate for coning in exclusion-zone (matrix-zone) can be obtained by idealizing the radius of fractured-zone with an equivalent radius of matrix-zone, so that the entire reservoir becomes a matrix-only reservoir as shown in Fig. 4.18. The concept behind such idealization is to

make both the system in Fig. 4.18 flow-equivalent, so they undergo the same pressure drawdown for the same production rate. The equivalent matrix-zone drainage size, $r_{e,eq}$ can be computed by using simple Darcy law as,

$$\left(\frac{\Delta P}{q}\right)_{system\ 2} = \left(\frac{\Delta P}{q}\right)_{system\ 1} \quad (4.24)$$

So, equivalent matrix-zone drainage size, $r_{e,eq}$ for a given combination of matrix-zone and fractured-zone arranged in series can be computed based on the above idealization approach, as,

$$\frac{k_m}{\ln\left(\frac{r_{e,eq}}{r_w+D}\right)} = \frac{k_f}{\ln\left(\frac{r_e}{r_w+D}\right)} \Rightarrow r_{e,eq} = (r_w + D)e^{\frac{k_m}{k_{f,m}} \ln\left(\frac{r_e}{r_w+D}\right)} \quad (4.25)$$

$$\frac{dr_{e,eq}}{dD} = e^{\frac{k_m}{k_{f,m}} \ln\left(\frac{r_e}{r_w+D}\right)} \times \left(1 - \frac{k_m}{k_{f,m}}\right) > 0 \quad (\text{always greater than zero}) \quad (4.26)$$

After replacing the combined radius of matrix-zone and fractured-zone with an equivalent matrix drainage radius, $r_{e,eq}$, semi-analytical critical-rate formula of an equivalent matrix-only reservoir as developed by Chaperon (1986) for short penetration, would be given by,

$$q_{cr,matrix-zone} = 0.0783 \times 10^{-4} \left[\frac{\Delta\rho k_o (h_o^2)}{\mu_o B_o} \right] \left[0.7311 + \frac{1.943}{\frac{r_{e,eq}}{h_o} \sqrt{\frac{k_v}{k_h}}} \right] \quad (4.27)$$

From Eqs. (4.25) and (4.26), we can write,

$$\frac{d\left(\frac{1}{r_{e,eq}}\right)}{dD} < 0, \text{ or } \frac{d(q_{cr,matrix-zone})}{dD} < 0 \quad (4.28)$$

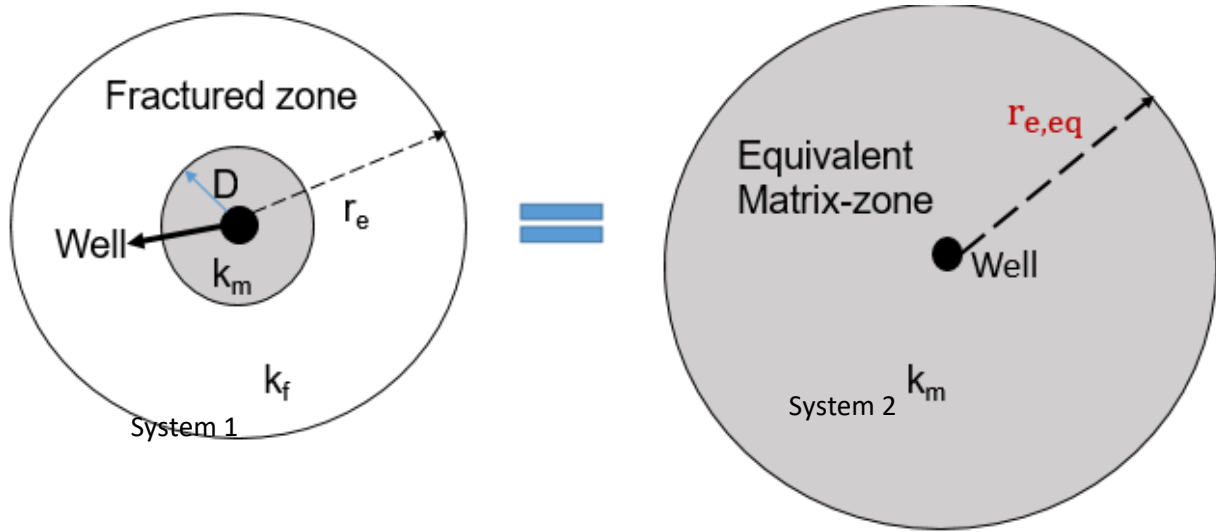


Fig. 4.18. Equivalent Matrix Zone idealized from exclusion zone and fractured zone arranged in Series

With the increase in radial size of matrix-zone (or the distance of the fracture network from the well), while the formula Eq. 4.22 suggest that the critical rate increases for coning in the fractured-zone as shown by line AD in Fig. 4.19, Eq. 4.28 implies that critical-rate is a decreasing function of matrix-zone radius for coning in the matrix-zone shown by line EC in Fig. 4.19. At certain point, the critical rate profiles for both the zones intersect at point B, as shown in Fig. 4.19. Obviously, critical-rate for the matrix-well would be the smaller critical-rate value (for two profiles) which would be the region below intersection point B.

In order to verify the critical rate model of matrix well for large well's distance to the fracture, we perform simulations on the base case NFR using the fracture properties shown in Table D1. The plot Fig. 4.19 shows that the predicted critical rate demonstrated by line ABC for the base case NFR matches well with the simulated critical rate shown by line AC. From the formula Eq. 4.22a, it is quite evident that fracture-well's (on-fracture well's) formula is a limit to the matrix-well's (off-fracture well's) formula, when the distance to the fracture reduces to zero (i.e. when $D=0$ in Eq. 4.22), demonstrated by point A. Maximum radial matrix-zone size for the

matrix-well is hypothetically equal to the half the maximum fracture spacing (1300 ft; Ozkaya and Minton 2005) in a radial setting. Beyond that, off-fracture well's critical-rate converges to that of matrix-only reservoir when its distance to fracture reaches the well's drainage size (i.e., point when fractured-zone diminishes) demonstrated by point C.

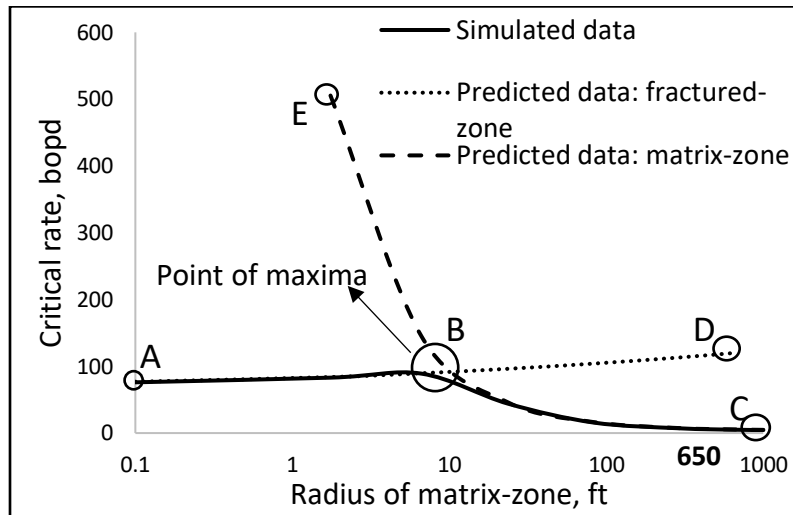


Fig. 4.19. Simulated and predicted critical rate as a function of radial sizes of matrix-zone for a given base case NFR- Appendix A (Tables A1 and A2)

Summary

Using the literatures reported on fracture network connectivity, fracture network can be classified into planar and channel fracture network (fracture corridors). Although planar fracture network could be modeled as orthogonal network of DPDP model (using idealized continuum approach) as reported in the literatures, modeling channel (fracture corridor) network would require discrete sheet-like network DPDP model. The study, further, showed how on/off-fracture well placement in these fracture networks can be modeled using CMG DPDP model. Following conclusions can be summarized from this study;

- 1) Planar fracture network can be classified into two types based on fracture spacing and flow performance: 1) densely distributed fracture network, 2) Sparsely distributed fracture network.
- 2) A 2D radial cylindrical DPDP simulator is used to model planar fracture network, whereas 3D discrete cartesian DPDP reservoir simulator is used for channel (fracture corridor) network.
- 3) The study showed that for different single-completed wells placed on/off fracture in the same densely-distributed planar fracture system, recovery performance hardly changes. Moreover, dual-completed (DWS) well recovers more than single-completed well and the recovery is not dependent on well's completion placement that makes DWS well a better performer eliminating any uncertainties associated with the well placement.
- 4) Effect of well placement on flow performance can be addressed using qualification of densely and sparsely distributed planar fracture network. The study derived an analytical model of minimum (critical) fracture spacing at which recovery between matrix vs. fracture well in the same NFR would differ – a basis of qualification of densely vs. sparsely distributed fracture network.
- 5) Modeling showed that the minimum fracture spacing model is not only a function of static NFR properties but also dynamic well-design and operational parameters. The model of critical fracture spacing is further verified by running a series of testing sample of simulated experiments representing wide variety of NFRs by varying parameters including fracture-to-matrix permeability ratio, fracture anisotropy ratio, penetration ratio and drainage radius. The analytical model results are found to be in good agreement with actual simulations.

- 6) The study showed that the critical fracture spacing is a strong qualitative indicator of the contrast in the ultimate recovery between fracture and matrix well with the increase in fracture spacing. Higher the critical spacing ($>10\text{ft}$), lower is the contrast which reveals operator do not need to worry about well placement issue in such NFRs. On the other hand, lower critical spacing ($<10\text{ft}$) signifies large difference in matrix and fracture well's recovery at higher fracture spacing. Moreover, typical planar fracture network NFRs demonstrate a lower critical spacing value, which implies that most of the planar network NFRs are sparsely distributed.
- 7) We consider the effect of off-fracture well placement in sparsely distributed planar fracture network to derive the matrix-well critical oil rate. By mechanistically including the effect of well's distance to the nearest fracture in a critical rate formula for fracture-well in NFR, we propose a new critical rate formula for wells completed in matrix block of fracture corridor-NFR. After comparing with the simulated data for matrix wells in base case NFR, the model matches well with the simulated data.
- 8) Two simultaneous coning phenomena was observed in these wells, one in fractured zone and other in matrix-zone. Coning in fractured-zone display continuous increase in the critical rates with increasing well's distance to fractures. Whereas, coning in matrix-zone display a continuous reduction in critical rate with increasing well's distance to fracture and the difference with that of matrix-only reservoir relates to their distance to nearest fracture and matrix-to-fracture permeability ratio. At certain point, the critical-rate for both the zones intersect and the region below this intersection point demonstrate the critical rate for the matrix-well system with different well placements in matrix-zone. It is also shown

the off-fracture well's critical-rate formula reduces to on-fracture well's formula when the matrix-zone size reduces to zero.

Chapter 5. Water-Cut Pattern and Well-Spacing

The Chapter investigates the water-cut pattern both for single porosity reservoir and NFR, and proposes a method to optimize the well spacing by relating it with water-cut and recovery. One of the characteristic water-cut patterns for an uncontained SPR with constant pressure bottom aquifer is when water-cut reaches ultimate water-cut as reported by Kuo and Desbrisay 1983 and Shirman and Wojtanowicz 2000. The latest model of ultimate water-cut, WCult, by Shirman and Wojtanowicz 2000 is,

$$\text{WCult} = \left(1 - \frac{q_{cr}}{Q}\right) \frac{Mh_w}{Mh_w + h_o} \quad (5.1)$$

However, in a real multi-well SPR with a finite drainage boundary, due to depletion of oil, water-cut would never stabilize but would undergo continuous increase until it reaches the value of 1. Thus, there is a need to perform both qualitative and quantitative analysis of post-breakthrough water-cut development and its pattern in relation to well spacing, both for single porosity reservoirs (SPR) and naturally fractured reservoirs (NFRs). The chapter would further evaluate the effect of typical water-cut patterns of NFR including water-cut stabilization on its recovery performance.

5.1 Water-Cut vs. Well Spacing in SPR

5.1.1 Effect of Well Spacing on Ultimate Water-Cut

A reservoir simulation study is carried out here to determine water cut development pattern

Section 5.1 and 5.2 of this chapter previously appeared as Journal paper 2018 on “Determination and Implication of Ultimate Water-Cut in Well-Spacing Design for Developed Reservoirs with Water Coning” published in *Journal of Energy Resources Technology* 140 (8), 082902. Reproduced with permission of ASME. See Appendix F for more details.

Section 5.3, 5.4 and 5.5 of this chapter previously appeared as Journal Paper 2020 on “Stabilized Water-cut in Carbonate Naturally-Fractured Reservoirs with Bottom-Water with an Implication in Well Spacing Design for Recovery Optimization” in *Journal of Energy Resources Technology* 142, no. 3 (2020), 082902. Reproduced with permission of ASME. See Appendix F for more details.

in the closed drainage area. A 2-D radial-cylindrical model is built with IMEX simulation software depicted in Fig. 5.1 using properties of reservoir #7 presented in Table 5.1. In the model, the oil-pay zone has a no-flow boundary and produced water is injected back to the aquifer at the constant-pressure boundary in order to represent a strong aquifer. Moreover, the production well is completed in the top half of the total oil-zone thickness and the capillary pressure transition zone is neglected.

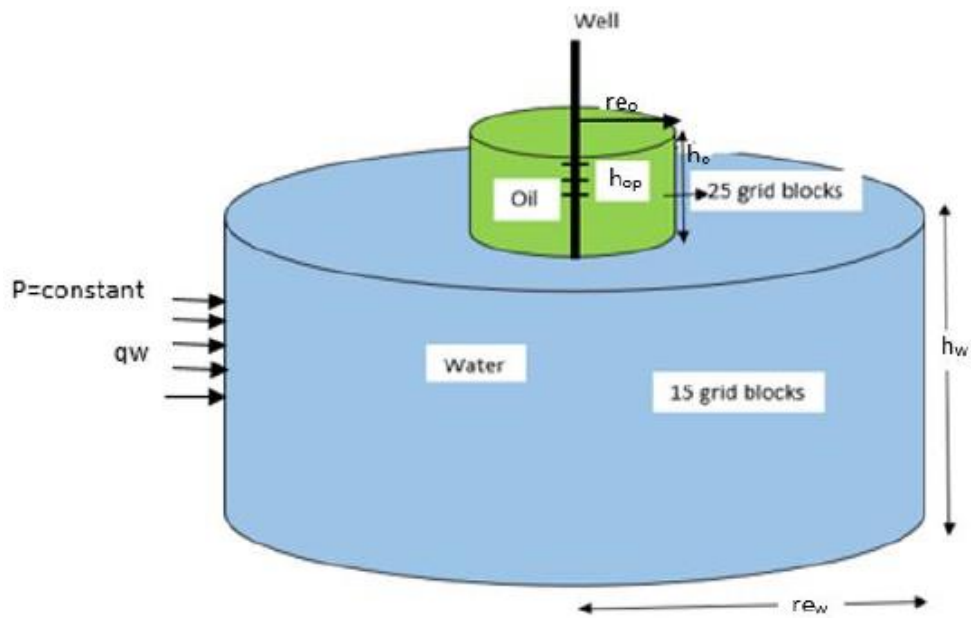


Fig 5.1. Radial model of oil with constant pressure bottom water

Table 5.1. Reservoir and Well data

Property	Unit	Value
Reference pressure	psi	6000
Formation oil volume factor	rb/stb	1.2
Water compressibility	1/psi	3.3202e--6
Oil compressibility	1/psi	1.50E-05
water viscosity	cp	0.5
Oil viscosity	cp	1.5, vary
oil density	lb/cuft	43.6559
Water density	lb/cuft	60.5489
Bubble point	psi	100

Firstly, we consider the effect of well spacing, $2r_e$, on the water cut and slope of water-cut change in time at constant production rate (2000 bpd, simulation run #7), shown in Fig. 5.2. At early times, there is a rapid increase of water cut during the water cone buildup stage followed by the WC slow-advancement stage. At the latter stage, for the BOR drainage system, WC reaches constant value of WCult. In contrast, for the NFB systems, WC never stabilizes and continues slow increase till WC=1. If well's drainage area is large enough such that the drainage size exceeds the lateral length of water cone at the end of water cone buildup (expansion) stage, the late-time WC slow-advancement stage for NFB system is controlled mostly by the oil-pay depletion as the effect of the water cone expansion becomes negligible and can be ignored. Thus, during this stage, the rate of water-cut increase is:

$$\frac{\Delta(WC)}{\Delta t} = \frac{(WC)_{t+\Delta t} - (WC)_t}{\Delta t} = \frac{\left(1 - \frac{q_{cr}}{Q}\right) \frac{M(h_w + \Delta h_w)}{M(h_w + \Delta h_w) + (h_o - \Delta h_o)} - \left(1 - \frac{q_{cr}}{Q}\right) \frac{M h_w}{M h_w + h_o}}{\Delta t} \quad (5.2)$$

And the pay-zone depletion is,

$$\Delta h_w = \Delta h_o = \frac{q_o \Delta t}{\pi r_e^2 \phi_m (1 - S_{wc} - S_{or})} = \frac{(1 - WC) Q \Delta t}{\pi r_e^2 \phi_m (1 - S_{wc} - S_{or})} \quad (5.3)$$

Substituting Δh_w and Δh_o from Eq. (5.3) in Eq. (5.2), we get:

$$\frac{\Delta(WC)}{\Delta t} = \frac{\left(1 - \frac{q_{cr}}{Q}\right) \frac{M \left(h_w + \frac{(1 - WC) Q \Delta t}{\pi r_e^2 \phi_m (1 - S_{wc} - S_{or})} \right)}{M \left(h_w + \frac{(1 - WC) Q \Delta t}{\pi r_e^2 \phi_m (1 - S_{wc} - S_{or})} \right) + \left(h_o - \frac{(1 - WC) Q \Delta t}{\pi r_e^2 \phi_m (1 - S_{wc} - S_{or})} \right)} - \left(1 - \frac{q_{cr}}{Q}\right) \frac{M h_w}{M h_w + h_o}}{\Delta t} \quad (5.4)$$

Oil water contact (OWC) advancement due to oil zone depletion may begin before the completion of water cone buildup stage, if the well-spacing is smaller than lateral length of water cone (defined here by threshold well-spacing). This may result in elevated slope of WC due to partly mixing of water cone expansion stage and oil depletion stage. Formula Eq. (5.4) explains different slopes of water-cut vs. time during late WC stage. Predictably, the slope reduces with the increase in well-spacing and, for well spacing greater than the threshold value ($2r_e = 4400$ ft, in

this case) the WC value at the beginning of late WC stage, can be assumed stabilized (since there is a clear separation between late slow WC advancement stage and the rapid water-cut increase stage due to water cone expansion) and equal to the constant value for the BOR drainage system. We define this condition as a pseudo-stabilized stage of water cut that occurs when the water cut increase rate becomes equal to Eq. 5.4 for well-spacing greater than the threshold well-spacing.

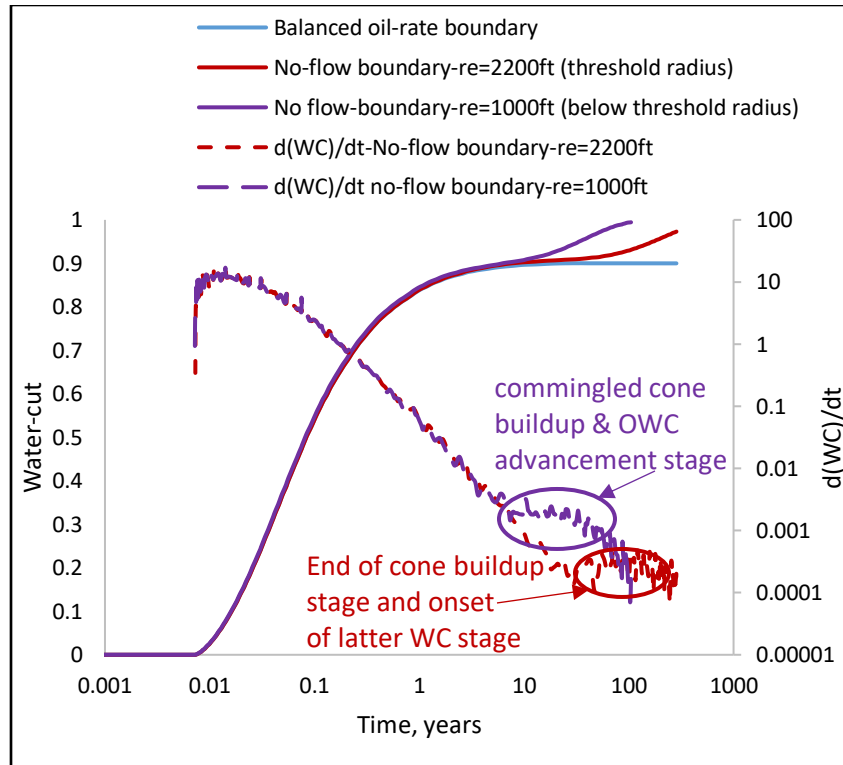


Fig. 5.2. Water cut pattern (Reservoir # 7) for different size of well spacing ($Q=2000\text{ bbl/day}$) depicting pseudo-stabilization at well-spacing equal to threshold spacing

For the example reservoir in Fig. 5.2 (with threshold well spacing 4,400ft), water-cut would almost stabilize after 4015 days of production at the pseudo WC_{ult} value=0.9, that is obtained by matching the simulated WC increase rate with the calculated increase rate from Eq. 5.4. For larger well spacing, the value of pseudo WC_{ult} would still be 0.9; however, for well spacing below threshold spacing (4,400ft), water cut would not be considered stabilized due to partly mixing of OWC advancement stage and the water cone buildup stage resulting in an elevated slope. *This*

implies that for every reservoir there is a minimum (threshold) value of well spacing below which water cut would never reach the pseudo stabilization stage.

5.1.2 Threshold Radius Correlation – Minimum Well Spacing

We determine threshold radius statistically using large number of simulated experiments for variety of well/reservoir system. Since Appendix D shows that the threshold radius is almost independent of production-rate, simulated experiments would be carried for any one production-rate (2000bbl/day chosen randomly). The resulting correlation would include reservoir properties ignored in Eq. (5.1): horizontal permeability, anisotropy ratio ($\frac{k_v}{k_h}$) and penetration ratio ($\frac{h_{op}}{h_o}$) (Note that Eq.5.1 considers only the effect of oil-pay thickness, mobility ratio and aquifer thickness). We use the Box and Behnken method (Cavazzuti 2013; Ferriera et al. 2007) to create a three-level factorial design matrix of simulated experiments shown in Table 5.4. Three level design would capture non-linear effects while minimizing the number of experiments (Cavazzuti 2013). Three levels of the reservoir properties are chosen based on the practical field-range values of these parameters (Table 5.2). The design stipulates a total of 54 different runs (reservoir/aquifer systems). For each system, a series of simulation runs is performed to determine the threshold radius - systematically increasing the size of drainage area until water cut becomes practically stable. The results - shown in Table 5.3 - are then used to develop empirical formula for threshold radius using the Response Surface method at production rate, $Q = 2000bbl/day$. The formula for threshold radius is:

$$r_{eTh} = 14920.6 - 3563.7M - 68.5h_w - 34586\frac{k_v}{k_h} + 99.65h_o + 288M^2 + 0.107h_w^2 + 31290\left(\frac{k_v}{k_h}\right)^2 + 1.5Mh_w - 0.55Mk_h - 10.13Mh_o - 0.087h_w h_o + 0.1k_h h_o \quad (5.5)$$

Table 5.2. Three-level values of different reservoir/aquifer system parameters

Levels	Oil-pay thickness, h_o	Mobility (M)	Aquifer thickness (h_w)	Horizontal permeability (k_h)	Penetration ratio (h_{op}/h_o)	Anisotropy ratio ($\frac{k_v}{k_h}$)
Low (-1)	25	1	20	50	0.2	0.01
Intermediate (0)	75	3	75	100	0.5	0.1
High (+1)	150	10	500	500	0.8	1

Table 5.3. Minimum well-spacing ($2r_{eTh}$) for various reservoir/aquifer system; $Q=2000$ bbl/day

Reservoir Aquifer System #	Oil-pay thickness, h_o	Mobility (M)	Aquifer thickness (h_w)	Horizontal permeability (k_h)	Penetration ratio (h_{op}/h_o)	Anisotropy ratio ($\frac{k_v}{k_h}$)	Threshold radius, ft (r_{eTh})
1	25	1	75	50	0.5	0.1	4000
2	25	1	75	500	0.5	0.1	7000
3	25	10	75	50	0.5	0.1	1000
4	25	10	75	500	0.5	0.1	1000
5	150	1	75	50	0.5	0.1	16000
6	150	1	75	500	0.5	0.1	28000
7	25	3	75	100	0.5	0.1	2200
8	150	10	75	50	0.5	0.1	4000
9	150	10	75	500	0.5	0.1	4000
10	75	1	20	100	0.2	0.1	16000
11	75	1	20	100	0.8	0.1	16000
12	25	3	75	100	0.8	1	1000
13	75	1	500	100	0.2	0.1	5000
14	75	1	500	100	0.8	0.1	5000
15	75	10	20	100	0.2	0.1	3000
16	75	10	20	100	0.8	0.1	3000
17	75	10	500	100	0.2	0.1	1350
18	75	10	500	100	0.8	0.1	1350
19	75	3	20	50	0.5	0.01	8000
20	75	3	20	50	0.5	1	7000
21	75	3	20	500	0.5	0.01	13000
22	75	3	20	500	0.5	1	12000
23	75	3	500	50	0.5	0.01	3000
24	75	3	500	50	0.5	1	1350
25	75	3	500	500	0.5	0.01	5000
26	75	3	500	500	0.5	1	3000

(Cont'd.)

Reservoir Aquifer System #	Oil-pay thickness, h_o	Mobility (M)	Aquifer thickness (h_w)	Horizontal permeability (k_h)	Penetration ratio (h_{op}/h_o)	Anisotropy ratio ($\frac{k_v}{k_h}$)	Threshold radius, ft (r_{eTh})
27	25	3	75	50	0.2	0.1	2000
28	25	3	75	50	0.8	0.1	2000
29	25	3	75	500	0.2	0.1	3500
30	25	3	75	500	0.8	0.1	3500
31	150	3	75	50	0.2	0.1	8000
32	150	3	75	50	0.8	0.1	8000
33	150	3	75	500	0.2	0.1	14000
34	150	3	75	500	0.8	0.1	14000
35	75	1	75	100	0.2	0.01	16000
36	75	1	75	100	0.2	1	8000
37	75	1	75	100	0.8	0.01	16000
38	75	1	75	100	0.8	1	8000
39	75	10	75	100	0.2	0.01	4000
40	75	10	75	100	0.2	1	850
41	75	10	75	100	0.8	0.01	4000
42	75	10	75	100	0.8	1	850
43	25	3	20	100	0.5	0.01	4500
44	25	3	20	100	0.5	1	4000
45	25	3	500	100	0.5	0.01	2000
46	25	3	500	100	0.5	1	1000
47	150	3	20	100	0.5	0.01	18000
48	150	3	20	100	0.5	1	16000
49	150	3	500	100	0.5	0.01	8000
50	150	3	500	100	0.5	1	4000
51	75	3	75	100	0.5	0.1	4400
52	75	3	75	100	0.5	0.1	4400
53	75	3	75	100	0.5	0.1	4400
54	75	3	75	100	0.5	0.1	4400

The formula gives statistically significant relationship between threshold radius (i.e well spacing) and five properties of the well-reservoir system: mobility, aquifer thickness, oil zone thickness, anisotropy ratio, and horizontal permeability. Other properties in Table 5.2 including penetration ratio are statistically insignificant. Moreover, possible application of pseudoWCult concept applies only to thin reservoirs ($h_o < 25ft$), where threshold well-spacing is within the practical range of well-spacing used in multi-well reservoirs. The next logical step is to develop a

generalized formula for pseudo-ultimate water-cut, pseudoWCult with no simplifying assumptions used in Eq. 5.1.

5.1.3 Pseudo Ultimate Water-Cut Formula

To derive a new ultimate water-cut model for NFB system, we consider well's deliverability reduction due partial penetration and the radial water inflow underneath the wellbore (as shown in Fig.5.3), ignored in the previous ultimate water-cut model Eq. 5.1 addressed in Chapter 2. In the derivation, we consider:

- 1) The pseudoWCult occurring for stabilized well inflow condition when $dWC/dt = 0.0009/yr \approx 0$;
- 2) Oil inflow distortion due to partial well's penetration of the oil payzone;
- 3) Water inflow to a final-size spherical water sink at the oil-water contact, OWC;
- 3) Small size of semispherical water inflow region comparing to the radial aquifer size;
- 4) Oil-zone bounded by a no-flow boundary, and strong aquifer having a constant pressure boundary.

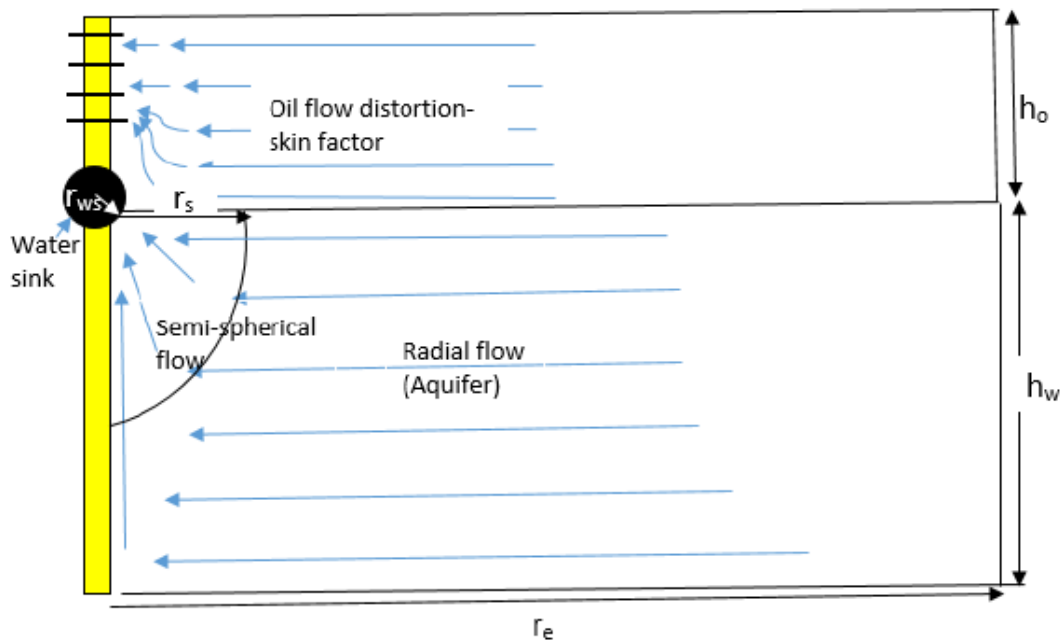


Fig.5.3. Oil and water inflow schematics representing the flow distortion due to partially-penetrating oil-zone and the semi-spherical flow due to water-sink

The new model of ultimate water-cut (Eq. C-9 in Appendix C) is given by:

$$\text{pseudoWCult} = \left(1 - \frac{q_{cr}}{Q}\right) \left\{ 1 + \frac{h_o}{Mh_w(\ln r_e/r_w + S)} \left[\ln r_e/r_w + \frac{h_w(1-\frac{1}{r_{Ds}})}{0.5h_{op}^3 \sqrt{k_v/k_h}} \ln \left(\frac{h_{op}}{r_w}\right) \right] \right\}^{-1} \quad (5.6)$$

where, S is the skin factor defined by Eq. (C-7), r_{Ds} is the dimensionless semi-spherical water inflow radius, r_s/r_{ws} , and r_{ws} is water-sink radius: $r_{ws} = \frac{0.5h_{op}}{\ln\left(\frac{h_{op}}{r_w}\right)}$, defined by Eq. C-2. Dimensionless water inflow radius, r_{Ds} is the only unknown parameter in Eq. (5.6). Practical use of the new ultimate water-cut formula (Eq.C-9)), requires known value of the semi-spherical water inflow radius, r_s . The value is determined, here, by matching the new formula with experimental (simulated) pseudo ultimate water-cut values in Table 5.4 using the dimensionless semi-spherical water inflow radius ($r_{Ds} = r_s/r_{ws}$) as a matching parameter. The matching correlates the water inflow radius with other parameters of reservoir-aquifer system such as mobility ratio, partial penetration, horizontal permeability, anisotropy ratio and aquifer thickness. The matching values of r_{Ds} are shown in Table 5.4.

The r_{Ds} values in Table 5.4 are very close to unity (i.e. the value of r_s is small and very close to r_{ws}) that makes the water flow distortion effect small and concentrated around the wellbore.

After running statistical analysis with SAS using 54 experimental runs again (from Table 5.4), we obtain the regression coefficients of all possible regressors for a 2nd order model. Subsequently, after eliminating insignificant parameters, we obtained a simple regression model of dimensionless water inflow radius as,

$$r_{Ds} = 1.2 - 8.9 \times 10^{-4}h_w - 0.21 \frac{h_{op}}{h_o} + 1.2 \times 10^{-6}h_w^2 + 5 \times 10^{-4} \frac{h_{op}}{h_o} \times h_w \quad (5.7)$$

Table 5.4. Semi-spherical water inflow radius using experimental matrix of Table 5.3

Reservoir Aquifer System #	Simulated pseudo WCult	D-less water inflow radius, r _{Ds}	Reservoir Aquifer System #	Simulated pseudo WCult	D-less water inflow radius, r _{Ds}	Reservoir Aquifer System #	Simulated pseudo WCult	D-less water inflow radius, r _{Ds}
1	0.751	1.045	19	0.530	1.075	37	0.550	0.99
2	0.745	1.05	20	0.524	1.075	38	0.527	0.994
3	0.968	1.044	21	0.527	1.074	39	0.928	1.1
4	0.967	1.048	22	0.521	1.076	40	0.953	1.1
5	0.416	1.045	23	0.872	1.065	41	0.925	0.993
6	0.412	1.046	24	0.941	1.06	42	0.920	0.99
7	0.900	1.045	25	0.874	1.065	43	0.727	1.075
8	0.881	1.047	26	0.938	1.07	44	0.746	1.078
9	0.881	1.043	27	0.894	1.1	45	0.899	1.065
10	0.374	1.14	28	0.916	0.99	46	0.964	1.06
11	0.229	1.01	29	0.894	1.1	47	0.379	1.074
12	0.912	0.99	30	0.916	0.99	48	0.364	1.076
13	0.836	1.053	31	0.769	1.1	49	0.850	1.063
14	0.758	1.077	32	0.633	1	50	0.911	1.066
15	0.867	1.13	33	0.765	1.1	51	0.795	1.05
16	0.752	1.01	34	0.631	1	52	0.795	1.05
17	0.981	1.053	35	0.605	1.07	53	0.795	1.05
18	0.967	1.077	36	0.654	1.09	54	0.795	1.05

We also find that the final regression model matches the simulation results with R-squared value at 0.98. To verify new formula Eq. 5.6, we compare calculated values from Eq. (5.1) and Eq. (5.6) for variety of well-reservoir systems shown in Table 5.3. The comparison plot is shown in Fig.5.4.

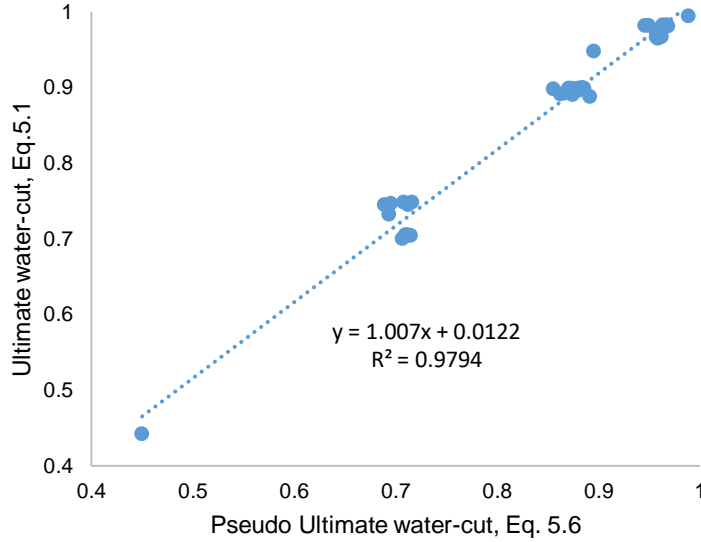


Fig. 5.4. Comparison of ultimate water-cut using presently-used formula, Eq.(5.1) and new formula, Eq.(5.6)

It appears from the unit-slope correlation plot that both formulas give practically the same results, i.e. Eq. (5.1) sufficiently predicts ultimate water-cut, $\text{pseudoWCult} \approx \text{WCult}$

The above observation leads to conclusion that the combined effects of flow distortion in the oil and water-zones does not affect upwards expansion of the water cone and the resultant value of water-cut. Additional well pressure drawdown due to partial penetration of oil pay-zone is hydraulically transmitted to the water-zone thus concurrently changing inflow of the two fluids without changing the water/oil ratio, i.e. water cut. When combined, the two effects counterbalance each other, so the overall effect is practically null. Comparing equations (5.1) and (5.6) gives,

$$\ln r_e/r_w + S \cong \ln r_e/r_w + \frac{h_w(1-\frac{1}{r_{Ds}})}{0.5h_{op} \sqrt[3]{k_v/k_h}} \ln \left(\frac{h_{op}}{r_w} \right)$$

Or,

$$S \cong \frac{h_w(1-\frac{1}{r_{Ds}})}{0.5h_{op} \sqrt[3]{k_v/k_h}} \ln \left(\frac{h_{op}}{r_w} \right) \tag{5.8}$$

The left side of Eq. 5.8 is the skin factor in the oil-zone due partial penetration and the right side expression determines “skin” in the water-zone due semi-spherical component of water flow. The formula Eq. (5.8) also provides for analytical estimation of the size of semi-spherical flow region in the aquifer, r_{DS} from the known value of partial penetration-skin in the oil pay-zone. Its value is very close to that from the r_{DS} correlation Eq. 5.7, thus it could effectively verify (or replace) the correlation Eq. 5.7.

5.2 Water-cut Stabilization Effect on Well’s Recovery in SPR

In reservoirs with bottom water, ultimate recovery is reached when water cut becomes equal to its economic limit, WC_{ec} , representing the breakeven (zero-profit) cost of daily production. The recovery process may include the pseudo WC_{ult} stage only if WC_{ult} is smaller than WC_{ec} , $WC_{ult} < WC_{ec}$. When WC_{ult} exceeds WC_{ec} , the recovery becomes unprofitable before the WC_{ult} stage is reached. Thus, the ultimate recovery depends on the value of “water-cut economic margin” defined here as $(WC_{ec} - WC_{ult})$ and may also relate to well-spacing.

Shown in Fig. 5.5 are plots of ultimate recovery from the same bottom-water reservoir. The two bottom plots correspond to small and negative WC economic margin. The plots demonstrate strong effect of well-spacing on recovery. They reveal that for the well spacing size smaller than minimum threshold value, $2r_{eTh} = 4400ft$, recovery increases with reduced well spacing. However, well-spacing above its minimum threshold value has practically no effect and recovery is very small. This is because - as shown in Fig. 5.6 - when well drainage area is smaller, at the same WC value more oil is displaced by wider water cone and by the water invasion at the outer boundary. For the large well spacing and the same water-cut value, however, the volumetric ratio of the reservoir invaded by water cone near wellbore and by water invasion at the boundary to total recoverable oil is small – hence smaller recovery.

When the WC margin is large (upper curve in Fig.5.5), recovery value is high and independent from well spacing. In such case, the production stage starting at pseudoWCult continues for long time resulting in the same recovery factor for any size of well-spacing. The effect of water-cut economic margin can be further illustrated with water invasion maps in Fig. 8. For the assumed value of $WC_{ec}=0.91$, the maps in Figs. 5.6a and 5.6b represent ultimate recovery when $WC=WC_{ult}=WC_{ec}$. For small (872ft) well-spacing, ultimate recovery factor, $RF_{ult} = 13.8\%$ and is six-fold greater than that for large well-spacing (4000ft). Thus, for the zero water-cut economic margin, smaller well-spacing would significantly increase recovery. On the other hand, if the economic water-cut value was $WC_{ec}=0.95$, then the maps in Figs. 5.6c-d would correspond to ultimate recovery with water-cut economic margin (0.95-0.91) of 4%. In such case, reducing well spacing from 4000ft to 872ft would practically not increase recovery (43% vs. 45%, respectively).

The above example also shows that relatively small change in the value of water-cut economic margin, 0.04, would give big increase of ultimate recovery factor, from 13.8% to 45% and from 2.12% to 43% for large and small well spacing, respectively. The effect can be explained by plotting recovery factor, RF_{ult} , vs. economic water-cut, WC_{ec} , Fig. 5.7. The plots indicate very small recovery for $WC_{ec}<WC_{ult}=0.91$, as the well's production must stop before the pseudoWCult stage is reached. They also demonstrate dramatic increase of RF_{ult} for small positive values of water-cut economic margin when $(WC_{ec}-WC_{ult})>0$. For such condition, the larger the value of water-cut economic margin is, the more irrelevant the well-spacing becomes- as the three plots (for different well-spacing) converge. It is important to note that oil-water contact advancement begins at the drainage boundary after the water cone growth is complete, as shown in Figs. 5.6.

In summary, the strongest effect on recovery is that of the WC economic margin - a difference between the WCec and WCult values. When WCult is much smaller than WCec, more oil can be recovered during the depletion stage. Moreover, for large values of WC economic margin oil recovery is not only high but is also practically independent from the well spacing (Fig. 5.5) so in this case, larger well-spacing (greater than threshold spacing) and higher production rate for faster recovery, should be considered in optimized design of reservoir development. Prior to optimization, however, a comparison of the pseudoWCult value with the economically-estimated value of WCec should be the first step in deciding on developing an oil pay-zone with water coning problem. When the WC economic margin is small or negative, oil recovery is small but could be increased by reducing well spacing below its threshold size. In such case, however, well spacing shall be designed by considering incremental recovery due to reduced spacing size without reaching the pseudoWCult stage of well's production.

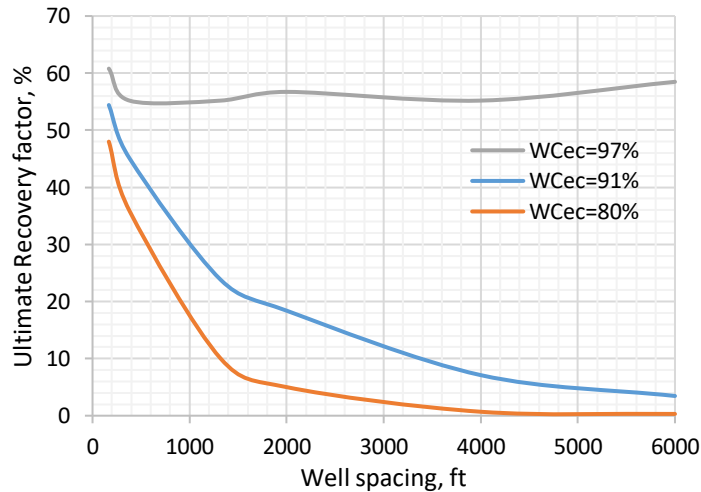
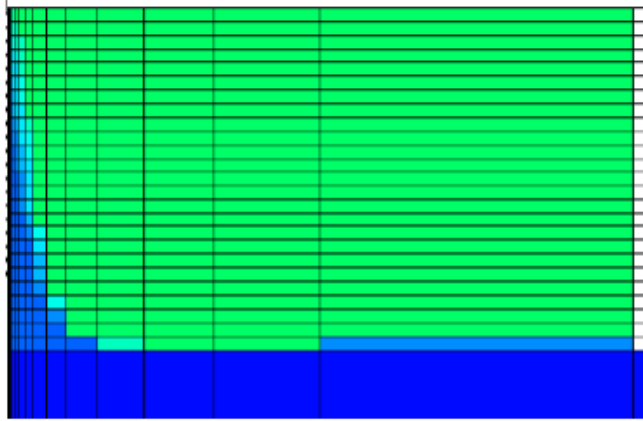
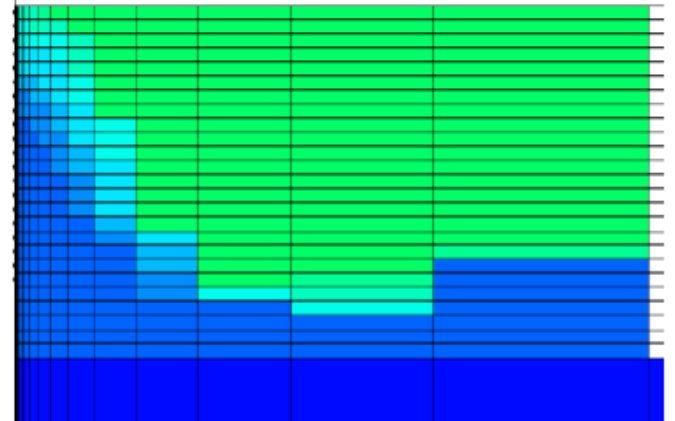


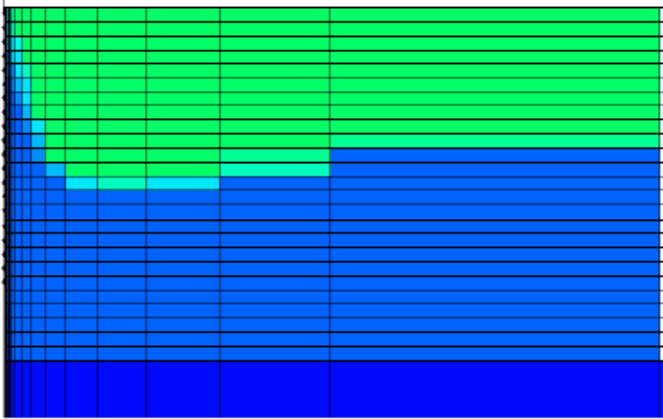
Fig. 5.5. Ultimate recovery vs. well-spacing (Reservoir # 7; Minimum (threshold) well-spacing=4400 ft, pseudoWCult=0.9): Recovery becomes independent of well-spacing at (WCec-pseudoWCult)>>0



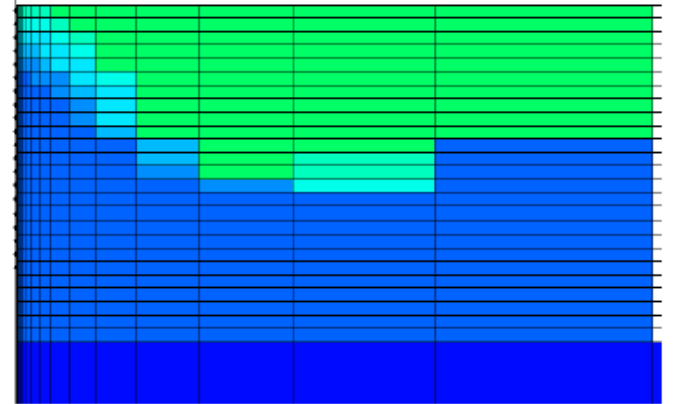
(a) Water saturation at WC=91% (Well-spacing=4000ft, Recovery=2.12%)



(b) Water saturation at WC=91% (Well-spacing=872ft, Recovery=13.8%)



(c) Water saturation at WC=95.2% (Well-spacing=4000ft, Recovery=43%)



(d) Water saturation at WC=95% (Well-spacing=872ft, Recovery=45%)

Figs. 5.6. Higher recovery for smaller well-spacing at $(WC_{ec}-pseudoWC_{ult}) \cong 0$ - Reservoir#12
(pseudoWC_{ult}=91%)

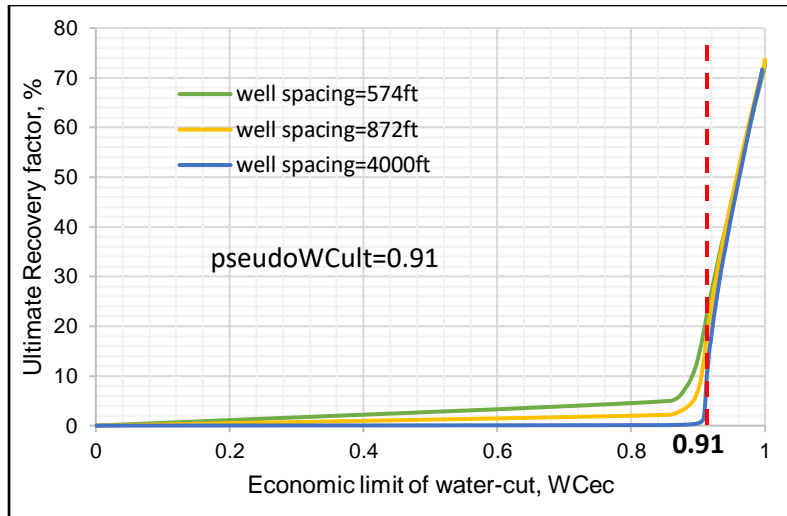


Fig. 5.7. Recovery factor vs. Water-cut (Reservoir # 12, pseudoWCult=0.91): Ultimate recovery increases with reduced well-spacing when $WC_{ec} \leq \text{pseudoWC}_{ult}$, whereas it converges when $(WC_{ec} - \text{pseudoWC}_{ult}) \gg 0$

5.3 Water-cut Pattern in NFR

Discussed in this section is the pattern and mechanism of WC development and stabilization in NFR (with planar fracture network) in comparison with single porosity reservoirs by running simulation experiments on a base case-NFR system. The simulation model is built using the following assumptions:

- 1) The well's drainage area is finite with no-flow closed boundaries representing a multi-well reservoir development project.
- 2) The NFR considered here is oil-wet. Numerous previous studies have shown that 90% of the carbonate reservoirs are either oil-wet, mixed-wet or neutral (Treiber and Owens 1972; Chilingar and Yen 1983; Cuiec 1984) of which 70% reservoirs being just oil-wet. However, the results in this study could also apply to neutral-wet reservoir, since capillary imbibition forces can be neglected due to dominant gravity effects for bigger block sizes (Kyte 1970).

3) The simulation study is carried out with a radial-cylindrical model using CMG IMEX reservoir simulator (Fig. 5.8). Oil pay has no-flow boundary, while aquifer is at constant pressure boundary to represent strong aquifers. Production well is completed in top 30% of the oil pay-zone (above free water-level) and capillary pressure is considered.

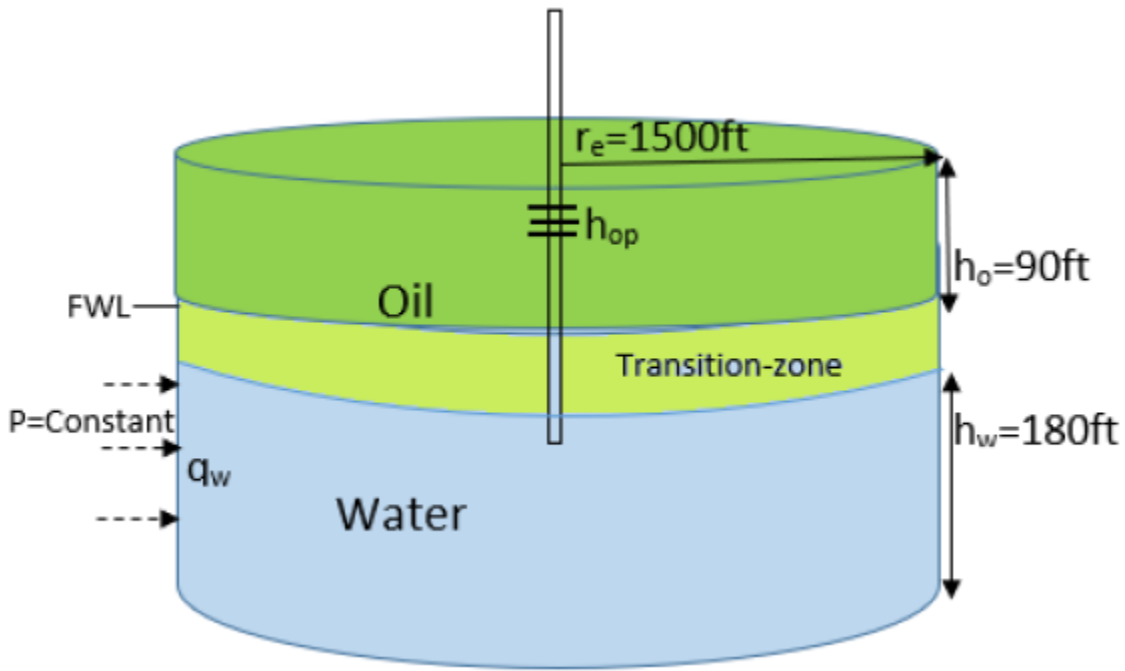
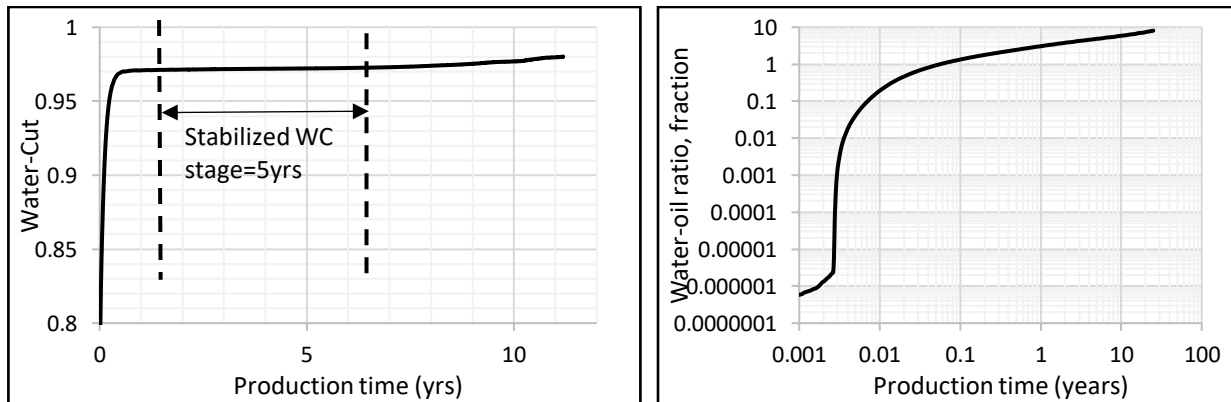


Fig. 5.8. Dual permeability radial model of oil pay-zone with bottom water (base case)

The study reveals development of stabilized water-cut stage in oil-wet carbonate NFRs for fracture-well. The water-cut pattern includes three stages - early water breakthrough with steep rise of water-cut followed with levelling and stabilization and the final stage of slow increase (Fig. 5.9a). In contrast, as shown in Fig. 5.9b, there is no stabilized WC stage in the matrix-only single-porosity reservoir (SPR) but there is a continuous slow increase of water-cut after it passes the pseudo water-cut value of $WC_{ult}=0.9$ (Prasun and Wojtanowicz, 2016) defined above (section 5.1) – corresponding to time when the water cone growth is complete and oil-water contact advancement dominates. The instant breakthrough in NFR indicate a channel-type invasion of

bottom-water, where late breakthrough in matrix-only reservoir shows the gradual development of water cone.

Furthermore, after the water breakthrough, shown in Fig 5.10, patterns of water cut development in the two types of reservoirs are clearly different; In NFR, there is an initial stage of rapid WC increase associated with monotonous reduction of slope, dWC/dt , from a very large value of 1500/year followed by stabilization stage when the slope reaches below the threshold minimal value of 0.0004/yr. Following stabilization period, slope again increases resulting in the final stage with progressive increase of WC till it reaches the value of 1. In the SPR, on the other hand, there is an S-shaped pattern of the WC plot (Chan 1995) (Fig. 5.9b) - with an initial increase of dWC/dt reaching its maximum value (at the plot's inflexion point, production time ≈ 4 days) corresponding to water cone's lateral expansion after the breakthrough.



(a) NFR, Stabilized WC value(WC_{stab}) = 0.97

(b) SPR, Well spacing=3000ft

Fig 5.9. WC pattern in NFR (a), and SPR (b) wells (3000ft well spacing and constant production rate) – base case data in Tables 5.5 to 5.7

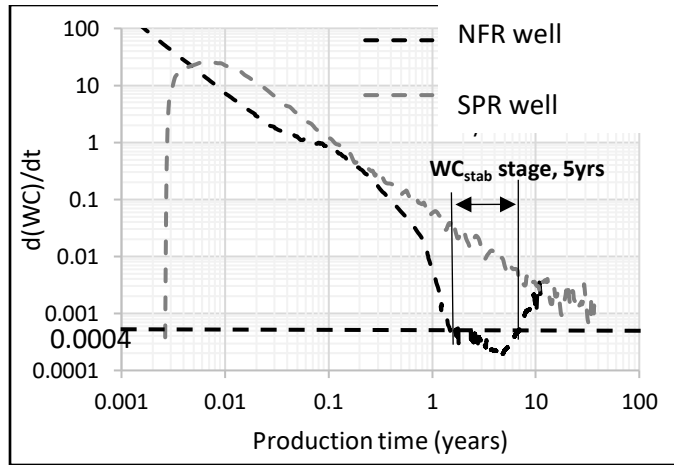


Fig. 5.10. Water-cut derivative patterns in NFR (Fig.5.9)

Table 5.5. Well in base-case NFR

Data	Unit	Base case	Range
Datum depth	ft	6000	6000
Initial Free water level	ft	6090	6090
Ratio of water zone to oil-zone thickness	fraction	2	2-5
Transition zone	ft	60	constant
Reservoir pressure at datum depth(P_i)	psi	3000	3000
Matrix porosity	fraction	0.1	0.05-0.15
Fracture porosity	fraction	0.001	0.0002-0.005
Fracture spacing	ft	6	0.1-20
Matrix permeability	md	1	0.1-10
Matrix anisotropy ratio	fraction	0.5	0.5
Matrix compressibility	1/psi	4.00E-06	4.00E-06
Fracture compressibility	1/psi	4.00E-05	4.00E-05
Perforated length	ft	27	30% of oil-zone thickness
Fracture horizontal permeability	md	300	100-500
Fracture anisotropy ratio	fraction	1	1-6
Well radius	ft	0.25	0.25
Outer radius of oil-zone	ft	2000	436-2000
Outer radius of water zone	ft	2000	436-2000
Total liquid production rate	bpd	13700	Varying
Well bottom flowing pressure	psi	1600	Constant

Table 5.6. Well in non-fractured single-porosity reservoir

Data	Unit	Conventional Reservoir
Datum depth	ft	6000
Free water level	ft	6030
Thickness of water zone	ft	200
Reservoir pressure at datum depth	psi	3000
Matrix porosity	fraction	0.1
Matrix horizontal permeability	md	200
Matrix anisotropy ratio	fraction	0.5
Matrix compressibility	1/psi	4.00E-06
Perforated length	ft	9
Well radius	ft	0.25
Outer radius of oil-zone	ft	3000
Outer radius of water zone	ft	3000
Liquid production rate	bbbl/day	2000

Table 5.7. Reservoir fluid properties

Data	Unit	Values	Range
Formation oil volume factor	rb/stb	1.10	-
Water compressibility	1/psi	3.00E-06	-
Oil compressibility	1/psi	1.50E-06	-
Water viscosity	cp	1	-
Oil viscosity	cp	1	1-10
Oil density	lb/cuft	52.0	48-58
Water density	lb/cuft	64	60.5-74.9
Bubble point pressure	psi	1000	-

In the oil-wet NFR, the beginning of stabilized WC stage occurs very early after one year, with small water cone in the rock matrix (Fig. 5.11b) and almost complete upward advancement of water in the fractures (Fig. 5.11a). Moreover, at the end of stabilized WC stage (after 6.5 years), there is practically no further water invasion in the fractures (Fig. 5.11c) while the water advancement in the matrix is almost complete (Fig. 5.11d).

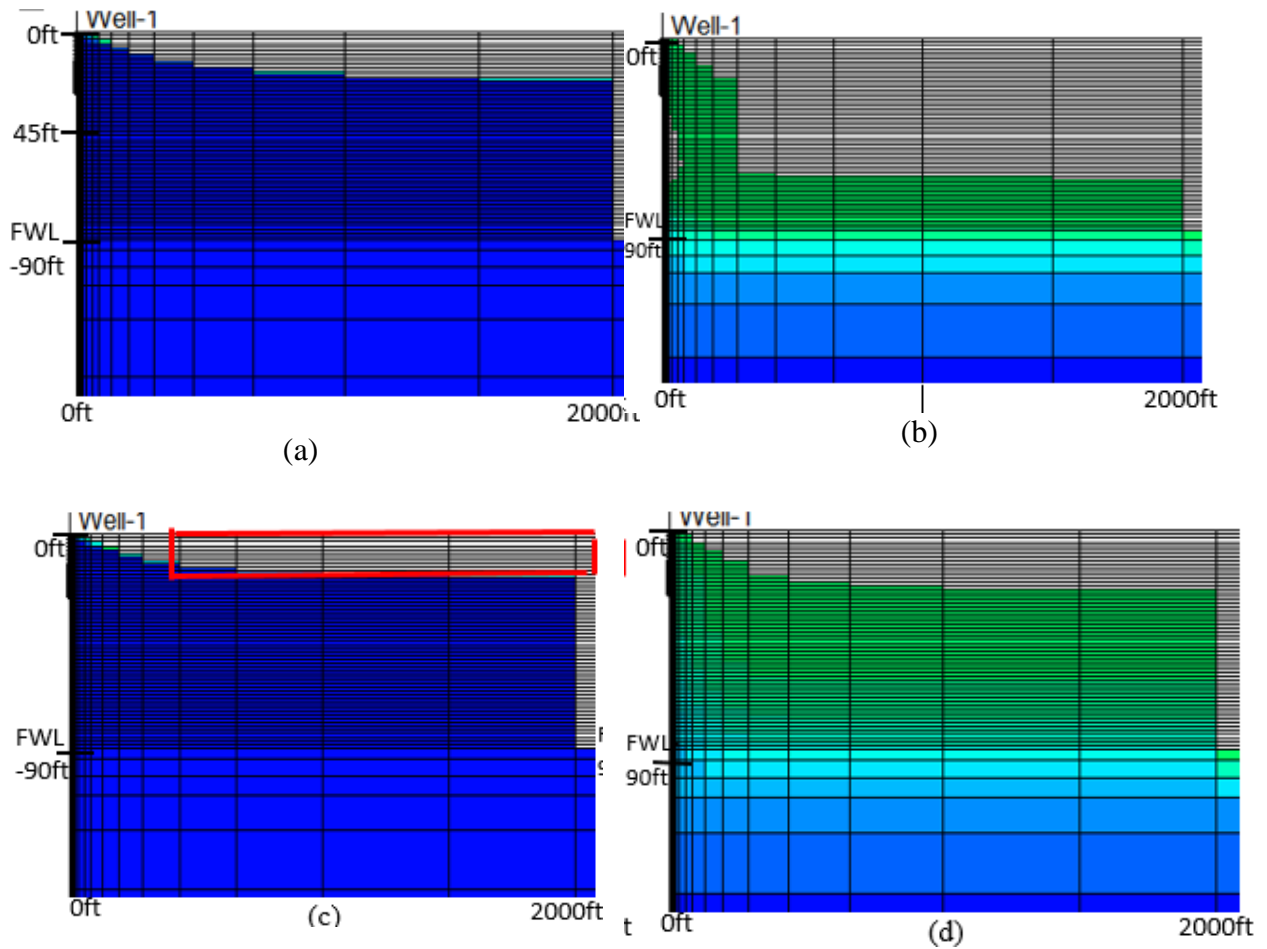


Fig. 5.11. Water invasion to a) fractures and b) matrix - start of stabilized WC stage after one year – base case NFR; Water invasion to c) fractures and d) matrix - end of stabilized WC stage (5 years) – base case NFR

Upwards water invasion to the NFR rock matrix results from the same three forces that control oil displacement by water during water-drive or water flood processes (Reiss 1980, Bourblaux et al. 2016):

- 1) Opposing capillary pressure due to forced imbibition of water into the oil-wet rock matrix.
- 2) Gravity drainage force which results from vertical segregation of oil (in matrix) and water (up in fracture-networks).
- 3) Viscous force due to the high liquid production rates at wellbore.

Water cut stabilization begins when the oil-water contact (OWC) moves up to the top of oil pay with little advancement of OWC in matrix blocks (Figs 5.11a and b). During this stage, the difference in elevation of OWCs results in gravity drainage and steady oil displacement from the matrix towards the fractures at the top of the oil-zone. This top layer of oil-filled fractures provides for oil exchange between matrix and fracture (shown in red envelope in Fig. 5.11c) and delivers oil to the well. The approximate average water saturation value at the end of stabilized WC stage for the base case NFR ($Q = 13700\text{bbl/day}$; $WC_{\text{stab}} = 0.97$; $T_{\text{stab}} = 5\text{yrs}$; well-spacing=3000ft) can be computed as,

$$S_{w,\text{stab}} = S_{\text{wc}} + \frac{Q \times (1 - WC_{\text{stab}}) \times T_{\text{stab}}}{\pi(r_e^2 - r_w^2) \times h_o \times \phi_m} \cong 0.15 + \frac{13700 \times 0.03 \times 5 \times 365 \times 5.615}{\pi(1500^2 - 0.25^2) \times 90 \times 0.1} \cong 0.22 \quad (5.9)$$

During the stabilized WC stage, the matrix water saturation (S_w) increases from 0.15 to 0.22. Within this range of water saturation, capillary pressure remains almost negligible as evident in Fig 5.12a, so it does not oppose oil displacement that results in constant displacement rate (Figs. 5.11b and 5.11d). The plot in Fig. 5.12a also shows that with the increasing matrix permeability, there is increasing range of near-zero P_c value at low water saturation (Namba and Hiraoka 1995) that would result in a longer period of stabilized WC stage. However, for the base case NFR, change of P_c with increasing water saturation becomes significant only for $S_w > 0.22$ (Fig. 5.12a), thus marking the end of WC stabilization stage. We define the increase rate of water-cut during stabilization stage as below the threshold value of 0.0004/year, which is defined when the slope of P_c vs. S_w is set as;

$$\frac{d(P_c)}{d(S_w)} \leq 1\text{psi/fraction}(S_w)$$

From the above discussion, it follows that capillary force during the WC stabilization stage can only be neglected at low water saturation values in the oil-wet NFRs. The water-wet or mixed-

wet formations display more significant P_c change for low S_w values (as evident from in Fig. 5.12b), and hence, should not demonstrate any water-cut stabilization stage as shown in Fig. 5.13. Further, from Eq. (5.9) it is evident that for thicker oil-zone, duration of stabilized WC stage becomes longer. Thus, we conclude that the water-cut stabilized stage is only characteristic for the oil-wet NFRs and is more prominent for thicker oil-zones.

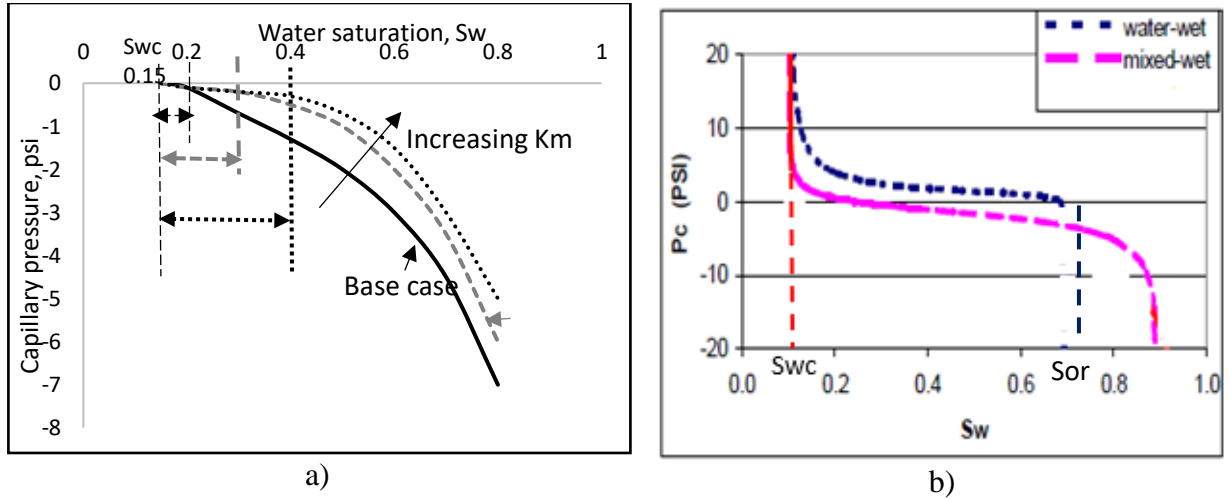


Fig. 5.12. Range of water saturation with negligible small capillary pressure – a) Effect of matrix permeability, K_m on the range of negligible small capillary pressure; b) Lack of negligible P_c range in water-wet and mixed-wet reservoirs (Masalmeh 2002)

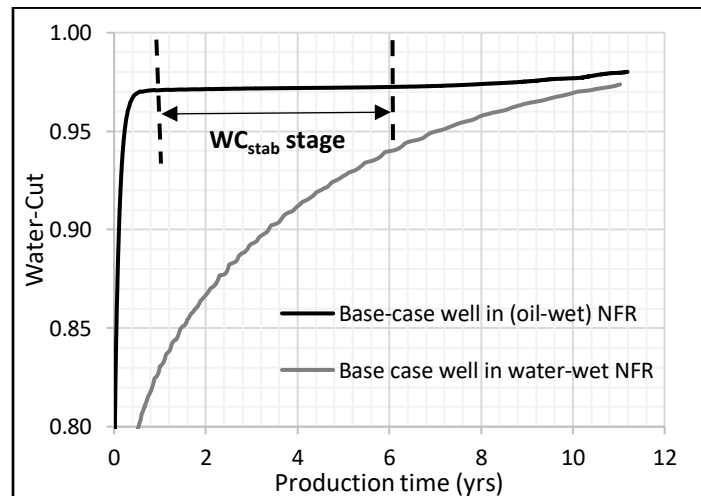


Fig. 5.13. Water-cut development pattern in oil-wet NFR and water-wet NFR (well-spacing=3000ft)

After the stabilized WC stage, capillary pressure would significantly increase with increasing water saturation in the matrix until oil saturation reduces to its residual value (Narr et al. 2006). There is a steady reduction of oil-displacement rate from the matrix during this process resulting from the opposing capillary pressure and shortening of matrix oil column evident from below formula (Boerrigter 1993):

$$Q_{m,o} = \frac{k_{mv}k_{ro}A_c}{\mu_o h_o} (\Delta\rho g h_o - Pc(S_w)) \quad (5.10)$$

At constant liquid production rate, the reduction of oil-rate results in gradual progression of WC. Analytically modeling the stabilized WC stage would help the operator decide the feasibility of project based on its comparison with the economic limit of water-cut, WC_{ec} ; where WC_{ec} represents the breakeven (zero-profit) cost of daily production.

5.4 Analytical Model of Stable Water-Cut in NFR

Mechanism of gravity drainage significantly contributes to oil displacement for vertically-connected fractures and capillary continuous matrix blocks so recovery would depend on the oil pay thickness (Pratap et al. 1997). However, viscous forces may be considerable depending on the matrix-fracture permeability contrast in NFR (Bourbiax et al. 2016). During stabilized WC stage, there is mostly flow of water in the fractures with small amount of oil from the matrix, so pressure drawdown mostly results from the flow in fractures as,

$$\Delta P_{well} = P_i - P_b - 600 = \frac{141.2QB_w\mu_w(\ln(r_e/r_w)+S)}{k_{fh}h_t} \quad (5.11)$$

Using the concept of average flow conductivity of the matrix block computed by integrating relative permeability integrated over matrix height, we can estimate oil displacement rate from the matrix due to viscous flow as,

$$Q_{m,viscous} = \frac{k_{mh} \int_0^{h_o} k_{ro}(z) dz}{141.2 B_o \mu_o (\ln(r_e/r_w) + S_m)} \times \Delta P_{well} = \frac{k_{mh} \int_0^{h_o} k_{ro}(z) dz \mu_w B_w Q (\ln(r_e/r_w) + S)}{k_{fh} h_t B_o \mu_o (\ln(r_e/r_w) + S_m)} \quad (5.12)$$

where, S is the partial penetration skin, given by (Papatzacoz 1987):

$$s = \left(\frac{1}{h_{pD}} - 1 \right) \ln \frac{\pi}{2r_D} + \frac{1}{h_{pD}} \ln \left[\frac{h_{pD}}{2+h_{pD}} \left(\frac{A-1}{B-1} \right)^{1/2} \right] \quad (5.13)$$

where, $r_D = (r_w/h_t) (k_{fv}/k_{fh})^{1/2}$, $h_{pD} = h_{op}/h_t$, $A = 4/h_{pD}$, $B = 4/3h_{pD}$

S_m is the partial penetration skin due to the well-inflow only in matrix which can be obtained from Eq. (5.13) after the following modifications:

$$r_D = (r_w/h_o) (k_{mv}/k_{mh})^{1/2}, \quad h_{pD} = h_{op}/h_o$$

Eq. 5.12 describes radial matrix-to-matrix flow conceptualized in the DPDP model discussed above. Additional component of the oil rate results from the effect of gravity forces that drive the oil displacement by water in matrix (Reiss 1980). The displacement represents the matrix-to-fracture flow at the top of oil-zone as discussed in the proposal. Assuming uniform displacement over the whole drainage area gives estimated oil rate as,

$$Q_{m,gravity} = 2.46 \times 10^{-5} \frac{k_{roe} k_{mv} (r_e^2 - r_w^2) \Delta \rho}{B_o \mu_o} \quad (5.14)$$

Thus, the total matrix oil rate is,

$$Q_{m,o} = Q_{m,viscous} + Q_{m,gravity} = \frac{k_{mh} \int_0^{h_o} k_{ro}(z) dz \mu_w B_w Q (\ln(r_e/r_w) + S)}{k_{fh} h_t B_o \mu_o (\ln(r_e/r_w) + S_m)} + 2.46 \times 10^{-5} \frac{k_{roe} k_{mv} (r_e^2 - r_w^2) \Delta \rho}{B_o \mu_o} \quad (5.15)$$

The approximate formula (5.15) implies that during the stabilized WC stage oil rate is constant resulting in constant value of water cut. For constant liquid production rate, Q_l , stabilized WC is,

$$WC_{stab} = \frac{(Q-Q_{m,o})}{Q} = 1 - \frac{1}{Q} \left[\frac{\int_0^{h_o} k_{ro}(z) dz k_{mh} \mu_w B_w Q (\ln(r_e/r_w) + S)}{k_{fh} h_t B_o \mu_o (\ln(r_e/r_w) + S_m)} + 2.46 \times 10^{-5} \frac{k_{ro} k_{mv} (r_e^2 - r_w^2) \Delta \rho}{B_o \mu_o} \right] \quad (5.16)$$

The stabilized value of water cut is typically very high due to the ratio of oil and water mobility in matrix and fracture, respectively. Most importantly, however, stabilized WC is strongly affected by production rate as shown in Fig 5.14. This is because, in NFR, production rate controls pressure drawdown (Eq. 5.11) and consequently, the viscous displacement of oil from matrix ($Q_{m,viscous}$).

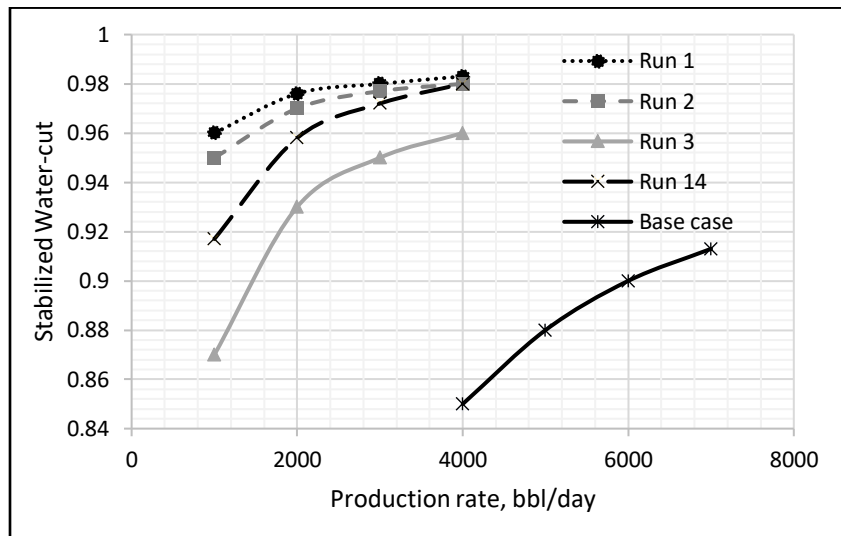


Fig. 5.14. Stabilized WC relationship with production-rate for different reservoirs in Table E-1

The stabilized WC formula in Eq. (5.16) is verified experimentally for variety of carbonate NFRs. A total of 16 simulated experiments have been designed using the Taguchi statistical design method described in Appendix E. The stabilized WC values from Eq. (5.16) closely match the experimental values as shown in Fig. 5.15, giving a unit-slope line at coefficient of determination (R-square) of 0.97.

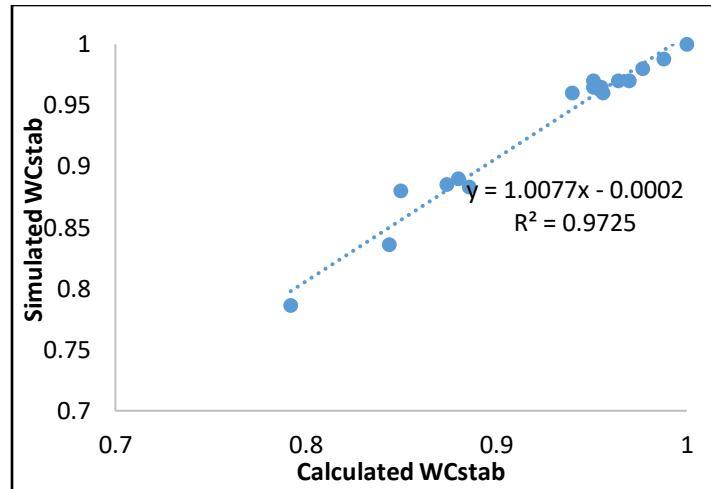


Fig. 5.15. Simulated vs. predicted stabilized water-cut values

5.5 Effect of Well Spacing and Production Rate on Stabilized Water-Cut Stage

Formula of Eq. 5.16 implies that stabilized water-cut, WC_{stab} would decrease with increasing well spacing (i.e. double the drainage radius). The relationship is confirmed (for the base case of NFR) with simulations in Fig. 5.16a where WC development is plotted for well-spacing varying from 2000ft to 6000ft. For larger well spacing – the stabilized WC stage duration shortens or WC may not stabilize at all so water-cut would continually increase. Absence of the stabilized WC stage can be explained by considering time difference of water invading fractures and oil outflow from matrix. Duration of stable WC stage depends on how fast the water invades the fractures, so they begin flowing mostly water at constant rate. During the stage, oil flows out of the matrix at constant rate so the water cut value remains constant. However, with increased well-spacing, there is shorter lag time between the processes of fracture water invasion and matrix oil release resulting in shortening of the stabilized WC stage. At this larger well spacing, the two processes overlap so there is no stabilized WC stage at all.

Demonstrated in Fig. 5.16a, is the strong effect of well spacing and production rate on the WC_{stab} stage duration (base case). The increase of stabilized WC stage would occur for larger well

spacing when production rate is increased. Moreover, for the same rate of production, the WC_{stab} stage rapidly reduces with increasing well spacing to become zero for larger well spacing values. In this section, multiple regression analysis is carried out to statistically correlate the stabilized WC stage duration as a function of well-spacing and production rate. We use the multi-level random experimental design with 5 levels of Q and 15 levels of W_s for improved precision. The W_s values are constrained by two limiting conditions: $T_{stab} > 0$, and $WC_{stab} < W_{cec}(0.98)$. The beginning and the end of stabilized WC stage is determined by minimum value of water-cut change rate $(\frac{d(WC)}{dt})$ set as,

$$\frac{d(WC)}{dt} < 0.001/year$$

The simulation results and the matrix of experiments are shown in Table 5.8.

Table 5.8. Stabilized WC stage duration (years) vs. well-spacing and production-rate (base case)

Q (bbl/day)	20	20	20	60	60	60	100	100	100	137	137	137	180	180	180
	00	00	00	00	00	00	00	00	00	00	00	00	00	00	00
Ws (ft)	12	26	20	24	30	40	280	380	460	320	400	500	600	500	380
	00	00	00	00	00	00	0	0	0	0	0	0	0	0	0
T _{stab} (years)	6	2	5	6	4.2	2	7.2	5	3	6.2	5	2.5	3	5.2	6.2
	6	2	5	6	5	2	5	5	3	5	5	2.5	3	5	5

Using multiple regression analysis, empirical correlation of the stabilized WC stage duration is correlated with well-spacing and production rate as,

$$T_{stab} = 5.89 + 0.00024Q - 4.7 \times 10^{-8}Q^2 - 7.25 \times 10^{-7}W_s^2 + 3.13 \times 10^{-7}QW_s \quad (5.17)$$

The regression model shows the good fit with experimental data at R-Squared value of 0.87.

As shown in Fig. 5.16b prolonged WC_{stab} stage (at smaller well spacing) develops earlier with higher values of water-cut. At high WC, oil rate is smaller but the WC_{stab} stage is longer.

Therefore, the question arises about finding this stage duration that would give maximal contribution to total recovery.

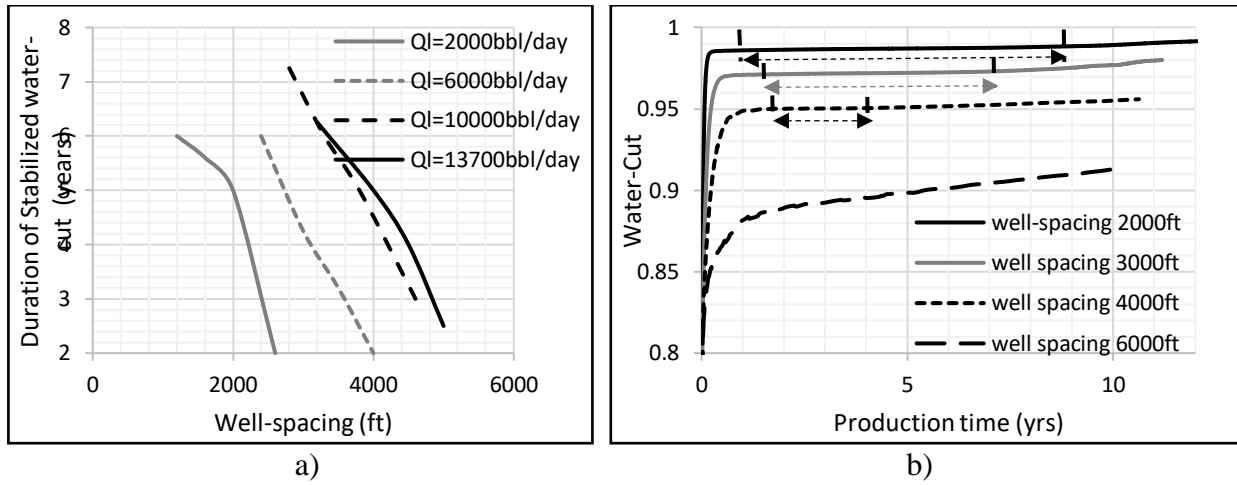


Fig. 5.16. Stabilized WC stage duration increases with reduced well spacing and increasing production-rate – a) Duration of stabilized WC stage as a function of well spacing and production rate (Base case NFR); b) WC development for different well-spacing (Base case NFR; $Q_l=13700$ bbl/day)

Physical mechanism of well spacing effect on water-cut pattern and recovery can be explained as follows. As the viscous force effects in highly fractured type II NFRs can be considered minimal, gravity force remains the major recovery mechanism. So, using Eq. (5.18), upward velocity of water invasion in matrix, $\frac{\Delta h}{\Delta t}$, during stabilized WC stage, can be approximated as,

$$\frac{\Delta h}{\Delta t} = \frac{Q_{m,gravity}}{\pi(r_e^2 - r_w^2)\phi_m(1 - S_{wc})} = \frac{2.46 \times 10^{-5} \frac{k_{roek_{mv}(r_e^2 - r_w^2)\Delta\rho}{B_o\mu_o}}{\pi(r_e^2 - r_w^2)\phi_m(1 - S_{wc})}}{\pi(r_e^2 - r_w^2)\phi_m(1 - S_{wc})} = 2.46 \times 10^{-5} \frac{k_{roek_{mv}\Delta\rho}{B_o\mu_o\pi\phi_m(1 - S_{wc})}}{\pi(r_e^2 - r_w^2)\phi_m(1 - S_{wc})} \quad (5.18)$$

Formula Eq. 5.18 demonstrates that the maximum upward rate of matrix water invasion is independent of well spacing. Initially, when the well spacing is large, water invasion rate in fractures is less than that specified by Eq. (5.18), so the upward water invasion (or oil displacement) velocity in matrix is constrained by the invasion rate in fractures (not by Eq. 5.18). As the well-spacing is reduced, it results in faster invasion of water in fractures, thus steadily

enhancing rate of gravity displacement from matrix to fracture, thereby resulting in the steep increase in total recovery. This happens till the water invasion rate in fractures becomes equal to Eq. 5.18 when the stabilized WC stage just begins. However, with the further reduction in well spacing when the stabilized WC stage occurs, water invasion rate in fractures exceeds that in Eq. 5.18, so the water invasion (or oil displacement) rate in matrix becomes a constant value given by Eq. 5.18, resulting in no further increase in recovery due to gravity effects. So, the only contribution to the minimal increase in recovery during this stage is the increase in weak viscous force (or pressure drawdown at the well) due to reduction in the drainage area.

5.6 Well Spacing Optimization

In this section, we assess contribution of the WC_{stab} stage to total recovery. A 3-D plot in Fig. 5.17 is the effect of well-spacing and production-rate on the total recovery (at 10 years) for the base case. In simulations, values of well spacing vary from the minimum well spacing calculated from Eq. 5.18 for $WC_{stab} = WC_{ec} = 0.98$, to maximum well spacing - randomly chosen as 5000ft. The 10 year oil recovery is low – not exceeding 12%. It is caused in part by the short project life but is also characteristic for oil-wet NFRs that reportedly does not exceed 18% (Haugen 2010). In the oil-wet NFR, capillary pressure opposes water invasion that, in turn, impedes oil production, as compared to the water-wet NFR where spontaneous imbibition enhances oil production.

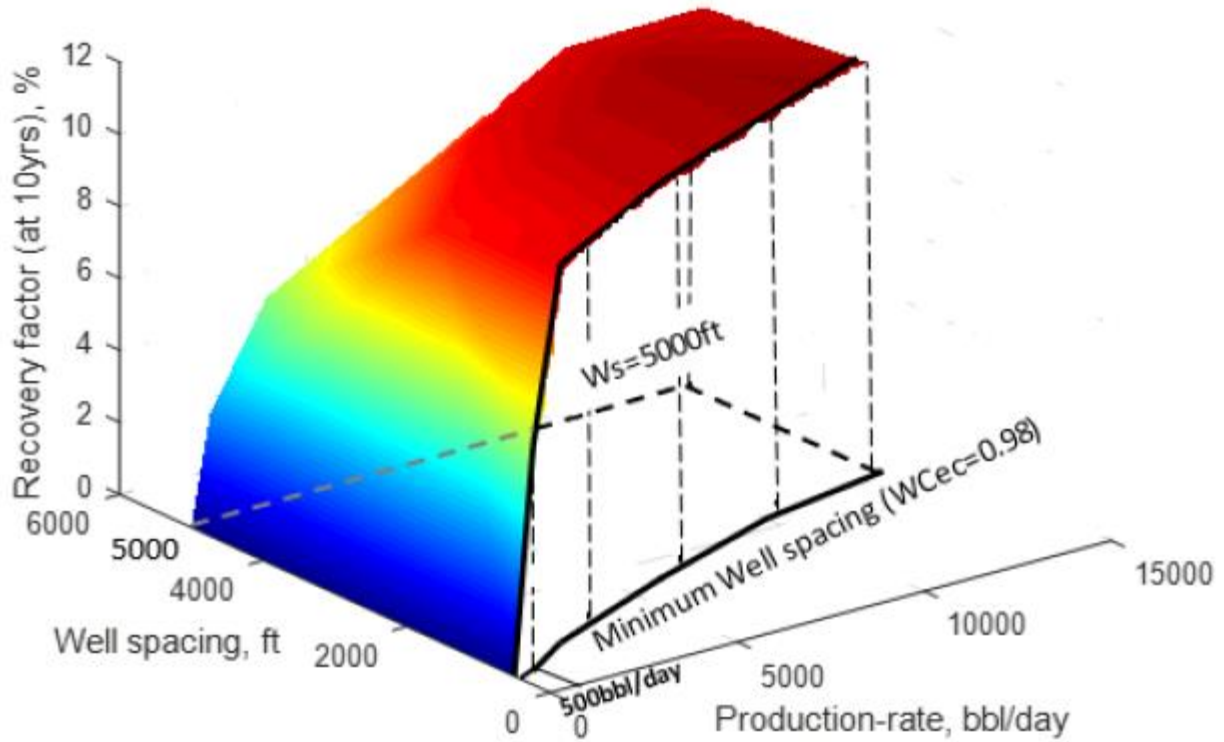


Fig. 5.17. 3-D total recovery (after 10years) as a function of well-spacing and production-rate for base case NFR

Fig. 5.18a shows the 10-year recovery, compared with 20-year recovery with constant production-rate of 4000 bbl/day, as a function of well spacing. Both figures (5.17 and 5.18a) demonstrate the steep increase in recovery with reduced well spacing followed by flattening of the plot with marginal increase in recovery. Moreover, Fig. 5.18a reveals that the beginning of the flattening of recovery plot coincides with the onset of stabilized water-cut stage irrespective of the project life (10 or 20 years). Small recovery improvement indicates insignificant contribution of the WC_{stab} stage for time-limited projects. Therefore, increasing the duration of stabilized WC stage by reducing the well spacing gives no meaningful recovery increase but higher capital and operating cost. Moreover, when disregarding the project duration, and considering ultimate recovery for $WC=WC_{ec}=0.95$, the WC_{stab} stage would reduce the recovery, as shown in Fig.

5.18b. So, all this implies that water cut stabilization stage needs to be avoided in order to optimize the recovery by setting the well spacing large enough to eliminate this stage.

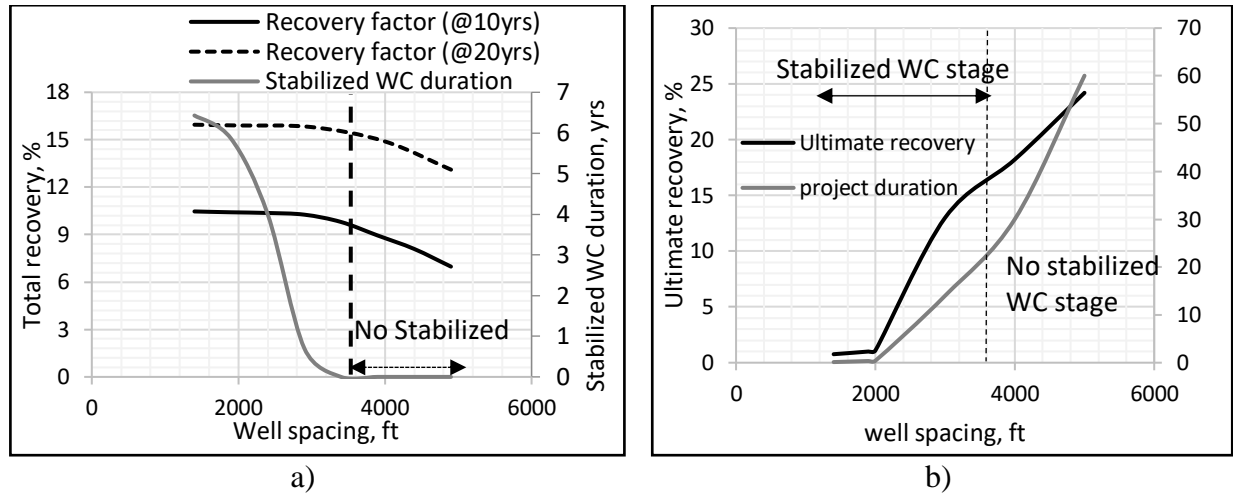


Fig. 5.18. a) Cross-sectional 2-D plot from 3-D surface plot of Fig. 11 at production-rate=4000bbl/day (representing the period of WC stabilization stage where total recovery increase is almost insignificant); b) Ultimate recovery (at 98% WCec) and duration of project as a function of well spacing for base case NFR, QI=4000bbl/day (demonstrates increase in ultimate recovery with increasing well spacing)

Increasing well spacing size above the value that eliminates the WC_{stab} stage – as shown in Fig. 5.18a would reduce the total recovery factor (RF) while increasing cumulative oil produced – as implied by Fig. 5.18b. This apparent contradiction results from the definition of RF - as ratio of cumulative oil to oil-in-place. By considering cumulative oil produced from NFR due combined action of viscous, gravity and capillary mechanisms, the RF vs. well spacing relationship is,

$$RF = \frac{Q_{m,viscous} \times \Delta t_p}{\pi \frac{W_s^2}{4} \phi_m (1-S_{wc}) h_o} + 2.46 \times 10^{-5} \frac{(k_{roek_{mv}} \Delta \rho \times \Delta t_p - 143.9 k_{roek_{mv}} \int_0^{\Delta t_p} \sum \left[\left(\frac{\partial PC}{\partial S_w} \right)_{S_w(t)} \frac{\partial S_w(t)}{\partial z} \right] dt}{\pi B_o \mu_o \phi_m (1-S_{wc}) h_o} \quad (5.19)$$

Where, capillary pressure would tend to oppose the matrix oil displacement by water and it would vary depending on the matrix water saturation reducing from maximum at the bottom to zero at matrix OWC. Since, matrix water saturation increases from bottom-up, opposing capillary pressure would theoretically pull the oil from top to bottom depending on the water saturation at

various heights. Total opposing flow rate (theoretical) would be the sum of flow-rates at different heights having different matrix water saturations at particular time, t, given by,

$$Q_{\text{capillary}}(t) = 0.00354 \frac{k_{\text{roe}} k_{\text{mv}} (r_e^2 - r_w^2)}{\mu_o B_o} \sum \left[\left(\frac{\partial P_c}{\partial z} \right)_{S_w(t)} \right] =$$

$$0.00354 \frac{k_{\text{roe}} k_{\text{mv}} (r_e^2 - r_w^2)}{\mu_o B_o} \sum \left[\left(\frac{\partial P_c}{\partial S_w} \right)_{S_w(t)} \frac{\partial S_w(t)}{\partial z} \right]$$

Where, Δt_p is the project duration, and $W_s = 2(r_e - r_w)$ is the well spacing.

Differentiating RF w.r.t W_s in formula 5.19, we get,

$$\frac{dRF}{dW_s} = -2 \frac{\Delta t_p}{\frac{\pi}{4} \phi_m (1 - S_{wc}) h_o W_s^3} \left[Q_{\text{m,viscous}} \left(1 - \frac{S_m - S}{\left(\ln \left(\frac{W_s}{2r_w} \right) + S_m \right) \left(\ln \left(\frac{W_s}{2r_w} \right) + S \right)} \right) \right] \quad (5.19a)$$

Since, $0 < \frac{S_m - S}{\left(\ln \left(\frac{W_s}{2r_w} \right) + S_m \right) \left(\ln \left(\frac{W_s}{2r_w} \right) + S \right)} < 1$ (for base case NFR, $\frac{S_m - S}{\left(\ln \left(\frac{W_s}{2r_w} \right) + S_m \right) \left(\ln \left(\frac{W_s}{2r_w} \right) + S \right)} = 0.017$), so

Eq. (5.19a) would always be negative.

So, the above formula 5.19 shows that although cumulative production would increase with well spacing (as implied by Fig. 5.18b), recovery factor would be a decreasing function of well spacing (Eq. 5.19a).

Increasing well spacing size would however, increase the ultimate recovery disregarding the duration of project. This is because with increasing well spacing, the duration of project (till WCec is reached) is no longer constant as it becomes a function of well spacing as shown in Fig. 5.18b. If the duration of project is assumed to be a linear function of well's drainage area, differentiating RF w.r.t W_s in formula 5.19, we get,

$$\frac{dRF}{dW_s} = \frac{Q_{\text{m,viscous}} \times \Delta t_p}{\frac{\pi}{4} \phi_m (1 - S_{wc}) h_o} \frac{S_m - S}{\left(\ln \left(\frac{W_s}{2r_w} \right) + S_m \right) \left(\ln \left(\frac{W_s}{2r_w} \right) + S \right)} +$$

$$d \left[\frac{2.46 \times 10^{-5} \frac{(k_{\text{roe}} k_{\text{mv}} \Delta \rho \times \Delta t_p - 143.9 k_{\text{roe}} k_{\text{mv}} \int_0^{\Delta t_p} \sum \left[\left(\frac{\partial P_c}{\partial S_w} \right)_{S_w(t)} \frac{\partial S_w(t)}{\partial z} \right] dt}{\pi B_o \mu_o \phi_m (1 - S_{wc}) h_o}}{dW_s} \right] \quad (5.19b)$$

Since Eq. 5.19b would always be positive, ultimate recovery factor would be an increasing function of well spacing as shown in Fig. 5.18b. The increased well spacing would cause an increase in ultimate recovery factor at lesser capital cost; however, the total duration of project may become exceedingly high which may not be acceptable for operators. Optimum well spacing obtained by eliminating the stabilized WC stage, would be higher compared to optimum well spacing (2800ft) obtained by maximizing the ultimate recovery after setting 10 years as the the maximum duration of project.

For a given production rate, optimum well-spacing for the base case NFR can be determined by setting the value of formula Eq. 5.17 to zero. So, the optimum well spacing can be rewritten as,

$$W_{s,opt} = \frac{3.13 \times 10^{-7} Q + \sqrt{9.8 \times 10^{-14} Q^2 + 29 \times (5.89 + 0.00024 Q - 4.7 \times 10^{-8} Q^2) \times 10^{-7}}}{14.5 \times 10^{-7}} \quad (5.20)$$

Similarly, optimum well-spacing for any NFR can be determined by developing a generalized correlation of stabilized WC stage duration for wide range of NFRs. So, the optimization problem can be formulated as: To maximize total recovery by finding optimum value of well-spacing, W_s that makes production process profitable at possibly the lowest value of stabilized water-cut below the economic limit of WC.

Well-spacing optimization example: In this example, we demonstrate the well-spacing design for the base case NFR. The optimum well-spacing for the base case optimization example satisfies $WC < WC_{ec}$ (0.98); so we assume well's daily production is economical. Using Eq. 5.20 for a given production-rate, $Q_{opt} = 4,000 \text{ bbl/day}$, we obtain optimum well spacing ($W_{s,opt}$) as, $W_{s,opt} \approx 3850 \text{ ft}$ which comes out close to the simulated optimum well spacing at 3600ft.

Substituting Q_{opt} and $W_{s,opt}$ in Eq. 5.16, we obtain; $WC_{stab} \approx 0.53$, which is much below the economic limit of WC. The low value of WC_{stab} demonstrates that the duration of profitable

production of oil after $WC_{stab} \approx 0.53$ would be longer and so the ultimate recovery would be higher (Fig. 5.18b) as compared to NFRs with reduced well spacing < 3000ft, which have WC stabilization (after the initial buildup), occurring very close to WC_{ec} , resulting in the production process being almost non-profitable.

Summary

In this study, water-cut pattern (ultimate water-cut) is related to the well spacing for multi-well single porosity and naturally fractured reservoirs with bottom water coning problem. Results of the study are summarized in the following conclusions:

- 1) In multi-well oil single porosity reservoirs with bottom water where wells produce from closed drainage areas, water-cut does not stabilize but continues slow increase at rate depending on the drainage area size, i.e. well spacing. This period of well production defined here as “slow water-cut progression period” is controlled by the oil depletion stage after the rapid increase of water-cut during water cone buildup stage.
- 2) It is found that when the well spacing becomes equal to or greater than minimum well spacing defined by the lateral extent of water cone, water-cut reaches the late pseudo stabilization stage governed entirely by oil depletion. So, in the same reservoir, the (pseudo) stabilized water-cut production stage may or may not happen-dependent upon well-spacing. The study provides a regression formula for the minimum well spacing (double size of the well’s drainage area threshold radius, r_{eTh} , above which the well would produce under condition of pseudo stabilized water-cut. The formula shows that pseudo WC_{ult} stage is practically possible only in thin reservoirs where minimum well-spacing is within the range of operating values of well-spacing for multi-well reservoirs. It

is also shown how to adjust minimum well spacing for different values of well's production rate.

- 3) Statistical comparison of the two formula using variety of bottom-water reservoirs with different well-spacing reveals that their results are similar ($\text{pseudoWCult} \cong \text{WCult}$), which means that:
 - (a) the effects of partial penetration and water inflow distortion are counter balanced and can be ignored; and,
 - (b) in multi-well bottom-water reservoirs, initial value of water-cut during the (pseudo) stabilized water-cut production stage, pseudoWCult , can be computed from the simple presently-used formula for WCult .
- 4) The pseudoWCult concept and value has potential practical use in designing well spacing for maximum ultimate oil recovery at maximum allowable well production rate. As the well's production must stop at the economic water-cut value, WCec , corresponding to the end of economical production, the difference of $(\text{WCec} - \text{WCult})$, dubbed here "water-cut economic margin", defines conditions for occurrence of the (pseudo) stabilized water-cut production and resulting incremental recovery. Computing water-cut economic margin should be the initial step in well spacing design followed with computation of the minimum size of well spacing-using formulas from this study. When the water-cut economic margin is negative or close to zero, well spacing smaller than its minimum (threshold) value should be considered and its size minimized for increased recovery.
- 5) As larger values of the water-cut economic margin result in increased ultimate recovery, priority should be given to bottom water systems with the largest water-cut economic margin. For a given reservoir with large water-cut economic margin, ultimate recovery is

not dependent on well spacing. In such case, possibly largest well spacing with maximum production rate should be designed to reduce capital cost and maximize Net Present Value of the project.

- 6) There are three stages of water-cut development in NFR-early water breakthrough with steep jump of water-cut followed with levelling and stabilization (stabilized water-cut) and the final progressive increase of water-cut. However, the water-cut stabilization is only a characteristic of oil-wet NFRs. The steep initial step-increase of water-cut gives a pattern of water channeling through fractures.
- 7) The stabilized water-cut stage in NFR begins when the water almost invades all fractures, so the fractures produce mostly water at constant rate, while oil is displaced from the matrix at constant rate. The stabilized water-cut stage ends when opposing capillary force begins effectively countering the gravity and viscous forces that reduces the oil displacement rate from the matrix.
- 8) A simple analytical model of oil displacement by water in matrix during stabilized water-cut stage is developed for oil-wet NFR by considering the driving force of gravity and viscous effect, while neglecting the capillary forces. This model gives a new analytical formula of stabilized water-cut. The new stabilized water-cut formula is verified by simulations using statistical method of experimental design for variety of NFRs. The comparison between the simulated and calculated stabilized water-cut value gives good match.
- 9) Duration of stabilized water-cut stage is related to the well spacing. Lowering the well-spacing would result in increased stabilized water-cut stage duration and the stabilized

water-cut value. Specifically, for the NFR base case, the stabilized water-cut duration is statistically correlated with Q_l and W_s .

- 10) The results show the water-cut stabilization stage does not significantly contribute to increase in recovery. In addition, the stage requires reducing well spacing which adds to the operating cost. Also, the ultimate recovery reduces with the increase in duration of duration of stabilized water-cut stage. So, stabilized water-cut stage should be avoided to optimize recovery and maximize profit.
- 11) A new method for finding optimum well-spacing by eliminating the stabilized water-cut stage, while maximizing recovery, is proposed. The method is demonstrated for the base case NFR. Further, the low value of stabilized water-cut at this optimum well spacing demonstrates that the profitable production can be sustained over the longer time, i.e. longer duration of the slow final progressive stage of water-cut till the water-cut reaches economic limit of water-cut.

Chapter 6. Oil Recovery from NFR with Fracture Corridors

After modeling the on/off corridor well placement in NFR with fracture corridors (previous chapter), the chapter reports the study performed to evaluate deterministic (considering known well placement) and probabilistic (considering uncertain well placement) recovery performance of single completed and DWS wells in distributed network, considering on-fracture (in-corridor) and off-fracture (in exclusion-zone) well completions.

Reliable predictions of well recovery are crucial for designing reservoir development. In the bottom-water naturally - fractured reservoirs (NFRs), comprising a network of distributed fracture “corridors,” spacing (and apertures) of the corridors varies throughout the reservoir. This makes oil well’s recovery a probabilistic variable as it depends upon uncertain well’s location in the network. The uncertainty is two-fold; it concerns well’s location within corridor network and well’s possible intersection with the nearest corridor. In any network’s location (with closely- or sparsely – spaced corridors), wells may intercept fracture corridors (fracture well) or go in-between two corridors in a matrix block (matrix-well). A simplified way of estimating well recovery is to ignore well’s location within corridor network and consider only probability and performance of fracture well and matrix well in a statistically-equivalent reservoir with uniform spacing and aperture equal to their expected values derived from their known statistics. Another (fully probabilistic) method considers the combined probabilities of the well’s location in the network and being a fracture well or matrix well. The study evaluates discrepancy between the two methods, explains its statistical nature, and demonstrates their implementation in a corridor-type NFR described in the literature.

Section 6.1, and 6.2.1 of this chapter previously appeared as OMAE paper (OMAE2019-96836) on “Probabilistic Estimation of Recovery From Naturally Fractured Bottom-Water Reservoir With Uncertain Well Placement in Fracture Network” in ASME 2019 38th International Conference on Ocean, Offshore and Arctic Engineering. Reproduced with permission of ASME. See Appendix F for more details.

6.1 Well Recovery vs. Completion Placement

In the study, recovery process is simulated by coupling the inner (near-well) zone's discrete single-porosity flow model with the outer zone Dual Porosity Dual Permeability (DPDP) simulator (Chapter 4). The matrix well's inner zone extends from the well to the nearest corridor (Fig. 4.5) and for the fracture well inner zone covers the corridor and adjacent matrix blocks (Fig. 4.6). In the simulations, matrix and fracture-wells are operated at maximum rate constrained by minimum downhole flowing pressure and the surface handling limit. Properties of the fracture corridor (type II NFR) is shown in Tables B2 and B3 (Appendix B). We would begin the study by comparing deterministic recovery performance of single and dual-completed well completion's placement in fracture corridor network.

6.1.1 Single-Completed Well

As discussed above, fracture corridors display large fracture spacing varying from 33 ft to 1300 ft (Ozkaya and Minton 2005). Therefore, in case of single-completed matrix-wells (completed in the exclusion zone), low-permeability rock matrix around the well significantly contributes to pressure distribution and the pressure drop across the well-adjacent rock matrix cannot be ignored. Consequently, a relevant comparison of fracture-well and matrix-well cannot be done by setting the same bottom-hole pressure in both wells because production rates become very different. So, we have no choice but to vary pressure drawdown and rates and to compare maximum recoveries of the two wells.

Figs. 6.1 compares water-cut vs. oil recovery plots for matrix-well and fracture-well (produced at their maximum recovery output) in type II sparsely distributed fracture corridor NFR (Table B2). Distance of matrix-well from corridors is 28 ft. We apply the maximum pressure drawdown 2000psi in matrix-well to stay above the bubble point pressure of 1000 psi. The matrix-

well would yield the maximum recovery at the maximum possible pressure drawdown. However, this principle doesn't apply to fracture-well as with increased drawdown, fracture-well demonstrates an increased severity of water-cut lowering the recovery at 97% water-cut. So, we vary the pressure drawdown for fracture-well and find the maximum recovery for small (100 psi) pressure drawdown over 20 years production time and water-cut below 97%.

Results show that the maximum possible recovery factor of matrix-well, 37%, exceeds that of fracture-well, 28%. This implies that in fracture corridor type II NFR, well completed in exclusion-zone could yield higher recovery at maximum possible pressure drawdown while the well completed in fracture corridor recovers less and requires tedious control of bottom pressure to prevent excessive water cut and still recovers less. Thus, in fracture corridor type II NFR, wells should be completed in the exclusion-zone.

The plots also show that the fracture-well undergoes instant water breakthrough followed by step increase of water-cut, but there is a delayed breakthrough in matrix-well followed by gradual increase of water-cut (Fig. 6.1A). This is because the bottom water quickly channels through permeable fractures connected to the fracture well, whereas in matrix-well water cone advancement in the rock matrix is delayed. In fracture-well, there is an initial stage of rapid WC increase followed with the instant reduction and stabilization of slope, dWC/dQ_o (Figs. 6.1B). In the matrix-well, on the other hand, there is an S-shaped pattern of the water-cut plot (Chan 1995) - with an initial increase of dWC/dQ_o reaching its maximum value (at the plot's inflexion point; $Q_o \approx 2 \times 10^3$ bbl/day) after the breakthrough (Figs. 6.1B).

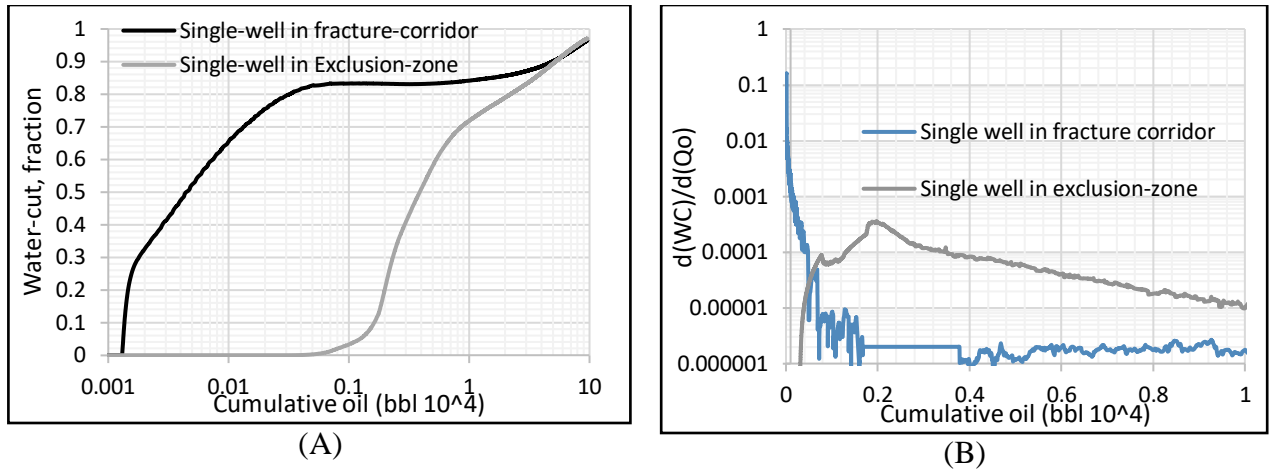


Fig. 6.1. Water-cut (A) and derivative (B) vs. cumulative oil for matrix- and fracture-wells in type II NFR with fracture corridors

6.1.2 Dual-Completed Well

In fracture corridors network, there are practically only two variants of DWS well completions placement –as shown in Fig. 6.2.

- 1) Top and bottom completions within or close to the vertical fracture-corridor;
- 2) Top and bottom completions in the exclusion zone.

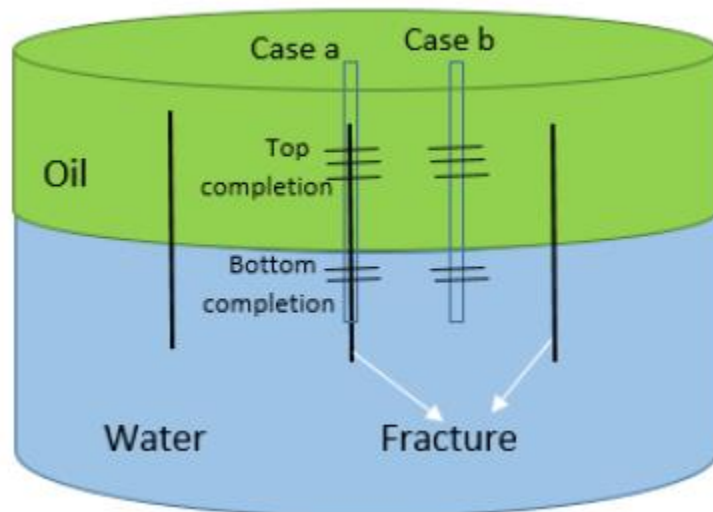


Fig. 6.2. DWS well completions placement in NFR with vertical fracture corridors

To compare two DWS variants in fracture corridor type II NFR (Table B3), we optimize well's operation for maximum recovery as described above using a 2000 psi pressure drawdown for matrix-well and 100 psi drawdown for fracture well. The same value of drawdown at the bottom completion does not induce inverse coning of oil.

The results in Table 6.1 and Fig. 6.3 show considerable improvement in recovery performance for both placement variants of DWS well comparing to a single-completed well. However, for both types of wells, placement of well completions in the exclusion-zone gives higher oil recovery. Table 2 presents also values of the optimized pressure drawdown (for maximum recovery) and resultant well's fluid production rate. Since the well is operated at constant pressure drawdown, production rate is shown only for the purpose of replicating our results. Interestingly, recovery is maximized for small production rates to avoid early termination of well's life due excessive (>97%) water-cut.

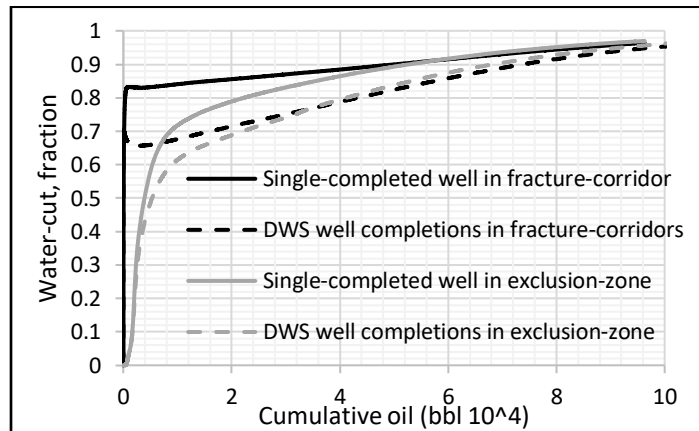


Fig. 6.3. Water-cut patterns for single-completed and DWS wells in type II NFR with fracture corridor network

Table 6.1. Well Recovery in Fracture-Corridor Network NFR (Type II*)

Well type	Completion (case)		Recovery factor (RF), %	Operation		
	Upper	Lower		Well's life, years	Pressure drawdown, psi	Production rate, bfpd
Single-completed	Corridor (a)	-	28	20	100 psi	150
	Exclusion-zone (b)	-	37	20	2000 psi	250
Dual-completed (DWS)	Corridor (a)	Corridor (a)	35	18	100 psi	210
	Exclusion-zone (b)	Exclusion-zone (b)	45	17	2000 psi	310

* Average NFR properties computed from the fracture corridor size distribution shown in next section: $F_w = 15.5ft$; $S_p = 56ft$; $k_f = 590md$

6.2 Probabilistic Prediction of Oil Recovery

Our study, above, assumes a certain (known) well completion's location in the fracture network. The oil well's recovery a probabilistic variable as it depends upon uncertain well's location in the distributed network of fracture corridors. The recovery performance of a well completed in a corridor (fracture well) or between two corridors (matrix well) is computed using numerical reservoir simulator by coupling a discrete model of the well's inflow zone with the DPDP flow model outside the zone. The well's inflow zone for matrix-well extends from well to the nearest corridor and is simulated by assigning zero fracture porosity to the grid block containing matrix-zone. For fracture well the well's inflow zone extends from well intercepting a discrete corridor to the nearest corridor and is simulated by assigning the nearest matrix-zone grid with a zero-fracture porosity.

It is found that corridor spacing and width is somehow related. For example, Bisdom et al. (2014) mapped 20 fracture corridors and reported a power-law relationship between fracture corridor spacing and $F_w[m]$, as

$$S_p = 1.45F_w^{1.54} \quad (6.1)$$

Where, ($F_W \in 2.4m - 9.5m$)

They also hypothesized a scale-invariant spatial distribution of fracture corridors. By following the concept, we may upscale their findings for the entire NFR with randomly-distributed fracture corridors having size range from 2.4 to 9.5m with size-dependent spatial distribution density,

$$F = 1/S_p = 0.69F_W^{-1.54} \quad (6.2)$$

Using the probability theory (Clauset 2011), we can convert the spatial distribution function, F, by dividing the F-value for any $F_W \in (2.4m, 9.5m)$ by the area, A, under the F-plot in Fig. 6.4.

$$A = \int_{2.4}^{9.5} 0.69F_W^{-1.54} dF_W = 0.42$$

Probability density function is,

$$p(F_W) = \frac{1}{A} \cdot F(F_W) = \frac{0.69F_W^{-1.54}}{0.42} = 1.65F_W^{-1.54} \quad (6.3)$$

and cumulative probability function is given by (Jensen et al. 1997),

$$P(F_W) = \int_{2.4}^{F_W} 1.65F_W^{-1.54} dF_W = 3(2.4^{-0.54} - F_W^{-0.54}) \quad (6.4)$$

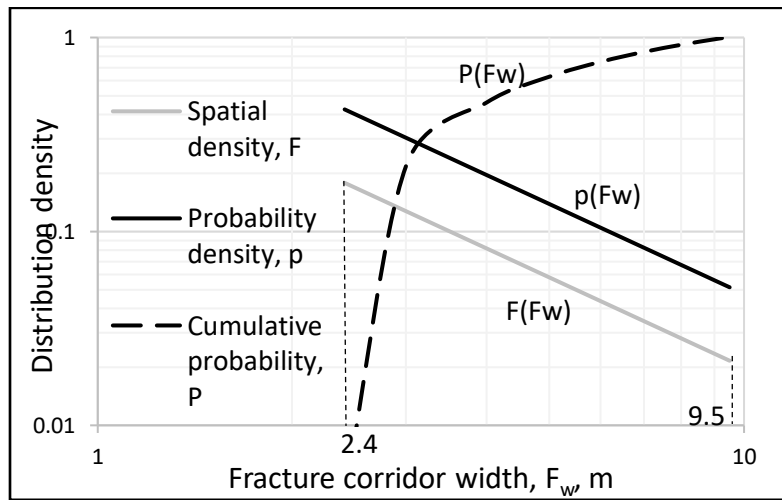


Fig. 6.4. Statistical measures of fracture corridors in example NFR (modified from Bisdom et al. 2014)

Formula Eq. 6.1 gives power-law distribution of the fracture corridor size that has also been confirmed by other researchers including Barton and Zoback 1992; Kakimi, 1980; Heffer and Bevan, 1990; Davy et al. 1990; Guerriero et al. 2010; Hooker et al. 2014). The coefficients of the power-law distribution can be estimated from the seismic survey or borehole image log (Hooker et al. 2014).

Wells drilled in NFR could have completions located either in fracture corridor – event C1, or exclusion-zone – event C2. Statistically, the two events are mutually exclusive and exhaustive, i.e. they cannot occur concurrently, and no other event is possible. Thus, the well’s recovery performances would depend upon random placement of the completion. Presented below is a expected and probabilistic estimation of recovery using published statistics of the field-case NFR, discussed above, and described by Eq. (6.1) through Eq. (6.4), with properties shown in Table 6.2.

6.2.1 Simplified Method for Well’s Recovery Prediction from NFR Statistics

In the simplified method, the corridor network statistics defines a statistically-equivalent reservoir with uniform corridor spacing and width equal to their expected values - central tendency measures. Probability of well completion intercepting fracture corridor, P(C1) is the ratio of the total area of all fracture corridors to the NFR area. The probability is the area under the corridor density plot, F, in Fig. 6.4 is calculated by integrating Eq. (6.2) as,

$$P(C1) = \int_{2.4}^{9.5} F(F_w) dF_w = \frac{0.69(9.5^{-0.54} - 2.4^{-0.54})}{-0.54} = 0.42 \quad (6.5)$$

Probability of the alternate event, C2 – well’s completion placed in the exclusion-zone is,

$$P(C2) = 1 - P(C1) = 0.58 \quad (6.6)$$

Oil recovery for the two well placement variants C1 and C2 is determined with a simulated sheet-like NFR – equivalent to actual reservoir – having expected values of the fracture corridor

size, $E(F_W)$ and spacing, $E(S_p)$. Considering probability density formula Eq. (6.3), the expected value of fracture corridor size, $E(F_W)$, (Jensen et al. 1997) is

$$E(F_W) = \int_{2.4}^{9.5} p(F_W) F_W dF_W = 1.65 \int_{2.4}^{9.5} F_W^{-0.54} dF_W = 4.74m (15.5ft) \quad (6.7)$$

To determine expected value of fracture spacing, we compute the expected value of $(F_W^{1.54})$ as,

$$E(F_W^{1.54}) = \int_{2.4}^{9.5} p(F_W) F_W^{1.54} dF_W = 11.7 \quad (6.8)$$

Considering the functional relationship between S_p and F_W in Eq. (6.1), the expected value of corridor spacing is,

$$E(S_p) = E(1.45F_W^{1.54}) = 1.45E(F_W^{1.54}) = 17m (56ft) \quad (6.9)$$

The expected value of effective permeability is,

$$E(k_f) = E\left(\frac{k_{ff} \times F_W}{S_p}\right) = E\left(\frac{k_{ff} \times F_W}{1.45F_W^{1.54}}\right) = E\left(\frac{k_{ff} \times F_W^{-0.54}}{1.45}\right) = \frac{k_{ff}}{1.45} E(F_W^{-0.54}) \quad (6.10)$$

Where, the expected value of $(F_W^{-0.54})$ is,

$$E(F_W^{-0.54}) = \int_{2.4}^{9.5} p(F_W) F_W^{-0.54} dF_W = 0.46 \quad (6.11)$$

This gives the effective permeability value in Tables B2 and B3,

$$E(k_f) = \frac{k_{ff}}{1.45} E(F_W^{-0.54}) = \frac{1960}{1.45} \times 0.46 = 590md$$

The simulation results shown in Table 6.2 reveal that a conventional (single-completed) well would recover either 28% or 37% of NFR oil-in-place (OIP) with 42% or 58% probability for randomly-placed completion in the fracture corridor or exclusion-zone, respectively. So, the expected value of recovery factor in a completely developed reservoir is 33% (28%*0.42+37%*0.58).

Table 6.2. Expected Recovery with Well in Fracture Corridor Network (NFR type II*)

Well type	Completion		Recovery	
	Upper	Lower	RF, %	Probability, %
Single-completed	Corridor (a)	-	28	42
	Exclusion-zone (b)	-	37	58
Dual-completed (DWS)	Corridor (a)	Corridor (a)	35	42
	Exclusion-zone (b)	Exclusion-zone (b)	45	58

*NFR estimates: $E(F_w) = 15.5ft$; $E(S_p) = 56ft$; $k_{ff} = 1960md$; $E(k_f) = 590md$

For a dual-completed DWS well, the two well completions are either placed in fracture corridors (variant a) or exclusion-zone (variant b), so the probabilities are the same as for the single-completed well: 42% and 58% respectively. The same sheet-like model of NFR with expected values of F_w , S_p and k_f is used to compute maximum recovery shown in Table 6.2. The recovery is determined by operating the well at constant optimum pressure drawdown (by trial-and-error) over the well's life constrained by the maximum value of water cut, 97%, or the well's production time, 20 years. The recovery factor values in Table 6.2 are consistently greater than those for single-completed well indicating that DWS well would produce either 35% or 45% of OIP with 42% or 58% probability if randomly completed in the fracture corridor or exclusion-zone, respectively. So, the expected reservoir recovery increases to 41% ($35\% * 0.42 + 45\% * 0.58$) which is almost 24% larger than that of single-completed well. A shortcoming of the simplified method is that it ignores the effect of the well's inflow zone size by considering only one (average) size in the statistically equivalent reservoir. Since the well's inflow zone controls well production, the size variation shall also be considered in computations of recovery. The objective of this study is to derive a new probabilistic method for computing distributed recovery factors for the fracture and matrix wells by considering uncertain wells' location in the corridor network.

6.2.2 Probabilistic Method for Well's Recovery Prediction from Well Placement Statistics

Placing oil well in the network of distributed fracture corridors makes the well's recovery a probabilistic variable as it depends upon uncertain well's location in the network. The uncertainty is two-fold; it concerns well's location within corridor network and well's possible intersection with the nearest corridor. In any network's location (with more closely- or more sparsely – spaced corridors), wells may intercept fracture corridors (fracture well) or go in-between two corridors in a matrix block (matrix-well). A fully probabilistic approach shall consider the combined probabilities of the near-well density of corridors and the well's collision with the corridors – i.e. being a fracture well or matrix well.

Determination of wells recovery predictions using probabilistic method would involve the following steps:

1) Derive the corridor distribution (in NFR) statistics using logs: Due to uneven distribution of fracture corridor network in an NFR, corridor spacing varies throughout the reservoir, and are also found to be typically related to other corridor attributes like width and length. As reported by Nelson [14], fracture corridor spacing, and width can be measured from horizontal bore hole image logs and geophysical attributes assuming parallel system of corridors. Number of corridors having width and spacing smaller than specified value can be measured, which would help obtain the relationship between cumulative frequency, spacing and width of corridor. Frequency as a function of corridor spacing can be normalized to a probabilistic distribution of corridor spacing.

2) Recovery modeling and estimation using NFR statistics: The recovery performance of matrix and fracture-well is modeled similar to the method chosen by Prasun and Wojtanowicz [12] by considering a discrete well's inflow zone and an outside zone of equivalent DPDP flow model. Only difference is that the simplified method estimates single value of well' recovery by considering only performance of fracture well and matrix well in a statistically-equivalent

reservoir with expected value of spacing and aperture. Whereas, the probabilistic method considers variation in well's recovery by considering different well's inflow zone locations in corridor spacing network and simulating their performance. Thereafter, the simulated recovery of matrix and fracture-wells is correlated as the continuous function of local corridor spacing inside the well's inflow zone using a best-fit curve.

3) Determination of overall recovery correlation: From the size of local corridor and exclusion-zone nearest to well's inflow zone, probability of being a matrix and fracture well can be determined. These probabilities can then be coupled with their respective matrix and fracture-well's recoveries to obtain the overall recovery correlation using statistical method of weighted average technique.

4) Determination of well's recovery distribution: Predictably, because of the distribution of corridor spacing network, there will be a discrete variation in well's recovery (placed at different locations in the network) each having a certain probability due to the probability of corridor spacing. The frequency (probability) of the occurrence of a recovery, once determined, can be normalized and integrated to obtain cumulative probability distribution.

In order to better understand the method, we would discuss its implementation in the example NFR [13] and compare its performance from the simplified method.

The fracture corridor spacing in the example NFR varies from 5.6m (18.8ft) to 46.5m (153ft) and fracture corridor widths in example NFR varies from 2.4m (8ft) to 9.5m (31ft). Assuming several locations in the reservoir with different intensity of corridor spacing would vary the size of the well's inflow zone. The well's inflow zone is the exclusion zone (matrix-zone) for matrix well and equals local corridor spacing – as shown in Fig 6.5A. For fracture well, the well's

inflow zone is equal to the sum of the intercepted corridor size and doubled size of the local corridor spacing – as shown in Fig. 6.5B.

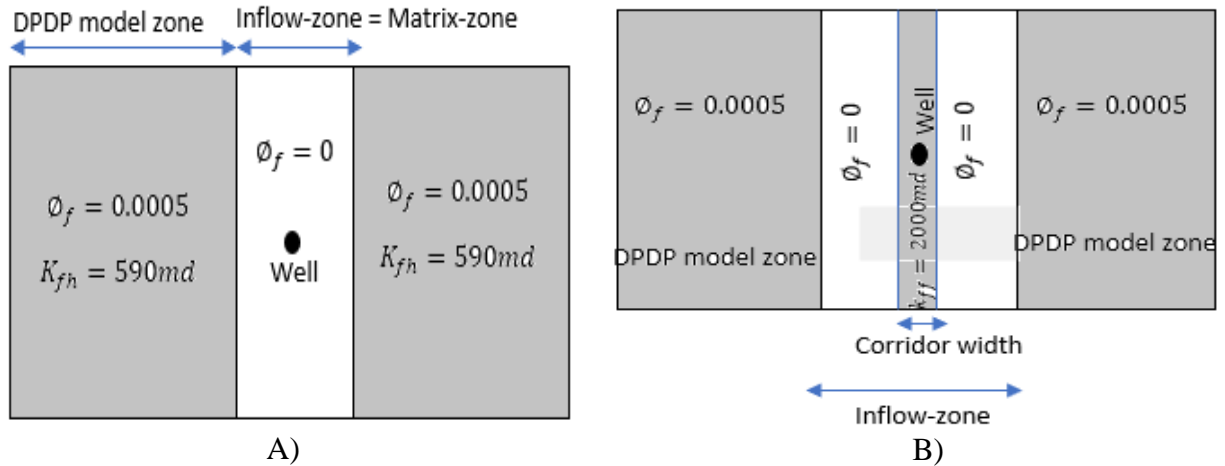


Fig. 6.5. A) Representation of matrix-well in a CMG DPDP flow model; B) Representation of fracture-well in a CMG DPDP flow model

Maximum well recovery is simulated using the NFR properties from Table A1 by assuming 20 years of well's production subjected to the maximum pressure drawdown (constrained by the bubble point pressure). For matrix well, the maximum pressure drawdown is 2000 psi and for fracture well, the optimum pressure drawdown is 100 psi. Table 2 shows the results.

Table 6.3. Effect of inflow zone size on recovery of fracture and matrix wells

Local corridor spacing, S_{pw} (ft)	Local corridor size, F_w (ft)	Well's inflow zone for fracture well, (ft)	Probability of fracture-well, $P(C1)$	Probability of matrix well $P(C2)$	Matrix well's recovery, $RF_{(C2)}$ %	Fracture well's recovery, $RF_{(C1)}$ %	Overall recovery, RF %
19	7.92	46	0.42	0.58	40	35	37.9
56	15.5	127.5	0.28	0.72	37	28	34.5
100	23.75	223.75	0.24	0.76	35.0	23.5	32.2
150	31.3	331.3	0.21	0.79	34.5	22	32.0

Using data from Table 6.3, matrix-well's recovery, $RF(C2)$, is correlated with local corridor spacing, S_{pW} (well's inflow zone size) as,

$$RF(C2) = 49.8S_{pW}^{-0.074} \quad (6.12)$$

The fracture-well's recovery correlation with the size of local corridor spacing is,

$$RF(C1) = 69.3S_{pW}^{-0.23} \quad (6.13)$$

Assuming a square drainage area with parallel dispersed system of corridors separated and surrounded by matrix block, probability of well intercepting the corridor, $P(C1)$ becomes a ratio of local corridor size, F_W and spacing, S_p , in a given location of well's inflow zone, given by (Table 6.3),

$$P(C1) = \frac{F_W}{S_{pW}} = \frac{0.79S_p[m]^{0.65}}{S_{pW}[m]} = 0.79S_{pW}[m]^{-0.35} \quad (6.14)$$

Probability of well intercepting matrix-zone separated by local corridor spacing, S_{pW} , $P(C2)$ becomes an alternate event, given by (Table 6.3),

$$P(C2) = 1 - P(C1) = 1 - 0.79S_{pW}[m]^{-0.35} \quad (6.15)$$

Overall recovery, RF , as a function of local corridor spacing would be a weighted average of fracture and matrix-well's recovery weighted by their probabilities ($P(C1)$ and $P(C2)$) for different well-inflow zone locations. From Table 6.3, relationship between local corridor spacing and total (overall) recovery can be correlated using the best-fit power law curve as shown in Fig. 6.6, which is given by,

$$RF = 49S_{pW}^{-0.088} \quad (6.16)$$

Figure 6.6 shows plots of the correlations of matrix well recovery, fracture well recovery and overall recovery.

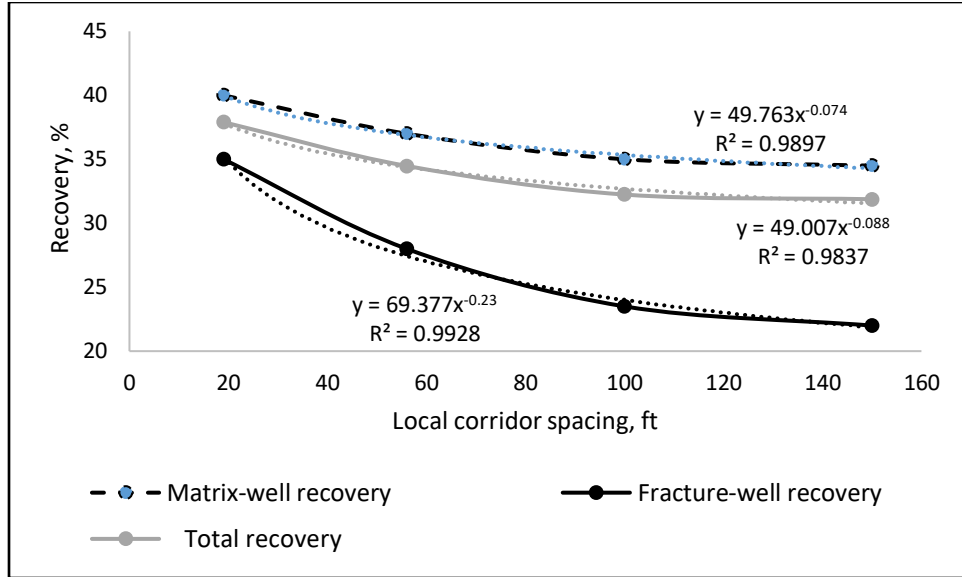


Fig. 6.6. Correlations of well recovery with local corridor spacing (size of well inflow zone)

Recovery plots indicate reduction of well recovery with increasing size of the well's inflow zone. The reduction can be explained as follows. In case of matrix well, there is a reduction in well's production rate due to the increase in near-well bore slightly permeable matrix zone size. Subsequently, the reduction in overall cumulative production for 20 years span of project life, results in a lower recovery.

Similarly, for fracture well, the final recovery significantly reduces with the increase in inflow zone sizes shown in Fig. 6.6. This happens because with the increase in well's inflow zone size, the corridor size or the corridor conductivity greatly increases resulting in a higher water-cut and hence, lower oil recovery.

6.2.2.1 Well's Recovery Distribution

From Eqs. (6.2) and (6.16), frequency of overall recovery, RF , would be given by,

$$F(RF) = 1.5 \times 10^{-19} RF^{11.36} \quad (6.17)$$

Cumulative probability distribution function, $CF(RF)$, is the probability that the variable takes a value less than or equal to RF . So, we can convert the frequency to cumulative probability

distribution by taking the integral of frequency between RF and its minimum value (equal to 32), and then dividing the resultant by cumulative frequency (Fig. 6.7), as

$$CF(RF) = \frac{\int_{32}^{RF} F(RF).dRF}{\int_{32}^{37.9} F(RF).dRF} = \frac{1.2 \times 10^{-20} (RF^{12.36} - 4 \times 10^{18})}{0.34} = 3.5 \times 10^{-20} (RF^{12.36} - 4 \times 10^{18}) \quad (6.18)$$

Probability density function would result from dividing the frequency by the cumulative frequency, as

$$P(RF) = \frac{1.5 \times 10^{-19} RF^{11.36}}{\int_{32}^{37.9} F(RF).dRF} = 4.4 \times 10^{-19} RF^{11.36} \quad (6.19)$$

Expected value of overall recovery can be derived as,

$$E(RF) = \int_{32.0}^{37.9} P(RF).RF dRF = \int_{32.0}^{37.9} 4.4 \times 10^{-19} RF^{11.36}.RF dRF = 36.6 \quad (6.20)$$

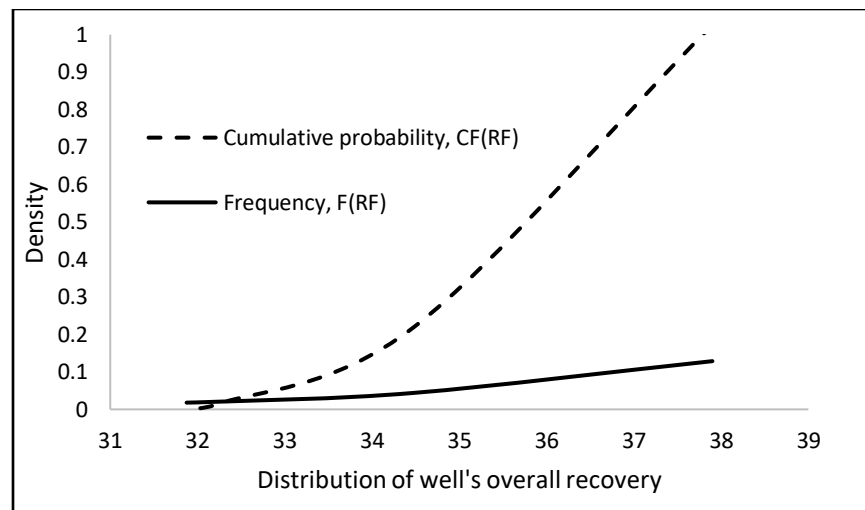


Fig. 6.7. Distribution of well's overall recovery

Table 6.4. Comparison of recovery for different well placements using probabilistic method from that obtained using simplified method

Methods of Recovery Estimation	Expected value of overall recovery	Recovery Discrepancy, % between the two methods
Method 1: Simplified method	33	10.9%
Method 2: Probabilistic method	36.6	

6.2.2.2 Discussions

Discussed here are two important questions resulting from the comparison study:

- Is the probabilistic estimation of recovery always higher than from the simplified method?
and,
- What is the advantage of knowing recovery distribution vs. just a single valued form the simplified method?

Comparing the expected recoveries using probabilistic method from that obtained using simplified method (Table 6.4), shows that the recoveries predicted from probabilistic method is greater than that from the simplified method for the subject NFR.

In order to extend the conclusion to other fields with similar corridor statistics, the study necessitates a mathematical proof of the theory, as shown below. In the proof, we shall consider the statistical theorem stating that convex transformation of a mean, $f(E[x])$ is less than or equal to the mean of the convex function, $E[f(x)]$ (Jensen, [15]), given by,

$$f(E[x]) \leq E[f(x)] , \text{ where } f \text{ is a convex function} \quad (6.21)$$

Physically, function f is convex if a line segment connecting two points on the graph of the function lies on or above the graph. Mathematically, function is convex if the second derivative is positive within the entire domain

With respect to this study, the above theorem states that if well's recovery is a convex function of corridor spacing (Fig. 6.6), then the mean value of recovery distribution (from the probabilistic method) is always greater than (or equal to) recovery value for the mean of corridor spacing distribution (from the simplified method).

As shown in Fig. 6.6 all three correlations of well recovery with the local corridor spacing are power functions written as,

$$RF_{Prob} = f(S_{pW}) = aS_{pW}^{-b} \quad (6.22)$$

In the simplified method, expected value of spacing, $E(S_{pW})$ defines a well's inflow zone size, so from Eq. (6.22), recovery becomes a function of this local corridor spacing, $E(S_{pW})$ as,

$$RF_{Simplified} = f(E(S_{pW})) \quad (6.23)$$

In the probabilistic method, we obtain the expected value of recovery – defined by central measures of tendency, from its distribution, so from Eq. (6.22), we get,

$$E(RF)_{Prob} = E(f(S_{pW})) \quad (6.24)$$

Second derivative of the function in Eq. (6.22) is

$$f''(S_{pW}) = ab(b+1)S_{pW}^{-(b+1)} \geq 0 ; \text{ so } f \text{ is a convex function.}$$

Using the Jensen's inequality from (Eq. 6.21), we get,

$$E(f(S_{pW})) \geq f(E(S_{pW})) \quad (6.25)$$

Therefore, from Eqs. (6.23), (6.24) and (6.25), we get,

$$E(RF)_{Prob} \geq RF_{Simplified} \quad (6.26)$$

This mathematically proves that the recovery obtained from probabilistic method would always be greater than that of simplified method for NFRs with distributed corridors.

Since probabilistic method provide us with an information on the variation in recovery along with the probability of its occurrence, it gives an operator an idea of the field performance or the revenue associated with risk assessment. Alternatively, by only providing the measure of central tendency of the corridor attribute and a single valued mean recovery, simplified method fails to consider the statistical distribution of corridor network and the recovery associated with it, thereby limiting the statistical spectrum of information. Failure to provide the probability

associated with the recovery limits the importance of simplified method in terms of reservoir performance evaluation and prediction.

Summary

In the study, two methods – simplified and probabilistic method of estimating well's recovery followed by their comparison is outlined for an example NFR implementation. Consequently, simplified method yields one value of recovery since it simplifies the NFR (with distributed fracture corridor network) to a single uniformly spaced statistically-equivalent reservoir using measures of central tendency, whereas the probabilistic method produces the matrix and fracture well's recovery correlation as a function of local corridor spacing. The spacing correlated recoveries corresponding to matrix and fracture well placement weighted by their probabilities can be combined to give a single distribution of overall recovery. Following conclusions can be deduced from the study,

- 1) For the field case NFR studied using simplified method, a complete reservoir development with single-completed wells would include 42 % fracture-wells recovering 28% and 58% matrix-wells recovering 37% of OIP, respectively – giving the total value of reservoir recover factor, $RF=33\%$. This also implied that well should be completed in exclusion-zone because of higher mean recovery.
- 2) The results also show some productivity advantage from using DWS technology in the field case NFR. Dual-completed DWS wells recover more oil ($RF=45\%$) with their two completions placed in an exclusion-zone rather than in fracture corridors ($RF=35\%$). Also, as the DWS wells recover more oil, the overall reservoir recovery factor, $RF=41\%$ would be almost 24% larger than that for single-completed wells.

- 3) Simulation results of matrix and fracture well's recovery as a function of well nearby local corridor spacing for example NFR demonstrates a power-law relationship, where both matrix and fracture well's recovery reduces with the increase in well's inflow zone size and recovery being more sensitive at low inflow zone sizes.
- 4) The overall recovery determined by weighted average of the matrix and fracture well's recovery weighted by their probabilities is found to be a power-law function, when correlated with the well's nearby local corridor spacing.
- 5) The probabilistic estimation gives higher values of expected recovery as compared to the simplified method – from 37% to 38% for matrix-well, and 28% to 30.36% for fracture-well. Moreover, the probabilistic method overestimates the total recovery by 10.9% from 33% (by simplified method) to 36.6%. The mathematical proof demonstrates that the recovery estimated from probabilistic method would always be greater than that from simplified method.
- 6) Another advantage of the probabilistic method is that it assigns probability to any value of recovery factor used in the reservoir management economics. For example, these results show that there is a considerable 30% probability of having recovery greater than the expected value of 36.6%. In practical applications, such information would help operators make reservoir development decisions based upon the risk-benefit considerations.

Chapter 7. Feasibility of Downhole Water Loop (DWL) Wells in NFRs

The chapter conducts a feasibility study of Downhole water loop (DWL) wells in NFRs with planar fracture network and fracture corridors. The study verifies the feasibility of DWL well by comparing the recovery performance of DWL well with the single-completed and DWS wells for their on and off-fracture variants. Once the feasibility is confirmed, a detailed model of DWL improved recovery performance is developed to screen potential NFR candidates for DWL application.

7.1 DWL Well Concept and Application

In a bottom-water reservoir with severe water coning, dual completed DWS well with completions above and below oil-water contact would help reduce water coning, however at the cost of additional water from water sink being produced at the surface. Studies on single porosity reservoirs (Shirman and Wojtanowicz 2000) have shown that disregarding water-cut from bottom completion significantly improves the recovery as compared to that of single completed well. However, the treatment and disposal costs associated with the additional water produced from bottom completion in DWS well would significantly cancel the gain due to additional recovery. Alternatively, with an additional completion further deep in the aquifer using downhole water loop (DWL) well would reinject the sink water back into the aquifer and thus eliminate the cost of surface water treatment and disposal. DWL wells feature two completions in the bottom aquifer: the upper one (water drainage) - for water coning reduction in the oil pay, and the lower one - for the drained water injection to the same aquifer). Injecting the produced water from drainage completion back into the aquifer serve two purposes: 1) help eliminate the problem of surface water disposal, and 2) also help maintain the aquifer strength. To date, DWL has been successfully implemented in conventional (non-fractured) oilfields (Jin 2013), however, no work has been done

to verify their feasibility in bottom-water naturally-fractured-reservoirs (NFRs) notorious for severe water problem.

7.2 DWL Well in NFRs with Fracture Corridor

Literatures (Ozkaya 2010, Ozkaya and Minton 2007; Bustos et al. 2010) reported in Chapter 2, indicate the severity of water coning in NFRs with fracture corridors as the underlying concern of reduced oil recovery from such NFRs. Although studies shown in chapter 6 concluded that the downhole water sink (DWS) wells in NFRs with fracture corridors yield higher recovery for both on and off-corridor well placements, they disregard the cost of additional water being produced at the surface due to bottom completion. Since DWL well would eliminate this additional water, there is a need to investigate the feasibility of DWL wells in such NFRs. This is because single porosity reservoirs have already demonstrated a strong pressure interference effect between the bottom water loop completions (Jin 2013), resulting in DWL well's reduced performance. The pressure interference effect between the water loop completions in the aquifer can be understood by flow streamlines for 2D flow in a DWL well system as shown in Fig. 7.1. We know that the change of pressure with respect to spherical radius (dp/dr) is inversely proportional to the spherical radius ($1/r^2$), and is proportional to the permeability. It means that at large radial (horizontal or vertical) distance from the wellbore, pressure gradient would be extremely small; so, if the water loop completions are separated by large vertical distance, there would be less pressure interference between the water loop completions. In contrary, for small vertical separation between the water loop completion placed in a higher vertical permeability NFR formation, would induce higher pressure interference reducing the performance of DWL well in NFRs.

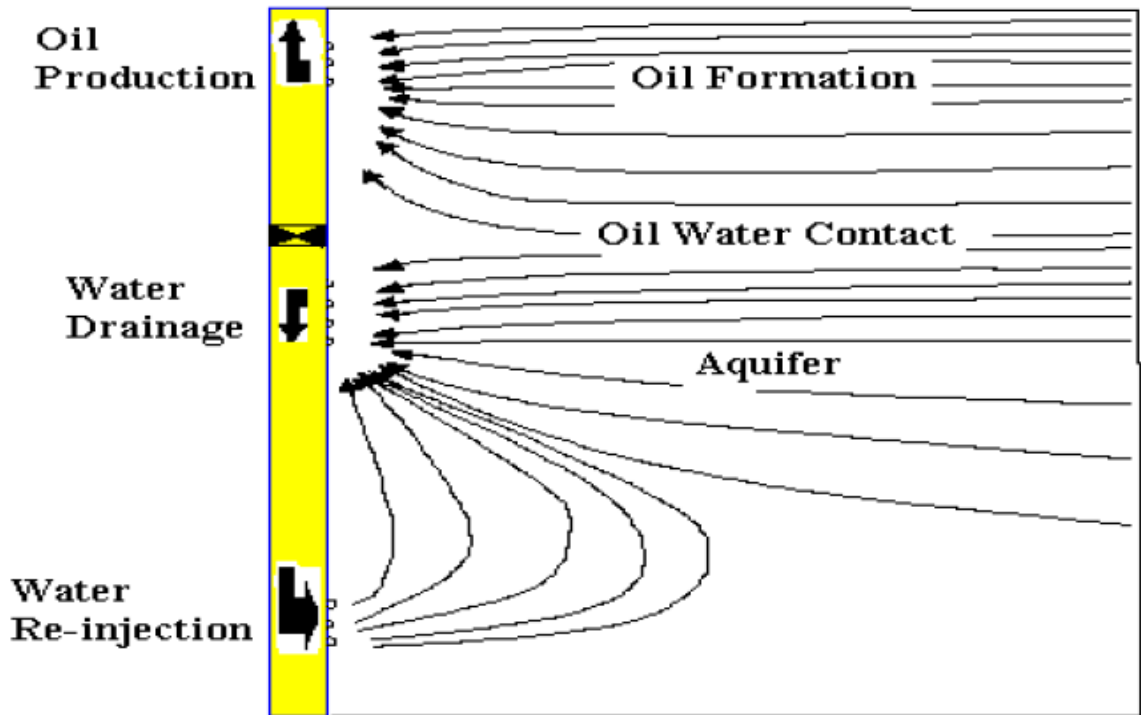


Fig. 7.1. Flow Streamlines in a 2D Downhole water loop well system (Jin 2013)

However, in NFRs with fracture corridor, demonstrating much higher vertical permeability, the pressure interference should be higher as compared to that in single porosity reservoirs, which may result in further reduced performance of DWL well. Similar to DWS well described in Chapter 6, we consider two possible placements DWL well completions in fracture corridors.

- 1) All the three completions intersect the fracture corridors;
- 2) All three completions in the exclusion zone away from the corridor.

7.2.1 DWL Well Penetrating Fracture Corridors

We employ a 3D Cartesian partially discrete DPDP model as described in Chapter 4 (Fig. 4.6) to simulate NFR with fracture corridors shown in Figs 7.2. Oil recovery is terminated when the upper completion water-cut reaches 97% for producing the top completion at the maximum possible rate of 5000 bbl/day constrained by the surface facilities. The water sink (bottom

drainage) completion operation is adjusted and optimized as discussed below and shown in Fig. 7.3. We assume large aquifer thickness of 500ft to provide for various separations between the downhole water loop completions - water drainage (sink) and water injection completion shown in Figs. 7.2.

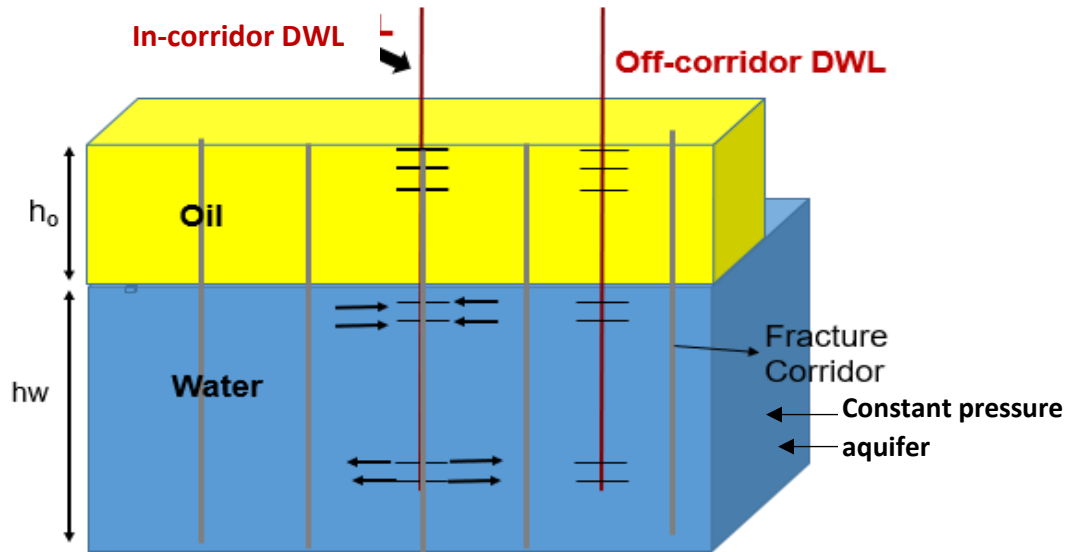


Fig. 7.2. Side View Schematic of DWL Well in NFR with Fracture Corridors

In our study, we assume the NFR is supported by strong aquifer which is modeled by a constant pressure aquifer as shown in Fig. 7.2. We consider base case NFR-well properties shown in Table B-3 (Appendix B), while varying reservoir-well properties such as corridor horizontal permeability, corridor spacing, corridor anisotropy ratio and mobility ratio to yield six different cases of DWL-NFR system shown in Table 7.1. The reason for the selection of these properties is based on the simulation results of chapter 4 which showed that only near well bore (well-inflow) region represented by partially discrete DPDP model controls the local water coning and hence the oil recovery of corridor-type NFR. The local near wellbore properties would include near wellbore corridor horizontal and vertical permeability, corridor spacing and fluid viscosity.

We begin the feasibility study by simulating the recovery of DWS well using series of different bottom completion water drainage rates and identifying the optimum DWS drainage rate for each of the four cases. As shown in Fig. 7.3, top completion recovery (at 97% water-cut) increases with the increase in water drainage rate, until there is no further significant increase in recovery, and we see the curve almost flattening. We select the optimum DWS water drainage rates and their respective DWS optimum recoveries (Table 7.1) before the oil recovery curve begins flattening (Fig. 7.3). In each of the cases, we place bottom water sink completion such that the oil-cut due to inverse oil coning is less than 0.0003. In determining the optimum drainage rate, we ignore the water produced from bottom completion (assuming they do not add treatment/disposal cost) and consider only the water produced from top completion in determining oil recovery at 97% economic limit of water-cut. We also determine DWS oil recovery (at $WC_{total}=WC_{econ}$) while considering the total water-cut both from top and bottom completion, which is found to be even lower than that of single-completed well as shown in Table 7.1.

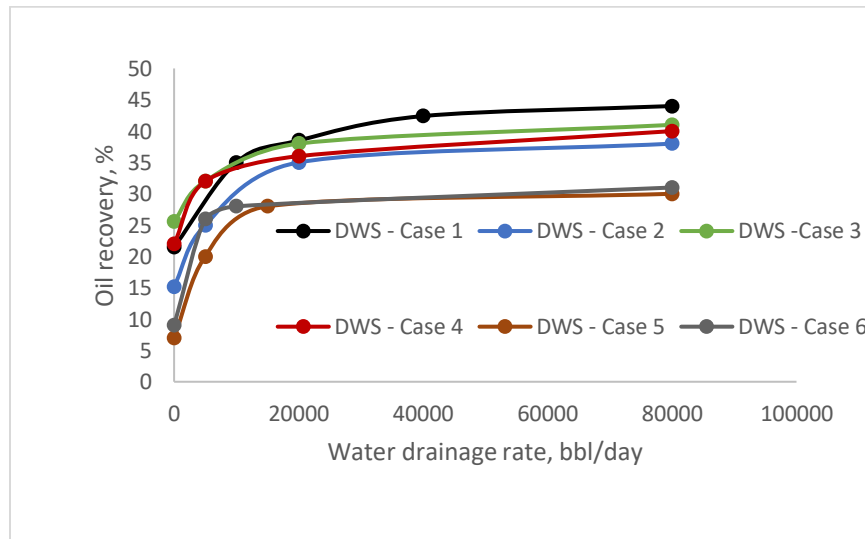


Fig. 7.3. DWS well recovery vs. water sink rate for six NFR cases shown in Table 7.1

Table 7.1. Single-completed, DWS and DWL well recovery in NFRs with fracture corridors (Top completion rate =5000bbl/day, Separation between water loop completions = 400ft)

Case	Corridor horizontal permeability, md	Corridor spacing, ft	Mobility ratio	Corridor anisotropy ratio	Optimum water sink rate, bbl/day	DWS recovery (WC _{top} = WC _{econ}), %	DWS recovery (WC _{total} = WC _{econ}), %	Single well recovery, %	DWL recovery, %
1	10000	50	1	10	30000	40	17	21.5	22
2	10000	200	1	10	20000	35	12.2	15.2	15.5
3	20000	50	1	10	20000	38	20.3	25.6	26.3
4	20000	200	1	10	15000	34.5	17.4	22	22.5
5	10000	50	2	5	17000	30	5.5	7	7.4
6	20000	200	2	5	8000	31	7.8	9	9.3

Since DWS well's recovery when total water-cut becomes equal to 97% for each of the cases is lower than that of single-completed well, we would not consider its implementation in NFRs with fracture corridors. This happens because when total water cut, WC_{total}, is considered the economic life of DWS well is shortened (and recovery reduced) comparing with the recovery when only top completion water cut, WC_{top} is considered.

As discussed before, increasing separation between the water loop completion in DWL well would help reduce the pressure interference and thus improve the recovery. However, increasing separation would be constrained by the aquifer thickness (450ft) and also by additional operating cost of drilling and completion. So, we study the impact of increasing separation length between the water loop completions on DWL well's recovery. The effect of separation is studied by running the series of simulations with increased separations for the same six cases shown in Table 7.1. The results, plotted in Fig. 7.4, show that DWL well's recovery does not increase and remains almost constant equal to single well completion recovery at zero separation between the water loop completions.

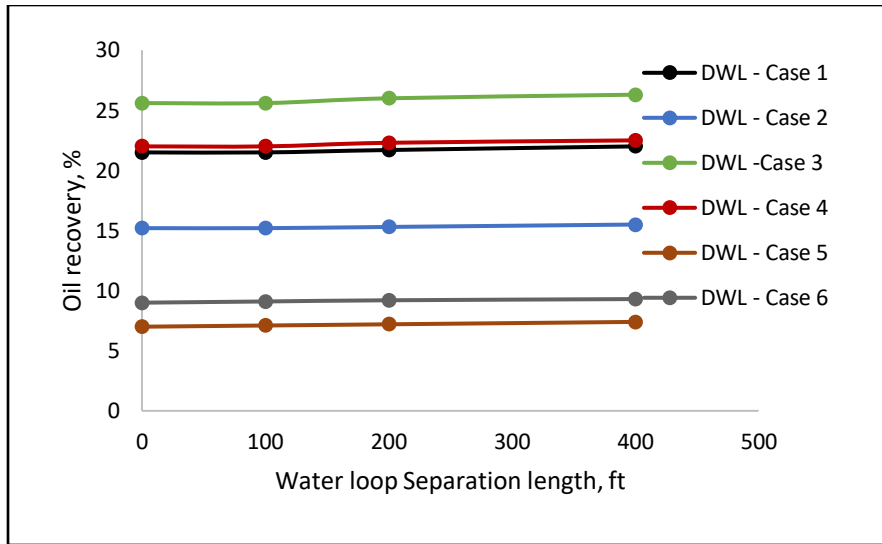


Fig. 7.4. No effect of water loop separation on DWL well recovery for six NFR cases in Table 7.1

The result indicates that strong pressure interference between the two water loop completions (within the aquifer thickness) entirely eliminates water coning control so the single completed wells are good enough and there is no benefit of DWL completion for wells located in the fracture corridors of this NFR.

To investigate this effect further, we analyze the downhole water loop's flow extend using the tracer simulation map technique by virtually adding one volume-percent of a tracer to the water injected at the DWL bottom completion. The tracer distribution map, shown in Fig. 7.5, reveals that almost all tracer stays inside the fracture corridor as - within a sheet-like corridor NFR - the corridors are not interconnected. Hence, the injected water returns to the water sink completion thus eliminating pressure drawdown at the completion and the resulting control of water coning in the oil payzone.

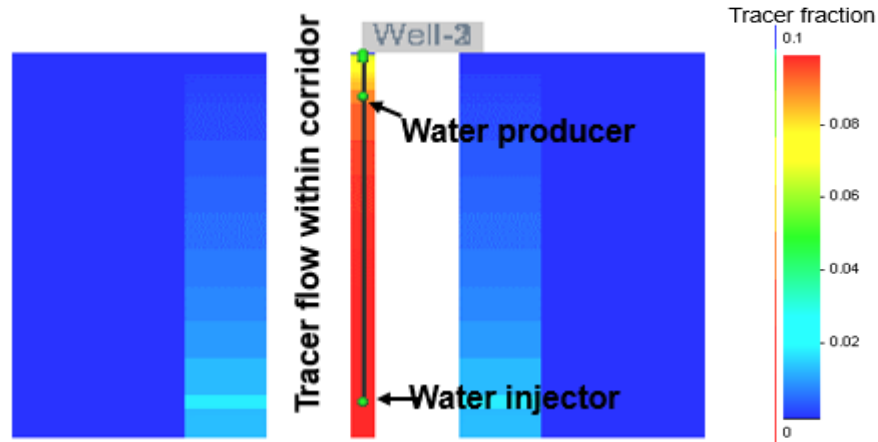


Fig. 7.5. Tracer map showing concentration of tracer in water injected via water injector in a DWL well located in fracture corridor

7.2.2 DWL Well Penetrating Exclusion-Zone

We again employ a 3D Cartesian discrete DPDP model as shown in Chapter 4 (Fig. 4.7) to simulate DWL in the center of an exclusion-zone. We operate both the top and sink completions by fixing the bottom-hole pressure equal to bubble point pressure, so the maximum possible pressure drawdown is achieved at both the completions. The constant bottom-hole pressure operation assumes that the simulator adjusts the rates for top completion accordingly to maintain the constant completion's pressure while drawing additional water from the sink. We operate at the maximum possible pressure drawdown only to produce the completions at its maximum rate capacity from the lower permeability matrix well completions. We also make sure that the oil-cut due to inverse oil coning at the water sink completion is minimal (< 0.0003) by adjusting the placement of bottom sink completion using trial-and-error approach. For DWL well, the third completion simply reinject back the water being produced from the water sink completion. Therefore, since in DWL well, only the top completion is responsible for water production, we would constrain the well-life at 97% water-cut from top completion. We use the same six NFR cases shown in Table 7.1 to simulate the DWS and DWL well in exclusion-zone surrounded by

fracture corridors. We simulated and plotted DWL well's oil recovery (at 97% water-cut) as a function of separation length between water loop completions shown in Fig. 7.6. We observe the insensitivity of the separation to the DWL well's recovery (Fig. 7.6) suggesting the strong interference between the water loop completions.

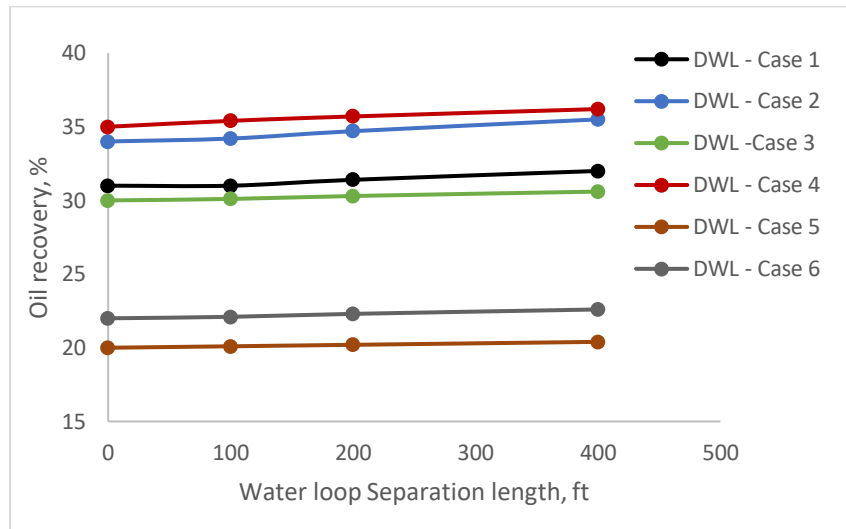


Fig. 7.6. Negligible effect of water loop separation on oil recovery with DWL well placed in exclusion-zone for six NFR cases in Table 7.2

Table 7.2. Recoveries for single completed, DWS and DWL well in NFRs with fracture corridors for four mixed-wet type NFR cases (Upper and bottom completion pressure drawdown = 2000psi, Separation between top/bottom completions = 400ft)

Case	Corridor horizontal permeability, md	Corridor spacing, ft	Mobility ratio	Corridor anisotropy ratio	Single well recovery	DWS recovery (WC _{top} = WC _{eco}) n. %	DWS recovery (WC _{total} = WC _{eco}) n. %	DWL recovery, %
1	10000	50	1	10	31	45	25	32
2	10000	200	1	10	34	47	30	35.5
3	20000	50	1	10	30	44	26	30.6
4	20000	200	1	10	35	46.5	31	36.8
5	10000	50	2	5	20	35	17	20.4
6	20000	200	2	5	22	36.2	18	22.6

The tracer map in Fig. 7.7 shows that the water injected by the well's bottom completion moves first through the exclusion-zone (Fig. 7.7a) to the nearest corridor (Fig. 7.7b-), then flows upwards in the corridor (Fig. 7.7b), and returns back to the well's sink completion through the exclusion zone (Fig. 7.7a). The tracer map explains strong pressure interference between the two water loop completions due high conductivity of the fracture corridor outside the exclusion zone surrounding the well. Even very large (up to 200 ft) exclusion zone does not provide sufficient hydraulic barrier between the two completion as they become hydraulically connected by the nearest corridor. In the result, there is negligible improvement in DWL recovery performance with increasing separation comparing to the single-completed well's performance.

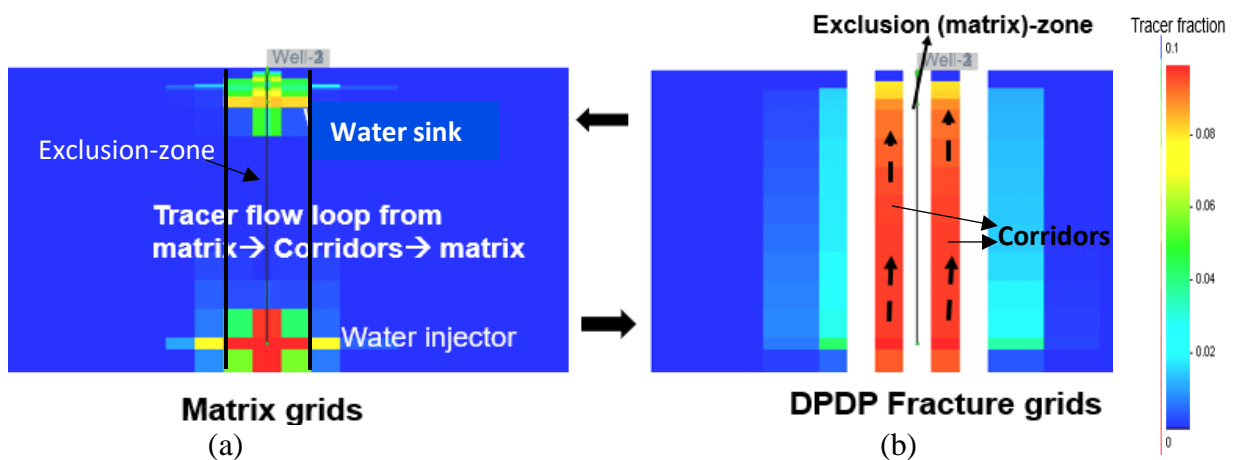


Fig. 7.7. Tracer concentration maps in (a) matrix-grids; and (b) DPDP fracture grids for DWL placed in NFR exclusion-zone

7.3 DWL Well in NFRs with Planar Fracture Network

We will consider two possible variants of DWL well completions placement in planar network.

- 1) All the three completions intersect the planar fracture;
- 2) All three completions in the matrix zone away from the fracture.

7.3.1 DWL Well Intersecting Planar Fracture Network

We employ a 2D radial-cylindrical dual porosity/dual permeability (DPDP) model of IMEX (CMG) (Fig. 7.8) to simulate NFR with planar fracture network shown in Figs 4.2 and 4.3B (Chapter 4). We assume large aquifer thickness of 500ft to provide for various separations between the downhole water loop completions - water drainage (sink) and water injection completion shown in Fig. 7.8.

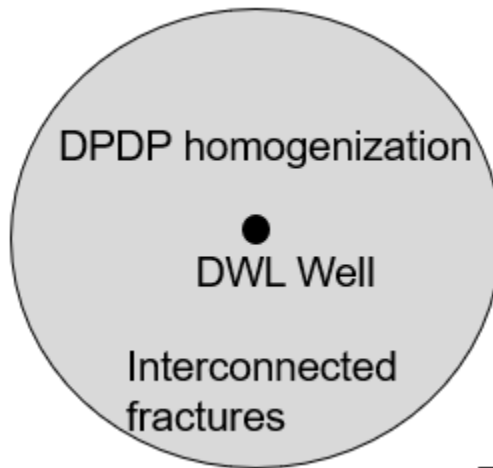


Fig. 7.8. Top view schematic of DWL well in NFR with planar fracture network

We consider base case NFR-well properties shown in Table B-3 (Appendix B), while varying reservoir properties such as fracture permeability, matrix permeability, and mobility ratio to yield four different cases of DWL-NFR system shown in Table 7.3. We only consider these properties for comparison because they constitute the main reservoir and fluid which control the Darcy-law flow rate in a single-porosity reservoir, and hence the oil recovery, assuming the reservoir dimensions do not play a significant role in oil recovery. Since the NFR with planar fracture network is modelled as DPDP equivalent flow system, where input simulator properties including effective fracture permeability allows for the fracture spacing and intrinsic fracture permeability variation; we do not consider them as the sensitivity parameters. We also assume that

the fracture vertical permeability is 5 times that of fracture horizontal permeability to simulate the most representative behavior of vertical/subvertical planar fractures type NFRs having anisotropy ratio varying from 1 to 10 (Prasun and Wojtanowicz 2019, Ozkaya 2010, Prasun and Wojtanowicz 2020).

We determine the water sink completion operation by simulating the recovery of DWS well using series of different bottom completion water drainage rates while the top completion is produced at the maximum possible rate of 5000 bbl/day limited by the surface facility. (Oil recovery is terminated when the upper completion water-cut reaches 97%). As shown in Fig. 7.9a, the DWS well's drainage rate increases oil recovery that eventually becomes practically constant and its plot flattens. Also, at zero drainage rate, DWS well behaves like a single-completed well. The recovery improvement with DWS is particularly evident for heavy oil reservoirs (Cases 1 and 2) where single-completed well recovers almost nothing. (A slim water cone rises very quickly with almost instant water breakthrough and rapid increase of water cut.)

We use the plots in Fig. 7.9a to find optimum values of DWS well water drainage rates (used in Table 7.3) at the points where the oil recovery plots begin to flatten out. Moreover, in determining the optimum drainage rate, we adjusted sink completion placement below oil-water contact, such that the oil-cut due to inverse oil coning is minimal (<0.0003). We also ignored the water produced from bottom completion (assuming they do not add treatment/disposal cost) and considered only computed water produced from the top completion to terminate the well production at 97% economic limit of water-cut. However, we also included in Table 7.3 actual values of DWS well oil recovery by considering total water-cut from the top and drainage completion equal to 97%. The results show that the actual DWS well recovery (when disposal cost

of all produced water is considered) becomes smaller than that of the single-completed well. he cost

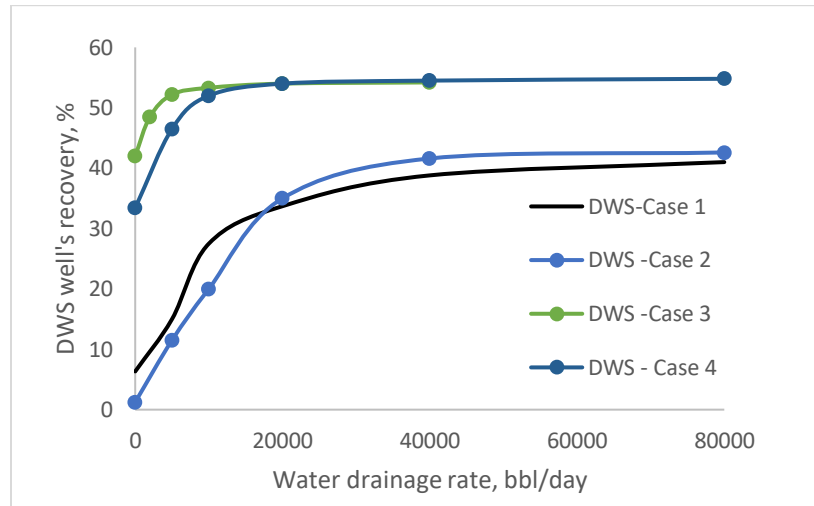


Fig. 7.9. Oil recovery vs. water drainage rate plot of on-fracture DWS well for four cases shown in Table 7.1

Table 7.3. Design of experiments for vertical DWS in planar network NFR (moderately water-wet) (Upper completion production rate = 5000bbl/day, Aquifer thickness= 450ft)

Cases	Fracture horizontal permeability, md	Matrix permeability, md	Mobility ratio, M	Water sink rate, bbl/day	DWS recovery (WC _{top} =WC _{econ}), %	DWS recovery (WC _{total} =WC _{econ}), %	Single well's recovery, %
1	600	5	3	40000	38.8	5.9	6.33
2	400	30	5	40000	41.6	1.2	1.25
3	300	40	1	5000	52.2	33.4	42
4	1000	100	2	10000	52	26.3	33.4

- All reservoir properties are shown in Appendix B (Table B3)

After determining the optimum water loop rates for DWS well (Table 7.3), we would use the same water sink rates in DWL well for those cases. We would study the impact of increasing separation length between the water loop completions on DWL well's recovery (at 97% water-cut) by running series of simulations for these four cases (Fig. 7.10).

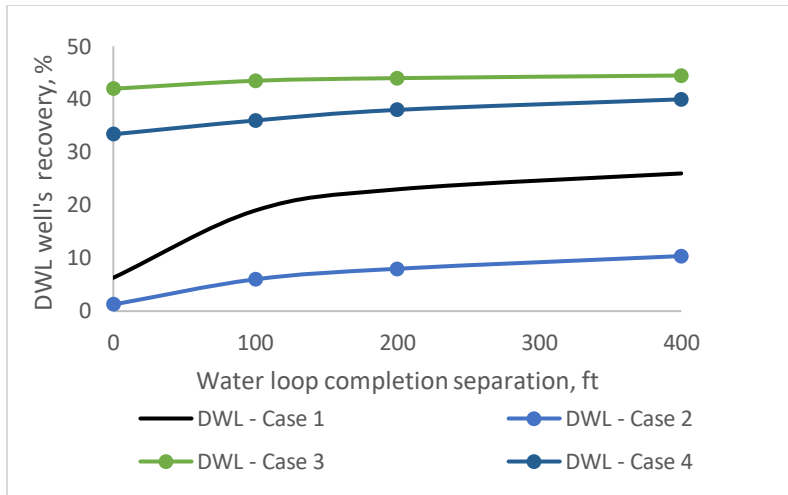


Fig. 7.10. Oil recovery vs. water loop completion separation length of on-fracture DWL well for four cases shown in Table 7.3

The plots in Fig. 7.10, show that there is a considerable effect of separation size on DWL’s recovery for cases 3 and 4 comparing to small effect for cases 1 and 2. The difference results from the high mobility ratio in case 1 and 2, where DWL well provides stronger suppression of water cones height and shape in oil-zone with increasing separation of two water loop completions. A reservoir with lower water cone would have more oil and less water flowing into the well resulting in lesser bypassed oil and higher recovery (Fig. 7.11 a and b). In contrast, , in the low-viscosity oil reservoir (case 3), the water saturation maps in Figs. 7.11 c and d display no significant change of the water cone shape and height due to increasing DWL completions separation that gives insignificant increase in oil recovery shown in Fig. 7.10.

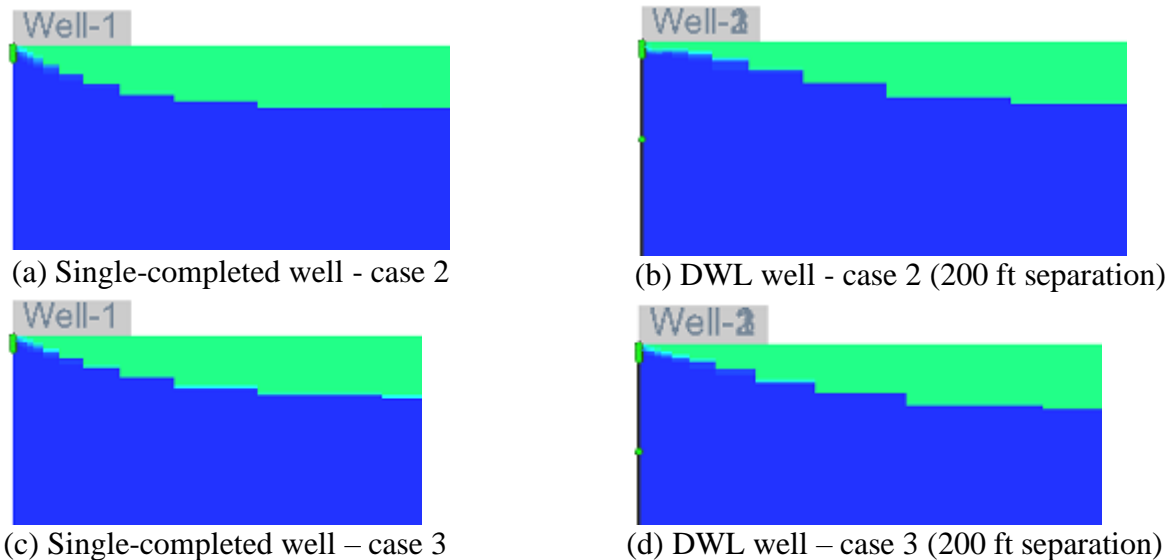


Fig. 7.11. Water saturation maps in NFR fracture grids (DPDP MODEL) (after 1 year of production) for Case 2 and 3 in Table 7.3

Moreover, in contrast to the non-performance of DWL wells with increased separation in NFRs with fracture corridors (Figs. 7.4 and 7.6), there is a significant improvement in the performance demonstrated by DWL well in NFR having planar fracture network (Fig. 7.10). This can be understood by comparing the tracer maps in Figs. 7.5 and 7.7, with that in Fig. 7.12, which shows how the tracer spreads laterally from the water injector to the surrounding region due to the connectivity of fractures. This means that relatively smaller amount of tracer (i.e. injected water) returns back to the water sink completion due to smaller pressure interference effect so that the water sink completion can better control water coning in the oil pay zone.

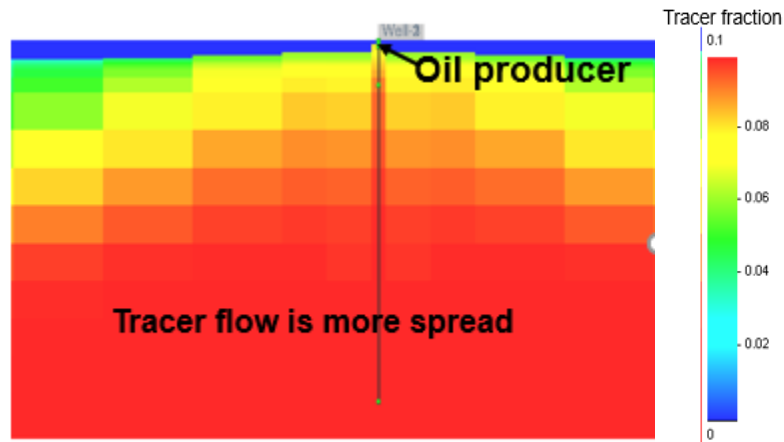


Fig. 7.12. Tracer map shows spatial spread of tracer around the water loop completions of DWL well in planar fracture network

Since the DWL wells' performance increases with the separation distance between the water loop completions the best performance becomes limited by the aquifer thickness (equal to 450ft in the study). For comparing DWL with two other types of wells we consider the maximum separation of equal to 400ft. A comparison of the DWS and single-completed wells' performance (from Table 7.3) with the simulated performance of DWL well is shown listed in Table 7.4 and depicted in Fig. 7.13. The results show that DWL well could be the best installation in NFRs with heavy oil and high values of mobility ratio – represented by Cases 1 and 2. In fact, DWL becomes the only well design option for significant recovery (RF=10.4% comparing to 1.25% or 1.2% for single-completed and DWS wells, respectively). Moreover, DWS well performance would strongly depend upon the cost of water disposal as this type of well in NFR has to produce a lot of water to control water coning and, therefore, has to be shut down early when the water disposal cost breaks even with the revenue from produced oil.

Table 7.4. Comparison of ultimate recovery between single-completed, DWS and DWL well for four cases shown in Table 7.3

Cases	Single Well's recovery, %	DWS (both completions) recovery, %	DWL recovery, %
Case 1	6.3	5.9	26
Case 2	1.25	1.2	10.4
Case 3	42	33.4	44.5
Case 4	33.4	26.3	40

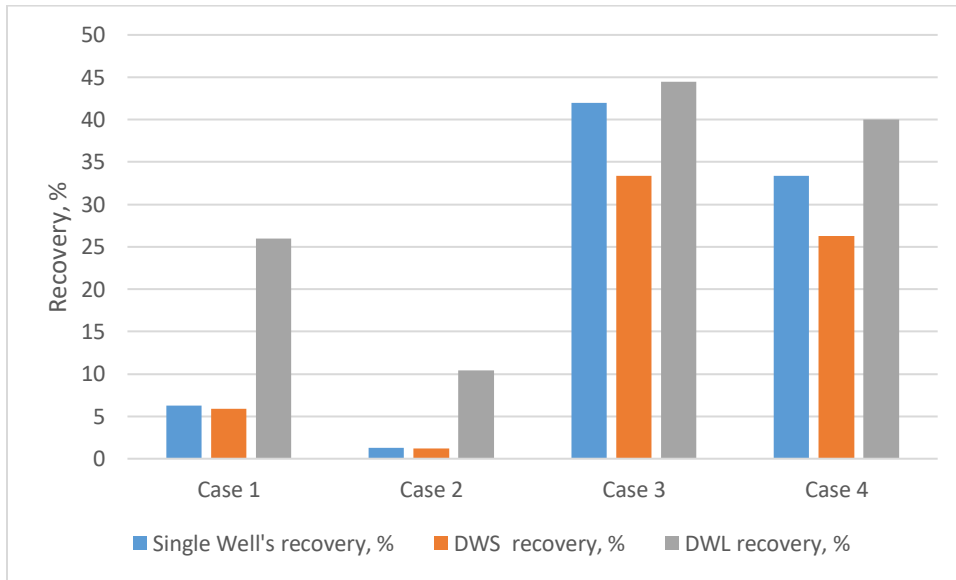


Fig. 7.13. Comparison of ultimate recovery with single-completed, DWS and DWL wells for four cases in Table 7.3

7.3.2 DWL Well Completed in NFR Matrix

In this section we consider a possible (though the least likely) scenario of the three types of wells (single-completed, DWS and DWL) with no completion intercepting fracture network. The scenario complements the study by being the least likely but extreme as all other possible cases of NFR wells would fall between the two extremes with some completions connected to the fracture network. This study involves again a series of simulation runs using 2D radial cylindrical DPDP model (CMG) by assigning zero fracture porosity to the matrix-zone (Fig. 4.3B) where all

the three DWL completions are completed in the middle matrix between two neighboring fractures. We operate both the top and water sink completions by adjusting the rate such that their bottom-hole flowing pressures are equal to bubble point pressure so the maximum possible pressure drawdown (2000 psi) is maintained at both completions. We create six reservoir cases shown in Table 7.5 by considering all parameters from Table 7.3 and additional variable - fracture spacing. We add fracture spacing because of the way DWL well placement in the rock matrix is modelled – as shown in Fig. 4.3 (Chapter 4). When completed in the matrix, DWL well’s performance is strongly dependent on the matrix zone size (equal to the fracture spacing). We also assume that the fracture vertical permeability is 5 times that of fracture horizontal permeability to simulate the most representative behavior of vertical/subvertical planar fractures type NFRs having anisotropy ratio varying from 1 to 10 (Prasun and Wojtanowicz 2019; 2020).

A comparison of recoveries with the three types of wells completed only in the NFR matrix is shown in Table 7.5. For the DWL installations, we analyze the relationship between well’s recovery and the water loop completions’ separation length shown in Fig. 7.14. We use the relationship to determine maximum recovery with DWL wells.

Table 7.5. Simulated optimum recovery comparison among single well, DWS well and DWL well for four cases (Table 7.3) (Top and bottom completion pressure drawdown = 2000psi, separation between top and bottom completion = 400ft)

Cases	Fracture horizontal permeability, md	Matrix permeability, md	Mobility ratio, M	Fracture spacing, ft	Single well’s recovery, %	DWS recovery (Top completion), %	DWS recovery (both completions), %	DWL well’s recovery, %
1	600	5	3	20	10	40	24.6	30
2	400	30	5	20	5	44	20.2	25
3	300	40	1	20	51.1	59	44.6	54.3
4	1000	100	2	20	41.2	52	38.1	46.5
5	300	40	1	10	51	58.8	44.9	53.6
6	400	30	2	10	41	52	39.3	46.3

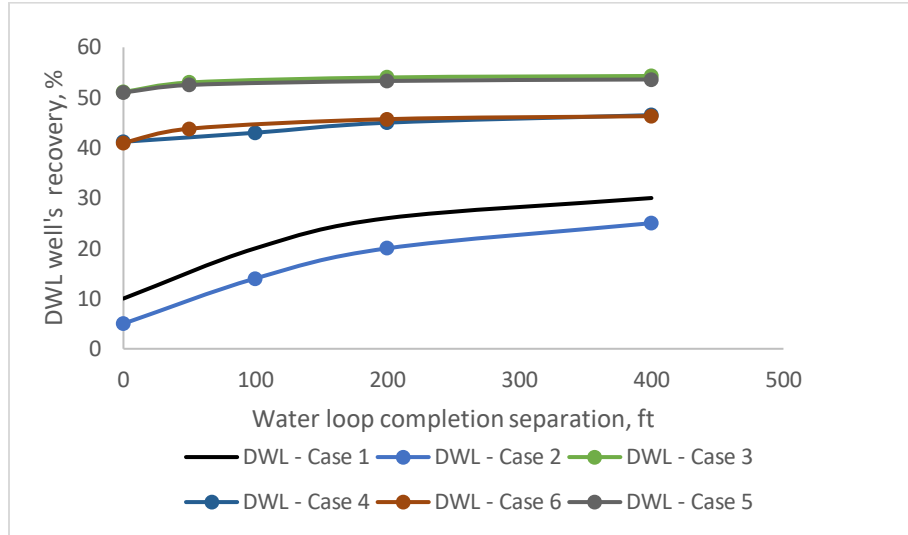


Fig. 7.14. Oil recovery vs. water loop completion separation length of DWL well completed in matrix-zone for four cases shown in Table 7.1

The plots in Fig. 7.15 indicate that, in some cases, DWL well's recovery increases with increase of separation size between the water loop completions until the aquifer thickness limit (=450ft) is reached. For comparison with other well types, we choose the maximum recovery of DWL well having 400-foot separation between water drainage-injection completions, shown in Table 7.5. Fig. 7.15 gives recovery comparison of the single, DWS, and DWL wells having all completions in the NFR matrix. Clearly, DWL well recovers more than single completed well and DWS well, particularly in Cases 1 and 2 (heavy oil- high oil/water mobility ratio) where significant improvement in recovery is similar to that of the on-fracture DWL well. Fig. 7.16 also shows that both single - completed and DWL wells intercepting matrix recover more than when they intercept fractures. This is because of the already higher recovery performance demonstrated by the single-completed well in matrix-zone (already shown in Chapter 4), making DWL overall recovery higher as compared to that of on-fracture DWL well completion.

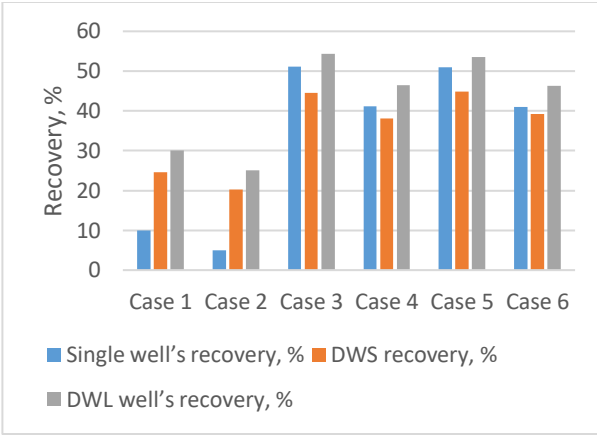


Fig. 7.15. Recovery of three well types with all completions placed in NFR matrix for six reservoir cases in Table 7.5

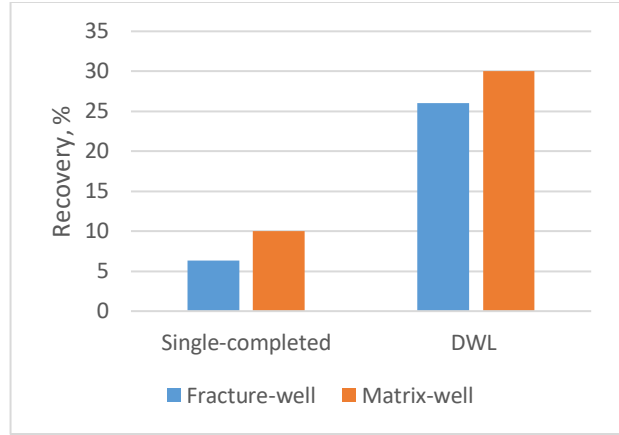


Fig. 7.16. Recovery of single-completed and DWL wells located in NFR matrix or fracture for heavy oil Case 1

In summary, the study of DWL performance in planar NFRs shows that: (a) the recovery increase with increasing water loop separation may be insignificant; (b) the rate of recovery increase reduces with separation; and, (c) maximum size of separation is limited by the aquifer thickness. Therefore, decision on DWL well construction in NFR should be based on predicted incremental recovery with DWL well comparing to a single-completed well. The prediction should be based upon a correlation developed in the next section of this work.

7.4 DWL Feasibility Model

In the study, we attempt to develop an empirical correlation of DWL well's recovery increase (as compared to a single-completed well) as a function of NFR properties, that could help to decide on DWL well's construction in NFRs with planar fracture network. The correlation is developed for DWL wells completed in the NFR matrix because, as shown in Chapter 4, most NFRs feature sparsely-distributed fracture networks so random well placement in the matrix is more likely. Moreover, because of higher probability of matrix-well placement and its higher recovery, the overall recovery from NFR would mostly depend on recovery from matrix wells.

Out of the various parameters affecting oil recovery with DWL well, initially, we identify the significant parameters. We perform this step by analyzing a multiple linear regression correlation using matrix of experiments based on fractional factorial design. For the analysis, We consider seven factors - fracture permeability, matrix permeability, fracture spacing, mobility ratio, pressure drawdown, oil pay thickness and fracture anisotropy ratio – to create matrix of experiments shown in Table 7.6. We also assume maximum size of the water loop completions' separation equal to 400 ft when the aquifer thickness is 450ft. Moreover, in the simulated operation of the DWL well, bottomhole flowing pressure in the top (oil pay) and the water sink completions is kept constant with the same pressure drawdown in both completions as described above. Table 7.6 summarizes results of the simulated well performance showing higher recovery with DWL well than that with single completed well for all combinations of the factors controlling the recovery process. Data in Table 7.6 are then used to select significant factors parameters that control the recovery process.

Table 7.6. Fractional factorial design of simulated impvememnt of recovery with DWL wells comparing to single-completed wells

Fracture horizontal permeability, md	Matrix permeability, md	Fracture spacing, ft	Mobility ratio	Maximum Pressure drawdown, psi	Oil pay thickness, ft	Fracture anisotropy ratio	DWL Recovery Increase, %
300	5	5	5	3000	60	5	5
800	5	5	1	1500	60	10	0.4
300	50	5	1	3000	30	5	6.4
800	50	5	5	1500	30	10	12.9
300	5	20	5	1500	30	5	6.1
800	5	20	1	3000	30	10	0.7
300	50	20	1	1500	60	5	1.5
800	50	20	5	3000	60	10	6.2

Significant parameters are selected using a linear multiple regression - correlation model based upon the results in table 7.7 is then analyzed using p-value (probability value) whose smaller

value suggest the strong evidence against null hypothesis assuming null hypothesis is true (where the null hypothesis: parameter coefficient =0). The parametric regression coefficients and the p-values are shown in Table 7.7. We only select the three most significant factors - mobility ratio, matrix permeability and fracture anisotropy ratio – having the p-value smaller than 0.05 (significance level), which indicates the very strong evidence of rejecting null hypothesis, so the parameter is statistically significant.

To determine feasibility of the matrix-placed DWL wells in NFRs, we develop a predictive correlation of expected increase of the recovery factor with DWL well, ΔRF_{DWL} , as compared to that of single - completed well as a function of the three significant factors – mobility ratio, fracture anisotropy ratio and matrix permeability. In the correlation design matrix, we also vary aquifer thickness to provide for different possible water loop separation size impacting the DWL well’s recovery. We use the Box-Behnkein design method to create matrix of experiments shown in Table 7.8 which comprises 27 combinations of four factors.

Table 7.7. Regression analysis of the NFR factors contributing to DWL recovery improvement

Parameters	Coefficient	P-value
Constant	6.3	0.0692
Fracture permeability	0.0006	0.4423
Matrix permeability	0.0822	0.0429
Fracture spacing	-0.17	0.0622
Mobility ratio	1.325	0.03
Maximum Pressure drawdown	-0.0004	0.2338
Oil pay thickness	-0.1083	0.05
Fracture anisotropy ratio	-2.1	0.046

Table 7.8. Matrix of Experiments created using Box-Behnkein design showing DWL recovery improvement as a function of NFR properties

Matrix permeability, k_m , md	Mobility ratio, M	Fracture Anisotropy ratio, k_{fv}/k_{fh}	Aquifer thickness, h_w , ft	DWL Increase in recovery, ΔRF_{DWL} %
5	1	5	200	0.9
50	1	5	200	0.2
5	5	5	200	1.2
50	5	5	200	4.6
5	3	1	200	0.8
50	3	1	200	3.2
5	3	10	200	0.6
50	3	10	200	1.4
5	3	5	50	0.2
50	3	5	50	0.3
5	3	5	500	2.8
50	3	5	500	5.3
30	1	1	200	0.2
30	5	1	200	5.8
30	1	10	200	0.1
30	5	10	200	3
30	1	5	50	0
30	5	5	50	0.6
30	1	5	500	1.1
30	5	5	500	7
30	3	1	50	0.3
30	3	10	50	0.1
30	3	1	500	7.6
30	3	10	500	4.8
30	3	5	200	3.1
30	3	5	200	3.1
30	3	5	200	3.1

Based upon the results in Table 7.8 a second-order correlation model, Eq. 7.1 and Table 7.9 describes incremental increase of recovery with DWL well, ΔRF_{DWL} , with respect to a single-completed well. The model gives good match of the calculated vs. simulated results in Table 7.8 with correlation coefficient R-squared = 0.94.

$$\begin{aligned} \Delta RF_{DWL} = & -3.434 + 0.06k_m + 0.8387M + 0.376\frac{k_{fv}}{k_{fh}} + 0.01h_w - 0.0019k_m^2 + 0.0235k_m \times \\ & M - 0.0038k_m \times \frac{k_{fv}}{k_{fh}} + 0.0001k_m \times h_w - 0.1598M \times M - 0.0673M \times \frac{k_{fv}}{k_{fh}} + 0.0027M \times \\ & h_w - 0.0082\frac{k_{fv}}{k_{fh}} \times \frac{k_{fv}}{k_{fh}} - 0.0005\frac{k_{fv}}{k_{fh}} \times h_w - 1.58E - 05h_w^2 \end{aligned} \quad (7.1)$$

Table 7.9. Regression analysis of the significant NFR factors contributing to DWL recovery improvement

Factors	Coefficient	p-value
Constant	-3.434	0.124
k_m	0.0607	0.292
M	0.8387	0.238
K_{fv}/K_{fh}	0.3761	0.212
h_w	0.0101	0.129
$k_m * k_m$	-0.0019	0.019
$k_m * M$	0.0235	0.023
$k_m * K_{fv}/K_{fh}$	-0.0038	0.362
$k_m * h_w$	0.0001	0.172
$M * M$	-0.1598	0.095
$M * K_{fv}/K_{fh}$	-0.0673	0.162
$M * h_w$	0.0027	0.01
$K_{fv}/K_{fh} * K_{fv}/K_{fh}$	-0.0082	0.652
$K_{fv}/K_{fh} * h_w$	-0.0005	0.193
$h_w * h_w$	-1.58E-05	0.073

In the final step, we reduce the correlation in Eq. 7.1 by eliminating insignificant factors having the p-value greater than 0.2, by running the regression analysis again with the remaining factors. The result is shown in Table 7.10 and the reduced correlation is in Eq. 7.2.

Table 7.10. Regression analysis of the significant NFR factors (based on p-value<0.2) correlation to DWL recovery improvement

Factors	Coefficient	p-value
Constant	-0.1993	0.776
h_w	0.0068	0.226
$k_m * k_m$	-0.0015	0.003
$k_m * M$	0.0284	0.001
$k_m * h_w$	0.0001	0.082
$M * M$	-0.0907	0.066
$M * K_{fv}/K_{fh}$	-0.0253	0.321
$M * h_w$	0.0029	0.002
$K_{fv}/K_{fh} * h_w$	-0.0004	0.242
$h_w * h_w$	-1.29E-05	0.082

$$\Delta RF_{DWL} = -0.199 + 0.007h_w - 0.0015k_m^2 + 0.0284k_m \times M + 0.0001k_m \times h_w - 0.09M \times M - 0.0253M \times \frac{k_{fv}}{k_{fh}} + 0.0029M \times h_w - 0.0004 \frac{k_{fv}}{k_{fh}} \times h_w - 1.29E - 05h_w^2 \quad (7.2)$$

We found that the model results still hold close agreement with the simulated results at R-squared value of 0.92.

Summary

In the study, we verify and investigate the feasibility of DWL well in NFRs with fracture corridors and planar fracture network for two different possible on/off fracture well placement. Following important conclusions can be reached from the study:

- 1) DWS top completion recovery improves significantly with the increase in water drainage rate, followed by a near-flattening curve both in NFRs with fracture corridors and planar fracture network. The value before reaching the near-flattening trend is used as the optimum DWS well's recovery in the study. However, DWS is notorious for producing large amount of water from water sink as well, which adds to the treatment and disposal cost. Hence, considering the total water-cut from both completions, results show that the

DWS recovers less than the single-completed well in both types of NFRs (planar network and corridor), which makes it as a non-profitable coning control method.

- 2) Although DWL eliminates the additional water-cut due to bottom water drainage completion, it fails to improve any recovery (in comparison to the single-completed well) both in on/off corridor placement because of strong pressure interference effect between the water loop completions.
- 3) However, in NFRs with planar fracture network, DWL manages to reduce the interference effect and provides considerable improved recovery performance. Clearly, the improvement in recovery would be a function of NFR properties. After identifying the significant NFR properties using fractional factorial design and regression analysis, we develop a non-linear empirical model of DWL recovery increase as a function of matrix permeability, mobility ratio, fracture anisotropy ratio and aquifer thickness.
- 4) Results show that DWL (both of their on/off fracture placements variants) well recovers significantly in planar network type NFRs when the mobility ratio is high. On-fracture DWL can recover 8-fold more than that of single-completed well (recovery increases from 1.25% for single-well to 10.4%). Comparing the on/off-fracture well placement in NFR with planar fracture network, we can conclude that off-fracture wells (single-completed and DWL well) recover more than that of their on-fracture variants.

Chapter 8. Conclusions

In this study, we develop a model or establish a relationship between different water coning control design metrics including critical oil rate, well placement, water-cut, well spacing and recovery, to improve the performance of NFRs with bottom water drive.

Firstly, we study the effect of well placement on water coning performance in NFRs. In order to model on/off fracture well placement, NFRs are categorized as two types based on the network pattern: planar and channel (fracture corridor) fracture network. A dual porosity/dual-permeability (DPDP) two-dimensional radial-cylindrical model is used for simulating planar networks and the 3-D Cartesian model - for simulating fracture corridor network. The study, further, classifies the planar fracture networks as densely and sparsely distributed networks. For a single-completed well, we study two possible locations of the well's completion: inside the fracture/corridor or in the matrix/exclusion-zone. For designing DWS wells, we consider four possible well completion placement combinations in densely-distributed planar NFRs and two combinations on/off fracture in sparsely-distributed planar NFRs.

Secondly, critical oil rate design metric for NFRs is developed by deriving a model for on-fracture completions in NFR from the mechanistic principle assuming vertical equilibrium of viscous and gravity forces for a hemispherical flow to a point source oil sink at the top of oil-pay using Chaperon's (1986) approach. The model is statistically calibrated for longer penetration ratio, using designed matrix of simulated experiments covering wide ranges of NFR properties, to derive a semi-analytical model of critical oil rate for on-fracture well in NFR. For off-fracture completion, we mechanistically model the effect of well's distance to the nearest fracture in a critical rate formula for fracture-well in NFR.

Thirdly, water-cut pattern, which is another design metric for water coning control, is investigated for single porosity reservoirs and NFRs. A new analytical formula of stabilized water-cut – a typical water-cut characteristics of an oil-wet NFR -- is developed by considering the driving force of gravity and viscous effect in matrix-blocks, while neglecting the capillary forces. Lastly, recovery of the single-well, DWS and DWL well is a strong metric for the water coning design control, which need to be evaluated. Due to the uncertainty of well placement in a distributed network of NFR, probabilistic recovery with risk assessment is a powerful tool to estimate the performance of NFR. Moreover, in the study, the feasibility of DWL well in NFR is investigated to assess their performance.

Following conclusions are reached from this study:

1. Literature review on critical-rate reveals that critical-rate model development in matrix-only reservoir is up-to-date, while there is a need of a new model for NFRs to address ignored effects of anisotropy ratio, water cone instability and off-fracture placement. Since NFRs are notorious for instant water breakthrough, and extremely high water-cut, we verified the economic viability of critical oil rate in NFR (fracture-well) by running series of simulations showing that the critical production rate in NFRs (with bottom-water) can reach as high as 200 bopd.
2. Two simultaneous coning phenomena was observed in these wells, one in fractured zone and other in matrix-zone. Coning in fractured-zone display continuous increase in the critical rates with increasing well's distance to the nearest fractures. Whereas, coning in matrix-zone display a continuous reduction in critical rate with increasing well's distance to fracture. At certain point, the critical-rate for both the zones intersect and the region below this intersection point demonstrate the critical rate for the matrix-well system with

different well placements in matrix-zone. It is also shown the off-fracture well's critical-rate formula reduces to on-fracture well's formula when the matrix-zone size reduces to zero.

3. In multi-well oil single porosity reservoirs with bottom water where wells produce from closed drainage areas, water-cut does not stabilize but continues slow increase at rate depending on the drainage area size, i.e. well spacing. This period of well production defined here as "slow water-cut progression period" is controlled by the oil depletion stage after the rapid increase of water-cut during water cone buildup stage.
4. It is found that when the well spacing becomes equal to or greater than minimum well spacing defined by the lateral extent of water cone, water-cut reaches the late pseudo stabilization stage governed entirely by oil depletion. So, in the same reservoir, the (pseudo) stabilized water-cut production stage may or may not happen-dependent upon well-spacing. The study provides a regression formula for the minimum well spacing (double size of the well's drainage area threshold radius, r_{eTh} , above which the well would produce under condition of pseudo stabilized water-cut. The formula shows that pseudoWCult stage is practically possible only in thin reservoirs where minimum well-spacing is within the range of operating values of well-spacing for multi-well reservoirs. It is also shown how to adjust minimum well spacing for different values of well's production rate.
5. A new formula for pseudoWCult is derived by considering all physical effects disregarded in the derivation of presently-used formula for WCult. Statistical comparison of the two formula using variety of bottom-water reservoirs with different well-spacing reveals that their results are similar ($pseudoWCult \cong WCult$).

6. The pseudoWCult concept and economic limit of water-cut (WCec) has potential practical use in designing well spacing for maximum ultimate oil recovery at maximum allowable well production rate. Computing water-cut economic margin, the difference of (WCec-WCult) should be the initial step in well spacing design followed with computation of the minimum size of well spacing-using formulas from this study. When the water-cut economic margin is negative or close to zero, well spacing equal to its minimum (threshold) value should be considered for increased recovery. For a given reservoir with large water-cut economic margin, ultimate recovery is not dependent on well spacing. In such case, possibly largest well spacing with maximum production rate should be designed to reduce capital cost and maximize Net Present Value of the project.
7. There are three stages of water-cut development in NFR-early water breakthrough with steep jump of water-cut followed with levelling and stabilization (stabilized water-cut) and the final progressive increase of water-cut. However, the water-cut stabilization is only a characteristic of oil-wet NFRs. The stabilized water-cut stage in NFR begins when the water almost invades all fractures, so the fractures produces mostly water at constant rate, while oil is displaced from the matrix at constant rate. The stabilized water-cut stage ends when opposing capillary force begins effectively countering the gravity and viscous forces that reduces the oil displacement rate from the matrix.
8. For the NFR base case, the stabilized water-cut duration is also statistically correlated with production rate and well spacing. Lowering the well-spacing and increasing the production rate would result in increased stabilized water-cut stage duration and the stabilized water-cut value. Identifying the economic viability of stabilized water-cut duration would help optimize well spacing for maximum recovery.

9. The results show the water-cut stabilization stage does not significantly contribute to increase in recovery. In addition, the stage requires reducing well spacing which adds to the operating cost. So, stabilized water-cut stage should be avoided to optimize recovery and maximize profit. As a result, a new method for finding optimum well-spacing by eliminating the stabilized water-cut stage, while maximizing recovery, is proposed.
10. For single-completed wells in densely-distributed planar fracture network, completions placement (at fracture or in matrix) has no effect on the well's recovery performance. This implies the existence of critical fracture spacing – the maximum spacing when the well's placement (on or off fractures) has no significant effect on the well's recovery. In densely-distributed planar network NFR, dual-completed (DWS) well recovers more than single-completed well and the recovery is not dependent on well's completion placement that makes DWS well a better performer with no concern about uncertain location of its two completions.
11. However, study on the comparison of on/off-fracture single well, DWS and DWL wells in sparse planar fracture network NFR demonstrated the following observations:
 - a.) Considering the total water-cut produced on the surface from all completions, DWS recovery performance is even below that of single-completed well whereas DWL recovers the most which is a function of the NFR properties. After identifying the significant NFR properties using fractional factorial design and regression analysis, we develop a non-linear empirical model of DWL recovery increase as a function of matrix permeability, mobility ratio, fracture anisotropy ratio and aquifer thickness. However, since the correlation is only developed for matrix-well placement, it ignores the

- probabilistic assessment of recovery for DWL well due to uncertainty of well completions placement on/off fractures.
- b.) DWL (both of their on/off fracture placements variants) well recovers significantly in planar network type NFRs when the mobility ratio is high. On-fracture DWL can recover 8-fold more than that of single-completed well (recovery increases from 1.25% for single-well to 10.4%). Moreover, study shows that off-fracture wells (single-completed and DWL well) would recover more than that of their on-fracture variants.
12. Modeling of critical fracture spacing – minimum spacing at which recovery of matrix vs. fracture well differs, -- showed that the minimum fracture spacing model is not only a function of static NFR properties but also dynamic well-design and operational parameters. The study showed that the critical fracture spacing is a strong qualitative indicator of the contrast in the ultimate recovery between fracture and matrix well with the increase in fracture spacing. Higher the critical spacing (>10ft), lower is the contrast which reveals operator do not need to worry about well placement issue in such NFRs. On the other hand, lower critical spacing (<10ft) signifies large difference in matrix and fracture well's recovery at higher fracture spacing. Moreover, typical planar fracture network NFRs demonstrate a lower critical spacing value, which implies that most of the planar network NFRs are sparsely distributed.
13. Alternatively, for single completed well in fracture corridor network NFR, the exclusion-zone location of well's completion gives higher recovery (37%) than the completion placed in the corridors, 28%. Thus, the wells should be preferably completed in the exclusion-zone. In such NFRs, DWL well fails to improve any performance due to the presence of strong pressure interference effects.

14. The probabilistic estimation which considers the probable location of well with respect to the corridor spacing distribution gives higher values of expected recovery as compared to the simplified method derived from the central tendency of the statistical distribution of NFR. The total recovery increases by 6.6% from 33% (by simplified method) to 35.2%. The mathematical proof demonstrates that the recovery estimated from probabilistic method would always be greater than that from simplified method. Moreover, advantage of the probabilistic method is that it would help assign probability to any value of recovery factor and therefore, would help operators make reservoir development decisions based upon the risk-benefit considerations.
15. For the field case NFR studied here, a complete reservoir development with single-completed wells would include 42 % fracture-wells recovering 28% and 58% matrix-wells recovering 37% of OIP, respectively – giving the total value of reservoir recover factor, $RF=33\%$. The results also show some productivity advantage from using DWS technology in the field case NFR. Of the total number of DWS development wells, probability of random placement of their two completions in fracture network (corridor vs. exclusion-zone) would be the same as for single-completed wells. However, as the wells recover more oil, the overall reservoir recovery factor, $RF=41\%$ would be almost 24% larger than that for single-completed wells.

Appendix A. Experimental Data on Critical Rate

Table A1. Well in a base case-NFR

Data	Unit	Base case NFR for fracture-well	Base case Fracture corridor NFR
Datum depth	ft	6000	6000
Thickness of oil zone above FWL	ft	40	40
Depth of WOC	ft	6070	6040
Water-zone thickness	fraction	50	50
Transition zone	ft	30	0
Reservoir pressure at datum depth(Pi)	psi	3000	3000
Matrix porosity	fraction	0.15	0.15
Fracture porosity	fraction	0.001	0.001
Fracture spacing	ft	6.6	300
Matrix permeability	md	50	40
Matrix anisotropy ratio	fraction	0.1	0.1
Matrix compressibility	1/psi	4.00E-06	4.00E-06
Fracture compressibility	1/psi	4.00E-05	4.00E-05
Perforated length	ft	8	8
Fracture horizontal permeability	md	145	1100
Fracture anisotropy ratio	fraction	1	5
Well radius	ft	0.25	0.25
Outer radius of oil-zone	ft	1000	1000
Outer radius of water zone	ft	1000	1000
Oil production rate	bopd	27	Varying

Table A2. Reservoir fluid properties

Data	Unit	Values	Range
Formation oil volume factor	rb/stb	1.10	-
Water compressibility	1/psi	3.00E-06	-
Oil compressibility	1/psi	1.50E-06	-
Water viscosity	cp	0.7	-
Oil viscosity	cp	0.7	0.7- 3.5
Oil density	lb/cuft	52.0	-
Water density	lb/cuft	64	-
Bubble point pressure	psi	1000	-

Table A3. Simulated critical rate of different NFRs for different penetration ratio (ho=40ft)

Cases	K _{fh} , md	K _{mh} , md	M	S _p , ft	r _c , ft	K _{fv} /K _{fh}	Simulated Critical rate, $q_{cr,fr}$, bopd					
							h _{op} /h _o =0.1	h _{op} /h _o =0.2	h _{op} /h _o =0.3	h _{op} /h _o =0.4	h _{op} /h _o =0.5	h _{op} /h _o =0.6
1	100	0.1	3	0.1	1000	5	4.9	4.8	4.5	4.2	3.7	3.2
2	100	0.1	3	18	1000	5	4.9	4.8	4.5	4.2	3.7	3.2
3	100	50	3	0.1	1000	5	6.5	6.3	6.0	5.5	4.9	4.2
4	100	50	3	18	1000	5	6.5	6.3	6.0	5.5	4.9	4.2
5	2000	0.1	3	0.1	1000	5	94.0	95.7	90.7	83.7	74.8	63.8
6	2000	0.1	3	18	1000	5	94.0	95.7	90.7	83.7	74.8	63.8
7	2000	50	3	0.1	1000	5	96.0	97.2	92.1	85.1	75.9	64.8
8	2000	50	3	18	1000	5	96.0	97.2	92.1	85.1	75.9	64.8
9	500	0.1	1	6	400	5	77.0	76.7	72.7	67.1	59.9	51.1
10	500	0.1	1	6	2000	5	65.0	70.2	66.5	61.4	54.8	46.8
11	500	0.1	5	6	400	5	15.8	15.3	14.5	13.4	12.0	10.2
12	500	0.1	5	6	2000	5	14.5	14.0	13.3	12.3	11.0	9.4
13	500	50	1	6	400	5	82.0	81.5	77.2	71.3	63.7	54.3
14	500	50	1	6	2000	5	67.0	74.6	70.7	65.2	58.3	49.7
15	500	50	5	6	400	5	16.8	16.3	15.4	14.3	12.7	10.9
16	500	50	5	6	2000	5	15.4	14.9	14.1	13.0	11.7	9.9
17	500	5	1	0.1	1000	1	78.7	76.3	72.3	66.7	59.6	50.9
18	500	5	1	0.1	1000	10	66.0	71.3	67.6	62.4	55.7	47.5
19	500	5	1	18	1000	1	78.7	76.3	72.3	66.7	59.6	50.9
20	500	5	1	18	1000	10	65.0	71.3	67.6	62.4	55.7	47.5
21	500	5	5	0.1	1000	1	15.7	15.3	14.5	13.3	11.9	10.2
22	500	5	5	0.1	1000	10	14.7	14.3	13.5	12.5	11.1	9.5
23	500	5	5	18	1000	1	15.7	15.3	14.5	13.3	11.9	10.2
24	100	5	5	18	1000	10	2.8	2.9	2.8	2.6	2.3	1.9
25	100	5	3	0.1	400	5	5.4	5.3	5.0	4.6	4.1	3.5
26	100	5	3	0.1	2000	5	5.0	4.8	4.6	4.2	3.8	3.2
27	100	5	3	18	400	5	5.4	5.3	5.0	4.6	4.1	3.5
28	100	5	3	18	2000	5	5.0	4.8	4.6	4.2	3.8	3.2
29	2000	5	3	0.1	400	5	105.6	102.4	97.0	89.6	80.0	68.3
30	2000	5	3	0.1	2000	5	85.0	93.7	88.8	82.0	73.2	62.4
31	2000	5	3	18	400	5	105.6	102.4	97.0	89.6	80.0	68.3
32	2000	5	3	18	2000	5	85.0	93.7	88.8	82.0	73.2	62.4
33	500	0.1	3	6	400	1	29.8	28.9	27.4	25.3	22.6	19.3
34	500	0.1	3	6	400	10	25.5	24.8	23.5	21.7	19.3	16.5
35	500	0.1	3	6	2000	1	24.8	24.1	22.8	21.0	18.8	16.0
36	500	0.1	3	6	2000	10	24.0	23.2	22.0	20.3	18.1	15.5
37	500	50	3	6	400	1	31.7	30.7	29.1	26.9	24.0	20.5
38	500	50	3	6	400	10	27.1	26.3	24.9	23.0	20.6	17.5
39	500	50	3	6	2000	1	26.4	25.6	24.2	22.4	20.0	17.0

(Cont'd.)

Cases	K _{fh} , md	K _{mh} , md	M	S _p , ft	r _e , ft	K _{fv} /K _{fh}	Simulated Critical rate, <i>q_{cr,fr}</i> , bopd					
							h _{op} /h _o =0.1	h _{op} /h _o =0.2	h _{op} /h _o =0.3	h _{op} /h _o =0.4	h _{op} /h _o =0.5	h _{op} /h _o =0.6
40	500	50	3	6	2000	10	23.0	24.7	23.4	21.6	19.3	16.5
41	100	5	1	6	1000	1	16.1	15.6	14.8	13.7	12.2	10.4
42	100	5	1	6	1000	10	15.1	14.6	13.8	12.8	11.4	9.7
43	100	5	5	6	1000	1	3.2	3.1	3.0	2.7	2.4	2.1
44	100	5	5	6	1000	10	3.0	2.9	2.8	2.6	2.3	1.9
45	2000	5	1	6	1000	1	313.2	303.7	287.9	265.7	237.3	202.5
46	2000	5	1	6	1000	10	270.0	283.7	268.9	248.3	221.7	189.1
47	2000	5	5	6	1000	1	62.6	60.7	57.6	53.1	47.5	40.5
48	2000	5	5	6	1000	10	55.0	56.7	53.8	49.7	44.3	37.8
49	500	5	3	6	1000	5	24.8	24.1	22.8	21.1	18.8	16.1
50	500	5	3	6	1000	5	24.8	24.1	22.8	21.1	18.8	16.1
51	500	5	3	6	1000	5	24.8	24.1	22.8	21.1	18.8	16.1
52	500	5	3	6	1000	5	24.8	24.1	22.8	21.1	18.8	16.1
53	500	5	3	6	1000	5	24.8	24.1	22.8	21.1	18.8	16.1
54	500	5	3	6	1000	5	24.8	24.1	22.8	21.1	18.8	16.1

Table A4. Simulated Critical rate for various well/NFR system (h_o=40ft)

Case s	K _{fh} , md	K _{mh} , md	M	S _p , ft	r _e , ft	K _{fv} /K _{fh}	h _{op} /h _o	<i>q_{cr,fr}</i> (simulated), bopd	w, mm	<i>k_{ff}</i> , m ²
1	500	5	3	0.1	400	1	0.5	22.7	0.06	2.67E-10
2	500	5	3	0.1	400	10	0.5	19.4	0.06	2.67E-10
3	500	5	3	0.1	2000	1	0.5	18.9	0.06	2.67E-10
4	500	5	3	0.1	2000	10	0.5	18.2	0.06	2.67E-10
5	500	5	3	18	400	1	0.5	22.7	0.32	8.53E-09
6	500	5	3	18	400	10	0.5	19.4	0.32	8.53E-09
7	500	5	3	18	2000	1	0.5	19.0	0.32	8.53E-09
8	500	5	3	18	2000	10	0.5	18.0	0.32	8.53E-09
9	100	5	3	6	1000	1	0.35	4.8	0.13	1.40E-09
10	100	5	3	6	1000	1	0.8	2.0	0.13	1.40E-09
11	100	5	3	6	1000	10	0.35	4.4	0.13	1.40E-09
12	100	5	3	6	1000	10	0.8	1.8	0.13	1.40E-09
13	2000	5	3	6	1000	1	0.35	92.0	0.35	1.03E-08
14	2000	5	3	6	1000	1	0.8	38.0	0.35	1.03E-08
15	2000	5	3	6	1000	10	0.35	86.3	0.35	1.03E-08
16	2000	5	3	6	1000	10	0.8	35.4	0.35	1.03E-08
17	500	0.1	3	6	400	5	0.35	23.3	0.22	4.10E-09
18	500	0.1	3	6	400	5	0.8	9.6	0.22	4.10E-09
19	500	0.1	3	6	2000	5	0.35	21.3	0.22	4.10E-09

(Cont'd.)

Case s	K_{fh} , md	K_{mh} , md	M	S_p , ft	r_e , ft	K_{fv}/K_{fh}	h_{op}/h_o	$q_{cr,fr}$ (simulated),	w, mm	k_{ff} , m^2
20	500	0.1	3	6	2000	5	0.8	8.8	0.22	4.10E-09
21	500	50	3	6	400	5	0.35	25.0	0.22	4.10E-09
22	500	50	3	6	400	5	0.8	10.0	0.22	4.10E-09
23	500	50	3	6	2000	5	0.35	22.7	0.22	4.10E-09
24	500	50	3	6	2000	5	0.8	9.3	0.22	4.10E-09
25	100	0.1	3	0.1	1000	5	0.5	3.7	0.03	9.15E-11
26	100	0.1	3	18	1000	5	0.5	3.7	0.19	2.92E-09
27	100	50	3	0.1	1000	5	0.5	4.9	0.03	9.15E-11
28	100	50	3	18	1000	5	0.5	4.9	0.19	2.92E-09
29	2000	0.1	3	0.1	1000	5	0.5	75.0	0.09	6.74E-10
30	2000	0.1	3	18	1000	5	0.5	75.0	0.51	2.15E-08
31	2000	50	3	0.1	1000	5	0.5	76.0	0.09	6.74E-10
32	2000	50	3	18	1000	5	0.5	76.0	0.51	2.15E-08
33	500	5	1	0.1	1000	5	0.35	56.0	0.06	2.67E-10
34	500	5	1	0.1	1000	5	0.8	27.0	0.06	2.67E-10
35	500	5	1	18	1000	5	0.35	66.0	0.32	8.53E-09
36	500	5	1	18	1000	5	0.8	27.0	0.32	8.53E-09
37	500	5	5	0.1	1000	5	0.35	13.2	0.06	2.67E-10
38	500	5	5	0.1	1000	5	0.8	5.4	0.06	2.67E-10
39	500	5	5	18	1000	5	0.35	13.2	0.32	8.53E-09
40	500	5	5	18	1000	5	0.8	5.4	0.32	8.53E-09
41	100	5	1	6	400	5	0.5	12.3	0.13	1.40E-09
42	100	5	1	6	2000	5	0.5	11.3	0.13	1.40E-09
43	100	5	5	6	400	5	0.5	2.5	0.13	1.40E-09
44	100	5	5	6	2000	5	0.5	2.3	0.13	1.40E-09
45	2000	5	1	6	400	5	0.5	240.0	0.35	1.03E-08
46	2000	5	1	6	2000	5	0.5	219.0	0.35	1.03E-08
47	2000	5	5	6	400	5	0.5	48.0	0.35	1.03E-08
48	2000	5	5	6	2000	5	0.5	44.0	0.35	1.03E-08
49	500	0.1	1	6	1000	1	0.5	59.0	0.22	4.10E-09
50	500	0.1	1	6	1000	10	0.5	55.0	0.22	4.10E-09
51	500	0.1	5	6	1000	1	0.5	11.8	0.22	4.10E-09
52	500	0.1	5	6	1000	10	0.5	11.1	0.22	4.10E-09
53	500	50	1	6	1000	1	0.5	63.0	0.22	4.10E-09
54	500	50	1	6	1000	10	0.5	59.0	0.22	4.10E-09
55	500	50	5	6	1000	1	0.5	12.6	0.22	4.10E-09
56	500	50	5	6	1000	10	0.5	11.7	0.22	4.10E-09
57	500	5	3	6	1000	5	0.5	19.0	0.22	4.10E-09
58	500	5	3	6	1000	5	0.5	19.0	0.22	4.10E-09
59	500	5	3	6	1000	5	0.5	19.0	0.22	4.10E-09
60	500	5	3	6	1000	5	0.5	19.0	0.22	4.10E-09
61	500	5	3	6	1000	5	0.5	19.0	0.22	4.10E-09
62	500	5	1	6	1000	5	0.5	56.0	0.22	4.10E-09

Appendix B. Properties of Single and Dual Completed Wells in NFR

Table B1. Single-completed and dual-completed well in moderately water-wet type III NFR

Data	Unit	Single-completed well in planar dense fracture-network	DWS well in planar dense fracture-network
Top of reservoir	ft	6000	6000
Bottom of reservoir (model)	ft	6100	6100
Oil water contact	ft	6060	6060
Transition-zone thickness	ft	40	40
Reservoir pressure at datum depth(Pi)	psi	3000	3000
Matrix porosity	fraction	0.2	0.2
Matrix permeability	md	30	30
Matrix anisotropy ratio	fraction	0.1	0.1
Matrix compressibility	1/psi	4.00E-06	4.00E-06
Fracture compressibility	1/psi	4.00E-05	4.00E-05
Fracture porosity	fraction	0.0005	0.0005
Mean Fracture spacing	ft	10	10
Fracture horizontal permeability	md	400	400
Fracture anisotropy ratio	ratio	5	5
Perforated interval thickness	ft	10	10
Well radius	ft	0.25	0.25
Outer radius of oil-zone	ft	1000	1000
Outer radius of water zone	ft	1000	1000
Bubble point pressure	psi	1000	1000
Oil viscosity	cp	4	4
Water viscosity	cp	0.8	0.8
Top Completion depth	ft	-	6000
Top Completion thickness	ft	-	10
Bottom completion depth	ft	-	6070
Bottom completion thickness	ft	-	10

Table B2. Single-completed well in mixed-wet type II NFR

Data	Unit	Densely-distributed fracture-network	Fracture-corridor system
Top of reservoir	ft	6000	6000
Bottom of reservoir (model)	ft	6100	6100
Oil-water contact	ft	6040	6040
Reservoir pressure at datum depth(P_i)	psi	3000	3000
Bubble point pressure	psi	1000	1000
Matrix porosity	fraction	0.1	0.3
Matrix permeability	md	5	30
Matrix anisotropy ratio	fraction	0.1	0.1
Matrix compressibility	1/psi	4.00E-06	4.00E-06
Fracture compressibility	1/psi	4.00E-05	4.00E-05
Fracture porosity	fraction	0.0005	0.0005
Fracture spacing	ft	6.6	-
Expected fracture spacing	ft	-	56
Effective horizontal permeability, k_f	md	600	-
Expected value of effective permeability	md	-	590
Corridor permeability, k_{ff}	md	-	1960
Fracture anisotropy ratio	ratio	5	5
Perforated interval thickness	ft	10	10
Well radius	ft	0.25	0.25
Outer radius/dimension of oil-zone	ft	1000	450×450
Outer radius/dimension of water zone	ft	1000	450×450
Oil viscosity	cp	2.5	1
Water viscosity	cp	0.8	0.8

Table B3. Properties of DWS well completed in mixed-wet type II NFR

Data	Unit	Densely-distributed fracture-network	Fracture-corridor system
Top of reservoir	ft	6000	6000
Bottom of reservoir (model)	ft	6100	6100
Initial Free water level	ft	6040	6040
Reservoir pressure at datum depth(P_i)	psi	3000	3000
Bubble point pressure	psi	1000	1000
Matrix porosity	fraction	0.1	0.3
Matrix permeability	md	5	30
Matrix anisotropy ratio	fraction	0.1	0.1
Matrix compressibility	1/psi	4.00E-06	4.00E-06
Fracture compressibility	1/psi	4.00E-05	4.00E-05
Fracture porosity	fraction	0.0005	0.0005
Fracture spacing	ft	6.6	-
Expected fracture spacing	ft	-	56
Effective horizontal permeability, k_f	md	600	-
Expected value of effective permeability	md	-	590
Corridor permeability, k_{ff}	md	-	1960
Fracture anisotropy ratio	ratio	5	5
Top Completion depth	ft	6000	6000
Top Completion thickness	ft	10	10
Bottom completion depth	ft	6070	6060
Bottom completion thickness	ft	10	10
Well radius	ft	0.25	0.25
Outer radius/dimension of oil-zone	ft	1000	450×450
Outer radius/dimension of water zone	ft	1000	450×450
Oil viscosity	cp	2.5	1
Water viscosity	cp	0.8	0.8

Appendix C. Derivation of PseudoWCult Formula

The pseudoWCult formula is derived for stabilized well inflow condition when $dWC/dt = 0.0009/\text{yr} \approx 0$. At this stage, oil and water inflows to the well are not purely radial as assumed in the derivation of the presently-used ultimate water cut formula, WCult, Eq. (5.1). As shown in Fig. 5.3, water flow in the aquifer comprises a small local semi-spherical flow region ($r_s - r_w$) around the water sink and large global radial flow region ($r_e - r_s \approx r_e - r_w$). Steady-state for hemispherical flow is described by:

$$\frac{q_w}{2\pi r^2} = -\frac{k_{spw}}{\mu_w} \frac{dp}{dr} \quad (\text{C-1})$$

Assuming water sink size, r_{ws} , equal to the equivalent spherical size of the well's completion (Moran and Finklea 1962; Joseph and Koederitz 1985), gives,

$$r_{ws} = \frac{0.5h_{op}}{\ln\left(\frac{h_{op}}{r_w}\right)} \quad (\text{C-2})$$

Semi-spherical flow of water from radius r_s (with pressure p_s) to the water sink (with well-bore pressure p_w) is,

$$\int_{r_{ws}}^{r_s} \frac{q_w dr}{r^2} = -\int_{p_w}^{p_s} \frac{2\pi k_{spw} dp}{\mu_w}$$

$$-q_w \left[\frac{1}{r_s} - \frac{1}{r_{ws}} \right] = -\frac{2\pi k_{spw} (p_s - p_w)}{\mu_w}$$

$$\text{or, } p_s - p_w = \frac{q_w \mu_w}{2\pi k_{spw}} \left[\frac{1}{r_{ws}} - \frac{1}{r_s} \right]$$

Where, r_s = semi-spherical water inflow radius

Substituting $k_{spw} = k_{sp} k_{rw}$ and $k_{sp} = \sqrt[3]{k_h^2 k_v}$, we get:

$$p_s - p_w = \frac{q_w \mu_w}{2\pi k_{rw} \sqrt[3]{k_h^2 k_v}} \left[\frac{1}{r_{ws}} - \frac{1}{r_s} \right] \quad (\text{C-3})$$

Size of semispherical water inflow region is small comparing to the aquifer size, so the radial water flow component is approximated as,

$$p_e - p_s = \frac{q_w \mu_w \ln^{r_e/r_w}}{2\pi k_h k_{rw} h_w} \quad (C-4)$$

Since the radial and spherical flows are in series, total pressure drop in the aquifer is,

$$p_s - p_w + p_e - p_s = \frac{q_w \mu_w}{2\pi k_{rw} \sqrt[3]{k_h^2 k_v}} \left[\frac{1}{r_{ws}} - \frac{1}{r_s} \right] + \frac{q_w \mu_w \ln^{r_e/r_w}}{2\pi k_h k_{rw} h_w}$$

and the water inflow rate is,

$$q_w = \frac{2\pi k_{rw} (p_e - p_w)}{\mu_w \left[\frac{\ln^{r_e/r_w} + \left(\frac{1}{r_{ws}} - \frac{1}{r_s} \right)}{k_h h_w + \sqrt[3]{k_h^2 k_v}} \right]} \quad (C-5)$$

Oil-inflow rate to a partially-penetrating well is,

$$q_o = \frac{2\pi k_h k_{ro} h_o (p_e - p_w)}{\mu_o (\ln^{r_e/r_w} + S)} \quad (C-6)$$

Where, the partial-penetration skin factor (Papatzacos 1986) is,

$$S = \left(\frac{1}{h_{pD}} - 1 \right) \ln \frac{\pi}{2r_D} + \frac{1}{h_{pD}} \ln \left[\frac{h_{pD}}{2+h_{pD}} \left(\frac{A-1}{B-1} \right)^{1/2} \right] \quad (C-7)$$

and,

$$r_D = (r_w/h_o) \left(k_v/k_h \right)^{1/2}$$

$$h_{pD} = h_{op}/h_o$$

$$A = 4/h_{pD}$$

$$B = 4/3h_{pD}$$

For stabilized inflow of oil and water, ultimate water cut is,

$$\text{pseudoWCult} = \left(1 - \frac{q_{cr}}{Q} \right) \frac{q_w}{q_w + q_o} \quad (C-8)$$

Substituting for q_w and q_o from eqs. (C-5) and (C-6) in (C-9) gives,

$$\text{pseudoWCult} = \left(1 - \frac{q_{cr}}{Q}\right) \left\{ 1 + \frac{h_o}{Mh_w(\ln r_e/r_w + S)} \left[\ln r_e/r_w + \frac{h_w(1 - \frac{1}{r_{Ds}})}{0.5h_{op} \sqrt[3]{k_v/k_h}} \ln \left(\frac{h_{op}}{r_w}\right) \right] \right\}^{-1} \quad (\text{C-9})$$

Critical rate (q_{cr}) in Eq. (C-9) can be computed from Chaperon (1986) as,

$$q_{cr} = 0.0783 \times 10^{-4} \left[\frac{\Delta\rho k_o (h_o^2 - h_{op}^2)}{\mu_o B_o} \right] \left[0.7311 + \frac{1.943}{\frac{r_e}{h_o} \sqrt[3]{\frac{k_v}{k_h}}} \right] \quad (\text{C-10})$$

Where, all parameters are in field units.

Appendix D. Effect of Production Rate on Minimum Well-spacing (Threshold Radius)

In this section, effect of production rate is studied on threshold well-spacing for five different reservoirs/aquifer systems from table 5.3 (3, 4, 12, 15 and 16). Production rate is varied from critical rate to the maximum rate for different reservoirs. Maximum rate is defined assuming pressure drawdown equal to 80% drop of reservoir pressure. From Fig. D-1, it is quite evident that threshold drainage radius is practically constant and rate-independent with more than 99% of the rate range.

Shown in Table D1 are limiting low values of production rates (as percent of maximum rates) above which threshold radius do not depend on rate for all reservoir/aquifer systems used in this study. Clearly, production rates do not have any effect on these parameters.

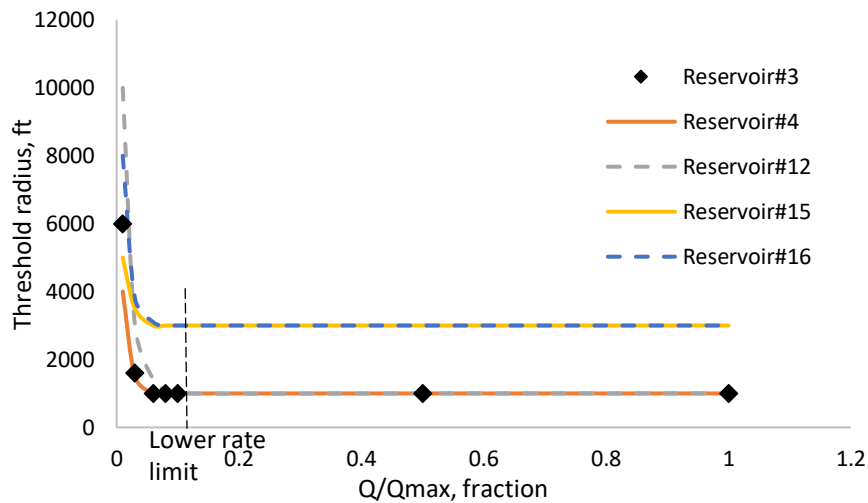


Fig. D-1. Minimum well spacing (twice the threshold radius) vs. production rate

Table D1. Lower limit of production rate interval (from Table 5.3) where r_{eTh} are rate-independent

Reservoir Aquifer System #	Lower rate limit (% of max. rate)						
1	0.10	15	0.02	29	0.02	43	0.04
2	0.03	16	0.05	30	0.02	44	0.06
3	0.05	17	0.08	31	0.02	45	0.02
4	0.03	18	0.10	32	0.03	46	0.03
5	0.03	19	0.02	33	0.04	47	0.02
6	0.06	20	0.07	34	0.01	48	0.02
7	0.05	21	0.01	35	0.10	49	0.04
8	0.01	22	0.05	36	0.01	50	0.01
9	0.15	23	0.05	37	0.06	51	0.07
10	0.06	24	0.02	38	0.06	52	0.02
11	0.04	25	0.10	39	0.03	53	0.07
12	0.07	26	0.02	40	0.04	54	0.10
13	0.04	27	0.07	41	0.05		
14	0.05	28	0.01	42	0.10		

Appendix E. Verification of Stabilized Water-Cut Formula

We compare the stabilized WC analytical formula with the results of WC simulations for variety of type II NFRs by considering different reservoir properties: fracture permeability, fracture porosity, fracture spacing, fracture anisotropy ratio, matrix permeability, matrix porosity, mobility ratio, oil-pay thickness, aquifer thickness, oil density, water density and drainage radius. The reservoir properties are varied considerably to represent the cases of type II NFRs (Meehan 2011; Buksh 1991; Jack and Sun 2003). In the study, we use the Taguchi method (NIST/SEMATECH 2012) for two-level experimental design of matrix of experiments (Table E-1). This method utilizes various levels fractional factorial design, and applies to large screening designs making the design more relevant. Based on the design, 16 simulation (IMEX) runs were performed to generate the simulated stabilized WC value and compared with calculated stabilized WC value (using Eq. 3.5) as shown in Table E-1 and Fig. 5.15. The unit-slope plot gives R-square of 0.97 and clearly verifies the analytical formula.

Table E-1. Type II NFR properties-Experimental design matrix

Run	1	2	3	4	5	6	7
Oil viscosity, μ_o	1	1	1	1	1	1	1
Horizontal fracture perm, Kfh	100	100	100	100	500	500	500
Matrix permeability, Kmh	1	1	1	1	5	5	5
Matrix porosity, Φ_m	0.05	0.05	0.15	0.15	0.05	0.05	0.15
Drainage radius, r_e	436	436	2000	2000	436	436	2000
Fracture anisotropy ratio, k_{fv}/K_{fh}	1	1	6	6	6	6	1
Fracture porosity	2E-04	2E-04	0.005	0.005	0.005	0.005	2E-04
Fracture spacing	0.1	20	0.1	20	0.1	20	0.1
oil-pay thickness, h_o	60	120	60	120	60	120	60
Aquifer thickness, h_w	120	600	120	600	300	240	300
Water density, ρ_w	60.5	74.9	60.5	74.9	74.9	60.5	74.9
Oil density, ρ_o	48	58	58	48	48	58	58
Total production-rate, Q_1	200	200	3900	12000	21000	10000	30000
Simulated WC_{stab}	0.836	0.786	0.96	0.89	0.98	0.988	0.88
Calculated WC_{stab}	0.844	0.792	0.94	0.88	0.977	0.988	0.85

Run	8	9	10	11	12	13	14	15	16
Oil viscosity, μ_o	1	10	10	10	10	10	10	10	10
Horizontal fracture perm, Kfh	500	100	100	100	100	100	500	500	500
Matrix permeability, Kmh	5	5	5	5	5	1	1	1	1
Matrix porosity, Φ_m	0.15	0.05	0.05	0.15	0.15	0.05	0.05	0.15	0.15
Drainage radius, r_e	2000	2000	2000	436	436	2000	2000	436	436
Fracture anisotropy ratio, k_{fv}/K_{fh}	1	1	1	6	6	6	6	1	1
Fracture porosity	2E-04	0.005	0.005	2E-04	2E-04	2E-04	2E-04	0.005	0.005
Fracture spacing	20	0.1	20	0.1	20	0.1	20	0.1	20
oil-pay thickness, h_o	120	120	60	120	60	120	60	120	60
Aquifer thickness, h_w	240	240	300	240	300	600	120	600	120
Water density, ρ_w	60.5	74.9	60.5	74.9	60.5	60.5	74.9	60.5	74.9
Oil density, ρ_o	48	48	58	58	48	48	58	58	48
Total production-rate, Q_1	29400	15000	1400	770	450	660	1900	3050	50
Simulated WC_{stab}	0.883	0.965	0.97	0.97	0.97	0.965	0.96	1	0.885
Calculated WC_{stab}	0.886	0.951	0.951	0.97	0.964	0.955	0.956	1	0.874

Appendix F. Previous Publication Agreements

The following is the response to my request to use the material in the article “Semi-analytical prediction of critical oil rate in Naturally Fractured Reservoirs with water coning” in my PhD dissertation. The content of this article is presented split and presented in Chapters 3 and 4.



Semi-analytical prediction of critical oil rate in naturally fractured reservoirs with water coning

Author: Samir Prasun, Andrew K. Wojtanowicz

Publication: Journal of Petroleum Science and Engineering

Publisher: Elsevier

Date: September 2019

© 2019 Elsevier B.V. All rights reserved.

Please note that, as the author of this Elsevier article, you retain the right to include it in a thesis or dissertation, provided it is not published commercially. Permission is not required, but please ensure that you reference the journal as the original source. For more information on this and on your other retained rights, please visit: <https://www.elsevier.com/about/our-business/policies/copyright#Author-rights>

BACK

CLOSE WINDOW

The following is the permission to publish below articles in my PhD dissertation:

1. Determination and Implication of Ultimate Water Cut in Well-Spacing Design for Developed Reservoirs With Water Coning, by Samir Prasun , A. K. Wojtanowicz, J. Energy Resour. Technol. Aug 2018, 140(8),
2. Stabilized Water-Cut in Carbonate Naturally Fractured Reservoirs With Bottom Water With an Implication in Well Spacing Design for Recovery Optimization,” by Samir Prasun, Andrew K. Wojtanowicz, J. Energy Resour. Technol. March 2020, 142(3)
3. Probabilistic Estimation of Recovery From Naturally Fractured Bottom-Water Reservoir With Uncertain Well Placement in Fracture Network,” by Samir Prasun, Andrew K. Wojtanowicz, Paper No: OMAE2019-96836

The content of articles 1 and 2 is presented in Chapter 5. The content of the article 3 is split and presented in Chapters 4 and 6.

RE: Urgent: Need permission to use my journal and conference papers in my PhD dissertation

Beth Darchi <DarchiB@asme.org>

Thu 4/16/2020 1:18 PM

To: Samir Prasun <sprasu1@lsu.edu>

Dear Mr. Prasun,

This permission has been revised to reflect all requests. It is our pleasure to grant you permission **to use all or any part of** the following ASME papers:

- Determination and Implication of Ultimate Water Cut in Well-Spacing Design for Developed Reservoirs With Water Coning, by Samir Prasun , A. K. Wojtanowicz, J. Energy Resour. Technol. Aug 2018, 140(8),
- Stabilized Water-Cut in Carbonate Naturally Fractured Reservoirs With Bottom Water With an Implication in Well Spacing Design for Recovery Optimization,” by Samir Prasun, Andrew K. Wojtanowicz, J. Energy Resour. Technol. March 2020, 142(3)
- Probabilistic Estimation of Recovery From Naturally Fractured Bottom-Water Reservoir With Uncertain Well Placement in Fracture Network,” by Samir Prasun, Andrew K. Wojtanowicz, Paper No: OMAE2019-96836

cited in your letter for inclusion in a PhD dissertation entitled Development of Water Coning Control Design Metrics in Naturally Fractured Reservoirs to be published by Louisiana State University, Baton Rouge.

Permission is granted for the specific use as stated herein and does not permit further use of the materials without proper authorization. Proper attribution must be made to the author(s) of the materials. Please note: if any or all of the figures and/or Tables are of another source, permission should be granted from that outside source or include the reference of the original source. ASME does not grant permission for outside source material that may be referenced in the ASME works.

As is customary, we request that you ensure full acknowledgment of this material, the author(s), source and ASME as original publisher. Acknowledgment must be retained on all pages where figure is printed and distributed.

Many thanks for your interest in ASME publications.

Sincerely,

Beth Darchi
Publishing Administrator
ASME

References

- Aguilera, R. 1998. Geologic Aspects of Naturally Fractured Reservoirs. *The Leading Edge*, 17(12): 1667-1670.
- Al-Afaleg, N.I. and Ershaghi, I. 1993. Coning Phenomena in Naturally Fractured Reservoirs. Presented at the Western Regional Meeting, Anchorage, Alaska, 26-28 May. SPE 26083.
- Alblooshi, Y. A., & Wojtanowicz, A. K. (2018, June). Dynamic Water Control in Naturally Fractured Bottom Water-Drive Reservoirs via Downhole Water Sink Well Deployment: First Experimental Study. In RDPETRO 2018: Research and Development Petroleum Conference and Exhibition, Abu Dhabi, UAE, 9-10 May 2018 (pp. 128-131). American Association of Petroleum Geologists, Society of Exploration Geophysicists, European Association of Geoscientists and Engineers, and Society of Petroleum Engineers.
- Amisigo, B.A. 2006. Modelling Riverflow in the Volta Basin of West Africa: A Data Driven Framework. PhD Thesis, Delft University of Technology, The Netherland.
- Arslan, O. (2005). Optimal operating strategy for wells with downhole water sink completions to control water production and improve performance. PhD dissertation, Louisiana State University, Baton Rouge, LA, USA.
- Bahrami, H., Shadizadeh, S.R. and Goodarzniya, I. (2004). Numerical Simulation of Coning Phenomena in Naturally Fractured Reservoirs. 9th Iranian Chemical Engineering Congress. Page 4845-4853, 23-25 Nov, 2004.
- Bailey, B., Crabtree, M., Tyrie, J., Elphick, J., Kuchuk, F., Romano, C. and Roodhart, L., 2000. Water control. *Oilfield review*, 12(1), pp.30-51.
- Barton, C. A., & Zoback, M. D. (1992). Self-similar distribution and properties of macroscopic fractures at depth in crystalline rock in the Cajon Pass Scientific Drill Hole. *Journal of Geophysical Research: Solid Earth*, 97(B4), 5181-5200.
- Bear, J., 2013. Dynamics of fluids in porous media. Courier Corporation.
- Birks, J. 1963. Coning Theory and its Use in Predicting Allowable Producing Rates of Wells in a Fissured Limestone Reservoir. *Iranian Petroleum Institute Bulletin*, Vol.12, 470-480.
- Bisdorn, K., Gauthier, B. D. M., Bertotti, G., & Hardebol, N. J. (2014). Calibrating discrete fracture-network models with a carbonate three-dimensional outcrop fracture network: Implications for naturally fractured reservoir modeling. *AAPG bulletin*, 98(7), 1351-1376.
- Bockel-Rebelle, M.O., Hassall, J.K., Silva, F.P., Lozano, J.A., Al Deeb, M., Salem, S.E.A., Vesseron, M. and Al Mehsin, K., 2004, January. Faults, fracture corridors and diffuse

- fracturing: ranking the main structural heterogeneities within onshore Abu Dhabi fields. In Abu Dhabi International Conference and Exhibition. Society of Petroleum Engineers.
- Boerrigter, P.M., Pieters, J., Wit, K., and Ypma, J.G.J. 1993. Fractured Reservoir Simulation: Case Studies. Presented at the SPE Middle East Oil Technical Conference and Exhibition, Bahrain, April 3-6. SPE-25615.
- Bourbiaux, B., Cacas, M.C., Sarda, S. and Sabathier, J.C., 1998. A rapid and efficient methodology to convert fractured reservoir images into a dual-porosity model. *Revue de l'institut Français du Pétrole*, 53(6), pp.785-799.
- Bourbiaux, B., Fournio, A., Nguyen, Q., Norrant, F., Robin, M., Rosenberg, E. and Argillier J. 2016. Experimental and Numerical Assessment of Chemical Enhanced Oil Recovery in Oil-Wet Naturally Fractured Reservoirs. *SPE Journal*, 21 (3). SPE-169140-PA.
- Bournazel, C. and Jeanson, B. 1971. Fast Water Coning Evaluation Method," Paper SPE 3628 presented at 46th ATCE, New Orleans, Oct.3-6.
- Buksh, G. 1991. Development of the Naturally Faculted ISND Shuaiba Reservoir. Presented at the Middle East Oil Show, Bahrain, 16-19 Nov. SPE 21354.
- Bustos, A.V., Eduardo, A.C., Febres, A., Antonio, V.P., Pemex, and Shen, F. 2010. Integrated Fractured Reservoir Characterization and Connectivity Study in the Cantarell Field. Paper SPE 132241 presented at the CPS/SPE International Oil & Gas Conference and Exhibition, Beijing, China, 8-10 June.
- Carlson, M.R. 2003. Practical Reservoir Simulation: Using, Assessing and Developing Results. PenWell Books, Tulsa, Oklahoma.
- Cavazzuti, M., 2013, "Optimization Methods; From Theory to Design Scientific and Technological Aspects in Mechanics," Springer-Verlag Berlin Heidelberg, 10.1007/978-3-642-31187-1.
- Chan, K.S. 1995. Water Cut Diagnostic Plots. Presented at the SPE ATCE, Dallas, TX, 22-25 Oct. SPE-30775-MS.
- Chaperon, I. 1986. Theoretical Study of Coning Toward Horizontal and Vertical Wells in Anisotropic Formations: Subcritical and Critical Rates. Paper SPE 15377 presented at the SPE 61st ATCE, New Orleans, LA, Oct. 5-8.
- Chilingar, G.V. and Yen, T.F. 1983. Some Notes on Wettability and Relative Permeabilities of Carbonate Reservoir Rocks II. *Energy Sources*, 7(1): 67-75.
- Clarkson, C.R., and Qanbari, F. 2015. A Semianalytical Forecasting Method for Unconventional Gas and Light Oil Wells: A Hybrid Approach for Addressing the Limitations of Existing Empirical and Analytical Methods. *SPE Reservoir Evaluation and Engineering*, 18(01).

- Clauset, A. 2011. Inference, Models and Simulation for Complex Systems. Lecture 0.
- Cuiec, L. 1984. Rock/Crude-Oil Interactions and Wettability: An Attempt to Understand Their Interrelation. Presented at the 59th Annual Technical Conference and Exhibition, Houston, TX, 16-19 Sept. SPE-13211-MS.
- Davy, P., Sornette, A., & Sornette, D. (1990). Some consequences of a proposed fractal nature of continental faulting. *Nature*, 348(6296), 56.
- Dershowitz, B., Lapointe, P., Elben, T., and Wel, L. 2000. Integration of Discrete Feature Network Methods with Conventional Simulator Approaches. *SPE Reservoir Evaluation and Engineering*, 3(02): 165-170. SPE 62498-PA.
- Dupuit, J.É.J., 1863. Études théoriques et pratiques sur le mouvement des eaux dans les canaux découverts et à travers les terrains perméables: avec des considérations relatives au régime des grandes eaux, au débouché à leur donner, et à la marche des alluvions dans les rivières à fond mobile. Dunod.
- Durlofsky, L.J. 1991. Numerical Calculations of Equivalent Gridblock Permeability Tensors for Heterogeneous Porous Media. *Water Resources Research*, 27 (5): 699–708.
- Elmouttie, M.K., Poulsen, B. and Krahenbuhl, G., 2015. Characterisation of Fracture Network Realisations for Geothermal Reservoir Flow Modelling. Proceedings World Geothermal Congress, Melbourne, Australia, 19-25 April.
- Ferreira, S.L.C., et al., 2007, “Box-Behnken Design: An Alternative for the Optimization of Analytical Methods,” *Analytica Chimica Acta*, 597(02).
- Ferrill, D.A. and Morris, A.P., 2008. Fault zone deformation controlled by carbonate mechanical stratigraphy Balcones fault system, Texas. *AAPG Bulletin*. 92, 359– 380.
- Figueiredo, B., Tsang, C.F., Niemi, A. and Lindgren, G., 2016. The state-of-art of sparse channel models and their applicability to performance assessment of radioactive waste repositories in fractured crystalline formations. *Hydrogeology Journal*, 24(7), pp.1607-1622.
- Gallagher, J., Prado, L., and Pieters, J. 1993. Simulation of Coning in a Thin Oil Rim in a Fractured Reservoir. Presented at the SPE Middle East Oil Technical Conference and Exhibition, Bahrain, 3-6 April. SPE 25613.
- Gilman, J.R. 1986. An Efficient Finite Difference Method for Simulating Phase Segregation in the Matrix Blocks in Double-Porosity Reservoirs. *SPE Reservoir Engineering*, 1: 403-413.
- Gilman, J.R., 2003, June. Practical aspects of simulation of fractured reservoirs. In *International forum on reservoir simulation (Vol. 23)*.
- Gilman, J.R., and Kazemi, H. 1988. Improved Calculations for Viscous and Gravity Displacement in Matrix Blocks in Dual-Porosity Simulators. *JPT*, 40(01): 60-70. SPE-16010-PA.

- Gomez, L., Gale, J. F. W., Laubach, S. E., and Cumella, S. 2003. Chapter 6, Quantifying fracture intensity: an example from the Piceance Basin. Peterson, K. M., Olson, T. M., and Anderson, D. S., eds, Piceance Basin 2003 guidebook. Rocky Mountain Association of Geologists, 96-113.
- Guerriero, V., Vitale, S., Ciarcia, S., & Mazzoli, S. (2011). Improved statistical multi-scale analysis of fractured reservoir analogues. *Tectonophysics*, 504(1-4), 14-24.
- Hooker, J. N., Laubach, S. E., & Marrett, R. (2014). A universal power-law scaling exponent for fracture apertures in sandstones. *Bulletin*, 126(9-10), 1340-1362.
- Gong, L., Fu, X., Gao, S., Zhao, P., Luo, Q., Zeng, L., Yue, W., Zhang, B. and Liu, B., 2018. Characterization and prediction of complex natural fractures in the tight conglomerate reservoirs: A fractal method. *Energies*, 11(9), p.2311.
- Gouth, F., Toub Blanc, A., and Mresah, M. 2006. Characterization and Modeling of a Fractured Reservoir Using a Novel DFN Approach. Presented at the 2006 Abu Dhabi International Petroleum Exhibition and Conference, Abu Dhabi, UAE, 5-8 Nov. SPE 102165.
- Guglielmi, Y., Elsworth, D., Cappa, F., Henry, P., Gout, C., Dick, P., & Durand, J. (2015). In situ observations on the coupling between hydraulic diffusivity and displacements during fault reactivation in shales. *Journal of Geophysical Research: Solid Earth*, 120, 7729– 7748.
- Guo, B., and Lee, R.L-H. 1993. A Simple Approach to Optimization of Completion Interval in Oil/Water Coning Systems. *SPE Reservoir Engineering*, 8(4). 249-255. SPE-23994-PA.
- Gupta, R., Smith Jr., P.G., Hu, L., Willingham, T.W., Cascio, M.L., Shyeh, J.J. and Harris, C.R. 2011. Enhanced Waterflood for Middle East Carbonate Cores- Impact of Injection Water Composition. Presented at the SPE Middle East Oil and Gas Show and Conference, Manama, Bahrain, 25-28 September. SPE 142668.
- Hamon, G. 1988. Oil/Water Gravity Drainage Mechanisms in Oil-Wet Fractured Reservoirs. Paper SPE 18366 presented at the SPE European Petroleum Conference, London, UK, 16-19 Oct.
- Hassall, J.K., Silva, F.P., Lozano, J.A., Al Deeb, M., Salem, S.E.A., Vesseron, M., and Mehsin, K.A. 2004. Faults, Fracture Corridors and Diffuse Fracturing: Ranking the Main Structural Heterogeneities within Onshore Abu Dhabi Fields. Presented at the Abu Dhabi International Conference and Exhibition, Abu Dhabi, UAE, 10-13 Oct. SPE 88676-MS.
- Haugen, A. 2010. Fluid flow in fractured carbonates: wettability effects and enhanced oil recovery. PhD Dissertation, University of Bergen, Bergen, Norway.

- Heffer, K. J., & Bevan, T. G. (1990, January). Scaling relationships in natural fractures: data, theory, and application. In European Petroleum Conference. Society of Petroleum Engineers.
- Hidalgo, O.J., Brito, L.E., Munoz, G.J., Paz, F., Flamenco, F. and Aguilera, R. 2009. Critical Oil Rates in Naturally Fractured Reservoirs to Minimize Gas and Water Coning: Case History of a Mexican Carbonate Reservoir. Presented at the 2009 SPE Latin American and Caribbean Petroleum Engineering Conference in Cartagena, Colombia, 31May-3June. SPE-121743.
- Horle, T., Firoozabadi, A., and Ishimoto, K. 1990. Laboratory Studies of Capillary Interaction in Fracture/Matrix Systems. SPE Reservoir Engineering, 5(03): 353-360. SPE-18282-PA.
- Hoyland, L.A., Papatzacos, P. and Skjaeveland, S.M. 1989. Critical-Rate for Water Coning: Correlation and Analytical Solution. SPE Reservoir Engineering, 4(4), 495-502. SPE-15855-PA.
- Jafari, A. and Babadagli, T., 2010, April. Prediction of the equivalent fracture network permeability using multivariable regression analysis and artificial neural network. In Proceedings of World Geothermal Congress, Bali, Indonesia(pp. 25-29).
- Jemberie, A. A. 2004. Information Theory and Artificial Intelligence to Manage Uncertainty in Hydrodynamic and Hydrological Models. PhD Dissertation, Delft University of Technology, The Netherlands.
- Jensen, J.L., Lake, L.W., Corbett, P.W.M., and Goggin, D.J. 1997. Statistics for Petroleum Engineers and Geoscientists. Prentice Hall PTR, New Jersey.
- Jin, L. 2013. A Feasibility Study of Multi-Functional Wells for Water Coning Control and Disposal. PhD Thesis, Louisiana State University, Baton Rouge, LA.
- Johns, R.T., Lake, L.W., Ansari, R.Z. and Delliste, A.M., 2005. Prediction of capillary fluid interfaces during gas or water coning in vertical wells. SPE Journal, 10(04), pp.440-448.
- Joseph, J.A., and Koederitz, L.F., 1985, "Unsteady-State Spherical Flow with Storage and Skin," SPEJ, 25(6), pp. 804-822.
- Joshi, S.D., 1991, Horizontal Well Technology, First Edition, Penn Well Books Tulsa, OK.
- Kakimi, T. (1980). Magnitude-frequency relation for displacement of minor faults and its significance in crustal deformation. Bulletin of the Geological Survey of Japan, 31, 467-487.
- Kirimi-Fard, M., Gong, B., and Durlofsky, L.J. 2006. Generation of Coarse-Scale Continuum Flow Models from Detailed Fracture Characterizations. Water Resour. Res. 42: W10423. doi: 10.1029/2006WR005015.

- Kuo, M.C.T., and Desbrisay, C.L., 1983, "A Simplified Method for Water Coning Predictions," 58th Annual Technical Conference and Exhibition, San Francisco, CA, Oct 5-8, Paper No. SPE 12067.
- Kyte, J.R. 1970. A Centrifuge Method to Predict Matrix-Block recovery in fractured reservoirs. SPE Journal, 10(2), 164-170, June 1970.
- Labastie, A. 1990. Capillary Continuity between Blocks of a Fractured Reservoir. Presented at the 65th Annual Technical Conference and Exhibition, New Orleans, LA, Sept. 23-26. SPE-20515.
- Lamb, H., 1945. Hydrodynamics, 1932. Cambridge UP, pp.236-241.
- Long, J.C.S., Gilmour, P., and Witherspoon, P.A. 1985. A Model for Steady State Fluid Flow in Random Three-Dimensional Networks of Disc-Shaped Fractures, Water Resour. Res., 21: 1105-1115.
- Longxin, M., Ruifeng, W., and Xianghong, W. 2015. Development Features and Affecting Factors of Natural Depletion of Sandstone Reservoirs in Sudan. Petroleum Exploration and Development, 42(3).
- Lorenz, J. C., and R. Hill, 1991. Subsurface fracture spacing: comparison of inferences from slant/horizontal core and vertical core in Mesaverde reservoirs in the Piceance Basin: SPE Rocky Mountain Regional Meeting/Low-Permeability Reservoir Symposium, April 15-17, 1991, Denver, SPE No. 21877, p. 705-716.
- Lorenz, J.C. and Hill, R.E., 1994. Subsurface fracture spacing: comparison of inferences from slant/horizontal core and vertical core in Mesaverde reservoirs. SPE Formation Evaluation, 9(01), pp.66-72.
- Martel, S.J. 1999. Analysis of Fracture Orientation Data from Boreholes. Environment and Engineering Geoscience, 5 (2), 213-233.
- Masalmeh, S.K. 2002. The Effect of Wettability on Saturation Functions and Impact on Carbonate Reservoirs in the Middle East. Presented at the SPE 10th Abu Dhabi International Petroleum Exhibition and Conference, Abu Dhabi, 13-16 Oct. SPE 78515.
- Matthews, J.D., Carter, J.N., and Dake, L.P. 1992. Investigation of Optimum Well Spacing for North Sea Eocene Reservoirs. Paper SPE 25030 presented at the European Petroleum Conference, Cannes, France, 16-18 Nov.
- Meehan, D.N. 2011. Using Analog Reservoir Performance to Understand Type I Fractured Reservoir Behavior with Strong Water Drives. Presented at the SPE Enhanced Oil Recovery Conference, Kuala Lumpur, Malaysia, 19-21 July. SPE 144177.

- Meyer, H.I. and Gardner, A.O. 1954. Mechanics of Two Immiscible Fluids in Porous Media. *J. Appl. Phys.* 25 (11): 1400-1406. <http://dx.doi.org/10.1063/1.1721576>.
- Meyer, H.I., and Searcy, D.F., 1956, "Analog Study of Water Coning," *Trans., AIME*, pp. 207-302.
- Moncada, K., Tiab, D., Escobar, F.H., Montealegre, M., Chacon, A., Zamora, R. and Nese, S.L., 2005. Determination of vertical and horizontal permeabilities for vertical oil and gas wells with partial completion and partial penetration using pressure and pressure derivative plots without type-curve matching. *CT&F-Ciencia, Tecnología y Futuro*, 3(1), pp.77-94.
- Moran, J.N., and Finklea, E.E., 1962, "Theoretical Analysis of Pressure Phenomena Associated with the Wireline Formation Tester," *Journal of Petroleum Technology*, 14(8), pp. 899-908, Paper No. SPE-177-PA.
- Muskat, M., 1937. *The Flow of Homogeneous Fluids Through a Porous Media*, Int. Human Resources Development Corp., Boston.
- Muskat, M. and Wyckoff, R.D. 1935. *An Approximate Theory of Water-coning in Oil Production*. *Trans. AIME*, Vol.114.
- Myers, R.H., and Montgomery, C.D., 1995, "Response Surface Methodology: Process and Product Optimization Using Designed Experiments," John Wiley and Sons, New York.
- Namani, M., Asadollahi, M. and Haghghi, M., 2007, January. Investigation of water coning phenomenon in Iranian carbonate fractured reservoirs. In *International Oil Conference and Exhibition in Mexico*. Society of Petroleum Engineers.
- Namba, T., and Hiraoka, T. 1995. Capillary Force Barriers in a Carbonate Reservoir under Waterflooding. Presented at the SPE Middle East Oil Show, Bahrain, 11-14 March. SPE 29773.
- Narr, W., Schechter, D.S. and Thompson, L.B. 2006. *Naturally Fractured Reservoir Characterization*, Chap. 4, 63. Richardson, TX: Society of Petroleum Engineers.
- Nelson, R.A. 2001. *Geologic Analysis of Naturally Fractured Reservoirs*. Second Edition, Gulf Professional Publishing.
- NIST/SEMATECH e-Handbook of Statistical Methods, <http://www.itl.nist.gov/div898/handbook/>, April 2012.
- Oda, M., 1985. Permeability tensor for discontinuous rock masses. *Geotechnique* 35 (4), 483-495.
- Ozkaya, S.I. 2010. Use of Exclusion Zone in Mapping and Modeling Fracture Corridors. *SPE Reservoir Evaluation and Engineering* 4 (13): 15-18. <https://doi.org/10.2118/120136-PA>.

- Ozkaya, S.I., 2013, March. Structural controls of fracture corridors in some Middle East Fields. In SPE Middle East Oil and Gas Show and Conference. Society of Petroleum Engineers.
- Ozkaya, S.I., and K.R. Minton. 2005. "Flow Potential of Fracture Corridors and Large Conductive-Fractures in a Clastic Field, Southern Basin-Oman." SPE Middle East Oil and Gas Show and Conference, Bahrain. 12-15 March. SPE 93030.
- Ozkaya, S.I. and Minton, K.R. 2007. Flow Potential of Fracture Corridors and Large Conductive Fractures in a Clastic Reservoir, Oman. Special Publication, Geological Society of London, 270: 245-263.
- Ozkaya, S.I., and Richard, P.D. 2006. Fractured Reservoir Characterization Using Dynamic Data in Carbonate Field, Oman. SPE Reservoir Engineering & Evaluation 9(3): 12-15.
- Papatzacos, P., 1986, "Approximate Partial-Penetration Pseudoskin for Infinite-Conductivity Wells," SPE Reservoir Engineering, 2(2), pp. 227-234, Paper No. SPE-13956-PA.
- Parsons, R.W. 1966. Permeability of Idealized Fracture Network. SPE Journal, 6(02):126-136. SPE 1289-PA.
- Perez-Martinez, E., Rodriguez-de la Garza, F., and Samaniego-Verduzco, F. 2012. Water Coning in a Naturally Fractured Carbonate Heavy Oil Reservoir-A Simulation Study. Presented at the SPE Latin American and Caribbean Petroleum Engineering Conference in Mexico City, Mexico 16-18 April. SPE-152545.
- Pine, R. J., & Batchelor, A. S. (1984). Downward migration of shearing in jointed rock during hydraulic injections. International Journal of Rock Mechanics and Mining Science and Geomechanics
- Pirson, S.J., 1977. Oil reservoir engineering. RE Krieger Publishing Company.
- Prasun, S. and Wojtanowicz, A.K. 2016. Determination and Implication of Ultimate Water-Cut in Well-Spacing Design for Reservoirs with Water Coning. Presented at the SPE Eastern Regional Meeting, Canton, Ohio, 13-15 Sept. SPE 184075.
- Prasun, S. and Wojtanowicz, A.K. 2018. Determination and Implication of Ultimate Water-Cut in Well-Spacing Design for Developed Reservoirs with Water Coning. Journal of Energy Resources Technology, 140(8): 082902-082902-12. doi: 10.1115/1.4039743.
- Pratap, M., Kleppe, J. and Uleberg, K. 1997. Vertical Capillary Continuity Between the Matrix Blocks in a Fractured Reservoir Significantly Improves the Oil Recovery by Water Displacement. Presented at the SPE Middle East Oil Show, Bahrain, 15-18 March. SPE 37725.
- Qin, W., Wojtanowicz, A.K., and Luo, P. 2016. Investigation of Well Production Mechanism in Heavy Oil Reservoirs Underlain by Strong Bottom Water. Presented at the Proceedings

of the ASME 2016 35th International Conference on Ocean, Offshore and Arctic Engineering, Busan, South Korea, June 19-24.

- Questiaux, J.M., Couples, G. and Ruby, N., 2010. Fractured reservoirs with fracture corridors. *Geophysical Prospecting*, 58(2), pp.279-295.
- Ray, D.S., Al-Shammeli, A., Verma, N.K., Matar, S., De Groen, V., De Joussineau, G., Ghilardini, L., Le Maux, T. and Al-Khamees, W., 2012. Characterizing and modeling natural fracture networks in a tight carbonate reservoir in the Middle East: a methodology.
- Reiss, L.H. 1980. *The Reservoir Engineering Aspects of Fractured Formations*. Appendix 5, 83-88. Houston, TX: Gulf Publishing Co.
- Rutqvist, J., Birkholzer, J., Cappa, F., & Tsang, C. F. (2007). Estimating maximum sustainable injection pressure during geological sequestration of CO₂ using coupled fluid flow and geomechanical fault-slip analysis. *Energy Conversion and Management*, 48(6), 1798– 1807.
- Saad, S.E.M., Darwch, T.D, and Assad, Y. 1995. Water Coning in Fractured Basement Reservoirs. Presented at the SPE Middle East Oil Show in Bahrain, 11-14 March. SPE-29808.
- Safari, R., & Ghassemi, A. 2015. 3D thermo-poroelastic analysis of fracture network deformation and induced micro-seismicity in enhanced geothermal systems. *Geothermics*, 58, 1– 14.
- Safari, R., & Ghassemi, A. 2016. Three-dimensional poroelastic modeling of injection induced permeability enhancement and microseismicity. *International Journal of Rock Mechanics and Mining Sciences*, 84, 47– 58. <https://doi.org/10.1016/j.ijrmms.2015.12.007>
- Schols, R.S. 1972. An Empirical Formula for the Critical Oil Production Rate. *Erdoel Erdgas, Z.*, 88(1): 6-11, January 1972.
- Shadizadeh, S.R. and Ghorbani, D. 2001. Investigation of Water/Gas Coning in Naturally Fractured Hydrocarbon Reservoirs. Presented at the Petroleum Society's Canadian International Petroleum Conference, Calgary, Alberta, Canada, 12-14 June. Paper 2001-014.
- Shibasaki, T., Edwards, E., Qotb, M., and Akatsuka, K. 2006. Identification of Key Fracture Effects on Fluid Flow and Iterative Approach for Effective Permeability Modeling of a Matrix-Dominated Carbonate Reservoir, Offshore Abu Dhabi. Presented at the 2006 Abu Dhabi International Petroleum Exhibition and Conference, Abu Dhabi, UAE, 5-8 Nov. SPE 101480.
- Shirman, E. I. (1996). A well completion design model for water-free production from reservoirs overlying aquifers (No. CONF-961003-). Society of Petroleum Engineers (SPE), Inc., Richardson, TX (United States).

- Shirman, E. I., & Wojtanowicz, A. K. (1997, January). Water cone hysteresis and reversal for well completions using the moving spherical sink method. In SPE Production Operations Symposium. Society of Petroleum Engineers.
- Shirman, E. I., & Wojtanowicz, A. K. (1998, January). More Oil With Less Water Using Downhole Water Sink Technology: A Feasibility Study. In SPE Annual Technical Conference and Exhibition. Society of Petroleum Engineers.
- Shirman, E.I. and Wojtanowicz, A.K. 1997. Water Coning Reversal Using Downhole Water Sink-Theory and Experimental Study. Presented at the SPE Annual Conference and Exhibition, San Antonio, Texas, Oct 5-8. SPE 38792.
- Shirman, E., Wojtanowicz, A. K., & Kurban, H. (2014). Enhancing oil recovery with bottom water drainage completion. *Journal of Energy Resources Technology*, 136(4), 042906.
- Shirman, E.I. and Wojtanowicz, A.K. 2000. More Oil Using Downhole Water-Sink Technology: A Feasibility Study. *SPE Production and Facilities*, 15(4): 234-240. SPE-66532-PA.
- Singh, S.K., Abu-Habbie, H., Khan, B., Akbar, M., Etchecopar, A. and Montaron, B., 2008. Mapping fracture corridors in naturally fractured reservoirs: an example from Middle East carbonates. *First Break*, 26(5).
- Snow, D.T., 1969. Anisotropic permeability of fractured media. *Water Resources Research*, 5(6), pp.1273-1289.
- Song, X.Y., Liu, Y.T., Jiang, X.E., Ding, Z.P. and Xue, L., 2019, January. A novel approach to assessing the anisotropic permeability parameters of fractured media. In IOP Conference Series: Materials Science and Engineering (Vol. 474, No. 1, p. 012043). IOP Publishing.
- Spence, G. H., Redfern, J., Aguilera, R., Bevan, T. G., Cosgrove, J. W., Couples, G. D., & Daniel, J. M. (Eds.). (2014, August). *Advances in the study of fractured reservoirs*. Geological Society of London.
- Tabatabaei, M., Ghalambor, A and Guo, B. 2012. An Analytical Solution for Water Coning in Vertical Wells. *SPE Production and Operations*, 27(2): 195-204. SPE 113106-PA.
- Tabola, D.P., and Baldwin, B.A. 1995. Capillary Continuity in Fractured Chalk Systems: An Experimental Study. Presented at the SCA conference. Paper no. 9526.
- Tan, Y., Li, H., Zhou, X., Jiang, B., Wang, Y. and Zhang, N., 2018. A Semi-Analytical Model for Predicting Horizontal Well Performances in Fractured Gas Reservoirs With Bottom-Water and Different Fracture Intensities. *Journal of Energy Resources Technology*, 140(10), p.102905.
- Thomas, L.K., Dixon, T.N., Evans, C.E., and Vienot, M.E. 1987. Ekofisk Waterflood Pilot. *JPT*, 39(02): 221-232. SPE-13120-PA.

- Thomas, L.K, Dixon, T.N., Pierson, R.G., and Hermansen, H. 1991. Ekofisk Nitrogen Injection. SPE Formation Evaluation, 6(02): 151-160. SPE-19839-PA.
- Treiber, L.E. and Owens, W.W. 1972. Laboratory Evaluation of the Wettability of 50 Oil-Producing Reservoirs. SPE Journal, 12(6): 531-540. SPE 3526-PA.
- Van Golf-Racht, T.D. and Sonier, F. 1994. Water Coning in a Fractured Reservoir. Presented at the SPE Annual Technical Conference and Exhibition, New Orleans, Sept. 25-28. SPE 28572.
- Voorn, M., Exner, U., Barnhoorn, A., Baud, P. and Reuschlé, T., 2015. Porosity, permeability and 3D fracture network characterisation of dolomite reservoir rock samples. Journal of Petroleum Science and Engineering, 127, pp.270-285.
- Van Sicken, C.D., 2002. Equivalent channel network model for permeability and electrical conductivity of fracture networks. Journal of Geophysical Research: Solid Earth, 107(B6), pp.ECV-1.
- Williams, M.P., Nivarthi, S.S., Al-Shehhi, B.H., and Edwards, E. 2011. Fracture Modeling in a Weakly Fractured Carbonate Reservoir, Offshore UAE. Presented at the SPE Reservoir Characterization and Simulation Conference and Exhibition, Abu Dhabi, UAE, 9-11 Oct. SPE 148018.
- Witherspoon, P.A., Wang, J.S., Iwai, K. and Gale, J.E., 1980. Validity of cubic law for fluid flow in a deformable rock fracture. Water resources research, 16(6), pp.1016-1024.
- Wojtanowicz, A. K., Xu, H., & Bassiouni, Z. A. (1991, January). Oilwell Coning Control Using Dual Completion With Tailpipe Water Sink. In SPE Production Operations Symposium. Society of Petroleum Engineers.
- Wojtanowicz, A. K., & Xu, H. (1992, June). A New In-Situ Method to Minimize Oilwell Production Water-Cut Using Downhole Water Loop. In Proceedings of the 43rd Annual Technical Meeting of the Petroleum Society of CIM, Calgary, AB, Canada, June (pp. 7-10).
- Wojtanowicz, A. K., & Shirman, E. (1996). An In-Situ Method for Downhole Drainage–Injection of Formation Brine in a Single Oil-Producing Well. Deep Injection Disposal of Hazardous and Industrial Wastes, JA Apps, and C.-F. Tsang, eds., Academic, New York, 403-420.
- Ye, Z., Janis, M., & Ghassemi, A. 2017a. Injection-driven shear slip and the coupled permeability evolution of granite fractures for EGS stimulation. Paper presented at the 51st U.S. Rock Mechanics/Geomechanics Symposium, San Francisco, CA.
- Ye, Z., Janis, M., Ghassemi, A., & Bauer, S. 2017b. Experimental investigation of injection-driven shear slip and permeability evolution in granite for EGS stimulation. Paper

presented at the 42nd Workshop on Geothermal Reservoir Engineering, Stanford, California, USA.

Zhang, X. and Koutsabeloulis, N.C., 2010, January. Estimate of permeability of fracture corridors/networks: From data acquisition to reservoir simulations. In International Oil and Gas Conference and Exhibition in China. Society of Petroleum Engineers.

Vita

Samir Prasun, Son of Raghubar Narain Barnwal and Chanda Barnwal, was born in India on May 1986. He received his B.Tech in Petroleum Engineering from Indian School of Mines, Dhanbad in 2009. After graduation, he joined University of Oklahoma as a research assistant, and completed his MS in Petroleum Engineering from there. After MS, he worked for Omak Technologies LLC as a reservoir engineer for a while and subsequently in Indian School of Mines as a lecturer. Subsequently, he decided to do his PhD from Louisiana State University in year 2015. During his PhD, he completed two internships, one in Bureau of Economic Geology and other in Exxon Mobil. He anticipates receiving PhD degree in Petroleum Engineering from Louisiana State University in August 2020.